TRANSFER AND DEVELOPMENT LENGTHS OF STEEL STRANDS IN FULL-SCALE PRESTRESSED SELF-CONSOLIDATING CONCRETE BRIDGE GIRDERS

BY

ANDREW M. POZOLO

THESIS

Submitted in partial fulfillment of the requirements
for the degree of Master of Science in Civil Engineering
in the Graduate College of the
University of Illinois at Urbana-Champaign, 2010

Urbana, Illinois

Adviser:

Professor Bassem Andrawes

ABSTRACT

Self-consolidating concrete (SCC) is a workable yet stable concrete which flows easily and consolidates under its own weight. Its unique properties can substantially reduce the labor required to pour complex or heavily reinforced structural members. Over the past decade, the American precast industry has taken significant strides to adopt SCC in commercial projects, though concern about early-age bond behavior has limited the material's application in prestressed members. A keen understanding of SCC's bond strength, including its impact on transfer and development lengths in prestressed members, is essential to safely implement SCC in prestressed design.

The Illinois Department of Transportation (IDOT) has sponsored a three-phase study exploring the bond behavior of steel strands in prestressed bridge girders. In the first phase, 56 pullout tests were conducted to compare the performance of seven-wire strands embedded in SCC and conventionally-consolidated concrete blocks. In the second phase, transfer lengths of prestressing strands in two SCC hollow box girders and two SCC I-girders were determined experimentally. In the third phase, the development length of strands in the two box girders was determined through a series of iterative flexural tests.

This thesis details the three phases of the IDOT study and compares results to industry standards and requirements of the American Concrete Institute and the American Association of State Highway and Transportation Officials. Results are also compared to analytical methods proposed in the literature. Additionally, a systematic method is developed to predict transfer lengths in full-scale specimens using pullout test data and finite element analysis. The proposed method may be useful when large-scale testing is impractical in terms of time or cost.

This thesis is dedicated to my parents, Gary & Cynthia.

ACKNOWLEDGMENTS

I first thank my advisor, Dr. Bassem Andrawes, for his continual guidance during my graduate studies at the University of Illinois. Without his support, this research would not have been possible. I also extend gratitude to Dr. Gregory Banas, Timothy Prunkard, and my fellow graduate students for assisting with experiments in the structural testing laboratory. In addition, I thank Michael Johnson and the workers at Prestressed Engineering Corporation in Blackstone, Illinois for cooperation during test specimen fabrication. I also acknowledge the Illinois Center for Transportation and the Illinois Department of Transportation for funding this project. Finally, I am forever grateful to my family and friends for their unyielding love and encouragement.

TABLE OF CONTENTS

CHAPTER 1: INTRODUCTION

1.1 MOTIVATION FOR RESEARCH PROJECT

Self-consolidating concrete (SCC) is a workable yet stable concrete which flows easily and consolidates under its own weight. Its unique properties can substantially reduce the labor required to pour complex or heavily reinforced structural members. Over the past decade, the United States (U.S.) precast industry has taken significant strides to adopt SCC, recognizing its potential to reduce material costs, labor costs, and turn-over time. Concern about early-age bond behavior, however, has thus far limited the material's application in prestressed members. Limited experimental data is available for full-scale prestressed SCC specimens, and studies assessing bond behavior in SCC have shown wide variability in their results. A keen understanding of SCC's bond strength, including its impact on transfer and development lengths in prestressed members, is essential to safely implement SCC in prestressed design.

In response to rising demand to adopt SCC in the state of Illinois, the Illinois Department of Transportation (IDOT) has sponsored a study exploring the application of SCC in full-scale prestressed girders. The study aims specifically at assessing the bond properties of prestressing strands in I-girders and hollow box girders cast with IDOT-approved SCC. Testing of SCC box girders is particularly notable because of the absence of similar testing in previous literature.

1.2 THESIS OUTLINE

This thesis presents the scope, methodology, and experimental results of research performed at the University of Illinois at Urbana-Champaign (UIUC) for the three-phase IDOT study. The thesis also presents comparisons of experimental data to previous research and outlines a method for predicting transfer lengths in full-scale specimens using pullout test data and finite element analysis. Chapter 1 discusses the motivation for this research.

Chapter 2 contains a literature review which highlights the properties of SCC, discusses code requirements for transfer and development lengths, and summarizes results from recent studies concerned with bond behavior of prestressed SCC specimens.

Chapter 3 presents experimental results from pullout tests conducted on 0.5-in. diameter, low-relaxation seven-wire steel strands embedded in SCC and NCC blocks. The tests are used to characterize strand behavior in SCC as acceptable when compared to behavior in NCC.

Chapter 4 outlines the design and analysis of two 28-ft. hollow box girders and two 48-ft. I-girders. The fabrication process and specimen geometry are described in detail. Theoretical prestress losses, shear capacities, and flexural capacities are presented. The design procedure for external FRP shear reinforcement is described, as is the application of CFRP to one box girder specimen.

Chapter 5 describes the transfer length measurements taken for the four full-scale girders. Experimental results are compared to requirements of the 2008 American Concrete Institute (ACI) building design code (ACI Committee 318) and the American Association of State Highway and Transportation Officials (AASHTO) LRFD Bridge Design Specifications (AASHTO 2004). Results are also compared to proposed analytical transfer length expressions from the literature.

Chapter 6 provides a thorough review of the flexural tests conducted to determine development length in the box girder specimens. Experimental results are compared to code requirements, theoretical design capacities, and analytical development length expressions from the literature. The shear-strengthening effect of externally bonded carbon fiber-reinforced polymer (CFRP) fabric is also noted.

Chapter 7 outlines a systematic method to predict transfer length using pullout test data incorporated into finite element analyses. The finite element program ANSYS (2007) is utilized to create models of the pullout blocks and girder specimens. Transfer length predictions from the analyses are compared to experimental results. The proposed method may be useful when large-scale testing is not feasible due to time, cost, or other prohibitive constraints.

Chapter 8 summarizes the major findings of the experimental and analytical portions of this research, with limitations or assumptions noted where appropriate.

Six appendices follow the main text of this thesis. Appendix A contains plots of all force-displacement responses obtained from the pullout tests. Appendix B provides fabrication drawings of the full-scale girder specimens; all pertinent reinforcement details and girder dimensions are included. Appendices C and D provide example calculations for prestress losses, shear capacities, and flexural capacities. Appendix E presents the strain profiles obtained for transfer length measurements in all four girders. Finally, Appendix F presents the end-slip behavior of strands during flexural testing of the two box girders.

CHAPTER 2: LITERATURE REVIEW

2.1 BACKGROUND ON SELF-CONSOLIDATING CONCRETE

Developed by researchers concerned with the durability of Japan's concrete infrastructure and the declining number of skilled laborers in Japan's workforce, self-consolidating concrete emerged as a structural material in the late 1980's (Okamura & Ouchi 2003). By altering typical concrete mixture proportions and incorporating various chemical admixtures, researchers created a concrete which would easily flow and consolidate under its own weight, drastically reducing the labor required in the casting process. Japan and Europe soon began implementing SCC in large-scale applications, particularly in bridges (Ouchi et al. 2003). Over the past decade, the United States precast industry has taken significant strides to adopt the material in prestressed design, recognizing its tremendous potential to reduce fabrication time, labor, and cost.

2.1.1 Definition and Plastic Properties of SCC

The U.S. Precast/Prestressed Concrete Institute (PCI) defines SCC as "a highly workable concrete that can flow through densely reinforced or complex structural elements under its own weight and adequately fill voids without segregation or excessive bleeding without the need for vibration," (PCI 2003-a). The PCI classifies a concrete mixture as SCC if it meets specified requirements for three criteria: (1) filling ability, (2) passing ability, and (3) stability. Adequate filling ability ensures concrete can completely flow under its own weight without vibration into formwork. Adequate passing ability ensures concrete can flow through openings near the size of its coarse aggregate without experiencing blockage. Passing ability is particularly important in specimens with irregular shapes or dense reinforcement. Finally, stability refers to concrete's resistance to segregation, or its ability to retain homogenous characteristics during placement. Table 2.1 lists suggested test methods for evaluating plastic properties of SCC (PCI 2003-a).

Table 2.1: Test Methods for Determining SCC Plastic Properties

Test Method	Measured Characteristic(s)
T_{50}	Relative viscosity
U-Box	Passing ability, self-consolidation
L-Box, J-Ring	Passing ability, fluidity
Visual Stability Index (VSI)	Segregation resistance
Slump Flow, Inverted Slump Flow	Flow separation resistance

The unique plastic characteristics of SCC are attained by altering the proportions of traditional concrete constituents including cement, water, coarse aggregate, and fine aggregate. A typical volume distribution of SCC mixture constituents is shown in Figure 2.1. When compared to NCC mixtures, SCC mixtures typically have lower aggregate volumes, smaller coarse aggregate sizes, and higher cementitious material contents. High-range water-reducers (HRWRs) or superplasticizers enhance the flow ability of SCC. Low aggregate volume and high flow ability would tend to promote segregation in the concrete; as such, mineral and chemical admixtures are incorporated to enhance segregation resistance. Mineral admixtures may include silica fume, fly ash, ground granulated blast-furnace slag, and pulverized limestone (Lange et al. 2008). Chemical additives designed to prevent segregation are known as viscosity modifying admixtures (VMAs).

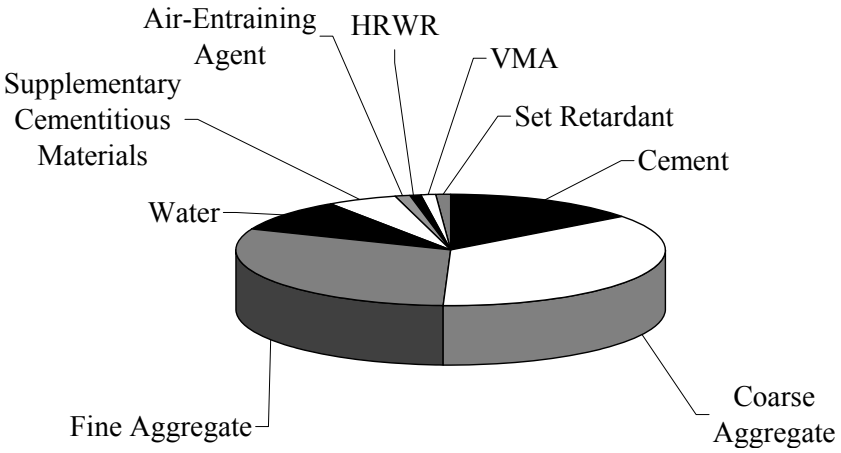

Figure 2.1: Typical SCC mixture constituents

2.1.2 Hardened Properties of SCC

The primary advantages of SCC are clearly derived from its plastic properties; however, these benefits would be negated if the hardened properties of SCC could not match those of traditional concrete. Lower coarse aggregate volumes suggest that the modulus of elasticity in SCC would be lower than in similar strength NCC (Bonen & Shah 2007). Additionally, aggregate significantly impacts long-term concrete shrinkage since it restrains volume change within the cement paste (Neville 1996). This could, in turn, affect prestress losses in SCC specimens. In a study by Schindler et al. (2007), hardened properties were measured

experimentally on cylinders cast with twenty-one SCC mixtures with varying water/cement (w/c) ratios, sand-to-total aggregate ratios, and cementitious material types. The researchers concluded that 112-day drying shrinkage strains in the SCC mixtures were of the same order of magnitude or less than corresponding strains in control specimens cast with NCC. The sand-to-total aggregate ratios appeared to have no significant effect on 112-day drying shrinkage strains or concrete compressive strength at any age. Finally, after 18 hours of curing, the modulus of elasticity in SCC was less than that in control specimens with comparable strength. After 56 days, however, moduli in SCC and NCC were comparable.

2.2 TRANSFER AND DEVELOPMENT LENGTH DEFINITIONS

A pretensioned concrete specimen is fabricated by casting concrete around prestressed strands, allowing the concrete to harden, and then releasing the strands. Upon release, specimens rely on bond between strands and concrete in transfer zones of the specimen to develop the imparted prestress. Three factors which may contribute to bond are adhesion between steel and concrete, friction between steel and concrete, and mechanical interlock (Janney 1954; Hanson & Kaar 1959). Since strands move relative to concrete upon release, it is generally accepted that bond due to pure adhesion is negligible; thus, friction and mechanical resistance are the two primary contributors to bond. Friction results from the wedging action of strands, commonly known as the Hoyer effect. When strands are initially stressed, they constrict in size; when released, they attempt to return to their original size, resulting in high radial pressure and frictional resistance. Additionally, the outer wires of helical strands tend to twist when released from tension; concrete surrounding the strands prevents twisting through mechanical interlock, thereby increasing bond. Specimens with adequate bond are able to reach their full shear and flexural design capacities without experiencing bond-slip failure at strand locations. Current design code requirements for transfer and development lengths were derived primarily from the work of Hanson and Kaar (1959) and are discussed in Section 2.2.1.

2.2.1 ACI and AASHTO Code Requirements

The 2008 ACI building design code defines transfer length as “the distance over which the strand must be bonded to the concrete to develop the effective prestress,” (ACI Committee 318). This distance is illustrated in Figure 2.2, which shows a theoretical strand stress profile at

the end of a prestressed specimen. The AASHTO LRFD design specifications require transfer lengths equal to $60d_b$, where d_b (in.) is the diameter of the strand (AASHTO 2004). The Chapter 11 ACI shear design guidelines, meanwhile, require transfer lengths equal to $50d_b$ (ACI Committee 318). Additionally, ACI flexural guidelines calculate transfer length L_t as in Equation 2-1, where f_{pe} is the effective prestress (ksi) and d_b is given in inches.

$$L_t = \frac{f_{pe} d_b}{3} \qquad \text{(Eq. 2-1)}$$

Development length is defined by the ACI as the transfer length plus "the additional length over which the strand must be bonded so that a stress f_{ps} may develop in the strand at nominal strength," (ACI Committee 318). This is quantified in Equation 2-2, where f_{ps} is the stress in the prestressed reinforcement at nominal strength (ksi), and f_{pe} (ksi) and d_b (in.) were previously defined. The second term in Eq. 2-2 is deemed the flexural bond length and is illustrated in Figure 2.2.

$$L_d = \frac{f_{pe} d_b}{3} + \left(f_{ps} - f_{pe}\right) d_b \qquad \text{(Eq. 2-2)}$$

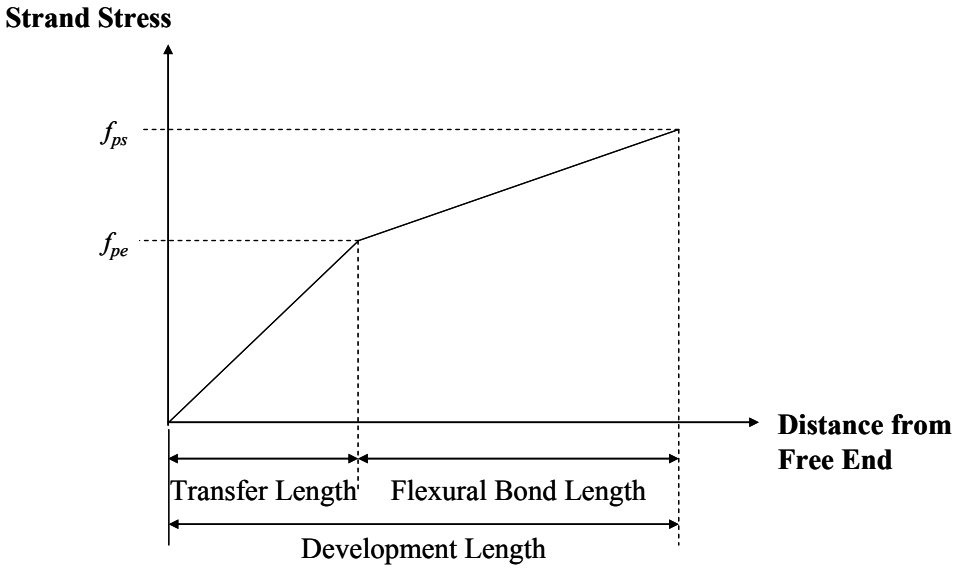

Figure 2.2: Strand stress variation along beam length

Equation 2-2 was first incorporated in the 1963 ACI Building Code and was adopted by AASHTO in 1973 (Buckner 1995). Later, Cousins et al. (1986) completed a study in which experimental transfer and development lengths of uncoated, un-weathered strands were found to exceed standard design predictions by a significant margin. As a result of this study and recognizing code requirements for bond were based on tests using outdated materials, the Federal Highway Administration (FHWA) issued a memorandum stating, among other items, that development length shall be taken as 1.6 times that which is determined by Equation 2-2. The 1.6 factor was formally presented at a joint meeting between the AASHTO Technical Committee for Prestressed Concrete and PCI Bridge Committee and, at present, remains in the AASHTO LRFD (2004) specifications.

2.2.2 Analytical Transfer Length Equations

Numerous studies were conducted in the past with the aim of analytically predicting transfer length of steel strands in NCC specimens. Analytical transfer length expressions from select studies conducted over the past forty years are presented in Table 2.2. The equations recommended by these studies were primarily derived using empirical data and suggest modifications to Equations 2-1 and 2-2. Among the goals of this thesis was to assess the viability of using these equations for prestressed SCC specimens, since no unique transfer length provisions currently exist for SCC.

As Table 2.2 shows, transfer length expressions varied in part based on whether the initial or effective prestress (i.e. f_{pi} or f_{pe}) was used. Five of the 15 references utilized f_{pe} in their analytical equations; the rest utilized f_{pi}. As noted in literature, using the initial prestress may be appropriate since transfer length is established when a specimen's prestressing force is released and does not significantly change thereafter (Marti-Vargas et al. 2007-b). Another parameter was the concrete compressive strength at transfer f'_{ci}. Three studies showed a correlation between f'_{ci} and L_t, three showed a correlation between $\sqrt{f'_{ci}}$ and L_t, and three utilized other relationships between concrete strength and L_t.

Table 2.2: Analytical Transfer Length Formulas (in ksi and inch units unless noted otherwise)

Reference	L_t Expression	Notes & Limitations
Based on Hanson and Kaar (1959)	$L_t = \frac{f_{pe} d_b}{3}$	
Olesniewicz (1975)	$L_t = \psi d_b \sqrt{\frac{f_{pe}}{f'_{ci}}}$	$\psi = 10$, average L_t
Zia and Mostafa (1977)	$L_t = \frac{1.5 f_{pi} d_b}{f'_{ci}} - 4.6$	f'_{ci} = 2-8 ksi
Nijhawam (1978)	$L_t = \frac{0.69 f_{pi} d_b}{f'_{ci}} + 10.3$	
Cousins et al. (1990)	$L_t = 0.5\left(\frac{U'_t \sqrt{f'_{ci}}}{B}\right) + \frac{f_{pe} A_p}{\pi d_b U'_t \sqrt{f'_{ci}}}$	Concrete strengths in psi; U'_t = 6.7 for uncoated strands; B = bond modulus (psi/in)
Bruggeling and Huyghe (1991)	$L_t = \frac{7 f_{pi} d_w}{12(0.13) f'_{ci}}$	$d_w = 0.33 d_b$ for 0.5-in., 7-wire strand
Balazs (1992)	$L_t = K d_b \sqrt[5]{\frac{f_{pi}^3}{f'^2_{ci}}}$	K = 4.64 ksi$^{(-1/5)}$, average L_t
Shahawy et al. (1992) Deatherage et al. (1994) Buckner (1995)	$L_t = \frac{f_{pi} d_b}{3}$	
Mitchell et al. (1993)	$L_t = 0.33 f_{pi} d_b \sqrt{\frac{3}{f'_{ci}}}$	f'_{ci} = 3.05-7.25 ksi
Russell and Burns (1996)	$L_t = \frac{f_{pe} d_b}{2}$	
Tadros and Baishya (1996)	$L_t = \frac{f_{pe} d_b}{0.8(3.04)}$	
Mahmoud et al. (1999)	$L_t = \frac{f_{pi} d_b}{\alpha_t f'^{0.67}_{ci}}$	α_t = 1.269 for steel strands
Marti-Vargas et al. (2007-b)	$L_t = \frac{\psi f_{pi} A_p}{0.282 \pi d_b f'^{0.67}_{ci}}$	$\psi = 1$, average L_t

2.3 EXPERIMENTAL TEST METHODS

2.3.1 Slump Flow Test – ASTM C1611/C1611M-09b

The slump flow test is designed to assess filling and passing ability of SCC with coarse aggregate size no greater than one inch. The test uses the standard cone defined in Section 5 of ASTM C143/C143M-10, oriented in either the normal or inverted position and held firmly in place at the center of a smooth, non-absorbent, rigid board. Cone dimensions are provided in Figure 2.3. The cone is filled with concrete in a continuous manner, and the SCC is not tamped or vibrated. The cone is raised over three seconds to a height of nine inches, during which time the fluid SCC expands outward from the board's center; this process is shown in Figure 2.4. Two diameter measurements are taken after the concrete stops flowing; the first is the largest diameter of the concrete patty, and the second corresponds to the diameter perpendicular to the first. The average of these two values is the slump flow, which should be reported to the nearest half-inch. SCC mixtures typically have slump flows between 22 in. and 30 in. If the two measured diameters are greater than two inches apart, the test must be repeated.

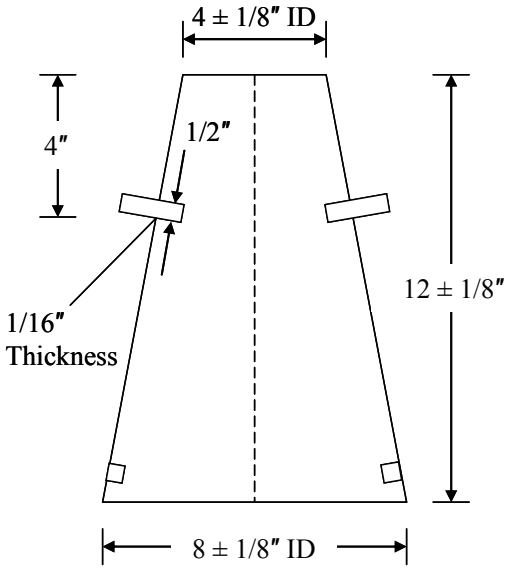

Figure 2.3: Standard cone dimensions for slump flow test (ASTM C143)

Figure 2.4: Slump flow test conducted on fresh SCC

The T_{50} test noted in the Appendix of ASTM C1611/C1611M-09b may be performed in conjunction with the slump flow test to evaluate the relative viscosity of SCC. The T_{50} value is the time it takes for the outer edge of SCC to reach a diameter of 20 inches. Values typically range between 2-5 seconds (W.R. Grace & Co. 2005).

2.3.2 Visual Stability Index (VSI) Test

The VSI ranking for SCC mixtures is a subjective visual characterization of concrete stability based on surface bleeding, mortar halos, and aggregate distribution. The test method is described in the Appendix of ASTM C1611/C1611M-09b. The VSI assessment should be made immediately after SCC stops flowing in a slump flow test. VSI values range from 0-3, with 0 corresponding to stable concrete and 3 indicating unacceptable concrete. Representative photos and descriptions from the ASTM standard are shown in Figure 2.5. A mixture with a VSI ranking of 2 should be retested and evaluated by quality control personnel to determine acceptability, while a mixture with a VSI ranking of 3 should be rejected.

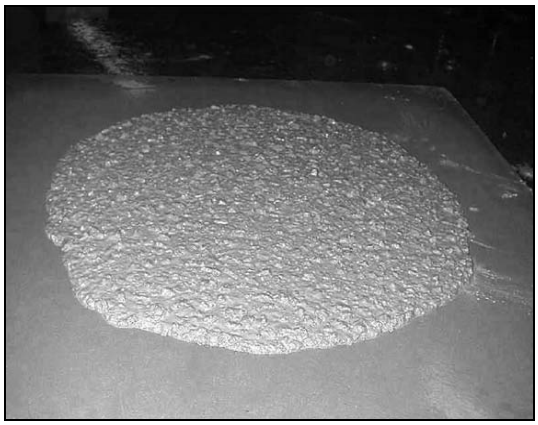

VSI = 0: High-quality SCC; homogenous with no evidence of bleeding.

VSI = 1: Acceptable SCC; slight bleeding observed as surface sheen.

VSI = 2: Borderline SCC; visible mortar halo and water sheen.

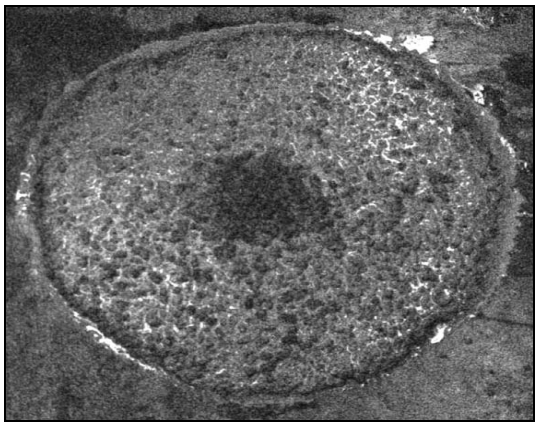

VSI = 3: Unacceptable SCC; prominent mortar halo, coarse aggregate concentrated at center.

Figure 2.5: Four SCC slump flows showing VSI ratings (ASTM C1611)

2.3.3 J-Ring Test – ASTM C1621/C1621M-09b

Designed to measure the passing ability of SCC, the J-Ring test follows the same procedure as the slump flow test, albeit with a J-Ring placed at the center of the board surrounding the slump cone. The 12-inch diameter ring rests atop sixteen 0.625-inch diameter rods that mimic reinforcement through which SCC would pass in a structural member. J-Ring dimensions are shown in Figure 2.6. Once filled, the cone is raised over three seconds to a height of nine inches, during which time the fluid SCC expands outward and through the J-ring as shown in Figure 2.7. The J-Ring flow is taken as the average diameter of the concrete patty in the same manner as the original slump flow. The J-Ring and original slump flows should be no greater than two inches apart.

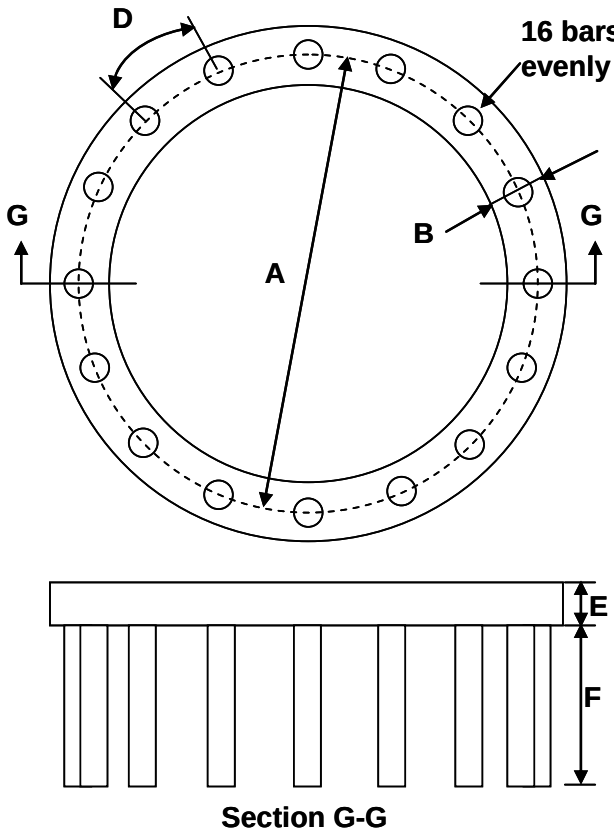

Dimension	(in)
A	12.0 ± 0.13
B	1.5 ± 0.06
C	0.625 ± 0.13
D	2.36 ± 0.06
E	1.0 ± 0.06
F	4.0 ± 0.06

Figure 2.6: Dimensions of standard J-Ring (ASTM C1621)

Figure 2.7: J-Ring test conducted on fresh SCC

2.3.4 L-Box Test

In the same spirit as the J-Ring test, the L-box test assesses the filling and passing ability of SCC. A typical L-box is shown in Figure 2.8 and comprises a vertical column separated from a horizontal box by a movable gate and reinforcement bars. The rebar configuration near the gate should represent the reinforcement expected in the specimens for which the SCC is being mixed. The horizontal portion of the L-box is approximately 32 inches long and 8 inches wide, while the vertical column is 4 inches wide.

Figure 2.8: L-box test conducted on fresh SCC

With the gate closed, the vertical L-box column is filled with concrete in a continuous manner; the concrete is not tamped or vibrated. After removing the gate, the concrete height at the end of the horizontal box is compared to the concrete height at the beginning of the horizontal box. The ratio between end and beginning heights should be greater than 75%. Visual inspection is also used to assess aggregate distribution and SCC passing ability.

2.3.5 Modified Moustafa Pullout Test

The PCI recommends the Moustafa pullout test to qualify bond characteristics of strands embedded in concrete as satisfactory (PCI 2003-a). Moustafa first performed pullout tests on lifting loop strands in 1974, considering 3/8-inch, 7/16-inch, and 1/2-inch diameter strands with

embedment lengths between 12-30 inches (Moustafa 1974). Each strand was loaded by hydraulic jacks, and the relative displacement between concrete and strand was monitored throughout loading until failure occurred. Since no bond quality standard exists for prestressing strands, Moustafa's method was adopted with slight modifications in subsequent research by Rose and Russell (1996) and Logan (1997) to study bond performance of strands intended for pretensioned applications. For consistency, the latter studies used 0.5-in. diameter strands embedded 18 inches in large block specimens. The pullout test is attractive given its simplicity and relatively low cost.

The PCI (2003-a) directly refers to Logan (1997) for a detailed outline of the modified Moustafa method. In his study, Logan tested 1/2-inch diameter strands embedded in blocks cast with the conventional concrete mixture shown in Table 2.3. The strands were obtained from six different manufacturers. Logan found the pullout test to accurately predict transfer and development characteristics in pretensioned specimens. Based on experimental results, acceptable 1/2-inch diameter strands should be capable of resisting at least 16 kips prior to slip initiation and 36 kips prior to failure. A summary of recommendations and guidelines for conducting the modified pullout test is presented below:

a) The test is recommended for concrete with compressive strength between 3500-5900 psi. The concrete pullout block is typically 24 inches wide, 24 inches deep, and 36 inches long with strands embedded 18 inches. However, block dimensions are flexible and depend on the number of tested strands.

b) A hydraulic jack with a minimum travel length of 12 inches should be used to pull the strands. The maximum load shall not exceed 50 kips.

c) The jacking load is applied gradually (20 kip/min) until strand cannot carry additional load.

d) Four types of data should be recorded during the test: (1) maximum load capacity, (2) approximate load at first slip, (3) approximate pullout distance at maximum load, and (4) a general depiction of failure. Typically, poorly bonded strand would slip 8-10 inches before reaching its ultimate load, but well-bonded strand would slip only 1-2 inches.

e) The test should be repeated as many times as needed and the data obtained should be used to compute an average failure load and standard deviation for each strand group.

Table 2.3: Normally-Consolidated Concrete Mixture from Logan (1997)

Material	Quantity (per yd^3)
Type III Cement	660 lbs
Crushed Gravel	1900 lbs
Sand	1100 lbs
Water Reducer	26 oz.
Water	35 gal
W/C Ratio	0.44

2.3.6 Transfer Length via 95% Average Maximum Strain Method (95% AMS)

Two methods are commonly used to experimentally measure transfer length: (1) the "draw-in" or "end-slip" method, and (2) the 95% Average Maximum Strain method (Russell & Burns 1993). The former method, which was not utilized in this study, calculates transfer length based on the relative displacement between strand and concrete after prestress release at the free ends of prestressed specimens; discussion of this method may be found in Balazs (1993) and Marti-Vargas et al. (2007-a). The latter method, which was utilized in this study, measures transfer length based on strain measurements throughout the transfer zone of a prestressed specimen. The procedure for the 95% AMS is detailed as follows:

a) Prior to prestress release, target points are affixed within a transfer zone of a specimen. The points are attached to the concrete surface at a depth equal to the strands' center of gravity. Initial measurements record the distance between each target point.

b) Immediately after prestress release and at any age thereafter, measurements are taken between all target points to determine the strain profile within the transfer zone.

c) Data may be smoothed by taking the strain at point "*a"* as the average of the strains at three adjacent points centered at "*a*" [e.g. $\varepsilon_{a,\,smooth} = 1/3 \cdot \sum (\varepsilon_{a-1}, \varepsilon_a, \varepsilon_{a+1})$]. An example of raw and smoothed strain data is shown in Figure 2.9.

d) The strain plateau region, or the distance over which strain is at a nearly constant maximum, is estimated visually. The average strain within the plateau is calculated. A line corresponding to 95% of this average strain is superimposed on the strain profile.

e) The intersection of the 95% AMS and the strain profile defines the transfer length (see Figure 2.9).

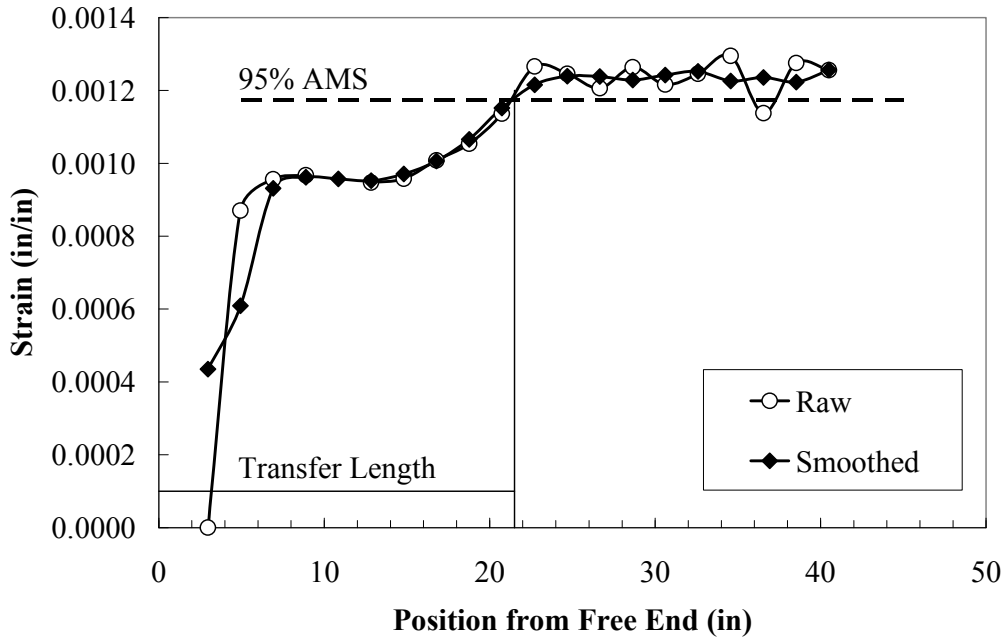

Figure 2.9: Example strain profile for determining transfer length using 95% AMS

2.3.7 Development Length via Flexural Tests

An iterative sequence of flexural tests may be used to determine development length in prestressed concrete members. Specimens are subjected to either three- or four-point bending, with the position of applied load (embedment length) varying between test iterations. If the specimen fails due to bond-slip or fails in shear, embedment length for the next trial is increased; if the specimen fails in flexure, embedment length for the next trial is decreased. The procedure is repeated until determining the minimum embedment length at which flexural failure occurs; this embedment length is taken as the development length.

2.4 TRANSFER AND DEVELOPMENT LENGTH TESTS ON SCC SPECIMENS

Recent studies investigating bond behavior in prestressed SCC members have focused on comparing experimental data from SCC specimens to data from conventionally-consolidated concrete specimens and current code provisions. The rest of this chapter summarizes the pertinent findings of these studies. A more extensive literature review of these studies was previously conducted by Andrawes et al. (2009).

2.4.1 Kansas State University

Sponsored by the Kansas Department of Transportation, this project aimed to characterize properties of pretensioned SCC bridge girders via pullout tests, transfer length tests, and development length tests (Larson et al. 2007). Pullout tests were conducted on 0.5-in. diameter strands embedded in blocks cast with a conventional concrete mixture utilized by Logan (1997). Meeting Logan's suggested criteria, the strands were deemed adequate for use in flexural test specimens.

The study considered small-scale rectangular beams with one bottom strand (SSB) or one top strand (TSB), as well as 21-in. deep T-beams, all of which were cast with SCC. Specimen geometry is presented in Figure 2.10. Span lengths for the rectangular and T-beams were 13.2 ft. and 15.5 ft., respectively. Transfer lengths were obtained using the end-slip method immediately after strand release, 18 days after release, and on the flexural testing day for each specimen. Average transfer lengths in the three specimen types were below the AASHTO requirement at all ages. However, average transfer lengths in TSB and T-beam specimens exceeded the ACI requirement for measurements taken after 18 days past prestress release.

Four-point bending tests were conducted to determine the flexural behavior of the beams. Strand embedment lengths equal to the code-predicted development length produced flexural failures. Subsequent flexural failures using shorter embedment lengths demonstrated that development lengths in the small-scale SCC specimens were 80% of the ACI/AASHTO predictions. No top-strand effect was observed in development length tests.

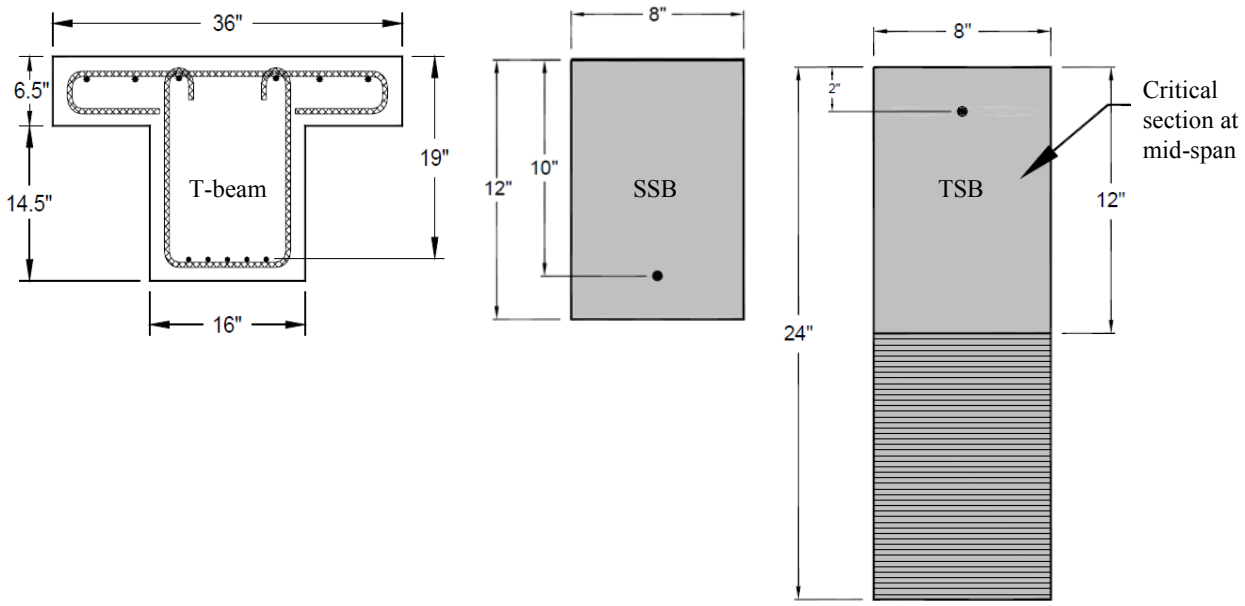

Figure 2.10: Specimen geometry for the study by Larson et al. (2007)

2.4.2 Lehigh University

Sponsored by the Pennsylvania Department of Transportation, this project had three objectives: (1) Investigate the material characteristics of SCC and conventional high early strength concrete (HESC), (2) Evaluate the transfer length, maximum moment, and maximum shear force of full-scale bulb-tee girders cast with SCC and HESC, and (3) Investigate the characteristics of bond between concrete and prestressing strands (Naito et al. 2006). The target compressive concrete strengths at 24 hours and 28 days were 6800 psi and 8000 psi, respectively. At 24 hours, both concretes had attained over 90% of their 28-day target strength.

To qualify the study's strands as acceptable, pullout tests were conducted on 0.5-in. diameter strands embedded in concrete similar to the mixture utilized by Logan (1997). At the test date, the concrete compressive strength was 4,000 psi. Although the average maximum pullout load was 31.5 kips, below the recommended 36 kips, researchers decided the strands were acceptable for the study based on past engineering experience.

The study considered 30-ft. long bulb-tee girders with the cross-sectional geometry depicted in Figure 2.11. Two specimens were cast for each SCC and HESC. Researchers used the 95% AMS method to evaluate transfer lengths in the girders. Transfer lengths were 15.8 in. and 15.7 in., respectively, for HESC and SCC specimens; hence, experimental values met

requirements of both the ACI (2008) and AASHTO (2004) design codes. No significant difference was observed between transfer lengths in the SCC and HESC girders.

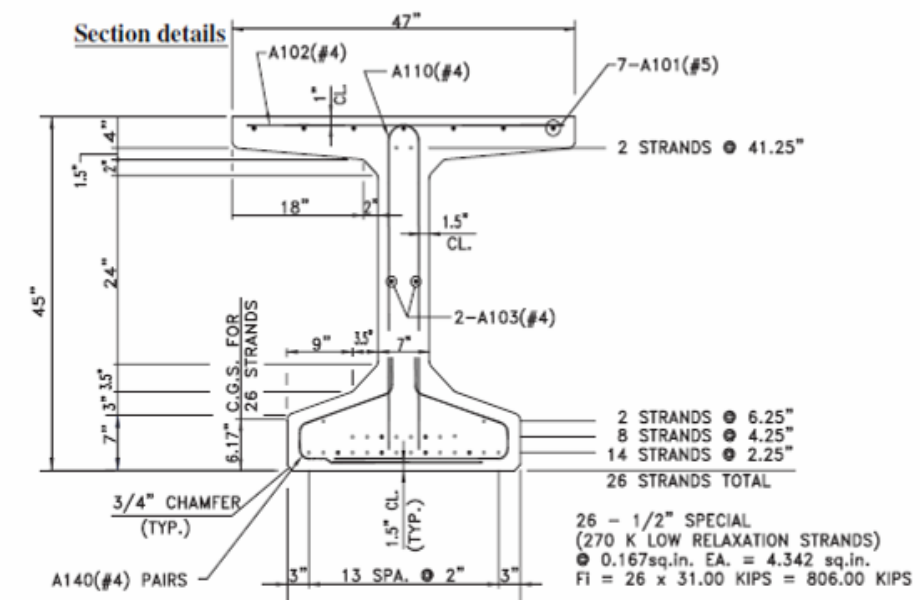

Figure 2.11: Bulb-tee specimen geometry for the study by Naito et al. (2006)

2.4.3 Michigan State University

This study investigated the effect of SCC mixture proportioning on bond behavior and the bond-related parameters of transfer and development lengths (Burgueno & Haq 2007). Researchers conducted strand pullout tests to evaluate bond strength, concrete surface strain calculations and end-slip measurements to characterize transfer length, and flexural tests to determine development lengths. Specimens were cast with three types of SCC and one conventional concrete, and the study considered variability in SCC composition by utilizing different amounts of VMA and HRWR admixtures. When strands utilized in the first phase of the project (Phase 1) were found to be unacceptable, a second phase (Phase 2) was added to the project scope; results from both phases are presented herein.

In both project phases, large-block pullout tests were conducted on 0.5-in. diameter strands with 18-in. embedment. The strands in Phase 1 were of poor quality, and those embedded in NCC were rusted. In Phase 2, strands were pre-qualified and clean in both SCC and NCC. Rust was estimated to increase bond strength by 30%. The effect of poor quality strand was highlighted by comparing the behavior of strands in SCC in both phases; poor quality strand was

found to have 103% lower bond strength than the pre-qualified strand. Removing the effects of rust and poor quality, researchers observed lower bond strength in SCC than in NCC.

All girders utilized for transfer and development length tests were 38-ft. long T-beams with the cross-section shown in Figure 2.12. The girders included two 0.5-in. diameter low-relaxation bottom strands, two #4 reinforcing bars within the top flange, and lateral stirrups placed every 12 inches throughout the entire span. Researchers used the 95% AMS and end-slip methods to evaluate transfer length. By comparing results from the two project phases, poor strand quality was estimated to increase transfer length by 17%. The effect of rust on transfer length was negligible. On average, SCC mixtures yielded transfer lengths which were 36% longer than in the NCC, though they were less than the value required by the ACI (2008).

Iterative flexural tests were conducted to determine the development length of strands in the girders. Because trials were limited, an ideal development length was linearly extrapolated for each concrete mix using test results and the beams' nominal moment capacities. Again, effects of rust and strand quality were removed prior to comparing results from both phases. Development lengths in SCC specimens were approximately 3% longer than those in NCC specimens; excluding one value, they all met ACI criteria. Additionally, the effect of SCC mixture proportioning was evident; the SCC with the highest fine aggregate content and lowest w/c ratio had the worst bond performance, while the SCC with the highest coarse aggregate content and highest w/c ratio had the best bond performance.

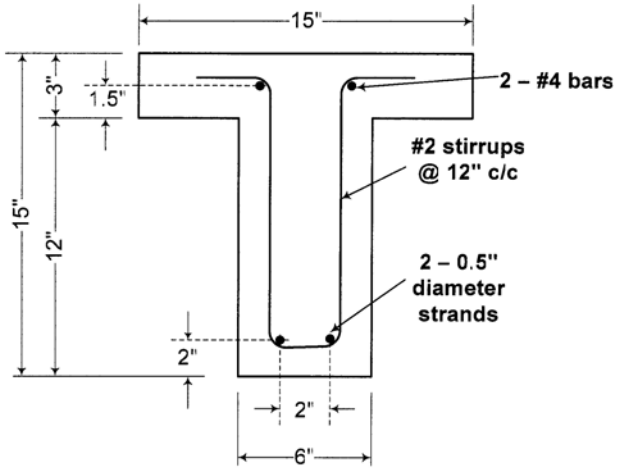

Figure 2.12: Girder cross-section for the study by Burgueno and Haq (2007)

2.4.4 North Carolina State University

Sponsored by the North Carolina Department of Transportation, this study measured transfer length and compared load-deformation characteristics in full-scale SCC and NCC specimens (Zia et al. 2005). Researchers utilized three 54.8-ft. long AASHTO Type III girders, two of which were cast with SCC and one of which was cast as a control specimen with NCC. The girders had 18 straight 0.5-in. low-relaxation strands and the cross-section shown in Figure 2.13. Researchers used the end-slip method as well as embedded steel bars instrumented with strain gauges to measure transfer lengths at ends of the three specimens. Using the end-slip method, transfer lengths in the SCC girders were found to be 32.3 in. and 50 in. In the control NCC girder, transfer length was estimated as 44.1 in. These values were approximately 40% greater than the AASHTO (2004) requirement of $60d_b$, or 30 in. Researchers were unable to determine transfer lengths using the embedded gauges since many were damaged during specimen production; however, the gauges which remained indicated that transfer lengths in both top and bottom strands were between 30 in. and 40 in. The researchers attributed the lower bond strength to the porous and soft fine aggregate utilized in all three concrete mixtures.

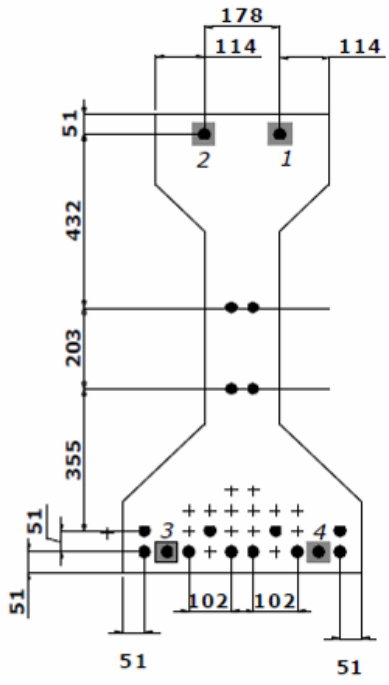

Figure 2.13: AASHTO Type III girder cross-section (in mm) for the study by Zia et al. (2005)

2.4.5 South Dakota State University

Research was conducted to investigate the performance of full-scale prestressed bridge girders cast with SCC containing limestone aggregates, which are commonly used in South Dakota concretes (Wehbe et al. 2009). The investigation entailed analyses of transfer length, prestress losses, flexural strength, and shear strength. The study considered three 40-ft. long MnDOT 36M girders, two of which were cast with SCC and one of which was cast as a control specimen with conventional concrete. Each specimen contained twelve straight 0.6-in. diameter, low-relaxation strands within the bottom flange, as shown in Figure 2.14. Both concrete mixtures had target strengths of 6,500 psi and 7,000 psi at release and 28 days, respectively.

Researchers planned to measure transfer lengths via concrete surface strain measurements and strain gauges attached to strands. However, surface strain measurements were highly erratic and were not used to estimate transfer lengths. From the strain gauges attached to the strands, transfer lengths were determined to be 30 in., 34.5 in., and 25.2 in., respectively, for the NCC, SCC1, and SCC2 specimens. Only the 34.5 in. value exceeded the $50d_b$ ACI requirement. The researchers concluded the structural performance of the prestressed SCC girders was comparable to that of the control specimen, and equations currently utilized to determine strength and stiffness of prestressed NCC girders are applicable to prestressed SCC girders.

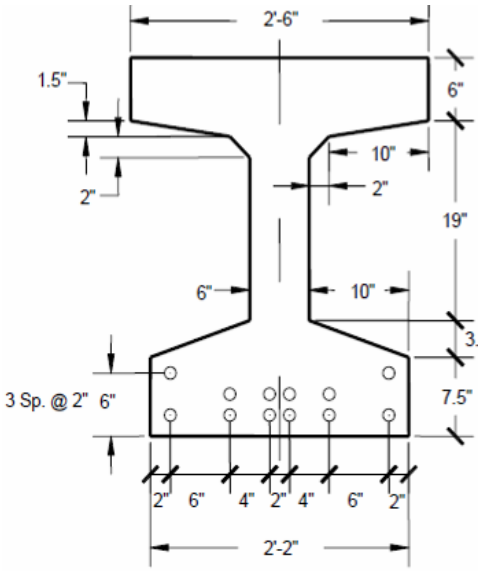

Figure 2.14: Section geometry for specimens studied by Wehbe et al. (2009)

2.4.6 University of Arkansas at Fayetteville

This project evaluated the transfer lengths of prestressing strands in SCC beams and compared them to ACI and AASHTO recommended values and transfer lengths in conventional concrete (Staton et al. 2009). The study utilized SCC with target strengths of 7000 psi at prestress release and 12000 psi at 28 days. Twelve 18-ft. long prestressed beams were cast; half used SCC and half used conventional concrete. The rectangular cross-section for the beams is shown in Figure 2.15; each beam had two 0.6-in. diameter bottom strands and two #6 bars in the compression zone.

Researchers used the 95% AMS method to measure transfer length. Additionally, vibrating wires were placed between the strands at each end of the beam to confirm the results from the strain gauges. A 2-10% difference was observed between the 95% AMS readings and the vibrating wire results. The measured transfer lengths in all six beams cast with SCC satisfied the ACI code requirement by a margin of 33% and the AASHTO code requirement by a margin of 44%. Transfer lengths did not vary significantly over time after three 3 days of prestress release; thus, the researchers suggested compressive strength had minor impact on transfer length.

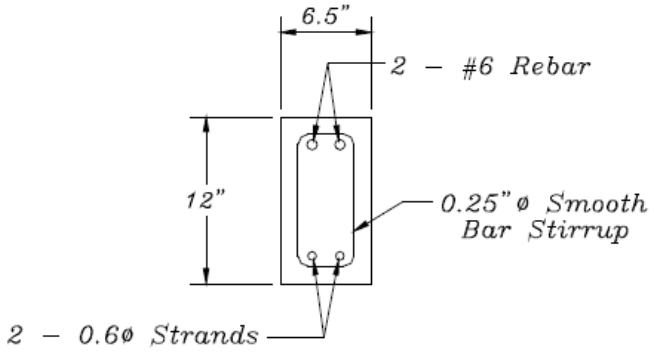

Figure 2.15: Specimen geometry for the study by Staton et al. (2009)

2.4.7 University of Florida

The Florida Department of Transportation sponsored a research project to compare the structural performance of AASHTO Type II bridge girders cast with SCC to those cast with conventional concrete (Labonte & Hamilton 2005). The project entailed analyses of production methods, plastic and hardened mixture properties, transfer length, and shear and flexural

behavior. The six full-scale test girders were 42 ft. long and had the cross-sectional geometry shown in Figure 2.16. Three of the girders were cast with SCC and three were cast with NCC; both concretes had a 28-day target compressive strength of 8500 psi.

Prestressing strands were released from tension by cutting in order to evaluate the impact cutting had on transfer length. Researchers estimated transfer lengths in two specimens using a slightly modified version of the 95% AMS method because they observed higher variation in strain readings than is typical. In the modified version, transfer length was determined using the intersection of the 95% AMS and a best-fit line through the origin and the first two data points of the strain profile. Experimental transfer lengths in the control specimen were determined to be 12.1 in. and 15.5 in. at the cutting and free ends, respectively; this yields a 28% difference. In the SCC specimen, transfer lengths were found to be 15.0 in. and 13.0 in. at the cutting and free ends, respectively; this yields a 15% difference. All experimental transfer lengths were well below ACI and AASHTO requirements, and the results revealed no significant difference between transfer lengths of strands in SCC girders and those of strands in conventional concrete girders.

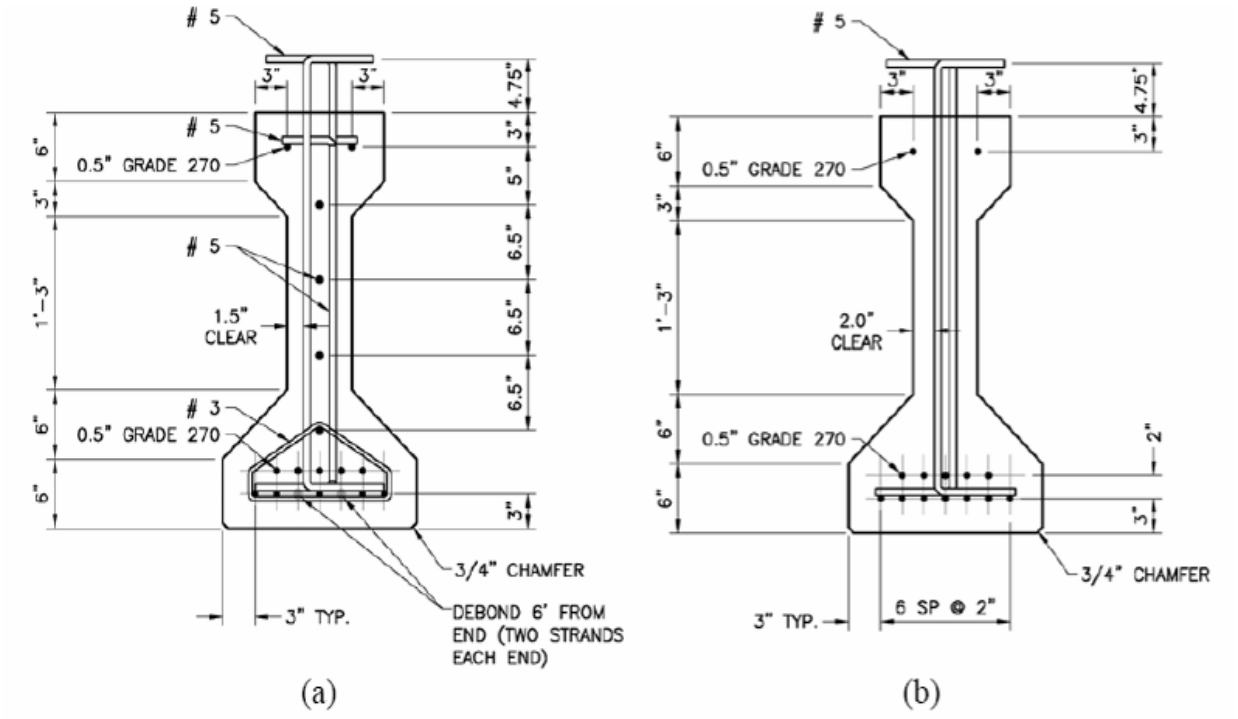

Figure 2.16: Specimen cross-section at (a) end and (b) midspan (Labonte & Hamilton 2005)

2.4.8 University of Nebraska-Lincoln

The Nebraska Department of Roads sponsored a research project to assess bond strength of SCC and transfer length of strands in pretensioned SCC bridge girders (Girgis & Tuan 2005). Researchers considered concrete mixtures and girder specimens used in three bridge projects; Mix #1 was an SCC used in the Oak Creek Bridge in Lancaster, NE, Mix #2 was an SCC used in the Clarks South Bridge in Merrick, NE, and Mix #3 was a conventional concrete used in the North Broadway Bridge in Sedgwick, KS.

The research team conducted Moustafa pullout tests on 0.6-in. diameter strands embedded 18-in. in large block specimens cast with the three concretes. At early ages, Mix #1, Mix #2, and Mix #3 had 43.4-kip, 54.2-kip, and 48-kip maximum pullout forces, respectively. At 28 days, Mix #2 and Mix #3 had maximum pullout loads of 65.7 kips and 63.1 kips, respectively. To compare results to the 36-kip minimum proposed by Logan (1997) for 0.5-in. diameter strands, researchers adopted a multiplier based on the ratio of strand diameters. This resulted in a benchmark pullout value of 43.2 kip, which all pullout loads exceeded.

The study utilized the 95% AMS method to evaluate transfer lengths in three specimens. The first specimen was a 72.5-ft. long NU1100 I-beam cast with Mix #1; the second specimen was a 90.2-ft. long NU900 I-beam cast with Mix #2; and the third specimens was a 124-ft. long NU1350 I-beam cast with Mix #3. Specimen dimensions and strand configurations may be seen in the cross-sections in Figure 2.17. Data was acquired from both sides of both ends of the girders at the bottom flanges. Average transfer lengths within Mix #1 and Mix #2 specimens were determined to be 36 in. and 43 in., respectively, which exceeded the 30-in. transfer length required by the ACI (2008). The average transfer length in Mix #2 also exceeded the 36 in. transfer length required by AASHTO LRFD Specifications (2004). The 20-in. average transfer length in the girder cast with conventional concrete met all code requirements. As such, transfer lengths of strands in the SCC girders were greater than those of strands in the conventional concrete girder by approximately 98%.

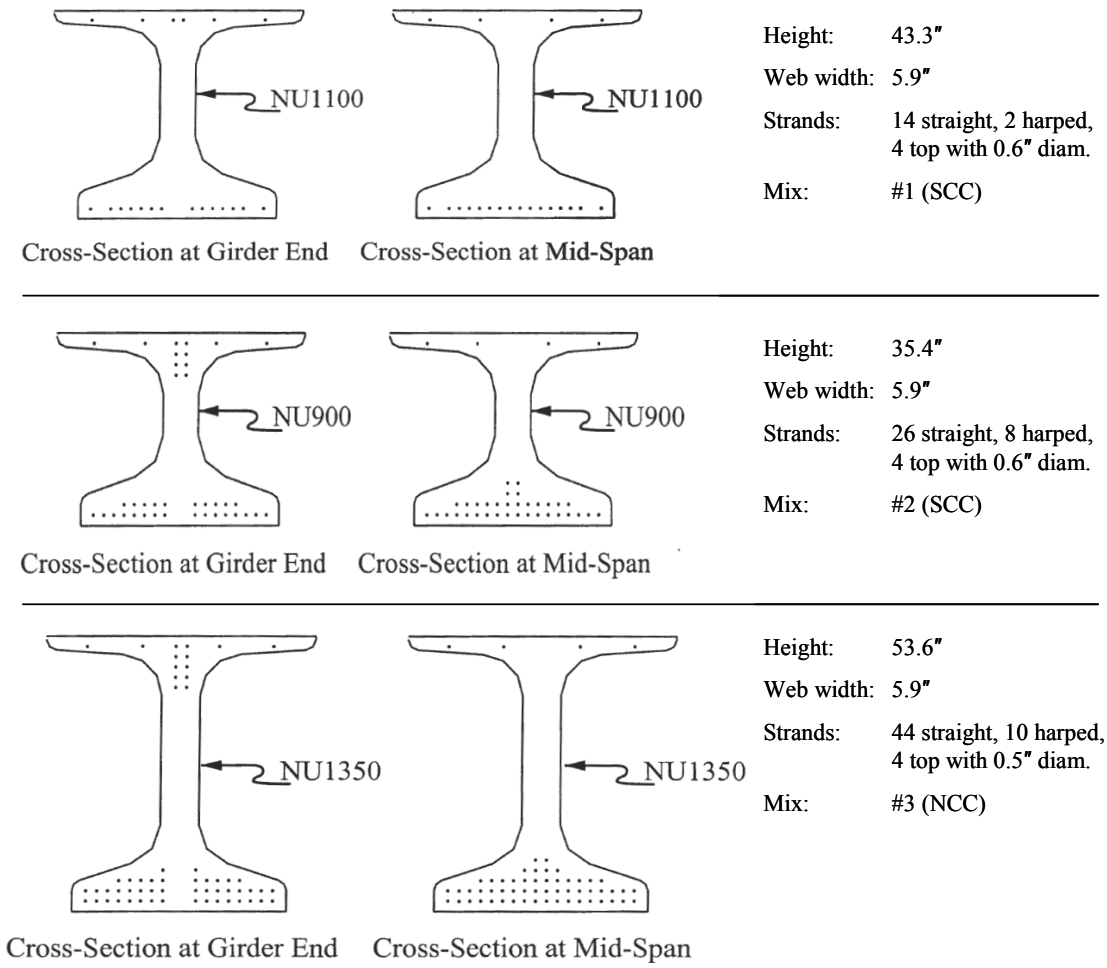

Figure 2.17: Transfer length specimens studied by Girgis and Tuan (2005)

2.4.9 Virginia Polytechnic Institute and State University

The Shockey Precast Group of Winchester, VA sponsored research to investigate bond strength, transfer length, and development length of strands in SCC girders (Trent 2007). The study considered three concrete mixtures, two of which were SCC (S1CCM, S1CCM2) and one of which was conventional concrete (S1CRM). All concretes had target compressive strengths of 3500 psi at 12 hours and 6500 psi at 28 days.

The 95% ASM method was utilized to determine transfer lengths in three prestressed specimens (one for each concrete mixture). The specimens had 6-in. square cross-sections with a single 9/16-inch diameter, 270-ksi low relaxation strand. Upon prestress release, the two edge specimens (S1CRM and S1CCM2) absorbed most of the energy before force transferred gradually to the middle specimen (S1CCM). Experimental transfer lengths were compared to

values recommended by ACI ($50d_b$ = 28.1 inches) and AASHTO ($60d_b$ = 33.7 inches). Results indicated two of three specimens (S1CRM and S1CCM) yielded acceptable transfer lengths. However, transfer lengths in the third specimen (S1CCM2) exceeded ACI requirements at 7 and 28 days after transfer. The transfer length values of the strands used in the SCC specimens were greater than those of strands in the conventional concrete specimen.

Twelve development length specimens were cast with the three concrete mixtures (four specimens per mixture). Specimens were 24-ft. long and had a T-beam cross-section as shown in Figure 2.18. An iterative scheme in which both ends of the specimens were subjected to flexural testing produced 10 bond failures and 14 flexural failures. An end-slip value of 0.01 inches was assumed as the threshold for defining a bond failure. Development lengths in the specimens cast with either SCC mixture were approximately 80%-83% of recommended ACI/AASHTO values. The study failed to determine a development length for the members cast with conventional concrete.

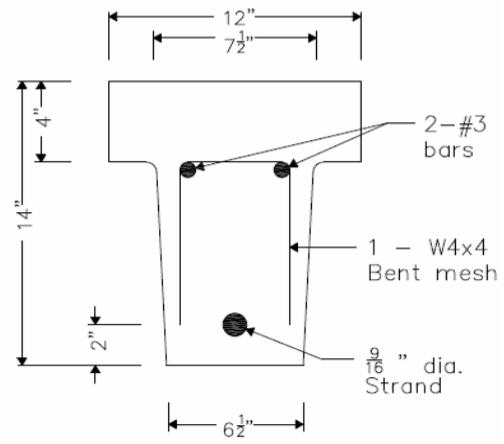

Figure 2.18: Cross-section development length specimens (Trent 2007)

2.4.10 SCC Mix Designs from Previous Large-Scale Studies

U.S. State Departments of Transportation are continually establishing guidelines for proper material proportioning to ensure adequate plastic and hardened behavior of new SCC mixtures. However, these requirements may significantly vary between institutions. As a result, the nine aforementioned studies tested specimens with fourteen different SCC mix compositions. The SCC mixture designs are summarized in Table 2.4; constituents are shown as required for one cubic yard of concrete. Nine of the mixtures in the table contained Type III cement, two

contained Type I/II cement, and three contained Type I cement. Type III cement is commonly used in prestressed members because its high early strength permits quick turnover times in fabrication plants. Four of the SCC mixtures also incorporated supplementary cementitious materials such as fly ash and ground granulated blast-furnace slag.

The chemical additives included in the mixes in Table 2.4 varied considerably. For instance, in the nine mixtures which utilized an air-entraining agent (AEA), the volume of AEA ranged from 1.8 oz. to 22.3 oz. per cubic yard. In seven mixtures the volume of VMA ranged from 10 oz. to 108 oz. per cubic yard. The amount of VMA is significant as it may adversely affect bond (Girgis & Tuan 2005). Finally, the amount of superplasticizer in the mixes varied from 14 oz. to 224 oz. per cubic yard. Where a dash is present in the table, either the SCC did not contain a particular material or the literature did not report a specific value for that material (i.e. the amount was indeterminate or varied between specimens and no range was presented).

Using results from earlier studies to predict bond adequacy of a proposed SCC mixture may be unsound when the studies' mixtures do not comply with standards applicable to the proposed SCC. If compared to current provisions set forth by the IDOT Bureau of Materials and Physical Research (2007), presented in Table 2.5, ten mixtures reported in the Table 2.4 would exceed the maximum cement factor of 705 lbs per cubic yard, eight would exceed the 50% limit for fine-to-total aggregate proportions, and three would have w/c ratios outside an allowable 0.32-0.44 range. Acknowledging this and recognizing the general need for further research on large-scale prestressed SCC specimens, the Illinois DOT sponsored a study exploring the bond behavior of strands in prestressed bridge girders cast with SCC adhering to current IDOT provisions.

Table 2.4: SCC Mix Designs from Studies on Prestressed SCC Specimens

Constituent	Units	A	B	C				D
Cement	Type	III	III	III	III	III	III	III
	lbs	750	849	750	700	700	700	810
Fly Ash	lbs	-	-	-	-	-	-	-
Coarse Agg.	lbs	1360	1651	1479	1380	1380	1435	1330
Fine Agg.	lbs	1500	1283	1628	1426	1426	1275	1300
Fine/Total Agg.		0.52	0.44	0.52	0.51	0.51	0.47	0.49
Water	gal.	27	33	31	33	33	37	41
W/C Ratio		0.30	0.32	0.34	0.39	0.39	0.44	0.42
AEA	oz.	5.0	2.0	13.1	5.3	12.3	22.3	2.4
HRWR	oz.	70	136	97	102	84	108	81
VMA	oz.	-	16	-	49	13	108	-
Set Retardant	oz.	-	-	525	-	410	327	32

Constituent	Units	E	F	G	H		I	
Cement	Type	I/II	I	I/II	III	III	I	I
	lbs	800	950	752	800	632	750	745
Fly Ash	lbs	-	-	168	150	100	-	-
Coarse Agg.	lbs	1454	1350	1307	1282	1311	1625	1650
Fine Agg.	lbs	1343	1474	1414	1417	1449	1340	1308
Fine/Total Agg.		0.48	0.52	0.52	0.53	0.53	0.45	0.44
Water	gal.	29	34	31	35	35	34	34
W/C Ratio		0.33	0.30	0.34	0.36	0.46	0.38	0.38
AEA	oz.	15.0	-	1.8	-	-	-	-
HRWR	oz.	224	105	64	14	14	-	-
VMA	oz.	-	19	-	10	10	-	-
Set Retardant	oz.	24	-	14	5	5	-	-

Legend	
A	Larson et al. (2007)
B	Naito et al. (2006)
C	Burgueno and Haq (2007)
D	Zia et al. (2005)
E	Wehbe et al. (2009)
F	Staton et al. (2009)
G	Labonte and Hamilton (2005)
H	Girgis and Tuan (2005)
I	Trent (2007)

Table 2.5: IDOT SCC Mixture Requirements

Requirement	Units	
Maximum Cement Factor	lbs/cy	705
Maximum Fine/Total Agg. Ratio	-	0.50
Allowable Range for W/C Ratio	-	0.32-0.44

CHAPTER 3: PULLOUT TESTS

Modified Moustafa pullout tests (see Section 2.3.5) were conducted to evaluate the bond characteristics of the seven-wire strands intended for use in this study's large-scale specimens. The tests method was utilized to verify comparable bond behavior between strands and SCC than between strands and a conventional concrete of similar design. The pullout test was attractive given its simplicity and relatively low cost. A total of fifty-six pullout tests were performed on 0.5-in. diameter, seven-wire low-relaxation strands embedded in SCC and NCC blocks. The strands had 270 ksi tensile strength and a modulus of elasticity equal to 28,700 ksi. Concrete compressive strengths and the strands' force-slip responses were recorded at curing ages of 1, 3, 7, and 28 days; this data was utilized to derive bond stress-slip relationships for SCC and NCC.

3.1 PULLOUT BLOCK SPECIMENS

Four pullout block specimens and thirty-two 6 in. x 12 in. cylinder specimens were cast simultaneously on February 2, 2009. Half of the specimens used SCC and half used NCC; details of the mixture compositions are presented at the end of this section. Each pullout block contained fourteen 0.5-in. diameter strands with 18 in. embedment and was 24 in. x 24 in. x 66 in. All block dimensions including strand spacing, longitudinal reinforcement, and clear cover are shown in Figure 3.1. Embedded strands were not tied to any of the nominal reinforcement which was utilized to control cracking and shrinkage. Strands extended 36 in. above the block surface to accommodate the pullout loading apparatus. Concrete was cast outdoors in a single casting bed with temperatures above the IDOT minimum of 25 degrees Fahrenheit. Space heaters were placed around the specimens and the casting bed was covered to ensure adequate overnight curing conditions. Specimens were shipped the following day to the Newmark Structural Engineering Laboratory at UIUC for 24-hr. tests.

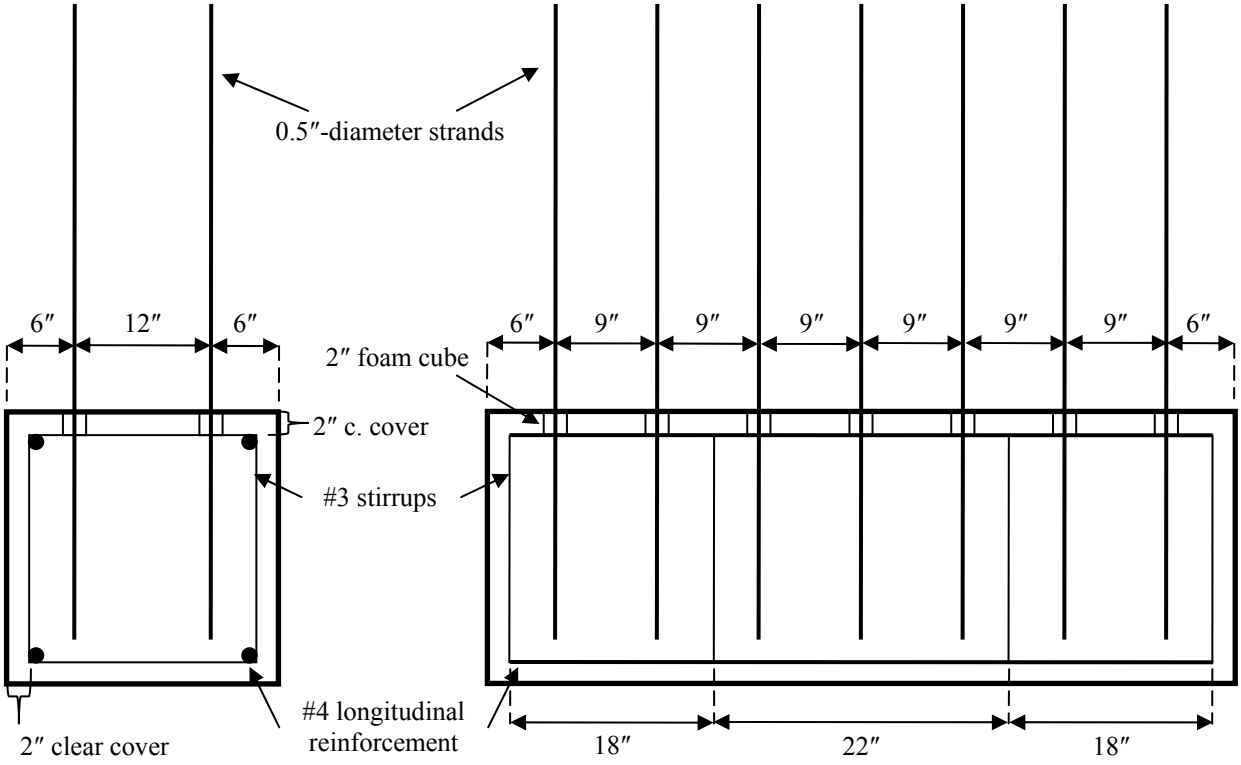

Figure 3.1: Pullout specimen design with dimensions in inches

Figure 3.2: Formwork for pullout specimens on casting day

Figure 3.3: Casting of pullout block specimen

Figure 3.4: Pullout block specimens after delivery to UIUC

The actual constituent proportions for the two concrete mixtures used in pullout block specimens are presented in Table 3.1. Pullout specimens were cast using one batch of SCC and one batch of NCC, both of which were 2 cubic yards in volume. Both mixtures contained Type III cement, coarse aggregate with maximum 0.5-in. nominal size, and natural sand fine aggregate. Use of a HRWR and an AEA ensured proper workability for each mixture. The amount of AEA was half the design volume because an issue with dosing equipment during specimen fabrication resulted in actual dosages which were half the values output on the batch tickets. The concretes contained no VMA, though the HRWR was promoted by the manufacturer as a single-component admixture having properties to improve segregation resistance. The SCC adhered to all current IDOT standards for precast/prestressed specimens (IDOT 2007).

Table 3.2 summarizes the results for plastic property tests conducted on pullout specimen concrete. A standard slump test (ASTM C143) was performed on the fresh batch of NCC, which had a 7-in. slump. Standard slump flow (ASTM C1611), J-Ring (ASTM C1621), L-box, and VSI tests were conducted for fresh pullout specimen SCC. Table 3.2 shows the SCC utilized in this study had moderate passing ability, moderate filling ability, and minimal segregation.

Table 3.1: Actual NCC and SCC Mixture Proportioning for Pullout Specimens

Mix Constituent	Units	Pullout NCC	Pullout SCC
Type III Cement	lbs/cy	670	662
Coarse Aggregate	lbs/cy	1849	1607
Fine Aggregate	lbs/cy	1180	1441
AEA	oz/cy	11	14
HRWR	oz/cy	45	81
Water	gal/cy	27	22
W/C	-	0.33	0.28
Coarse/Fine Aggregate	-	1.57	1.12
Fine/Total Aggregate	-	0.39	0.47

Table 3.2: Fresh Mixture Properties for Pullout Specimen Concrete

		Pullout SCC	Pullout NCC
Temperature	°F	63	62
Entrained Air	%	5.7	6.3
Slump Flow	in.	22.0	-
J-Ring Spread	in.	20.0	-
L-Box Ratio	%	75	-
VSI	-	0-1	-
Slump	in.	-	7

3.2 PULLOUT TEST SETUP

The servo-controlled assembly in Figure 3.5 was utilized to apply load to strands in the pullout tests. The 120-kip capacity hydraulic ram had a 13-in. stroke, a 6.25-in. outer diameter, and a 3-in. bore diameter. A linear variable differential transducer (LVDT) attached to the ram's cylinder monitored displacement of an aluminum plate secured to the top of the piston. Strands were loaded at a constant displacement-controlled rate of 0.4 in/min, resulting in loading rates below the maximum 20 kip/min as set forth by Logan (1997). Load was applied continuously until strands were completely pulled out or fractured. Five criteria were obtained for each pullout test: (1) First slip load, (2) Peak pullout load, (3) Displacement at first slip, (4) Displacement at peak load, and (5) Depiction of failure. The former four criteria were taken from the force-displacement response for each strand, while the latter criterion was made by visual observation.

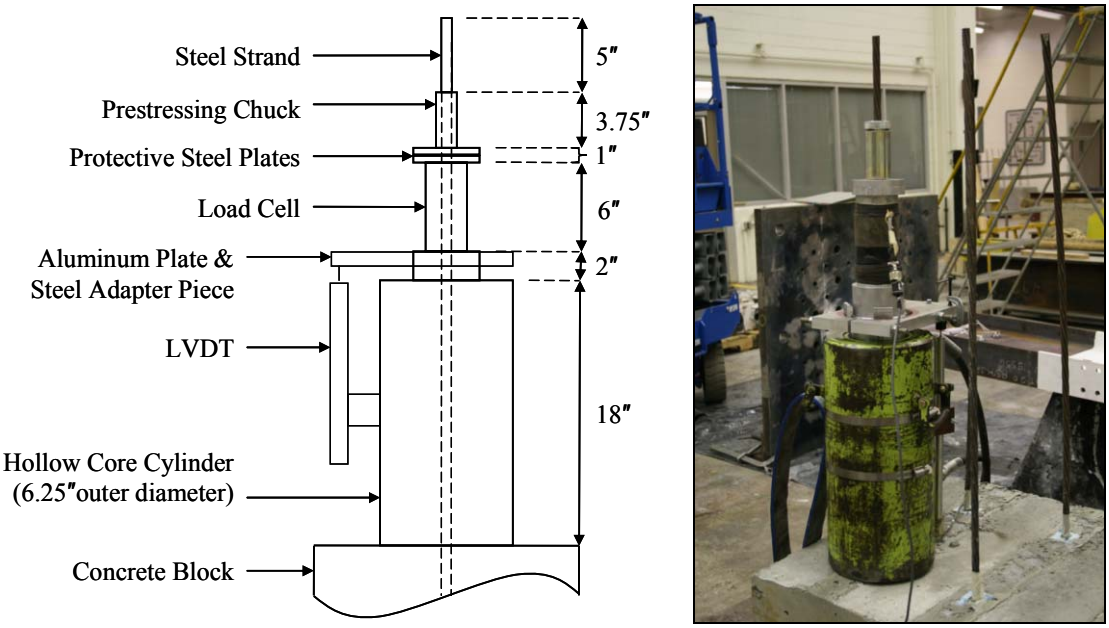

Figure 3.5: Servo-controlled assembly utilized to perform pullout tests

3.3 PULLOUT TEST RESULTS

Fourteen pullout tests were conducted on each testing date, or 1, 3, 7, and 28 days after concrete placement; half of the tests were on SCC specimens and half were on NCC specimens. Each strand was assigned a label corresponding to the day of testing and the type of concrete in which the strand was embedded; for example, the label "S3-A" corresponds to the first ("A") of seven strands embedded in SCC ("S") tested three days ("3") after concrete placement. The force-displacement responses for all tests are presented in Appendix A.

For discussion purposes, Figure 3.6 displays the responses of the seven strands embedded in SCC tested three days after concrete placement. Each response in the figure shows regions of linear and nonlinear behavior typical of all the results regardless of concrete age or type. Linear behavior was observed when a strand remained fully bonded to concrete and steel deformed elastically. Localized bond failure then brought about a reduction in pullout stiffness at the point when a strand first slipped relative to concrete ("first slip" point). Progressive bond failure caused a gradual reduction in pullout stiffness until the strand reached a maximum capacity ("peak pullout" point). After reaching this maximum load, one of two types of behavior were observed: (1) load resistance gradually declined, indicating a bond failure, or (2) load resistance abruptly dropped, indicating the fracture of one or more of the wires in the steel strand.

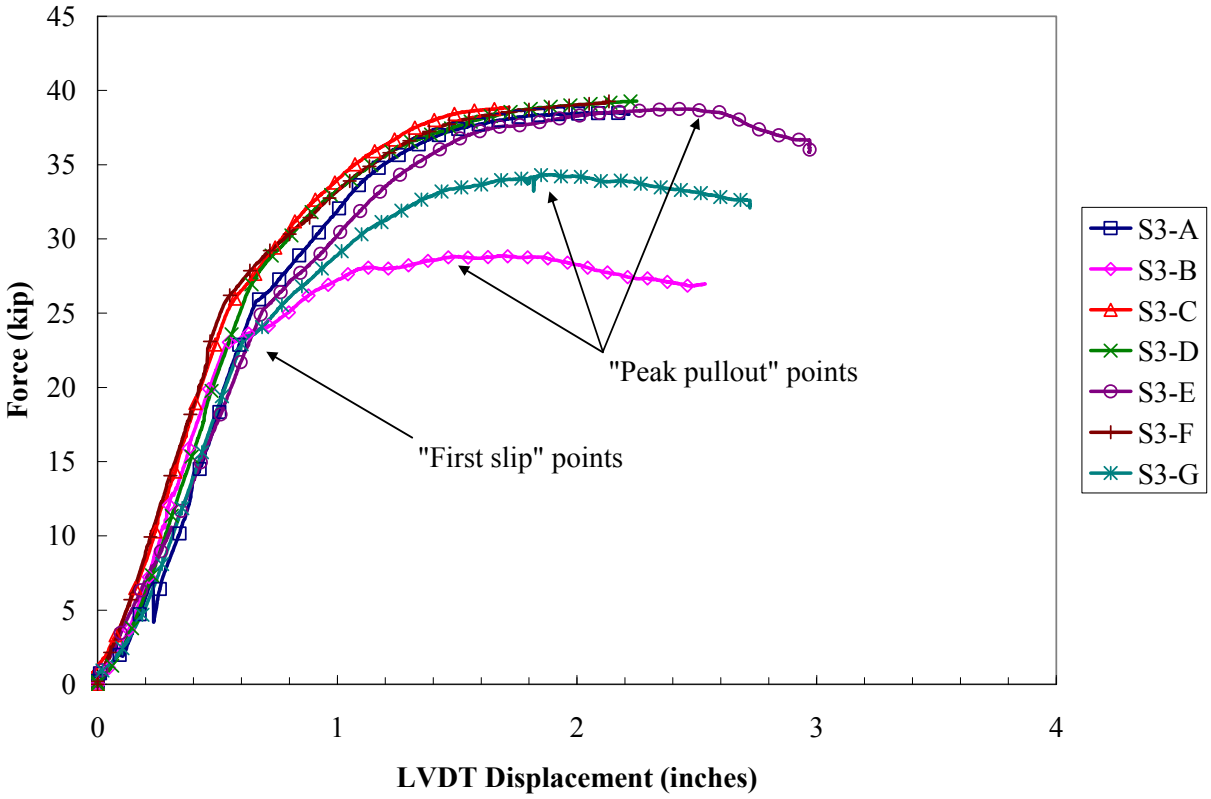

Figure 3.6: Force-displacement responses for strands in SCC 3 days after casting

Table A.1 in Appendix A contains the first slip loads and peak pullout loads for all tested strands. One strand (N3-E) yielded no data because the LVDT became dislodged during testing, requiring an abrupt stop of the loading mechanism; the LVDT and load cell were recalibrated prior to testing the next strand. Figure 3.7 shows the average absolute first slip and peak pullout loads at all ages with an assumed error of ±one standard deviation. Average absolute first slip loads increased over time, ranging in SCC from 23.8-25.3 kips and in NCC from 23.5-26.3 kips. Average absolute peak loads also increased over time, ranging in SCC from 36.1-38.3 kips and in NCC from 30.4-36.2 kips

When comparing bond performance in different concretes, it is prudent to consider normalization techniques. Numerous studies on bond behavior have shown a correlation between bond strength and $(f_c)^{1/2}$, where f_c is the concrete compressive strength (Chan et al. 2003; Esfahani et al. 2008). ACI provisions, moreover, state that development lengths of reinforcing bars are inversely proportional to $(f_c)^{1/2}$, which implies a linear relationship between bond strength and $(f_c)^{1/2}$ (ACI Committee 318). However, methods of normalization vary among

studies depending upon the concrete strength range, confinement within specimens, and country in which testing occurs. Previous research and most European design codes consider bond strength to vary proportionally with $(f_c)^{1/3}$ (Mitchell & Marzouk 2007). Other studies have found a more precise correlation between bond strength and $(f_c)^{1/4}$ (Darwin et al.1996). Based on similarities to the studies discussed in Section 2.4, the current study assumes a linear relationship between bond strength and $(f_c)^{1/2}$, and Figure 3.8 shows first slip and peak pullout loads normalized using $(f_c)^{1/2}$ to better assess the bond behavior of SCC and NCC using a common datum.

The average compressive cylinder strengths for both concretes at various testing ages are shown in Figure 3.9 with an assumed error of ±one standard deviation. Both concretes achieved adequate strength for initial tests and strengthened over time, exceeding 5 ksi after 28 days. It should be noted, however, that individual cylinder specimens for either concrete type showed wide variability in strength at the same age (i.e. SCC cylinder strengths at 28 days ranged from 3.5-9.1 ksi). Indeed, cylinder strengths reported for both concrete types prior to shipping pullout specimens to UIUC were greater than 4 ksi. Normalized first slip loads differed between SCC and NCC by an average of 10% for all tests. Only the 1-day tests showed first slip normalized loads in SCC higher than those in NCC (see Figure 3.8). Normalized pullout loads differed between SCC and NCC by as much as 25% at 1 day and as little as 1% at 3 days. Only the 7-day tests produced lower normalized pullout loads in SCC than in NCC. From the pullout capacities, it was concluded that the strands in this study displayed sufficient bond to SCC; therefore, they were utilized in subsequent full-scale girder testing.

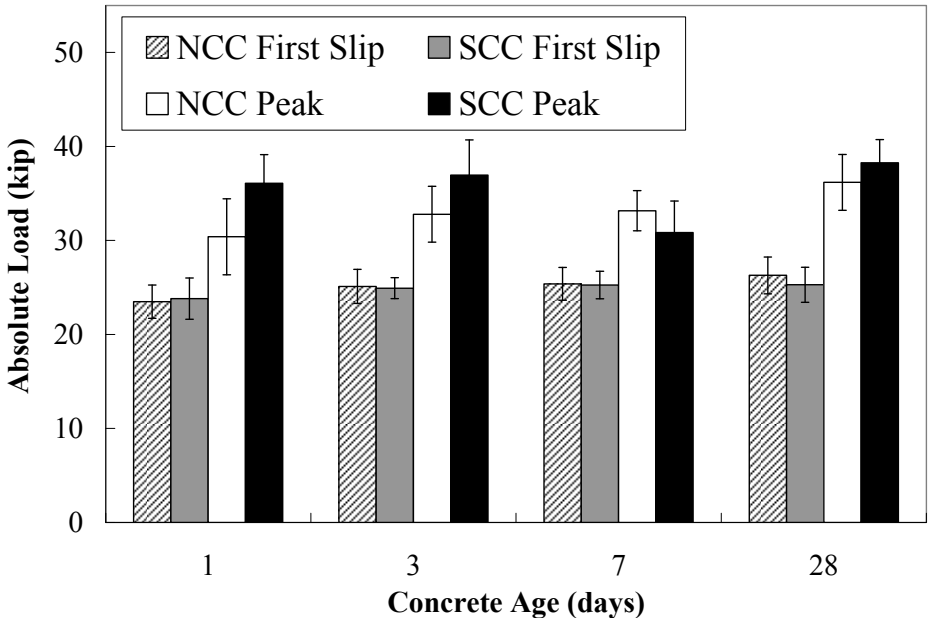

Figure 3.7: Average absolute first slip and peak pullout loads at various ages

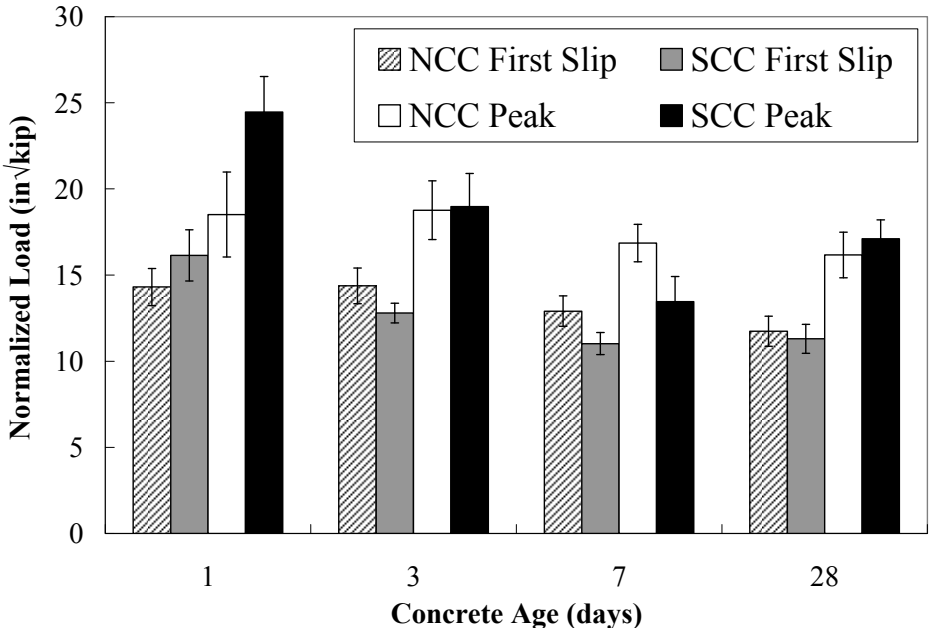

Figure 3.8: Average normalized first slip and peak pullout loads at various ages

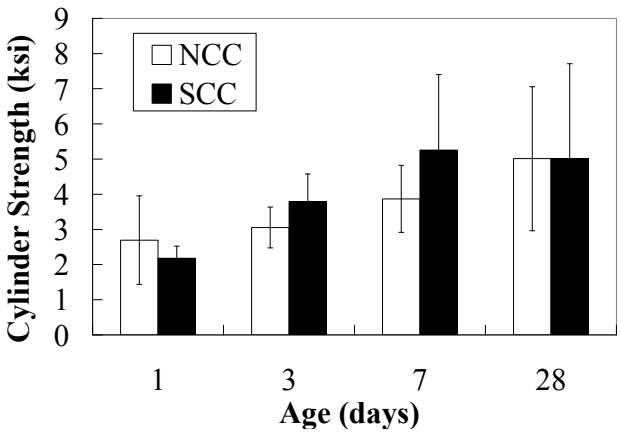

Figure 3.9: Average compressive cylinder strengths for pullout specimens at various ages

CHAPTER 4: FULL-SCALE GIRDER DESIGN AND ANALYSIS

This chapter contains all design, analysis, and fabrication information for the four SCC girders cast for transfer and development length tests at UIUC. Results of transfer length tests are discussed in Chapter 5, and results of development length tests are discussed in Chapter 6. This chapter details the design loading conditions, design capacities, and predicted development lengths within the girder specimens.

4.1 SPECIMEN DESCRIPTION

Two full-scale hollow box girders and two full-scale I-girders were cast for transfer and development length tests using the same SCC and strands as in the pullout blocks. The two girder types were selected because of their frequent use in Illinois bridge construction. The box girders were 28 ft. long and 27 in. deep, and each was prestressed with sixteen 0.5-in. diameter strands. All strands were straight, fully bonded to concrete, and stressed to 202 ksi prior to casting. The cross-sectional geometry and strand configuration for the box girders are provided in Figure 4.1. The hollow in the center of each girder was formed by a Styrofoam® block 23 ft. in length; hence, for 30 in. from either end, the beam's cross-section was not hollow. Fabrication drawings showing transverse reinforcement, longitudinal reinforcement, lifting loops, and other pertinent details may be found in Appendix B. As shown in the appendix, shear reinforcement within the box girders comprised overlapping #4 stirrups spaced every 9 in. throughout the center span and every 6 in. at the beam ends. Lifting loops were placed 15 in. from either end of the beams.

The two I-girders were 48 ft. long and 42 in. deep, and each was prestressed with twelve 0.5-in. diameter strands. Strands were straight, fully bonded to concrete, and stressed to 202 ksi prior to casting. The cross-sectional geometry and strand configuration for the I-girders are shown in Figure 4.2. Again, fabrication drawings showing all pertinent specimen details may be found in Appendix B. Transverse reinforcement within the I-girders comprised #4 stirrups throughout the web and bent #3 bars in both flanges; these were spaced every 12 in. throughout the center span and every 6 in. at the beam ends. Additional, overlapping #4 stirrups were placed at within the end zones to prevent shear failure. Lifting loops were placed 39 in. from either end.

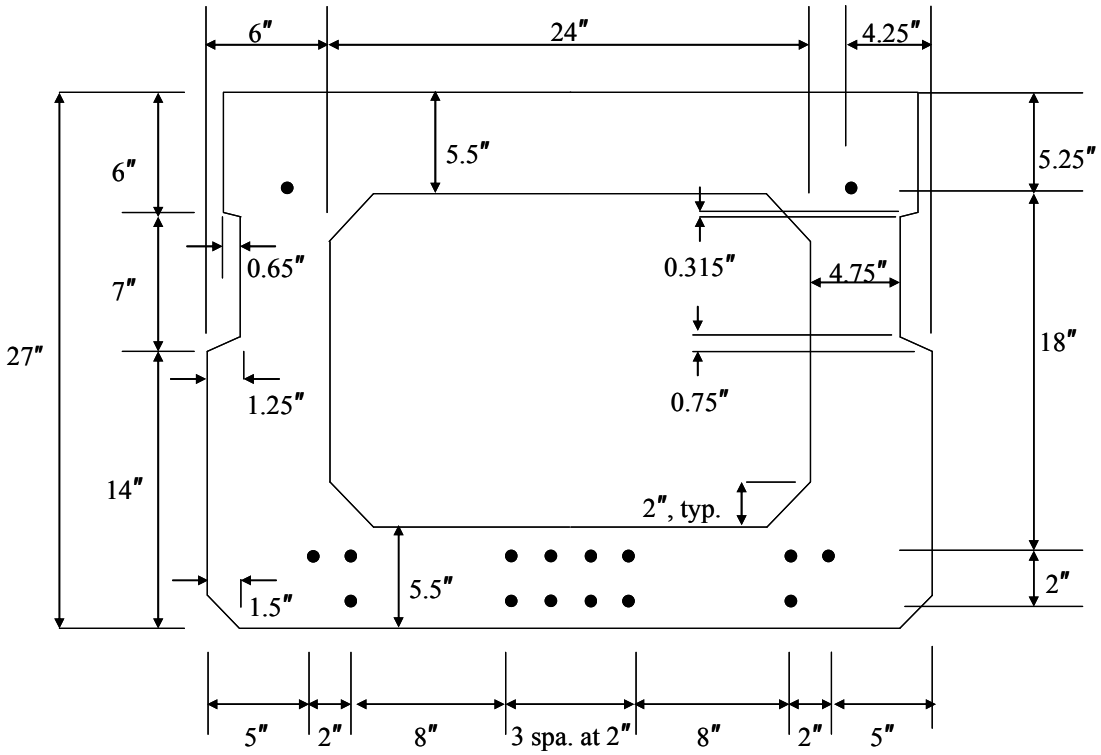

Figure 4.1: Cross-sectional geometry and strand configuration for box girder specimens

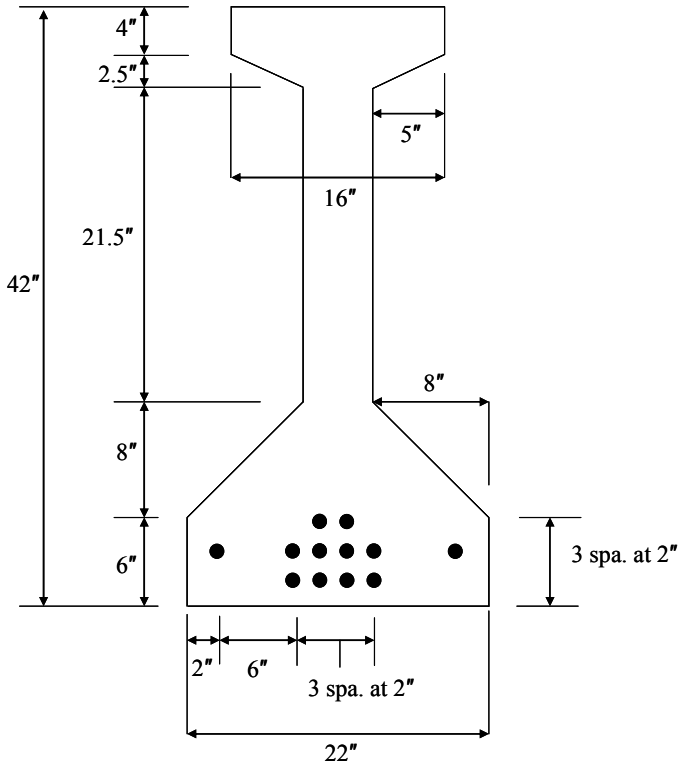

Figure 4.2: Cross-sectional geometry and strand configuration for I-girder specimens

4.2 SPECIMEN FABRICATION

All four full-scale specimens were cast sequentially on August 26, 2009 using eight batches of SCC. All batches were 3 cubic yards in volume except for the 0.5-cubic yard Batch 8. Table 4.1 presents the actual constituent proportions for all eight batches. Proportioning of the AEA required modification throughout casting but did not affect overall mixture acceptability. Table 4.2 summarizes the results for plastic property tests conducted on girder specimen concrete. Standard slump flow, J-Ring, L-box, and visual stability index tests were conducted for the first batch of SCC. Results showed the SCC had good passing ability, good filling ability, and minimal segregation. For subsequent batches, only the slump flow test was performed. Temperature and entrained air were checked for all batches of concrete.

Table 4.1: Actual Mixture Proportioning for Batches of Girder Specimen SCC

Constituent	Units	Batch 1	Batch 2	Batch 3	Batch 4	Batch 5	Batch 6	Batch 7	Batch 8
Type III Cement	lbs/cy	660	660	660	660	660	660	660	664
Coarse Agg.	lbs/cy	1578	1581	1577	1569	1571	1585	1571	1714
Fine Agg.	lbs/cy	1420	1420	1420	1420	1420	1422	1421	1476
AEA	oz/cy	17	20	25	28	32	32	32	32
HRWR	oz/cy	80	80	80	80	80	80	80	84
Water	gal/cy	31	30	31	30	30	31	31	30
W/C	-	0.39	0.38	0.39	0.39	0.39	0.39	0.39	0.38
Coarse/Fine Agg.	-	1.11	1.11	1.11	1.11	1.11	1.12	1.11	1.16
Fine/Total Agg.	-	0.47	0.47	0.47	0.48	0.47	0.47	0.47	0.46

Table 4.2: Fresh Mixture Properties for Batches of Girder Specimen SCC

		Batch 1	Batch 2	Batch 3	Batch 4	Batch 5	Batch 6	Batch 7	Batch 8
Temperature	°F	69	70	71	70	72	70	70	70
Entrained Air	%	4.0	4.0	5.2	5.2	5.4	6.2	6.0	3.8
Slump Flow	in.	25.75	23	24.5	23	22.88	24	23.25	25.5
J-Ring Spread	in.	25.38							
L-Box Ratio	%	0.92							
VSI	-	0-1							

The casting bed configurations for the four girders are provided in Figure 4.3. Per the figure, Box-1 and Box-2 hereafter refer to the box girder specimens, and I-1 and I-2 hereafter refer to the I-girder specimens. Specimen Box-1 was cast first with Batches 1-2 (see Tables 4.1 and 4.2); then, specimen Box-2 was cast with Batches 2-4, specimen I-1 was cast with Batches 4-6, and specimen I-2 was cast with Batches 6-8. The box girders were cast monolithically starting at their south ends; the I-girders were cast starting at their north ends (see Figure 4.3). A monolithic pour of a hollow girder is typically more problematic when using conventional concrete than when using SCC because formwork for the center void obstructs the flow of concrete. No mechanical vibration or tamping was utilized during casting. Casting and strand release locations were noted in order to analyze whether they affected transfer length at either girder end. All girders had a specified 5000 psi release strength and 6000 psi 28-day target strength at 28 days. Seventy 4 in. x 8 in. cylinders were cast during fabrication to determine concrete compressive strength at later ages. Figures 4.4 through 4.15 illustrate the fabrication process for the four girders.

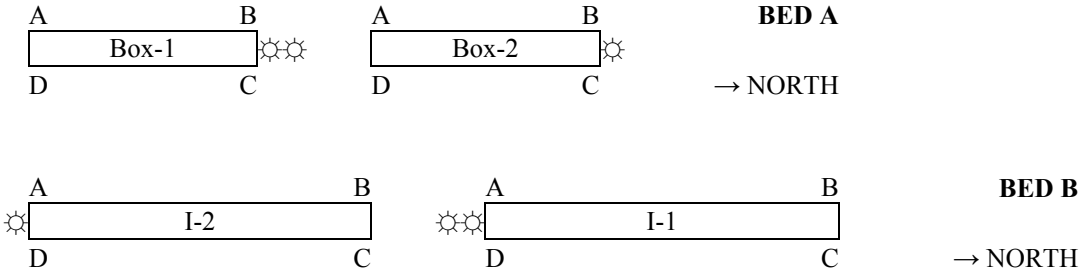

Box-1	Started casting at A-D	Strands first cut at ☼, then cut at ☼☼
Box-2	Started casting at A-D	
I-1	Started casting at B-C	Strands first cut at ☼, then cut at ☼☼
I-2	Started casting at B-C	

Figure 4.3: Diagram showing casting locations, cutting locations, and beam orientation

Figure 4.4: Box girder formwork prior to casting

Figure 4.5: End zone of box girder prior to casting

Figure 4.6: Box girder half-filled during casting

Figure 4.7: Completely filled box girder

Figure 4.8: Box girders covered for overnight curing

Figure 4.9: Box girders moved from bed after 3 days

Figure 4.10: I-girder formwork prior to casting

Figure 4.11: End zone of I-girder prior to casting

Figure 4.12: Partially filled I-girder during casting

Figure 4.13: Completely filled I-girder

Figure 4.14: I-girders covered for overnight curing

Figure 4.15: I-girders moved from bed after 3 days

Approximately one month after casting, when all transfer length measurements had been completed, specimens were shipped to UIUC. Prior to flexural tests, composite SCC slabs were cast atop the I-girders to simulate the effective portion of a bridge deck. The slab for girder I-1 was cast on April 23, 2010, and the slab for girder I-2 was cast on April 28, 2010. Provided by a local fabricator, the slab SCC differed slightly from the concrete utilized to cast the girders, though the 28-day target strength remained the same. The actual constituent proportions for the deck SCC are provided in Table 4.3. As shown, the concrete incorporated Type I/II cement, unlike the girders which utilized Type III cement for rapid strength gain. The AEA manufacturer differed between mixtures, and only 5 oz. per cubic yard was required for the deck concrete. The brand of HRWR also differed between mixtures, but the required quantity remained the same. Each deck was cast using a single, 7-cubic yard batch of concrete. No mechanical vibration or tamping was utilized during casting.

The slabs were 8 in. x 30 in., extended the entire length of the specimens, and utilized nominal reinforcement to meet temperature and shrinkage requirements. The transverse reinforcement in the slabs comprised evenly-spaced #4 bars. Slab dimensions were selected to ensure strands would yield prior to concrete crushing during flexural tests. Figures 4.16 through 4.21 show the deck fabrication process; decks were allowed to cure, covered with tarps, for one week prior to formwork removal.

Table 4.3: Actual SCC Mixture Proportioning for I-Girder Decks

Mix Constituent	Units	SCC
Type I/II Cement	lbs/cy	658
Coarse Aggregate	lbs/cy	1557
Fine Aggregate	lbs/cy	1489
AEA	oz/cy	5
HRWR	oz/cy	91
Water	gal/cy	30.1
W/C	-	0.38
Coarse/Fine Aggregate	-	1.05
Fine/Total Aggregate	-	0.49

Figure 4.16: Formwork for I-girder deck

Figure 4.17: Reinforcement for I-girder deck

Figure 4.18: Casting of I-girder deck

Figure 4.19: Leveling the surface of I-girder deck

Figure 4.20: Completely filled I-girder deck formwork

Figure 4.21: I-girder deck after formwork removal

4.3 SECTION PROPERTIES

This section briefly summarizes the geometrical properties used in the analysis of each specimen type. Table 4.4 contains the properties of both the hollow and filled cross-sections within the box girder. As shown in the fabrication drawings in Appendix B, the box girder cross-section is hollow for only 25 ft. within the specimen; for 30 in. from either end, the section is completely filled. Table 4.5 contains I-girder properties with and without the composite deck. For simplicity, the concrete in the girder and slab comprising the composite section were assumed to have the same strength; hence, no transformed moment of inertia or section properties are presented. Volume-to-surface (V/S) ratios utilized in calculating prestress losses are also listed in the tables.

Table 4.4: Box Girder Section Properties

Hollow Section Properties		
A_c	568.8	in
h_t	27.0	in
d_p	21.5	in
e_o	8.04	in
y_t	13.29	in
y_b	13.71	in
I_g	49684	in^4
Z_b	3739	in^3
Z_t	3624	in^3

Filled Section Properties		
A_c	896.8	in
h_t	27.0	in
d_p	21.5	in
e_o	8.12	in
y_t	13.63	in
y_b	13.37	in
I_g	57452	in^4
Z_b	4297	in^3
Z_t	4215	in^3

Strand Properties		
# Strands	16	
CG Strands:	5.25	in
A_{ps}	2.448	in^2

Girder Properties		
Surface Area	65074	in^2
Volume	210780	in^3
V/S Ratio	3.24	in

Table 4.5: I-Girder Section Properties

Original Section Properties		
A_c	464.5	in
h_t	42	in
d_p	38.3	in
e_o	14.0	in
y_t	24.35	in
y_b	17.65	in
I_g	90822	in^4
Z_b	5145.1	in^3
Z_t	3730.2	in^3

Section Properties with Deck		
A_c	704.5	in
h_t	50	in
d_p	46.3	in
e_o	23.6	in
y_t	22.7	in
y_b	27.3	in
I_g	219262	in^4
Z_b	8028.8	in^3
Z_t	9663.2	in^3

Strand Properties		
# Strands	12	
CG Strands:	3.67	in
A_{ps}	1.836	in^2

Girder Properties (without deck)		
Surface Area	79265	in^2
Volume	267552	in^3
V/S Ratio	3.37	in

4.4 PRESTRESS LOSSES

Throughout the life of a prestressed concrete member, the stress in its prestressing strands decreases in an asymptotic manner. This reduction in tensile stress is termed "prestress losses." Proper estimation of prestress losses will accurately predict the effective prestress f_{pe} utilized in design. The effective prestress directly relates to transfer and development length; as such, this study utilized several methods to predict f_{pe} values within the four girder specimens. Values were calculated for the girder specimens 28 days after casting and at the time of flexural testing. This section outlines the AASHTO, ACI, and PCI methods for calculating prestress losses and summarizes the f_{pe} values predicted for the four girder specimens. Example calculations for the girders may be found in Appendix C.

The combined effects of concrete and steel behavior over time, as well as mechanical action during specimen fabrication, equate to the total losses within a specimen. Losses may occur during three stages of a pretensioned specimen's life: (1) prior to transfer, (2) at transfer, and (3) after transfer. Prior to transfer, friction losses occur due to steel relaxation. At transfer, instantaneous losses occur due to elastic shortening of concrete. Finally, additional steel relaxation, concrete creep, and concrete shrinkage continue to reduce tensile strand stress after transfer and throughout the lifespan of the specimen.

4.4.1 AASHTO Methods

The AASHTO LRFD Design Specifications (2004) provide two methods for calculating prestress losses: (1) the approximate lump sum method, and (2) the separate lump sum method. The outline of each method herein utilizes terminology as presented in the specifications. Total losses for either method may be represented by Equation 4-1, which combines the effects of elastic shortening (Δf_{pES}), concrete shrinkage (Δf_{pSR}), concrete creep (Δf_{pCR}), and steel relaxation (Δf_{pR}). For pretensioned members, instantaneous losses due to elastic shortening are taken per Equation 4-2, where the concrete stress f_{cgp} at the center of gravity of prestressing steel at the time of transfer is calculated using Equation 4-3.

$$\Delta f_{pT} = \Delta f_{pES} + \Delta f_{pSR} + \Delta f_{pCR} + \Delta f_{pR} \qquad \text{(Eq. 4-1)}$$

$$\Delta f_{pES} = \frac{E_{ps}}{E_{ci}} f_{cgp} \quad \text{(Eq. 4-2)}$$

where: E_{ps} = elastic modulus of prestressing steel
E_{ci} = elastic modulus of concrete at time of transfer
f_{cgp} = concrete stress at strand CG from self-weight, prestress force at transfer

$$f_{cgp} = \left(\frac{f_{pi} A_{ps}}{A_c} + \frac{f_{pi} A_{ps} e^2}{I} \right) - \frac{M_{sw} e}{I} \quad \text{(Eq. 4-3)}$$

The approximate lump sum method estimates the combined effect of all time-dependent losses based on specimen and strand type. For box girders with Grade 270 strands, the upper bound estimate of time-dependent losses Δf_{pTD} is taken per Equation 4-4, where *PPR* is the partial prestressing ratio. For low-relaxation strands, AASHTO permits Eq. 4-4 to be reduced by 4 ksi. For I-girders with Grade 270 strands, the average estimate of time-dependent losses is calculated using Equation 4-5, which may be reduced by 6 ksi for low-relaxation strands. Both equations are valid for pretensioned members cast with normal-weight concrete, stressed after reaching 3.5-ksi strength, and either steam or moist cured.

$$\Delta f_{pTD} = 21.0 + 4.0 PPR \quad \text{(Eq. 4-4)}$$

$$\Delta f_{pTD} = 33 \left[1 - 0.15 \left(\frac{f'_c - 6}{6} \right) \right] + 6 PPR \quad \text{(Eq. 4-5)}$$

The separate lump sum method provides refined estimates for individual components of time-dependent losses. Losses due to concrete shrinkage and creep are calculated using Equations 4-6 and 4-7, respectively. The change in concrete stress Δf_{cdp} in Equation 4-7 is calculated at the same section for which f_{cgp} is calculated. Losses due to steel relaxation are calculated separately for the time prior to prestress transfer (Δf_{pR1}) and the time after transfer (Δf_{pR2}) using Equations 4-8 and 4-9, respectively, for lox-relaxation strands. The time *t* is taken as the number of days between strand prestressing and transfer.

$$\Delta f_{pS} = 17.0 - 0.15 H \quad \text{(Eq. 4-6)}$$

where: H = relative humidity

$$\Delta f_{pC} = 12.0 f_{cgp} - 7.0 \Delta f_{cdp} \geq 0 \quad \text{(Eq. 4-7)}$$

where: Δf_{cdp} = change in stress at strand CG due to permanent loads absent at transfer

$$\Delta f_{pR1} = \frac{\log(24.0t)}{40.0}\left(\frac{f_{pJ}}{f_{py}} - 0.55\right) f_{pJ} \quad \text{(Eq. 4-8)}$$

$$\Delta f_{pR2} = 0.30\left[20.0 - 0.4\Delta f_{pES} - 0.2(\Delta f_{pSR} + \Delta f_{pCR})\right] \quad \text{(Eq. 4-9)}$$

4.4.2 PCI Method

The PCI Design Handbook (2004) outlines a method to predict prestress losses for normal design conditions. As the handbook states, typical prestress losses range from 25 ksi to 50 ksi in normal-weight concrete members, and from 30 ksi to 55 ksi in lightweight concrete members. The method outlined below utilizes terminology as written in the design handbook; variables repeated from previous text are not redefined. First, total losses are represented by Equation 4-10, which combines losses due to elastic shortening (*ES*), concrete creep (*CR*), concrete shrinkage (*SH*), and steel relaxation (*RE*). The individual components of loss are calculated using Equations 4-11 through 4-14.

$$TL = ES + CR + SH + RE \quad \text{(Eq. 4-10)}$$

$$ES = \frac{K_{es} E_{ps} f_{cir}}{E_{ci}} \quad \text{(Eq. 4-11)}$$

where: K_{es} = 1.0 for pretensioned members
f_{cir} = net compressive stress in concrete at strand CG at transfer

$$CR = \frac{K_r E_{ps}}{E_c}\left(f_{cir} - f_{cds}\right) \quad \text{(Eq. 4-12)}$$

where: K_r = 2.0 for normal weight concrete, 1.6 for light weight concrete
f_{cds} = stress at strand CG due to superimposed dead loads applied after transfer
E_c = elastic modulus of concrete at 28 days

$$SH = \left(8.06 \times 10^{-6}\right) K_{sh} E_{ps} \left(1 - 0.06\frac{V}{S}\right)\left(100 - RH\right) \quad \text{(Eq. 4-13)}$$

where: K_{sh} = 1.0 for pretensioned members
V/S = volume-to-surface ratio
RH = average ambient relative humidity

$$RE = \left[K_{re} - J\left(SH + CR + ES\right)\right] C \qquad \text{(Eq. 4-14)}$$

where: J = coefficient from PCI Table 4.7.3.1
K_{re} = coefficient from PCI Table 4.7.3.1

The net compressive stress f_{cir} in concrete at the strands' center of gravity at transfer, as referenced in Eq. 4-11, is calculated using Eq. 4-15. Meanwhile, the stress f_{cds} in concrete at the strands' center of gravity due to superimposed dead loads applied after transfer is calculated using Equation 4-16. For Grade 270 low-relaxation strands, the coefficients J and K_{re} in Eq. 4-14 are taken as 0.040 and 5000, respectively. The coefficient C in Eq. 4-14 may be obtained from PCI Table 4.7.3.2, but it may also be calculated using either Equation 4-17 or 4-18.

$$f_{cir} = K_{cir}\left(\frac{P_i}{A_g} + \frac{P_i e^2}{I_g}\right) - \frac{M_g e}{I_g} \qquad \text{(Eq. 4-15)}$$

where: K_{cir} = 0.9 for pretensioned members
P_i = initial prestressing force
M_g = bending moment due to self-weight and permanent loads at transfer

$$f_{cds} = \frac{M_{sd} e}{I_g} \qquad \text{(Eq. 4-16)}$$

where: M_{sd} = moment due to superimposed dead and sustained loads after transfer

$$\frac{f_{pi}}{f_{pu}} \geq 0.54: \quad C = \frac{\left(\frac{f_{pi}}{f_{pu}}\right)}{0.21}\left[\frac{\left(\frac{f_{pi}}{f_{pu}}\right)}{0.9} - 0.55\right] \qquad \text{(Eq. 4-17)}$$

$$\frac{f_{pi}}{f_{pu}} < 0.54: \quad C = \frac{\left(\frac{f_{pi}}{f_{pu}}\right)}{4.25} \qquad \text{(Eq. 4-18)}$$

4.4.3 ACI Committee 209 Method

While ACI Committee 343 (1995) utilizes the AASHTO separate lump sum method to estimate prestress losses, ACI Committee 209 (2008) suggests an alternative approach incorporating refined creep and shrinkage effects. The method outline below utilizes terminology

as presented in the ACI manual; variables repeated from previous text are not redefined. Total losses are represented using Equation 4-19; the four terms in the equation represent losses due to elastic shortening, concrete creep, concrete shrinkage, and steel relaxation, respectively.

$$\lambda_t = (nf_c) + (nf_c)v_t\left(1 - \frac{F_t}{2F_o}\right) + \frac{(\varepsilon_{sh})_t E_s}{1 + n\rho\xi_s} + (f_{sr})_t \qquad \text{(Eq. 4-19)}$$

where: λ_t = total losses
n = modular ratio of steel to concrete at time of loading
f_c = concrete stress such at steel CG due to prestress and dead load
v_t = creep coefficient at any time
F_t = total loss of prestress at any time minus the initial elastic loss
F_o = prestress force at transfer, after elastic loss
$(\varepsilon_{sh})_t$ = shrinkage strain at any time
ρ = reinforcement ratio
ξ_s = cross section shape coefficient
$(f_{sr})_t$ = stress loss due to steel relaxation in prestressed member at any time

As the ACI manual suggests, F_o, A_g, and I_g are frequently used as approximations to F_i, A_t, and I_t in Equation 4-19, with $F_o = F_i(1\text{-}n\rho)$. Approximate values for the ratio F_t/F_o may be obtained for normal-weight concrete from ACI Table 4.4.1.2 (ACI Committee 209). For a time span of three weeks to one month between prestressing and sustained load application, the ratio is taken as 0.10; for a time span of two to three months, the ratio is taken as 0.14; at ultimate, the ratio is taken equal to 0.18. For low-relaxation strands, values of stress loss due to steel relaxation may be obtained using ACI Table 4.4.1.3 (ACI Committee 209). For specimens with $0.65 < f_{pi}/f_{py} < 0.80$, steel relaxation may calculated using Equation 4-20, where t is the time after initial stressing in hours. The ultimate steel relaxation may be taken equal to $0.025(f_{si})$.

$$(f_{sr})_t = 0.005(f_{si})\log(t) \qquad \text{(Eq. 4-20)}$$

Values for the creep coefficient and shrinkage strain at any time are calculated using Equations 4-21 and 4-22, respectively, where v_u is the ultimate creep coefficient, $(\varepsilon_{sh})_u$ is the ultimate shrinkage strain, and t is the time after loading. In the absence of specific data, recommended values for v_u and $(\varepsilon_{sh})_u$ are $2.35\gamma_c$ and $0.000780\gamma_{sh}$, respectively, for moist-cured concrete; γ_c and γ_{sh} are correction factors derived based on loading age, relative humidity,

specimen geometry, and initial moist curing (ACI Committee 209). For brevity, the correction factors are not described in detail here, though they are included in example calculations in Appendix C.

$$v_t = \frac{t^{0.60}}{10 + t^{0.60}} v_u \qquad \text{(Eq. 4-21)}$$

$$\left(\varepsilon_{sh}\right)_t = \frac{t}{35 + t}\left(\varepsilon_{sh}\right)_u \qquad \text{(Eq. 4-22)}$$

According to ACI Committee 209, the correlation between measured and computed prestress losses is reasonable but not accurate. With general knowledge of the environmental conditions, load history, or concrete constituent properties of a specimen, calculated prestress losses may be expected to correlate to actual losses within 15-20%. A more rigorous method of computing prestress losses is the time-step method, where time-dependent losses are evaluated at successive intervals over a specified length of time. In doing so, the interdependent effects of relaxation, creep, and shrinkage, all of which occur at different rates, are included in analysis. However, since the estimated long-term losses using the aforementioned methods were reasonable, the time-step method was not utilized in this study.

Examples C.1-C.3 in Appendix C contain example prestress loss calculations for specimen Box-1 to illustrate the execution of the aforementioned methods. Table 4.6 lists the effective prestress in the box girders calculated using various methods; Table 4.7 lists the same for the I-girders. For comparison, effective prestress was calculated using design and actual concrete strengths, as well as curing ages of 28 and 365 days. To illustrate the time-dependent behavior of prestress losses, total losses calculated via the ACI Committee 209 procedure are plotted for specimen Box-1 in Figure 4.22.

As the two tables show, the difference in design and actual concrete strengths had little impact on calculated effective prestress (less than 2 ksi difference). The time-dependent behavior of creep and shrinkage are clearly evident in the f_{pe} values calculated using the ACI Committee 209 method at concrete ages of 28 and 365 days. The AASHTO approximate lump sum, separate lump sum, and ACI Committee 209 methods predict effective prestress in the box girders with reasonable precision. However, the PCI method calculates effective prestress in the box girders at approximately 6 ksi larger than the other three methods. Much greater variability is seen in the

effective prestress within the I-girders; nearly a 15 ksi difference exists between predictions from the AASHTO approximate lump sum and PCI methods.

Table 4.6: Effective Prestress within Box Girder Specimens using Various Prediction Methods

Box Girder 1	**Design**	**Actual**	
Initial Concrete Strength	5000 psi	5660 psi	
28-Day Concrete Strength	6000 psi	7500 psi	
	Effective Prestress (ksi)		
Age (days):	28	28	365
AASHTO Total Lump Sum	168.0		
AASHTO Sep. Lump Sum	165.7	166.1	
PCI Method	170.3	172.2	
ACI 209 Method	177.9	178.8	166.5

Box Girder 2	**Design**	**Actual**	
Initial Concrete Strength	5000 psi	5460 psi	
28-Day Concrete Strength	6000 psi	7010 psi	
	Effective Prestress (ksi)		
Age (days):	28	28	365
AASHTO Total Lump Sum	168.0		
AASHTO Sep. Lump Sum	165.7	166.1	
PCI Method	170.3	171.6	
ACI 209 Method	177.9	178.5	166.2

Table 4.7: Effective Prestress within I-Girder Specimens using Various Prediction Methods

I-Girder 1	**Design**	**Actual**	
Initial Concrete Strength	5000 psi	4880 psi	
28-Day Concrete Strength	6000 psi	6870 psi	
	Effective Prestress (ksi)		
Age (days):	28	28	365
AASHTO Total Lump Sum	158.5	159.2	
AASHTO Sep. Lump Sum	166.9	166.9	
PCI Method	173.1	173.8	
ACI 209 Method	178.4	178.2	165.8

I-Girder 2	**Design**	**Actual**	
Initial Concrete Strength	5000 psi	4710 psi	
28-Day Concrete Strength	6000 psi	6740 psi	
	Effective Prestress (ksi)		
Age (days):	28	28	365
AASHTO Total Lump Sum	158.5	159.1	
AASHTO Sep. Lump Sum	166.9	166.9	
PCI Method	173.1	173.6	
ACI 209 Method	178.4	178	165.5

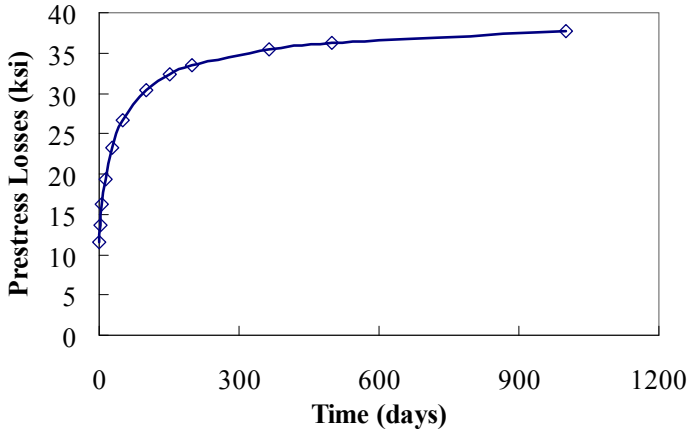

Figure 4.22: Prestress losses in Box-1 calculated per ACI Committee 209

4.5 DEVELOPMENT LENGTH PREDICTIONS

Development lengths in the four specimens were predicted using Equation 2-2. Both the effective prestress f_{pe} and the nominal strand stress f_{ps} may vary depending on method of calculation. Effective prestress was calculated using four different methods (Section 4.4). The nominal strand stress was calculated using two methods, the first of which was the AASHTO code approximation shown in Equation 4-22.

$$f_{ps} = f_{pu}\left(1 - \frac{kc}{d_{ps}}\right) \qquad \text{(Eq. 4-22)}$$

where: c = neutral axis depth
d_{ps} = depth of center of gravity of prestressing steel
k = defined by Equation 4-23

$$k = 2\left(1.04 - \frac{f_{py}}{f_{pu}}\right) \qquad \text{(Eq. 4-23)}$$

Nominal strand stress was also calculated using constitutive stress-strain material properties of 270-ksi prestressing strand. In this iterative method, three strain components are calculated for an assumed nominal stress f_{ps}; if the sum of the three strains is within reasonable tolerance of the corresponding strain on the strand's stress-strain curve, the f_{ps} is acceptable. The procedure is outlined in Equations 4-24 through 4-27. The first strain is due to the effective prestressing load, without self-weight; the second strain is due to the load required to negate the effect of camber; the third strain is the additional strain required to reach ultimate failure. Only the third strain depends on the assumed nominal stress.

$$\varepsilon_1 = \frac{f_{pe}}{E_{ps}} \qquad \text{(Eq. 4-24)}$$

$$\varepsilon_2 = \frac{1}{E_c}\left(\frac{Fe}{A} + \frac{Fe^2}{I}\right) \qquad \text{(Eq. 4-25)}$$

$$\varepsilon_3 = \frac{0.003\left(d_{ps} - c\right)}{c}, \quad \text{where} \quad c = \frac{A_{ps} f_{ps}}{0.85 f_c b \beta_1} \qquad \text{(Eq. 4-26)}$$

$$\varepsilon_{total} = \varepsilon_1 + \varepsilon_2 + \varepsilon_3 \approx \varepsilon_{stress-strain} \rightarrow OK \qquad \text{(Eq. 4-27)}$$

Nominal stress predictions from the two methods differed by no greater than 4 ksi. Development lengths calculated using effective prestress values from four methods (Section 4.4) and nominal stress from the stress-strain (SS) and AASHTO methods are shown in Table 4.8. The effective prestress was taken after all losses. Specific values are presented only for one specimen per type of beam because differences in predictions for two specimens of the same beam type were negligible. For the box girder, development length predictions shown in the table ranged between 68.5 in. and 72.4 in.; for the I-girder, predictions ranged from 73.9 in. to 81 in. From available test data, the actual effective prestress in the box girders was found to be 162 ksi (see Section 6.3.1, Table 6.4). Using this f_{pe} and the AASHTO approximation for f_{ps}, the development length in the box girders was predicted as 72.9 in., slightly exceeding the values in Table 4.8. From flexural test data, it was shown that the effective The development length predictions do not incorporate the 1.6 multiplier specified by the FHWA and AASHTO (see Section 2.2.1).

Table 4.8: Development Lengths Calculated using Various Methods

Box Girder 1	**Design f'_c = 6 ksi**		**Actual f'_c = 7.5 ksi**		
Methods	*SS*	*AASHTO*	*SS*	*AASHTO*	
AASHTO Total Lump Sum	69.3	70.9	70.0	71.8	
AASHTO Sep. Lump Sum	70.0	71.7	70.6	72.4	
PCI Method	68.5	70.1	68.6	70.3	
ACI 209 Method	70.1	71.7	70.4	72.2	**Range**
Minimum	68.5	70.1	68.6	70.3	**68.5**
Average	69.5	71.1	69.9	71.7	**70.5**
Maximum	70.1	71.7	70.6	72.4	**72.4**

I-Girder 1	**Design f'_c = 6 ksi**		**Actual f'_c = 6.9 ksi**		
Methods	*SS*	*AASHTO*	*SS*	*AASHTO*	
AASHTO Total Lump Sum	80.2	78.7	81.0	78.8	
AASHTO Sep. Lump Sum	77.5	75.9	78.5	76.2	
PCI Method	75.6	73.9	76.3	73.9	
ACI 209 Method	77.8	76.2	78.8	76.5	**Range**
Minimum	75.6	73.9	76.3	73.9	**73.9**
Average	77.8	76.2	78.7	76.4	**77.2**
Maximum	80.2	78.7	81.0	78.8	**81.0**

4.6 DESIGN CAPACITIES

To maintain consistency with real bridge girders, the girders in this study were designed for realistic AASHTO (2004) loading scenarios; specimen geometry and reinforcement (see Appendix B) were unaltered from what would typically be utilized in practice. The hollow box girders were designed to withstand AASHTO HL-93 loading, which utilizes the HS20-44 design truck or tandem load in addition to a design lane load. The design truck comprises 72 kips distributed to three axles. The distance between the front and middle axle is constant, while the distance between the middle and rear axles may vary from 14 ft. to 30 ft. The design tandem comprises two 25-kip loads spaced 4 ft. apart and is used to represent heavy military vehicles. The design lane load which represents vehicular traffic is taken as 0.64 kip/ft. All components of the HL-93 loading are shown in Figure 4.23. The two I-girders were designed to withstand AASHTO HS20-44 loading, which utilizes the HS20-44 design truck and design lane load, but does not consider tandem loading.

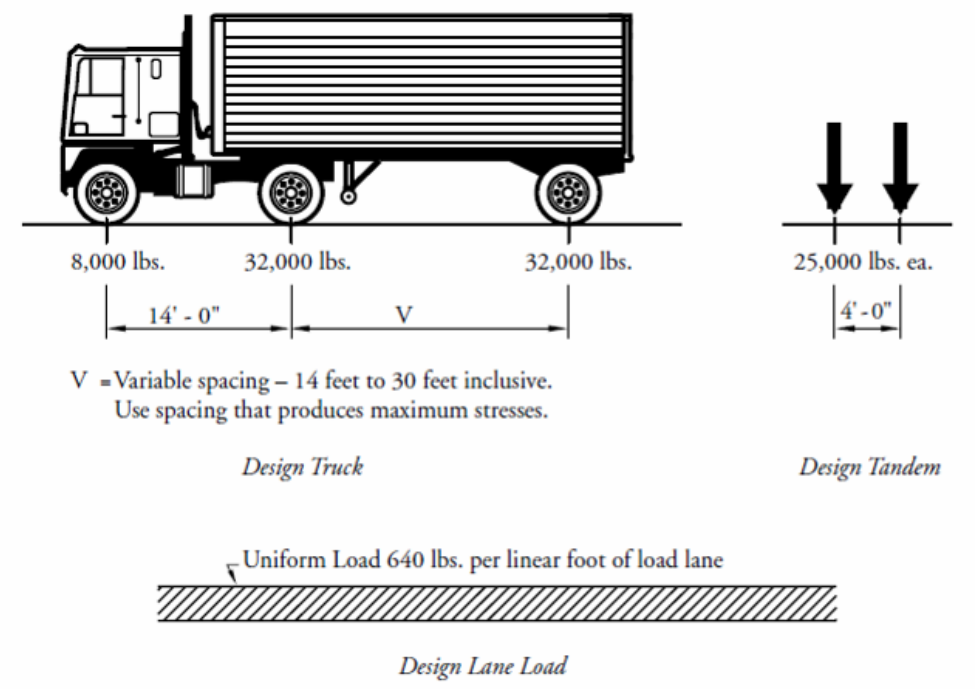

Figure 4.23: Components of HL-93 loading (PCI 2003-b)

A MATLAB® code was utilized to generate the shear and moment envelopes for both specimen types. The code incorporated all loading scenarios including variable axle distance and vehicle position, load factors specified by AASHTO, and dead load due to beam self-weight and a superimposed bridge deck. The superimposed dead load was taken as 1.0 kip/ft., equivalent to a 10-ft. wide, 8-in. thick deck. All analyses utilized a 1.75 live load factor, a 1.25 dead load factor, and a 1.33 impact factor; the impact factor accounts for the 33% dynamic load allowance specified by AASHTO and was applied only to the design truck and tandem loads. The code also incorporated shear and moment distribution factors used to distribute loads from a full lane to an individual girder. The demand envelopes for the box girders are shown in Figure 4.24, and the envelopes for the I-girders are shown in Figure 4.25. The figures also display as-built sectional capacities for each specimen; shear capacities were calculated using both ACI and AASHTO methods, flexural capacity was calculated using the AASHTO f_{ps}, and all calculations utilized the 6000 psi design strength. Example calculations for each method may be found in Appendix D.

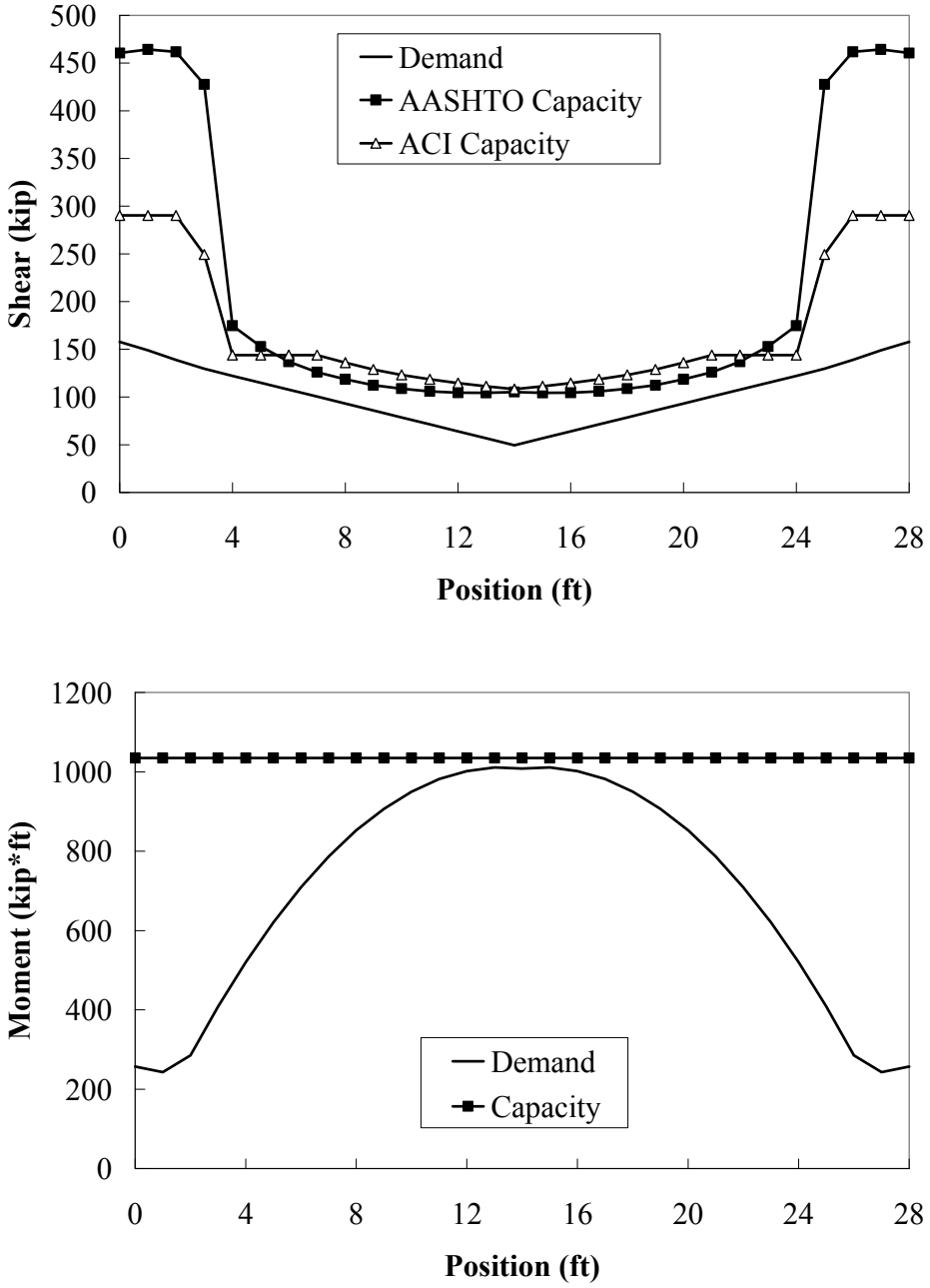

Figure 4.24: Shear (top) and moment (bottom) envelopes and sectional capacities for box girders

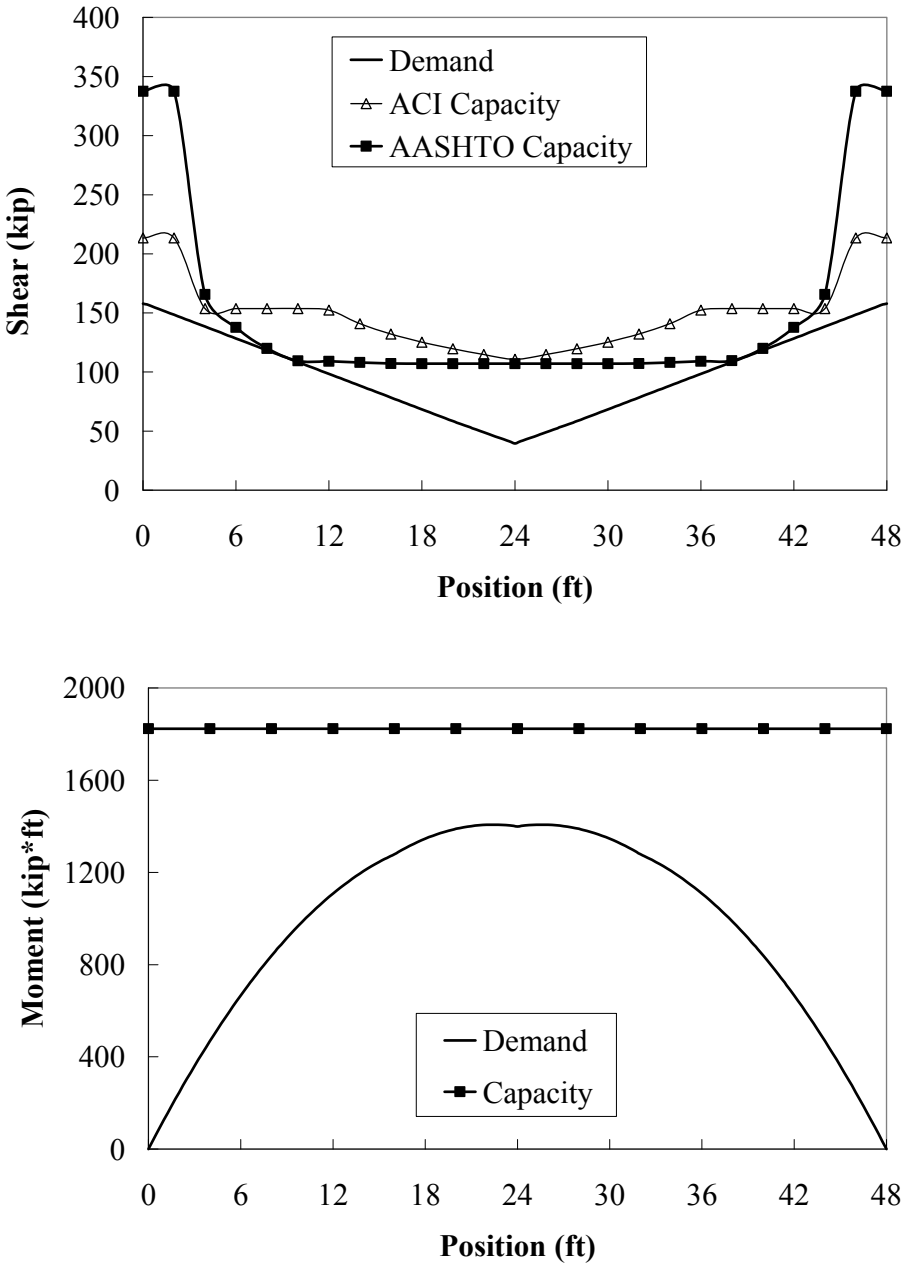

Figure 4.25: Shear (top) and moment (bottom) envelopes and sectional capacities for I-girders

The shear and moment distribution factors were taken as 1.0 for the box girder analysis, conservatively applying the entire load to one member. As seen in Figure 4.24, the box girder is most critical in shear where the center void terminates, 30 in. from either end of the specimen. More refined analysis may show higher shear capacities at this location, but high stress concentration at the hollow/filled interface makes shear failure likely in the region. The

theoretical moment capacity of 1035 kip-ft is adequate for the 28-ft. specimen under the prescribed loading.

The capacities shown in Figure 4.25 were calculated using the composite I-girder, with an 8 in. thick and 30 in. wide slab. Demand was calculated using assumed 6-ft. center-to-center beam spacing, resulting in shear and moment distribution factors of 75% and 60%, respectively. Akin to the box girder, the I-girder is more vulnerable in shear than in flexure; especially between 4 ft. and 10 ft. from either end of the specimen. Within this region the stirrup area decreases from 0.8 in^2 to 0.4 in^2 and stirrup spacing increases from 6 in. to 12 in. on center (see Figure B.5). The theoretical moment of the composite section was found to be 1800 kip-ft; as the figure shows, the as-built girder is adequate for the prescribed loading. The nominal stress at ultimate failure (f_{ps}) was calculated as 263 ksi and 266.4 ksi using an AASHTO approximation and strain compatibility, respective.

4.7 SUPPLEMENTARY SHEAR REINFORCEMENT

As discussed in Section 4.6, one of the key characteristics of the specimens used in this study is that they were designed for realistic AASHTO (2004) load conditions, resulting in girders which were more vulnerable in shear than flexure within the vicinity of the development length. As such, it was anticipated that the girders would fail in shear prior to reaching nominal moment capacity at the loaded section. To maintain consistency between the tested specimens and real bridge girders, no additional internal shear reinforcement was added; however, in one trial an attempt was made to increase the shear strength of the girder in the shear-vulnerable region through the use of external Carbon Fiber Reinforced Polymer (CFRP) sheets. Studies by Norris et al. (1997) and Kachlakev and McCurry (2000) have shown bonded FRP to be effective in strengthening concrete members in shear. One benefit of using CFRP sheets is that the external application had no impact on the flow of the concrete during casting or the bond between concrete and internal strands. This section summarizes the ACI Committee 440 (2008) design procedure for external FRP reinforcement and describes the application process for specimen Box-2.

4.7.1 ACI Design Procedure for External FRP Reinforcement

ACI Committee 440 (2008) outlines a design procedure for strengthening of concrete specimens using externally-bonded FRP, an extremely efficient material whose relevance in structural applications continues to grow. The procedure draws upon basic design principles and recent experimental results to predict the actual strength contribution of FRP systems. The nominal shear strength of a member reinforced with FRP may be calculated using Equation 4-28. The strength reduction factor Ψ_f derives from reliability analyses and is taken equal to 0.85 for three-sided wraps and equal to 0.95 for fully wrapped reinforcement. The nominal FRP shear strength V_f is determined in essentially the same manner as the nominal strength of steel stirrups. As shown in Equation 4-29, V_f accounts for the orientation and CL-to-CL spacing of FRP strips. Where strips are placed adjacent to one another, forming a continuous wrap, the spacing term s_f is taken equivalent to the width of the entire wrap. The depth d_{fv} is the distance from the top of the FRP to the depth of tensile steel. The combined nominal steel and FRP shear strength must not exceed the limit in Equation 4-30.

$$\Phi V_n = \Phi(V_c + V_s + \Psi_f V_f) \qquad \text{(Eq. 4-28)}$$

where: V_c = concrete shear strength from Ch. 11 of ACI 318-08
V_s = steel contribution to shear strength from Ch. 11 of ACI 318-08
V_f = FRP contribution to shear strength from Section 11.4 in ACI 440.2R-08
Ψ_f = 0.85 for 3-sided wraps, 0.95 for full wraps (Table 11.1, ACI 440.2R-08)

$$V_f = \frac{A_{fv} f_{fe} (\sin\alpha + \cos\alpha) d_{fv}}{s_f} \qquad \text{(Eq. 4-29)}$$

where: A_{fv} = total cross-sectional area of FRP acting in shear: $2t_f w_f n_{layers}$
f_{fe} = effective stress in FRP

$$V_s + V_f \le 8 b_w d \sqrt{f_c'} \qquad \text{(Eq. 4-30)}$$

The effective stress f_{fe} in Eq. 4-29 is the product of the FRP's tensile modulus and the effective strain ε_{fe}; the effective strain is calculated by applying reduction factors to the ultimate FRP strain ε_{fu} to account for concrete strength and wrapping configuration. For U-wraps, where reinforcement covers only three sides of a specimen, adjustment factors may be calculated in

using Equations 4-31 through 4-35 in accordance with Section 11.4.1.2 of ACI 440.2R-08. For the case of fully-wrapped FRP, the effective strain may be taken as a maximum $0.004 \leq 0.75\varepsilon_{fu}$. The 0.004 limit is imposed to preclude failure due to loss of aggregate interlock, which has been observed in experimental tests (ACI Committee 440). For long-term effects, ACI Table 9.1 provides environmental reduction factors applied to the ultimate FRP strength and strain provided by manufacturers; the factor for interior exposure to carbon fiber is 0.95.

$$\varepsilon_{fe} = \kappa_v \varepsilon_{fu} \quad \text{(Eq. 4-31)}$$

$$\kappa_v = \frac{k_1 k_2 L_e}{468\varepsilon_{fu}} \quad \text{(Eq. 4-32)}$$

$$k_1 = \left(\frac{f'_c}{4000}\right)^{2/3} \quad \text{(Eq. 4-33)}$$

$$k_2 = \frac{d_{fv} - L_e}{d_{fv}} \quad \text{(Eq. 4-34)}$$

$$L_e = \frac{2500}{(nt_f E_f)^{0.58}} \quad \text{(Eq. 4-35)}$$

4.7.2 External CFRP Wrap for Specimen Box-2

To increase the shear strength of one end of specimen Box-2, a CFRP wrap was applied in the shear-vulnerable region prior to testing. Five coupon tests were conducted to evaluate the tensile modulus and strength of the composite formed with unidirectional carbon fabric and a saturating epoxy resin. Coupons were 0.6 in. x 14 in., and each had 4-in. long perforated plastic tabs at either end for gripping within the loading apparatus. The specimens were formed by saturating two 0.014-in. thick layers of fabric with an epoxy resin designed to have a 120-minute pot life. Specimens were cured for 36 hours prior to testing. The average tensile modulus and ultimate strength of the composite coupons were 19694 ksi and 284 ksi, respectively. The coupon specimens consistently failed at the location of grips due to high stress concentration or fracture of the plastic tabs; therefore, the average modulus and strength values were probably conservative.

Following the method described in Section 4.7.1, it was determined that two layers of 0.014-in. thick, unidirectional carbon fabric wrapped entirely around an 18-in. wide section of

the girder (see Figure 4.26) would provide sufficient shear strength for the intended loading. No portion of the wrap was placed less than 20.3 in. away from the point of load; in this configuration, the CFRP would not interfere with plastic hinge development, nor would it cover the end of the specimen where shear was already adequate. The girder was first prepared by roughening the smoothed concrete surface with an electric diamond-toothed grinder to facilitate better adhesion between the FRP and concrete. The effect of grinding is illustrated in Figure 4.27. After the roughened surface had been cleaned, a first coat of epoxy resin was applied directly to the concrete. Then, the first layer of carbon fabric was pressed onto the epoxy and held firmly in place. An absorbent roller was utilized to impregnate the fabric with another layer of epoxy resin, as shown in Figures 4.28 and 4.29. The process was repeated for the second layer of fabric. The final wrap is shown in Figure 4.30. Care was taken to ensure the fabric was completely saturated, and excess resin was removed by lightly pulling a rubber squeegee along the contour of the beam.

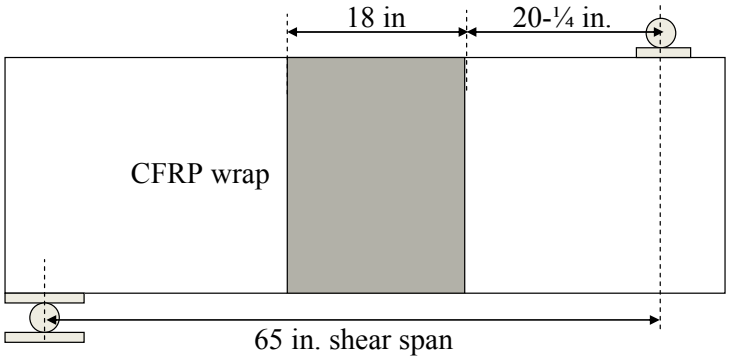

Figure 4.26: CFRP Wrap Location on Box-2

Figure 4.27: Surface roughened with toothed grinder

Figure 4.28: Placing the first epoxy/fabric on Box-2

Figure 4.29: First epoxy/fabric layer applied to Box-2

Figure 4.30: Final CFRP wrap on specimen Box-2

CHAPTER 5: TRANSFER LENGTH

After fabrication, transfer lengths in the four full-scale girders were measured between August 27, 2009 and September 28, 2009. Measurements were taken at 16 locations to obtain average transfer lengths for the eight girder ends and each girder as a whole. Experimental data was compared to ACI (2008) and AASHTO (2004) requirements. Additionally, transfer lengths were compared to analytical predictions proposed in the literature.

5.1 MEASUREMENTS

After 20 hours of moist curing, forms for all girders were removed to provide access for attaching surface-strain target points, which were used to obtain longitudinal strain profiles at the ends of specimens. For each girder, 0.39-in. diameter stainless steel target points were glued to each side of both ends at a depth corresponding to strands' center of gravity; five-minute metal-concrete epoxy was used, and concrete surfaces were wiped clean prior to application. Figure 5.1 and Figure 5.2 show targets attached to specimens Box-1 and I-1, respectively. Targets were spaced 2 in. apart on specimens Box-1 and I-1, 4 in. apart on specimens Box-2 and I-2, and were extended approximately 45 in. from the end of each beam. Prior to releasing the pretensioned strands, initial distance measurements were taken between each pair of target points using a mechanical gauge with 4-in. length.

Strands were released after 24 hours of curing; Box-1 and Box-2 had reached 5660 psi and 5460 psi strengths, respectively, while I-1 and I-2 had reached 4880 psi and 4710 psi strengths, respectively. Although the latter two girders did not meet the specified 5000 psi release strength, it was deemed appropriate to release all four specimens so that subsequent measurements could proceed on the same day. Strands were flame-cut (see Figure 4.3 for cutting locations), and distances between target points were measured immediately after release. In conjunction with the initial target point measurements, these readings were then used to develop a strain profile for all sides and ends of the beams. The specimens were moved from their casting beds to the fabrication plant yard after 1-day measurements were complete. The beams remained unmoved in the yard for measurements taken 3, 7, 14, and 28 days after concrete placement.

For each day of transfer length measurements, seven concrete compressive cylinder tests were performed to determine the strength of the beams. The top and bottom cylinder surfaces

were made smooth with an electric grinder prior to testing on-site at the fabrication plant. One cylinder each from SCC Batches 1-3 and SCC Batches 5-8 (see Tables 4.1 and 4.2) were tested, and beam strengths were determined based according to batch distribution within the beams. The resultant concrete strengths over time for each beam are listed in Table 5.1. The 6000-psi design strength was reached by the box girders within 3 days and by the I-girders within 14 days.

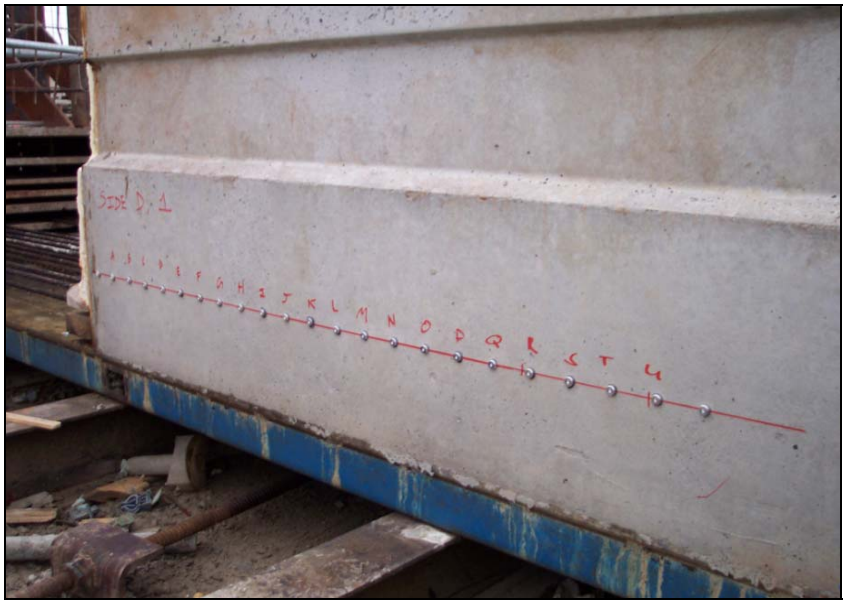

Figure 5.1: Target points attached to specimen Box-1, Side D

Figure 5.2: Target points attached to specimen I-1, Side A

Table 5.1: Girder Specimen Strength (f_c, in psi) as Determined by Compressive Cylinder Tests

Age (days):	1	3	7	14	28
Box-1	5660	6140	6680	7460	7500
Box-2	5460	6300	6760	7450	7010
I-1	4880	5480	5940	6550	6870
I-2	4710	5470	5980	6590	6740

5.2 DISCUSSION OF TRANSFER LENGTH RESULTS

The 95% AMS method (see Section 2.3.6) was utilized to determine experimental transfer lengths via surface strain measurements. Strain profiles obtained for all sixteen transfer length locations (refer to Figure 4.3) are presented in Figures E.1-E.16 in Appendix E. An example set of strain profiles is shown in Figure 5.3 for the far end of specimen I-1 at Location D. At various ages, individual transfer lengths were obtained for both sides of both ends of each girder. Then, average transfer lengths were calculated for the eight end locations ($L_{t\text{-}end}$) and for each girder as a whole ($L_{t\text{-}avg}$). At the far end of specimen I-2, no transfer lengths were obtainable at Location A since strain profiles showed no distinct plateau (see Figure E.15). However, readings at Location D (see Figure E.16) at the same end clearly displayed plateau regions. $L_{t\text{-}end}$ values reported for I-2's far end, therefore, were based solely on measurements at Location D.

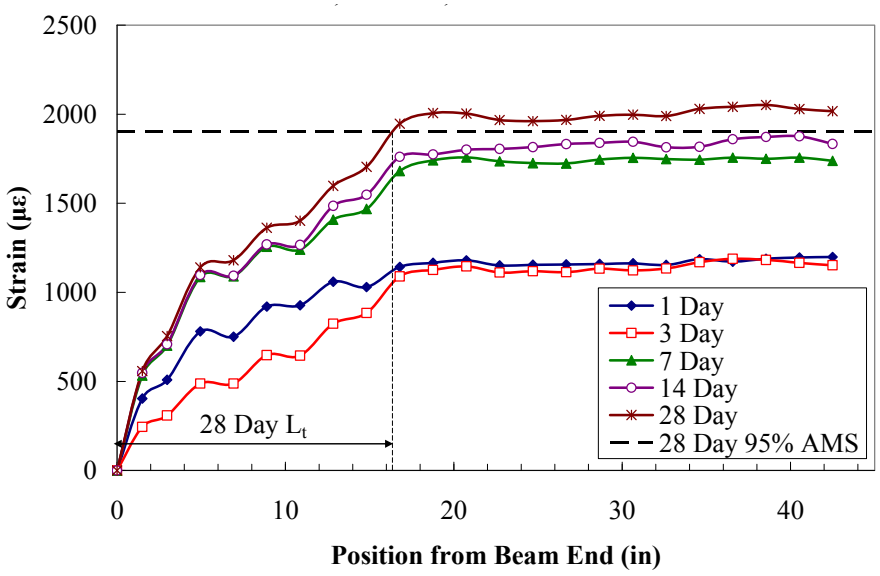

Figure 5.3: Strain profiles for the far end of specimen I-1 at Location D

Table 5.2 contains all $L_{t\text{-}end}$ values obtained in the study. At I-2's far end, transfer lengths exceeded the ACI $50d_b$ (25 in.) provision at all ages by up to 30% and exceeded the AASHTO $60d_b$ (30 in.) provision at 1-day and 3-day measurements by up to 8.3%. At the other seven ends, transfer lengths were consistently below these two code requirements. No 28-day data was available for I-2's far end because strain readings at Location D were incomplete due to human error. A bolded value in Table 5.2 indicates the end at which transfer length was largest within a girder at each age.

A number of factors acting in combination could have produced different transfer lengths at two ends of the same beam: concrete casting location, strand cutting location, and, because beams were cast with multiple batches of concrete, compressive strength at transfer. The far ends of Box-2 and I-2 experienced the most immediate force transfer due to strand cutting and had the lowest concrete compressive strengths within their respective girder types. Accordingly, transfer lengths at the far ends of Box-2 and I-2 were longer than those at their opposite ends by 11% and 57%, respectively. The effects of cutting location and concrete strength were not considered independently; however, their combined action appeared to significantly impact transfer length. Table 5.2 also contains ratios between $L_{t\text{-}end}$ values at starting and far ends for each girder. Average "Starting/Far" ratios ranged from 0.63 in specimen I-2 to 1.19 in specimen I-1, suggesting transfer length is independent of casting location. The $L_{t\text{-}end}$ values are also shown over time in Figure 5.4. No consistent increase in transfer length was observed as concrete aged.

Table 5.2: Transfer Lengths at all Beam Ends ($L_{t\text{-}end}$, in inches)

	Age (days):	**1**	**3**	**7**	**14**	**28**
Box-1	Starting End	18.1	18.9	18.1	19.3	20.3
	Far End	**24.5**	**20.2**	**24.0**	**19.6**	**24.1**
	Starting/Far	0.74	0.94	0.75	0.98	0.84
Box-2	Starting End	19.8	19.3	18.7	17.7	18.1
	Far End	**21.6**	**20.6**	**19.8**	**20.0**	**21.4**
	Starting/Far	0.92	0.94	0.94	0.89	0.84
I-1	Starting End	**24.6**	**23.1**	**22.4**	**22.6**	**21.8**
	Far End	18.6	19.5	19.1	19.6	19.5
	Starting/Far	1.32	1.19	1.17	1.16	1.12
I-2	Starting End	18.5	19.6	20.6	19.8	21.0
	Far End	**32.3**	**32.5**	**29.7**	**29.9**	-
	Starting/Far	0.57	0.60	0.69	0.66	-

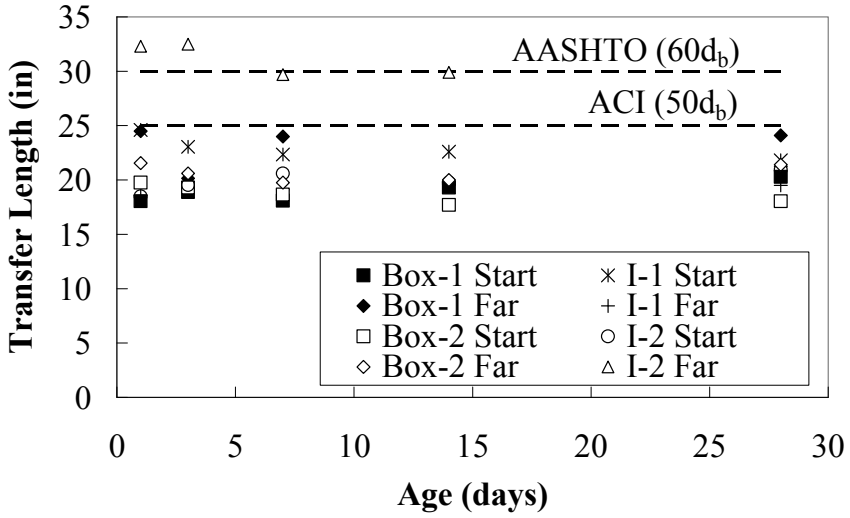

Figure 5.4: $L_{t\text{-}end}$ values at various ages compared to ACI and AASHTO requirements

At all ages, the average transfer length ($L_{t\text{-}avg}$) for each girder was calculated by taking the average of the girder's two $L_{t\text{-}end}$ values presented in Table 5.2. $L_{t\text{-}avg}$ values are presented in Table 5.3 for comparison to ACI and AASHTO provisions. No 28-day $L_{t\text{-}avg}$ value was calculated for specimen I-2 because data for its far end was not available, as previously mentioned. Ratios $L_{t\text{-}avg}/50d_b$, $L_{t\text{-}avg}/(f_{pe}d_b/3)$, and $L_{t\text{-}avg}/60d_b$ in Table 5.3 with values less than unity indicate adequate transfer lengths with respect to code requirements. The ratio $L_t/(f_{pe}d_b/3)$ was calculated using experimental data only from 28-day tests, since the ACI Code prediction utilizes the effective prestressing force after all prestress losses.

As seen in the table, average transfer lengths in three of the four specimens consistently met the most stringent transfer length requirement ($50d_b$). However, average transfer lengths within specimen I-2 exceeded $50d_b$ prior to 14-day measurements. This is attributed to the unusually large transfer lengths obtained at the specimen's far end, for reasons suggested previously. Overall, experimental transfer lengths were 86% of $50d_b$, 72% of $60d_b$, and 69% of $f_{pe}d_b/3$. Therefore, it is reasonable to presume the bond properties of the tested SCC are sufficient to meet current design requirements; the final phase of this project described in Chapter 6 seeks to confirm this presumption. Data in Table 5.2 and Table 5.3 shows no correlation between transfer length and girder type.

Table 5.3: $L_{t\text{-}avg}$ Values at Various Ages Compared to ACI and AASHTO Requirements

			ACI ($50d_b$)	ACI ($f_{pe}d_b/3$)	AASHTO ($60d_b$)
	Age (days)	$L_{t\text{-}avg}$ (in)	$L_{t\text{-}avg}/L_{t\text{-}calc}$	$L_{t\text{-}avg}/L_{t\text{-}calc}$	$L_{t\text{-}avg}/L_{t\text{-}calc}$
Box-1	1	21.3	0.85	-	0.71
	3	19.5	0.78	-	0.65
	7	21.1	0.84	-	0.70
	14	19.5	0.78	-	0.65
	28	22.2	0.89	0.73	0.74
Box-2	1	20.7	0.83	-	0.69
	3	20.0	0.80	-	0.67
	7	19.2	0.77	-	0.64
	14	18.9	0.75	-	0.63
	28	19.7	0.79	0.65	0.66
I-1	1	21.6	0.86	-	0.72
	3	21.3	0.85	-	0.71
	7	20.7	0.83	-	0.69
	14	21.1	0.84	-	0.70
	28	20.7	0.83	0.68	0.69
I-2	1	25.4	1.02	-	0.85
	3	26.0	1.04	-	0.87
	7	25.2	1.01	-	0.84
	14	24.8	0.99	-	0.83
	28	-	-	-	-
Box Beam Average:			**0.81**	**0.69**	**0.67**
I-Beam Average:			**0.92**	**0.68**	**0.77**
Overall Average:			**0.86**	**0.69**	**0.72**

5.3 COMPARISON TO ANALYTICAL TRANSFER LENGTH

Because of the time and cost associated with experimentally determining transfer length, numerous studies were conducted in the past with the aim of predicting analytically the transfer lengths of prestressed steel strands in NCC specimens. The transfer length equations recommended by these studies were primarily derived using empirical data. One goal of this study was to assess the viability of these equations in predicting transfer lengths in prestressed SCC specimens. Therefore, experimental transfer length data obtained in this study was compared to transfer lengths predicted by the analytical expressions discussed in Section 2.2.2.

The average correlation between experimental ($L_{t\text{-}exp}$) and predicted ($L_{t\text{-}calc}$) transfer lengths is shown for box and I-girders in the final two columns of Table 5.4. When an analytical expression utilized f_{pe}, correlation ratios were calculated using only 28-day experimental data. A

ratio $L_{t\text{-}exp}/L_{t\text{-}calc}$ less than unity shows an expression to overestimate transfer length. All equations in Table 5.4 overestimated the average transfer lengths obtained in this study. However, experimental data showed better correlation to predictions incorporating initial prestress and concrete compressive strength, regardless of whether f'_{ci} or $\sqrt{f'_{ci}}$ was used, than to predictions incorporating effective prestress or no concrete strength. The formulas proposed by Marti-Vargas et al. (2007-b) and Zia and Mostafa (1977) most accurately predicted box beam transfer lengths with $L_{t\text{-}exp}/L_{t\text{-}calc}$ ratios of 0.95. Marti-Vargas et al. (2007-b) also most accurately predicted I-beam transfer lengths with a $L_{t\text{-}exp}/L_{t\text{-}calc}$ ratio of 0.99.

Table 5.4: Correlation between Experimental and Analytical Transfer Lengths

Reference	L_t Calculation ($L_{t\text{-}calc}$)	$L_{t\text{-}exp}/L_{t\text{-}calc}$	
		Box Beams	I-Beams
Based on Hanson and Kaar (1959)	$L_t = \frac{f_{pe} d_b}{3}$	0.69	0.68
Olesniewicz (1975)	$L_t = \psi d_b \sqrt{\frac{f_{pe}}{f'_{ci}}}$	0.73	0.68
Zia and Mostafa (1977)	$L_t = \frac{1.5 f_{pi} d_b}{f'_{ci}} - 4.6$	0.95	0.91
Nijhawam (1978)	$L_t = \frac{0.69 f_{pi} d_b}{f'_{ci}} + 10.3$	0.91	0.96
Cousins et al. (1990)	$L_t = 0.5\left(\frac{U'_t \sqrt{f'_{ci}}}{B}\right) + \frac{f_{pe} A_p}{\pi d_b U'_t \sqrt{f'_{ci}}}$	0.45	0.42
Bruggeling and Huyghe (1991)	$L_t = \frac{7 f_{pi} d_w}{12(0.13) f'_{ci}}$	0.79	0.78
Balazs (1992)	$L_t = K d_b \sqrt[5]{\frac{f_{pi}^3}{f'^2_{ci}}}$	0.80	0.86
Shahawy et al. (1992) Deatherage et al. (1994) Buckner (1995)	$L_t = \frac{f_{pi} d_b}{3}$	0.63	0.73
Mitchell et al. (1993)	$L_t = 0.33 f_{pi} d_b \sqrt{\frac{3}{f'_{ci}}}$	0.87	0.93
Russell and Burns (1996)	$L_t = \frac{f_{pe} d_b}{2}$	0.46	0.45
Tadros and Baishya (1996)	$L_t = \frac{f_{pe} d_b}{0.8(3.04)}$	0.56	0.55
Mahmoud et al. (1999)	$L_t = \frac{f_{pi} d_b}{\alpha_t f'^{0.67}_{ci}}$	0.85	0.88
Marti-Vargas et al. (2007-b)	$L_t = \frac{\psi f_{pi} A_p}{0.282 \pi d_b f'^{0.67}_{ci}}$	0.95	0.99

CHAPTER 6: DEVELOPMENT LENGTH

After completion of the final 28-day transfer length tests, the four girder specimens were transported to the Newmark Structural Engineering Laboratory at UIUC, where development length tests were conducted. Testing of the two box girders was conducted first, followed by testing of the two I-girders. At the time this thesis was composed, development length tests on the I-girders were not complete; thus, this chapter presents details only of test setup, observations, and results for the two box girder specimens. A total of four flexural tests were executed to determine the development length of strands in the box girders (see Section 2.3.7). Concrete cracking, concrete strain, deflection, and strand end-slip were monitored continuously throughout each test. Experimental results presented herein are compared to current ACI (2008) and AASHTO (2004) requirements, as well as theoretical shear and moment capacities.

6.1 THREE-POINT FLEXURAL TEST SETUP

6.1.1 Loading Frame

The structural loading frame utilized during testing was designed to apply forces up to 600 kip to the girder specimens. The loading frame components are shown in Figure 6.1, with pertinent dimensions called out in the frame plan shown in Figure 6.2 and frame elevations shown in Figures 6.3 and 6.4. The 4 built-up columns were bolted to the structural testing floor. Two pairs of channels, each with 19-in. depth, 11.13-in. flange width, and 0.625-in. web width, extended between the columns and were bolted to the columns. A 29.9-in. deep I-beam stiffened with 0.325-in. thick 36 ksi plates was oriented in the longitudinal direction of the test specimens and was attached to the channels using mechanical clamping devices.

Attached to the I-beam were two manually-controlled hydraulic rams with 300-kip capacity each. Load cells were secured to the rams' pistons by threaded rods and were protected by 0.75-in. thick aluminum caps on top and bottom. When activated, the rams pressed the load cells onto a bearing block created by adding two web plates, six bearing stiffeners, and a 1-in. thick bottom flange plate to a 24-in. long W12X58 beam, as shown in Figure 6.5. The block rested atop a 3-in. diameter rod which, in turn, rested atop a 5 in. x 2 in. x 24 in. plate, forming a pinned support at the load point as shown in Figure 6.6. For each test, a pinned support was

placed beneath the end of the girder nearest the applied load, while a roller support was placed at the opposite end. Support details are shown in Figure 6.7. The bottom bearing plates on either end were affixed to 5 ft. x 2.5 ft. x 10.5 ft. concrete reaction blocks, utilized to prevent damage to the structural testing floor. The fully assembled testing frame may be seen in Figure 6.8.

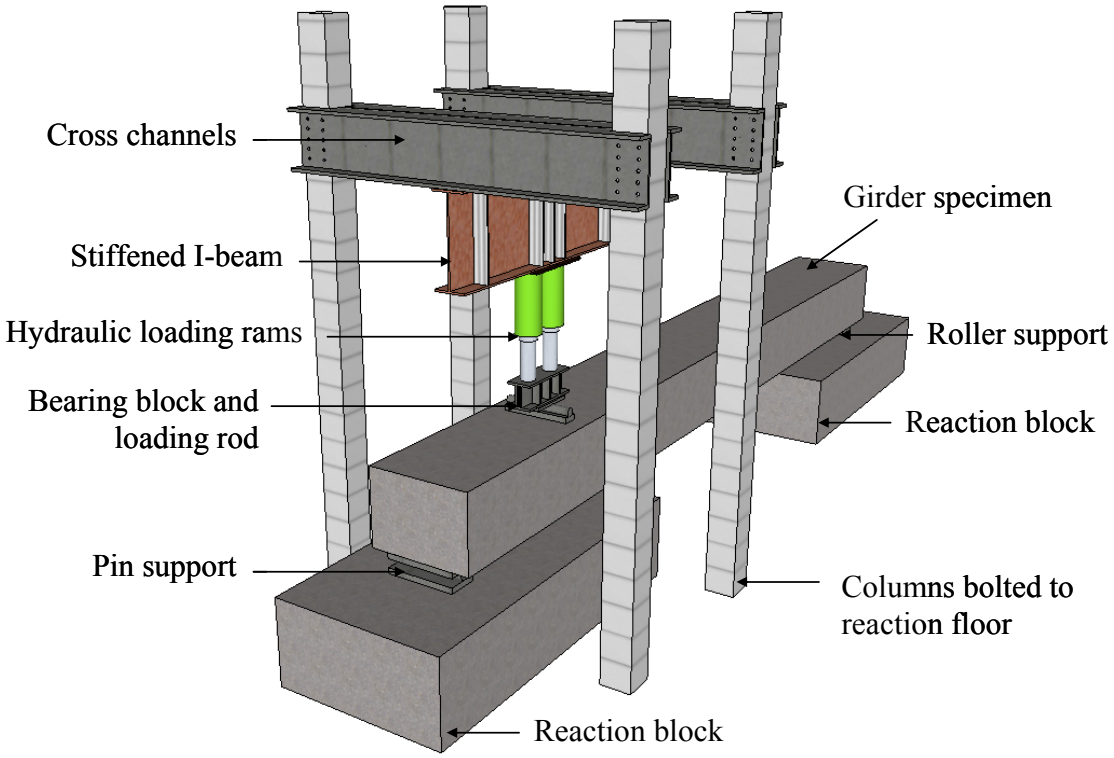

Figure 6.1: Schematic of loading frame components and assembly for flexural tests

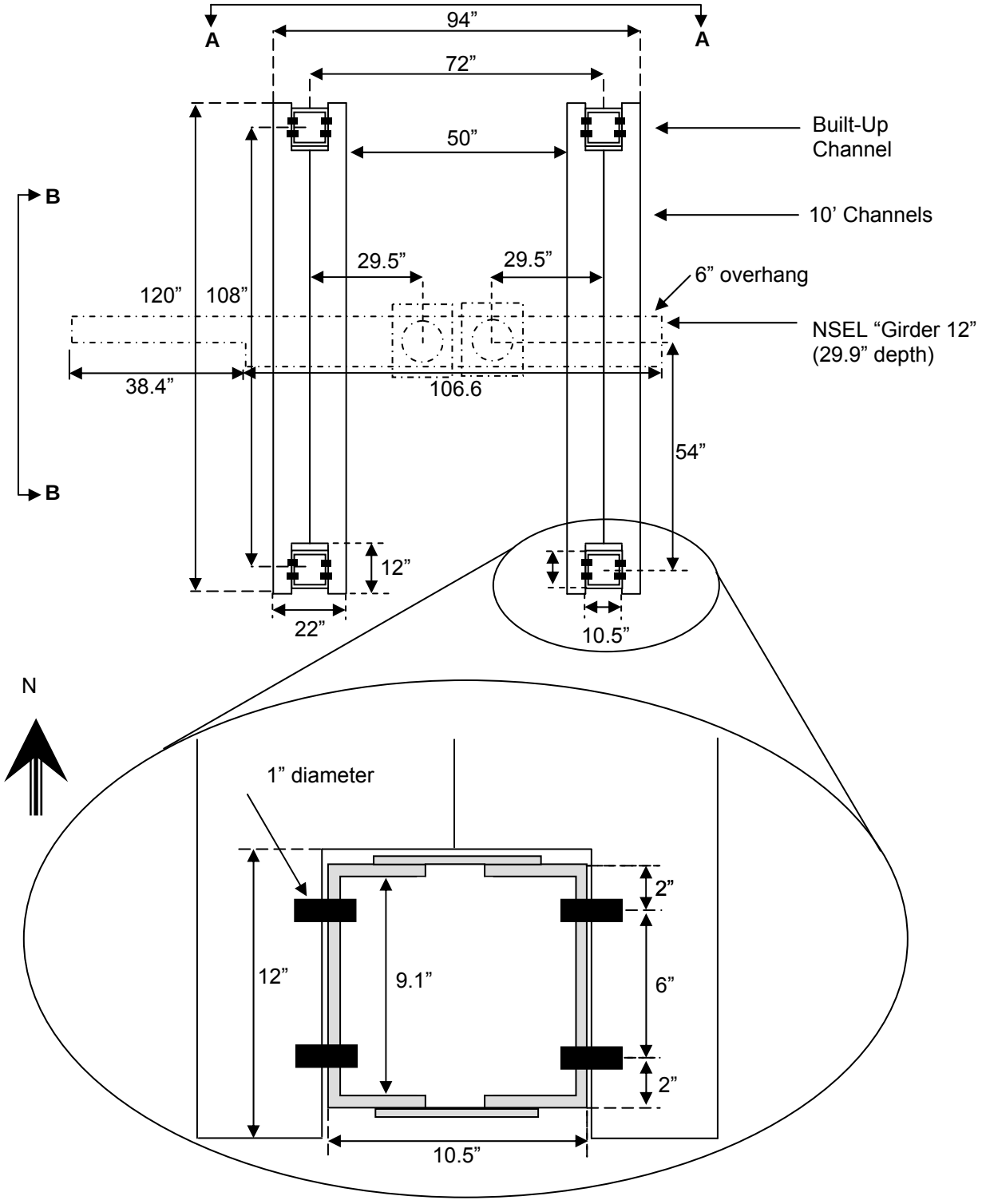

Figure 6.2: Plan of flexural test loading frame

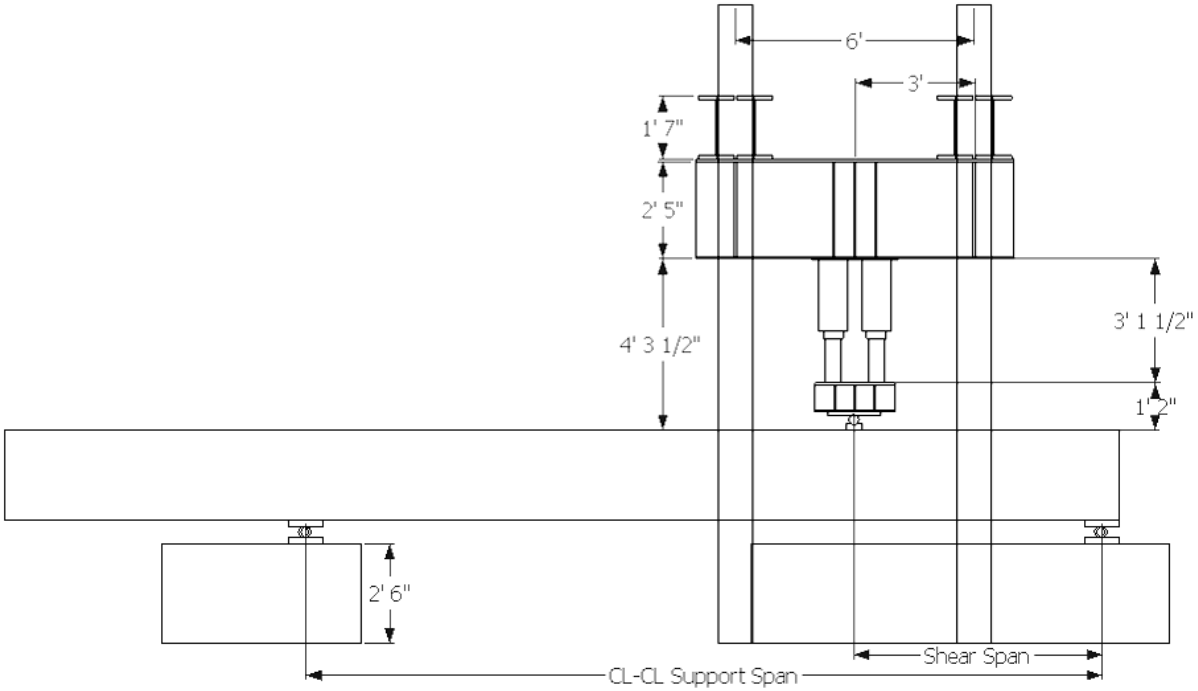

Figure 6.3: Elevation A-A of flexural test loading frame

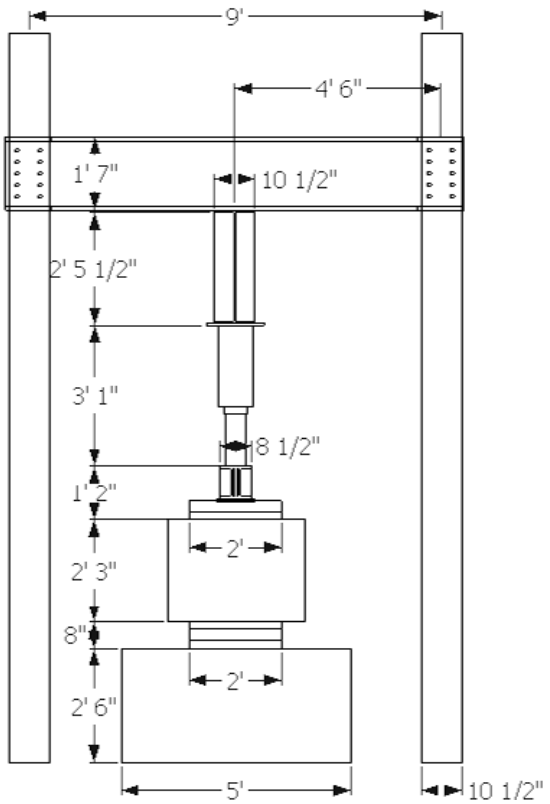

Figure 6.4: Elevation B-B of flexural test loading frame

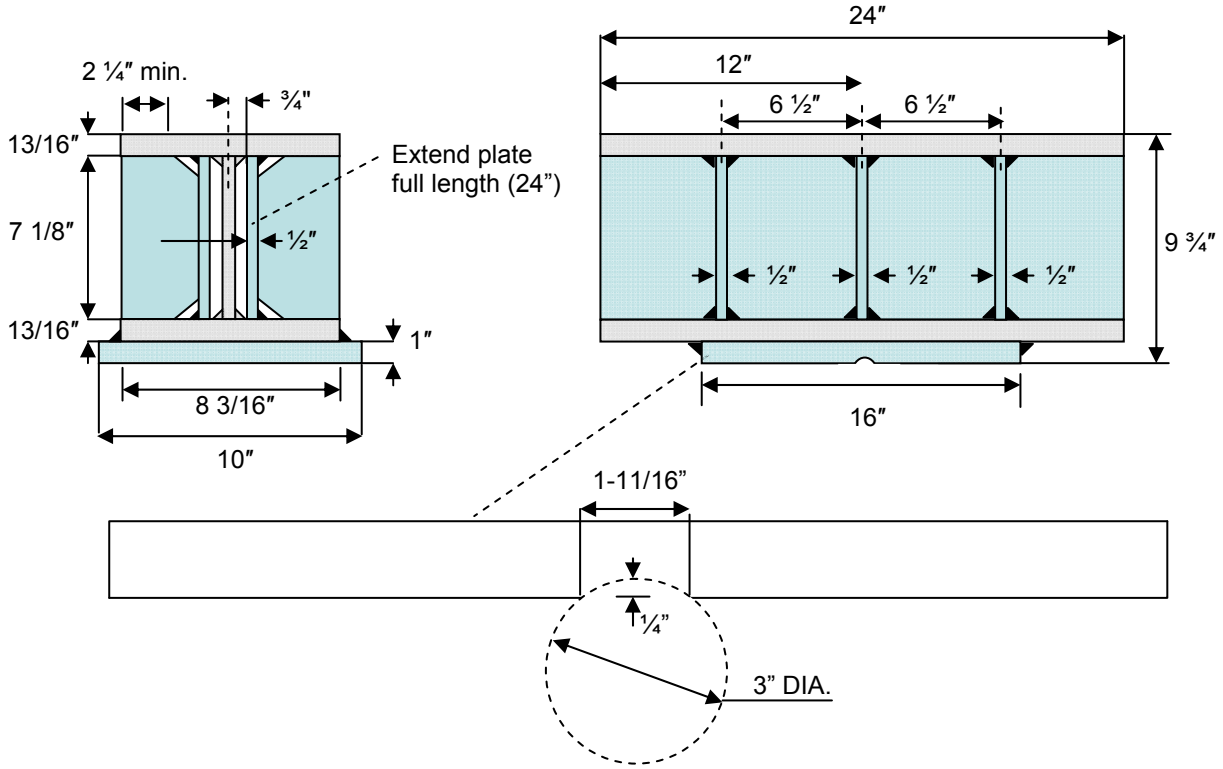

Figure 6.5: Bearing block design for flexural tests

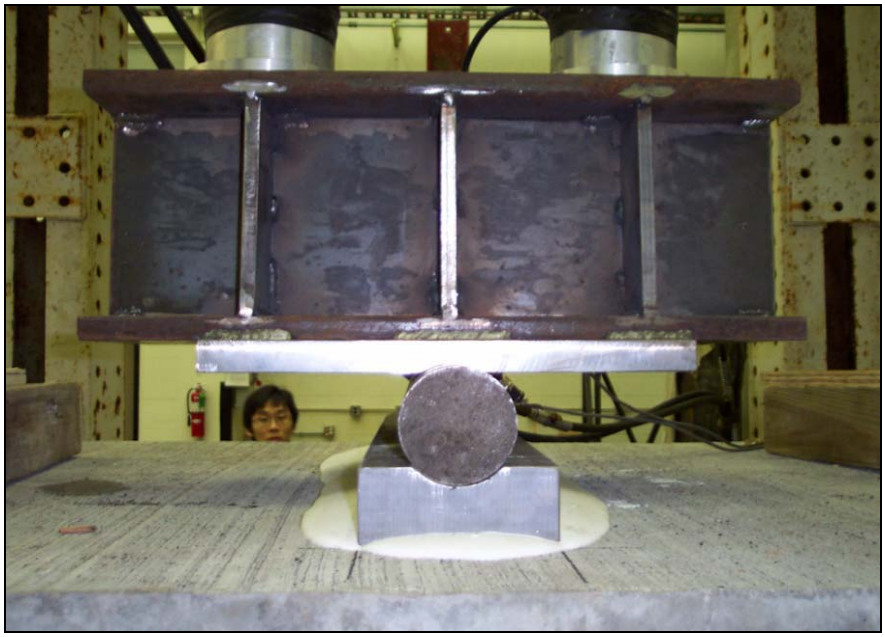

Figure 6.6: Bearing block and pinned support at point of loading

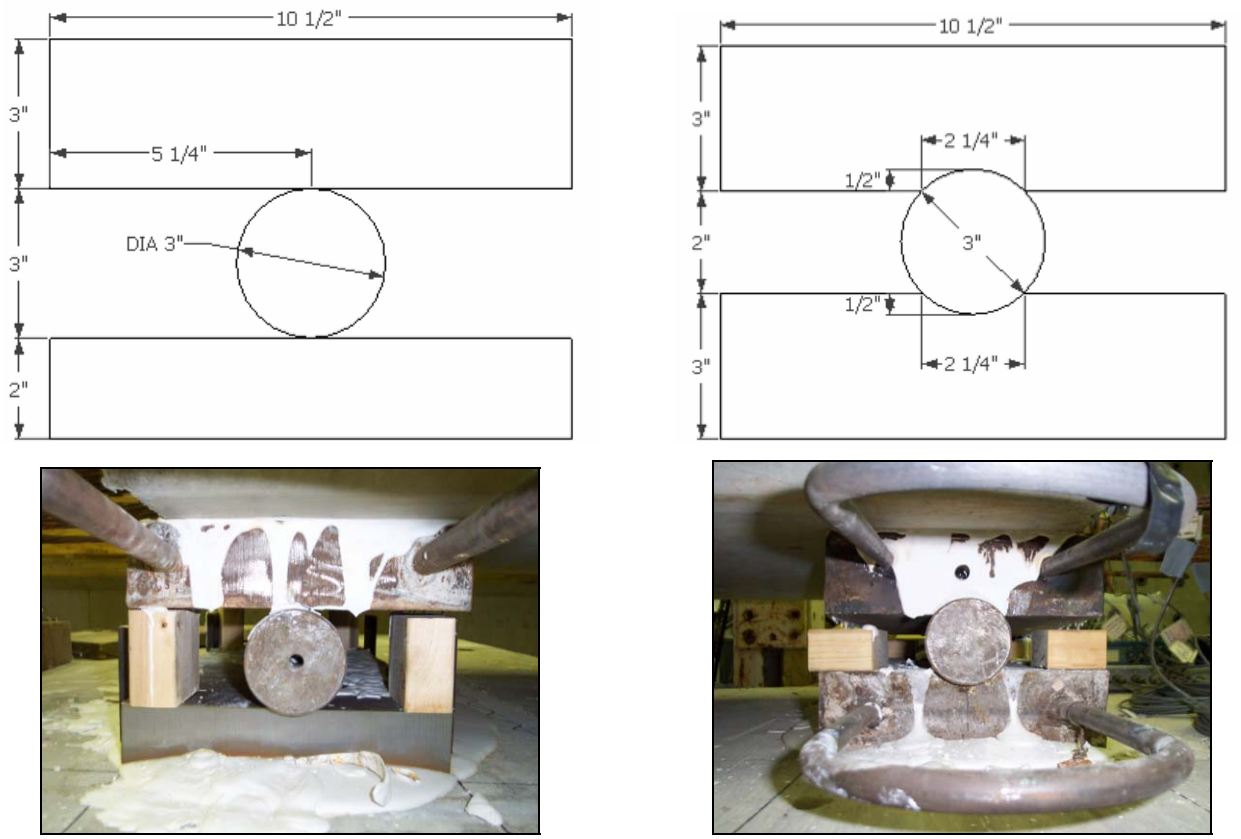

Figure 6.7: Roller (left) and pin (right) support in flexural test setup

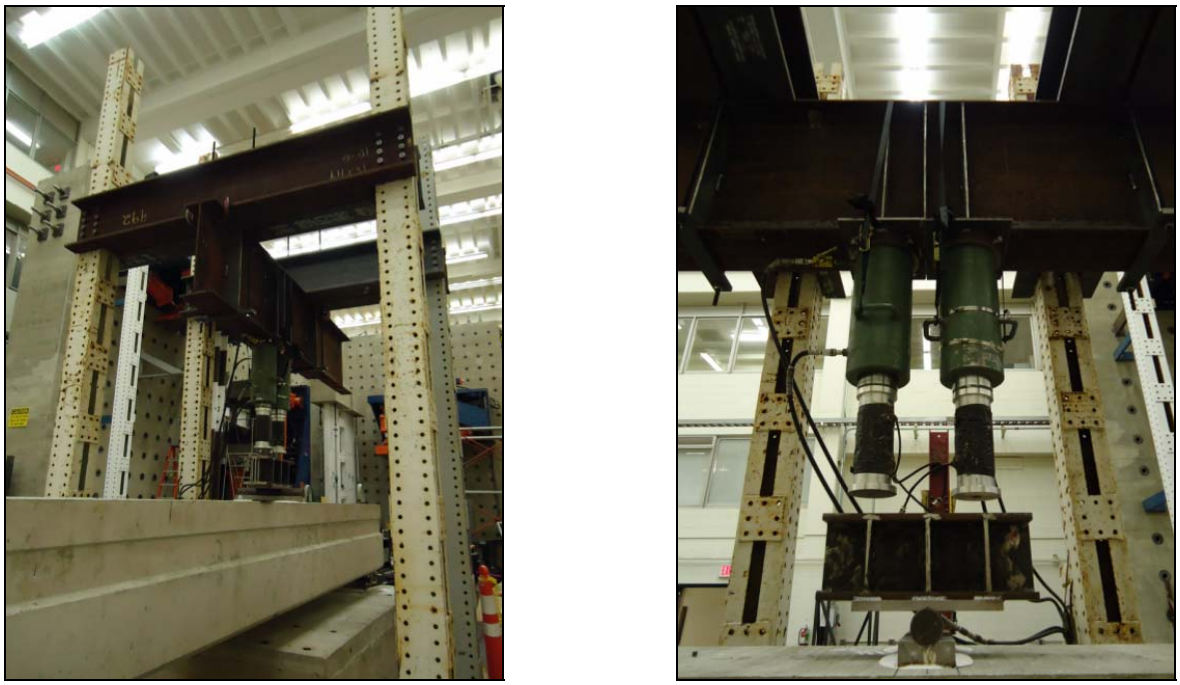

Figure 6.8: Fully assembled testing frame (left) and loading mechanism (right)

6.1.2 Instrumentation

For each test, instrumentation was set in place to measure the applied load, strand end-slip, concrete strain, and beam deflection. End-slip was continuously monitored via LVDTs attached to prestressing strands at the girder end nearest the applied load. LVDT configurations for the box girders are shown in Figure 6.9. Three LVDTs with a range of ±0.10 in. were affixed using aluminum angles and hose clamps, and five LVDTs with a range of ±0.50 in. were affixed using wooden connector pieces and hose clamps; both attachments are shown in Figure 6.10.

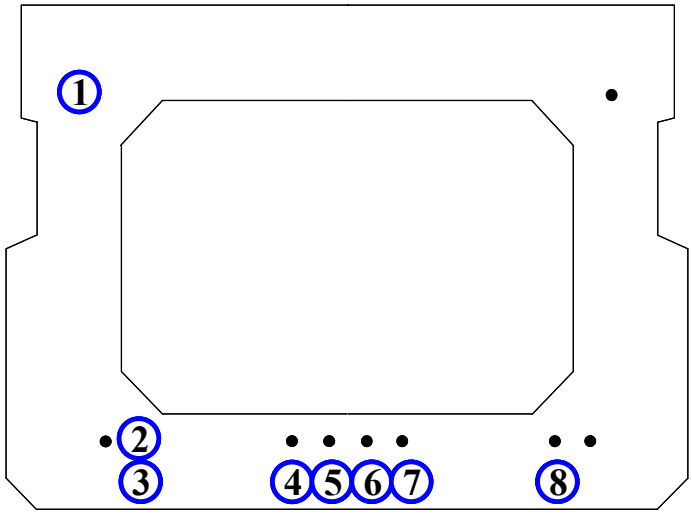

Figure 6.9: End-slip LVDT configuration for box girder tests

Figure 6.10: Spring-loaded ±0.10 in. (left) and guided ±0.50 in. (right) LVDTs

All tests utilized concrete surface strain gauges to obtain experimental strain profiles under the point of loading. The gauge type was model PL-90-11-5LT from Texas Measurements, Inc., with gauge length of 3.54 in. and a 2% strain limit. The position of the surface strain gauges are shown in Figure 6.11. To attach each gauge, the appropriate concrete area was first roughened to a fine sandpaper finish and cleaned. Then, a primary layer of polyester adhesive was applied to the concrete; a flat plastic tab was gently pressed onto the adhesive and set in place overnight. Once the polyester coating had hardened, the plastic tab was removed and the gauge was mounted to the flat surface with cyanoacrylate epoxy.

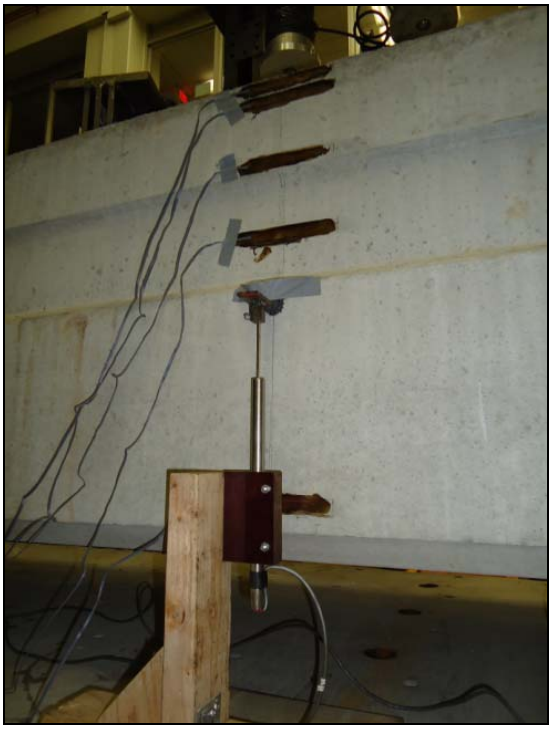

Figure 6.11: Concrete surface strain gauges and LVDT under point of loading

Vertical deflection was measured at two locations during each test. The point directly beneath the applied load was monitored with an LVDT with ±3 in. range; it was attached to the beam as shown in Figure 6.11. Deflection of the specimen at the midpoint between supports was also monitored with an LVDT with ±3 in. range; it was attached to the beam as shown in Figure 6.12. All instruments were connected via wire transducers to a 32-channel data logger.

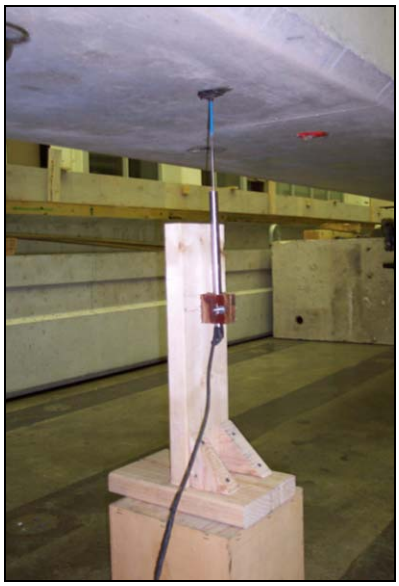

Figure 6.12: LVDT attached to specimen at midpoint between supports

As previously mentioned, 300-kip capacity load cells were attached to both hydraulic cylinders to continuously monitor the applied load throughout testing. Load cells had outer diameters of 4.723 in. and reached maximum capacity at 10,000 psi. The aluminum adapter pieces between the pistons and load cells were 0.75-in. thick and had 5.5-in. outer diameters. The aluminum caps between the load cells and bearing block were also 0.75-in. thick and had 6-in. outer diameters to increase bearing area on the block.

6.2 DEVELOPMENT LENGTH TESTS

Each 28-ft. box girder was tested twice under three-point bending. Strand embedment for each test was controlled by varying the location of bearing supports relative to the loading frame, which remained stationary and bolted to the reaction floor. For a girder's first test, the supports shown in Figure 6.7 were nearly flush with the girder ends; thus, centerlines of the bearing plates were 5.25 in. to 6 in. from specimen edges. After the first test, the partially damaged specimen was removed from the testing frame and rotated 180 degrees. The reaction block furthest from the loading frame was shifted to prevent the damaged portion of the specimen from bearing on the support. Finally, the girder was placed under the loading frame for a second flexural test. The location of the supports and point of loading for each box girder test are shown in Figure 6.13.

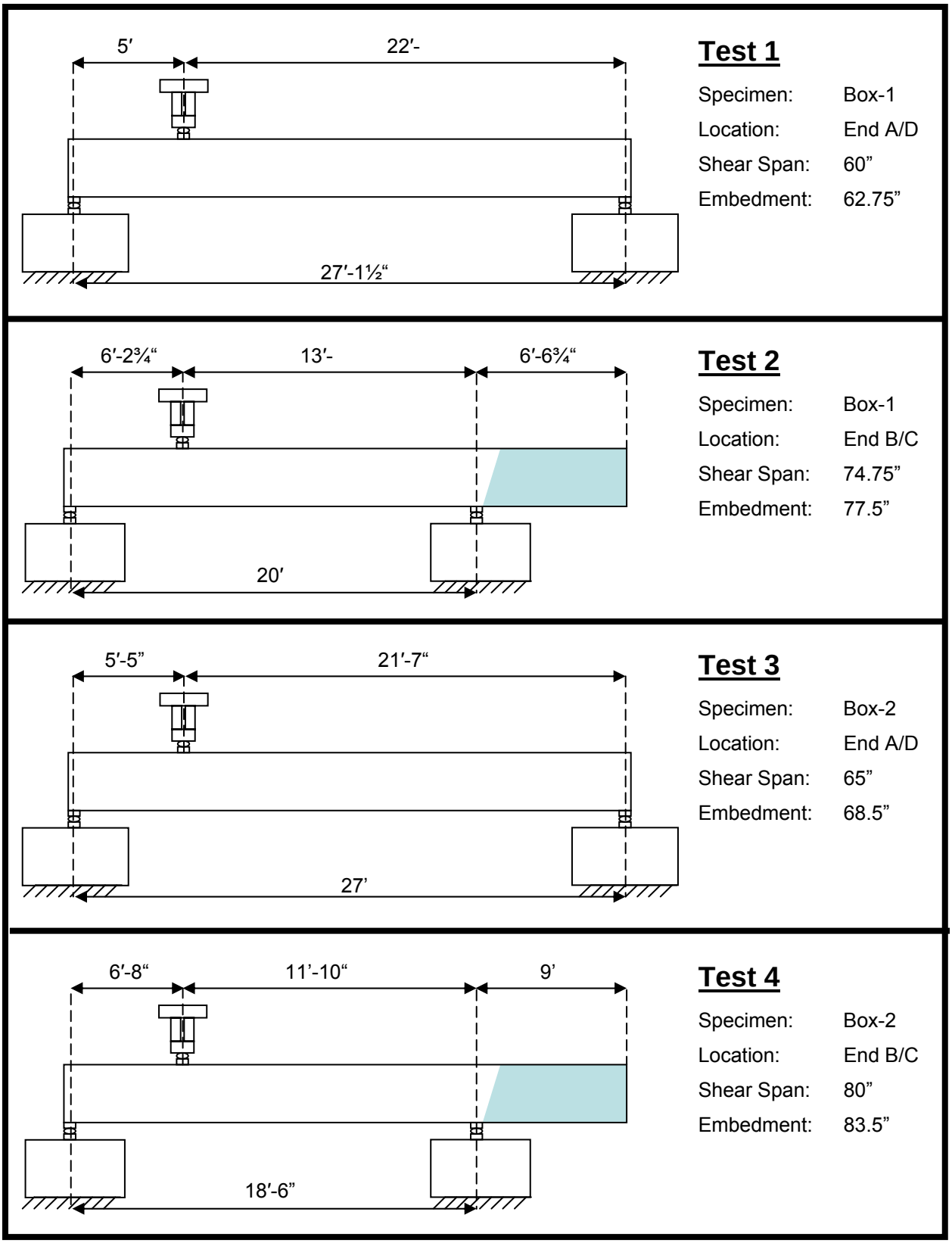

Figure 6.13: Support and load positions for all box girder tests (not to scale)

An electric pump was utilized to advance the two hydraulic rams until the bottom caps of the load cells were in contact with the bearing block. To afford better control throughout testing, the rams were disconnected from the electric pump and reconnected to a manual pump; both the electric and manual pumps had 10,000 psi capacity. The hydraulic system was connected in parallel to ensure each ram advanced at the same rate. The rams were advanced continuously until the applied load was within 50 kips of the load predicted to cause flexural cracking. Then, specimens were loaded in increments of 3 kips. Once cracking initiated, time was allotted between load steps to monitor crack formation and allow load to settle.

Care was taken to monitor end-slip, cracking patterns, and load resistance to determine the most probable failure mode in each test. Shear failure was characterized by prominent diagonal cracking within the shear span and abrupt decreases in load capacity. Flexural failure was characterized by symmetric cracking about the point of load, concrete crushing and high strain in the compression flange under the applied load. Constant load resistance and steadily increasing strand end-slip were indicative of bond failure. When embedment in a specimen approaches the development length, the specimen may display characteristics of more than one failure mechanism; such behavior may be termed flexure-shear, flexure-slip, or shear-slip failure. Tests were stopped once a dominant failure mechanism was evident.

6.2.1 Flexural Test 1: Specimen Box-1, South End (A/D)

The first development length test was performed on the south end of specimen Box-1 (refer to Figure 4.3). The date of testing was April 12, 2010; 229 days after casting. The total centerline-to-centerline (CL-to-CL) distance between supports was 27.125 ft. The beam was placed under the loading frame such that the shear span, or distance between the CL of loading and CL of the pinned support, was 5 ft. The embedment was taken as the distance from the beam end to the face of the loading plate; in this case, 62.75 in. The chosen embedment was approximately 12 in. less than the predicted development length.

The loading protocol for the test was described in Section 6.2. The first visible cracks, both shear and flexural, occurred at an applied load of 165 kip. Shear cracking became dominant at 176 kip, after which flexural cracks did not significantly widen. The maximum resisted load was 197.4 kip; including the moment due to self-weight, this corresponds to a maximum

experimental moment of 841.1 kip-ft. The load-deflection response for the specimen is shown in Figure 6.14. The flexural cracking observed visually corresponded well with the onset of nonlinear behavior in the figure. Deflection at the point of loading was 0.47 in. when the peak load was reached; however, the maximum deflection at the conclusion of the test was 0.76 in.

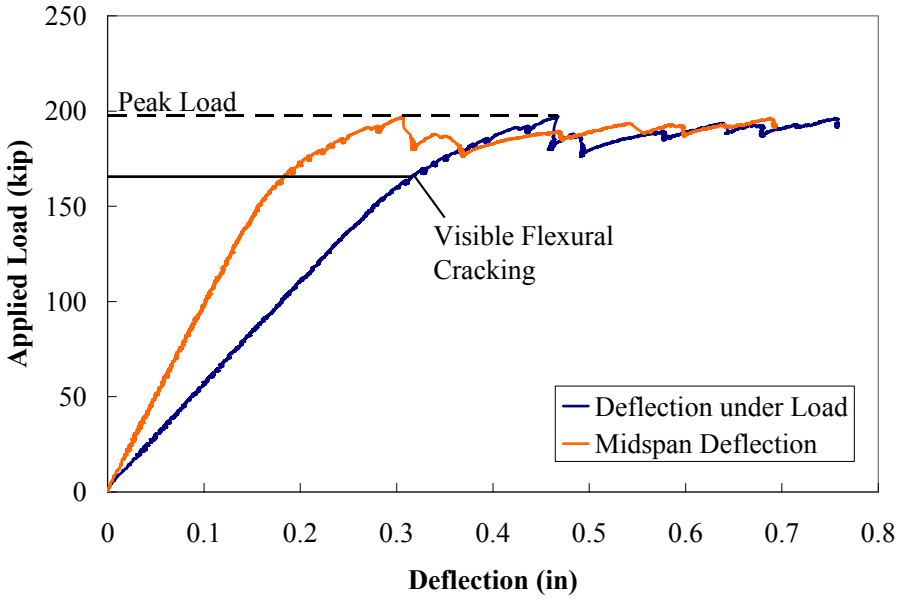

Figure 6.14: Load-deflection response for Box-1, South End

The final cracking pattern for the first test may be seen in Figures 6.15 through 6.18. Only three flexural cracks formed throughout the test. Two primary shear cracks formed in the web and propagated diagonally upward toward the point of loading and downward toward a point 30 in. from the end of the specimen, where the hollow within the beam ends. Strand slip occurred only after shear cracks had propagated across the strands in the tension flange. It is important to note that crack propagation across the strands effectively shortened the embedment length. In Figure 6.19, end-slip is plotted with respect to the applied load for the strand which slipped furthest into the girder. The term "significant shear cracking" in the figure refers to the load at which shear became the prominent failure mode. The end-slip responses of all strands in the girder are shown in Figure F.1 through Figure F.8 in Appendix F. Though the beam remained capable of resisting load, the test was stopped when end-slip of bottom strands exceeded 0.2 in. The maximum end-slip values for individual strands are shown in Table 6.1.

Figure 6.15: Crack pattern for Box-1, South End, Side A

Figure 6.16: Primary shear cracking for Box-1, South End, Side A

Figure 6.17: Crack pattern for Box-1, South End, Side D

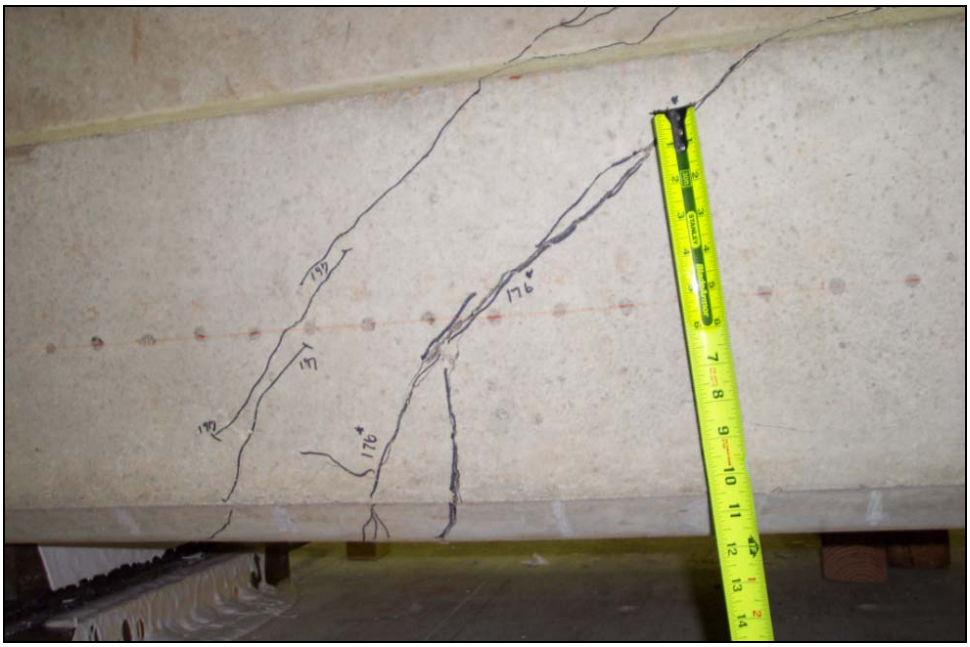

Figure 6.18: Primary shear cracks for Box-1, South End, Side D

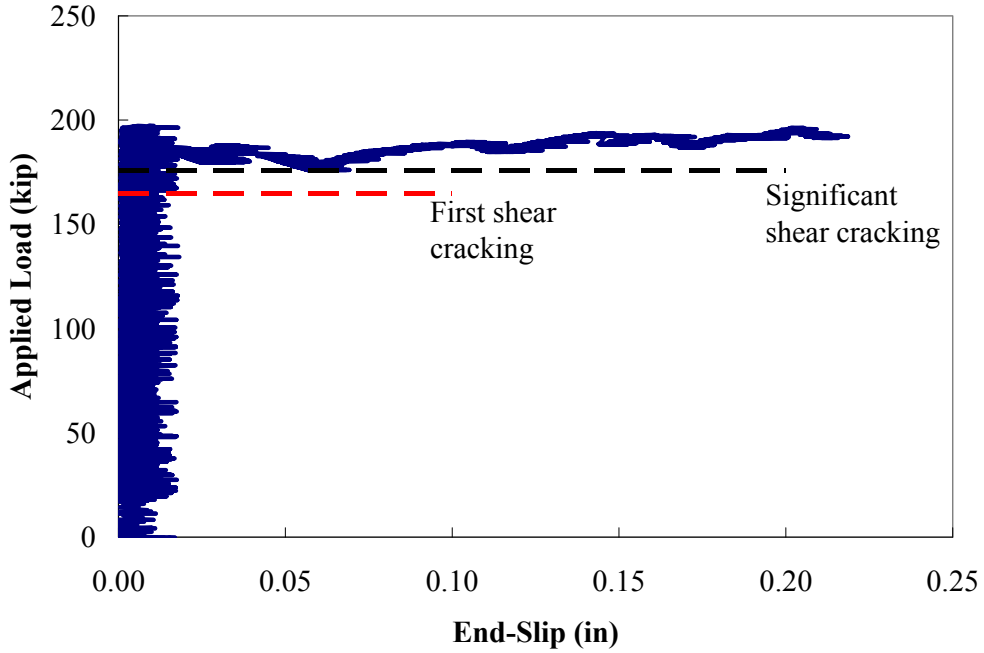

Figure 6.19: End-slip response of strand with greatest total slip (#7) for Box-1, South End

Table 6.1: Maximum End-Slip of Individual Strands for Box-1, South End

Strand	End-Slip (in)
1	0.017
2	0.209
3	0.194
4	0.191
5	0.212
6	0.208
7	0.219
8	0.167
Bottom Strands	**0.198**
Outer Strands (3 & 8)	**0.180**
Center Strands (4-7)	**0.207**

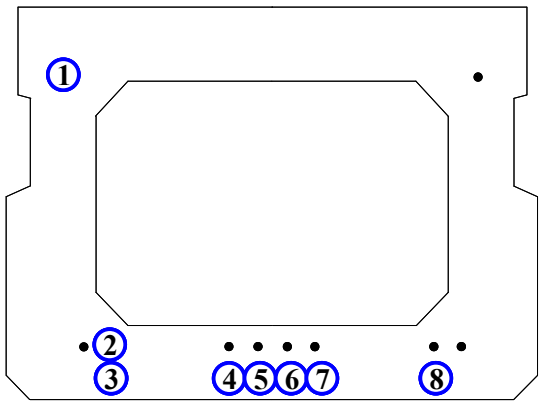

The longitudinal strain was monitored throughout the test at 5 locations under the point of loading. The strain output, adjusted for the initial strain in the concrete due to self-weight and the effective prestress, is shown in Figure 6.20. The distances listed in the legend indicate the location of each strain gauge with respect to the bottom fiber of the beam. Using a linear strain assumption, the maximum compressive strain at the top concrete fiber was 942 microstrain.

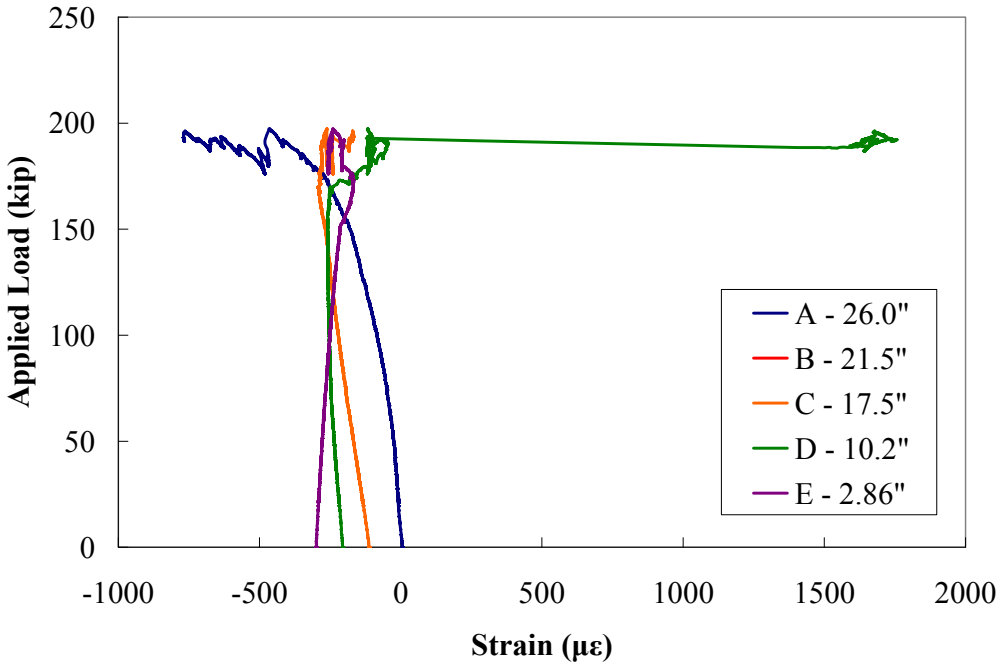

Figure 6.20: Longitudinal strains under loading for Box-1, South End

6.2.2 Flexural Test 2: Specimen Box-1, North End (B/C)

The second development length test was performed on the north end of specimen Box-1 (refer to Figure 4.3). The date of testing was April 26, 2010; 243 days after casting. The total CL-to-CL distance between supports was 20 ft. The beam was placed under the loading frame such that the shear span was 6.23 ft. The 77.5 in. embedment for this iteration was selected based on the obvious shear failure observed in the first test.

The first visible flexural cracks occurred at an applied load of 149 kip. The behavior of the beam remained heavily flexural until shear cracking initiated under 218-kip loading. The specimen reached a peak load of 227 kip; including the moment due to self-weight, this corresponds to a maximum experimental moment of 995.7 kip-ft. The load-deflection response for the specimen is shown in Figure 6.21. As shown in the figure, after reaching the maximum load, resistance declined due to flexural cracking, shear cracking, and strand-slip. The hydraulic rams were pushed downward, though the beam could not again attain the maximum load; the specimen failed abruptly in shear at a load of 218 kip. Deflection under the point of loading was 0.85 in. at the peak load; however, the maximum deflection at failure was 1.41 in.

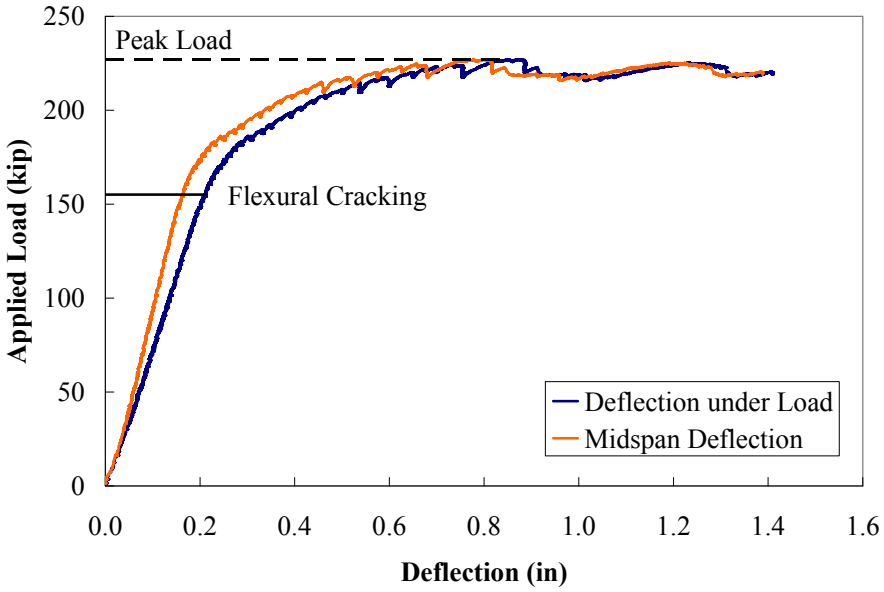

Figure 6.21: Load-deflection response for Box-1, North End

The flexural cracking pattern is clearly visible in Figure 6.22, which shows Side C of the specimen immediately prior to failure. Figure 6.23 shows the same location after abrupt shear failure occurred in the following load step. Figure 6.24 and Figure 6.25 show the ultimate damage on Side B of the specimen, including cracking under the point of loading. As in the first trial, the primary shear crack extended from the point of loading to the point where the hollow within the beam terminates. Had the beam's shear capacity been sufficient for the laboratory test loading condition, the specimen would likely have failed in flexure at an embedment of 77.5 in. Akin to the behavior observed in the first test, strand slip occurred only after a shear crack had propagated across the strands in the tension flange. In Figure 6.26, end-slip is plotted with respect to the applied load for the strand which slipped furthest into the girder. The end-slip responses of all strands in the girder are shown in Figure F.9 through Figure F.16 in Appendix F. The maximum end-slip values for individual strands are shown in Table 6.2.

Figure 6.22: Crack pattern immediately prior to failure for Box-1, North End, Side C

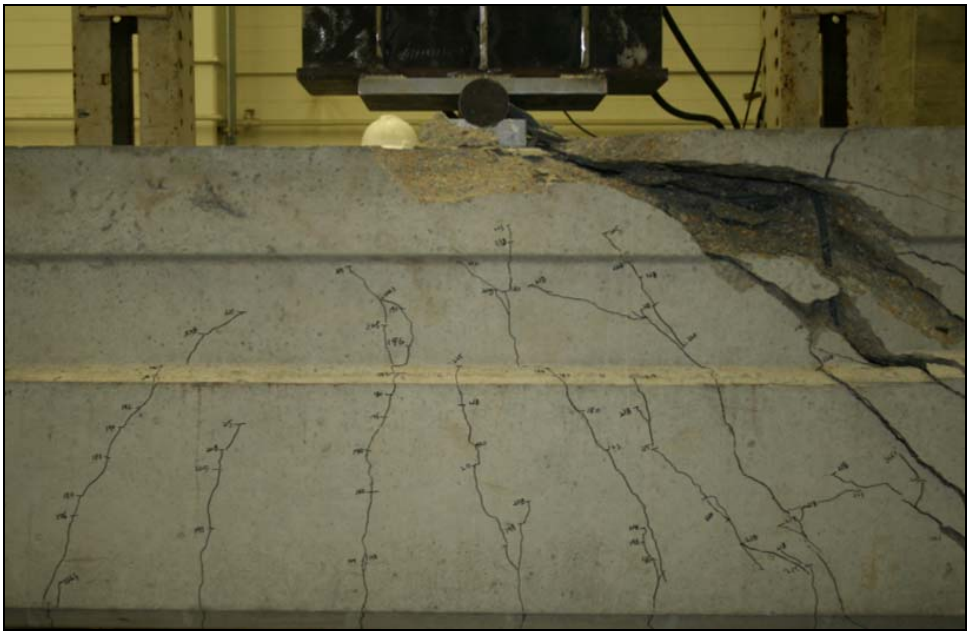

Figure 6.23: Crack pattern after failure for Box-1, North End, Side C

Figure 6.24: Primary shear crack for Box-1, North End, Side B

Figure 6.25: Concrete crushing at the face of the loading plate for Box-1, North End, Side B

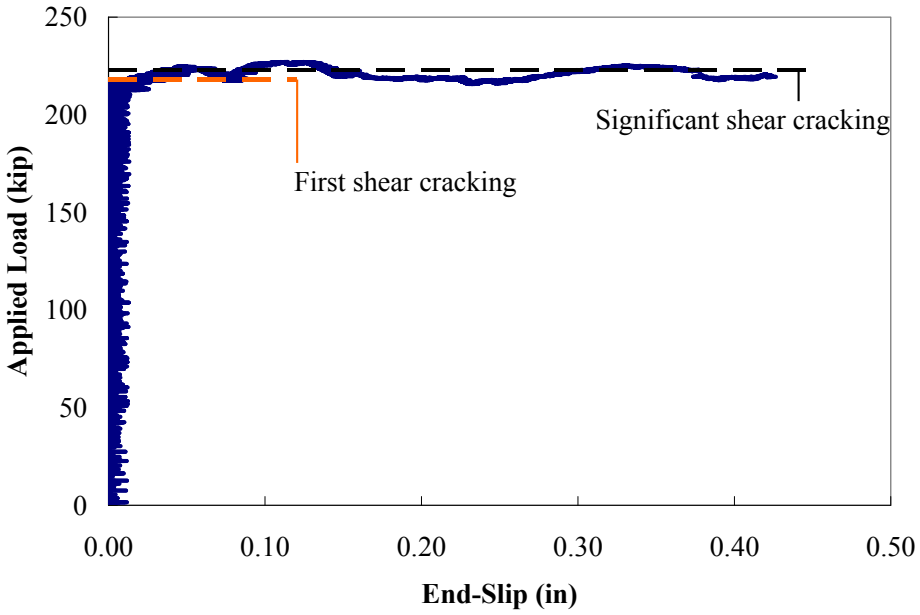

Figure 6.26: End-slip response of strand with greatest total slip (#5) for Box-1, North End

Table 6.2: Maximum End-Slip of Individual Strands for Box-1, North End

Strand	End-Slip (in)
1	0.001
2	0.229
3	0.241
4	0.406
5	0.427
6	0.354
7	0.425
8	0.367
Bottom Strands	**0.370**
Outer Strands (3 & 8)	**0.304**
Center Strands (4-7)	**0.403**

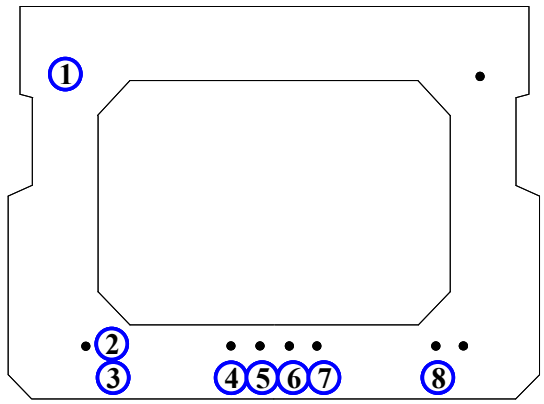

The longitudinal strain was monitored throughout the test at 5 locations under the point of loading. The strain output, adjusted for the initial strain in the concrete due to self-weight and the effective prestress, is shown in Figure 6.27. The distances listed in the legend indicate the location of each strain gauge with respect to the bottom fiber of the beam. Using a linear strain assumption, the maximum compressive strain at the top concrete fiber was 2257 microstrain.

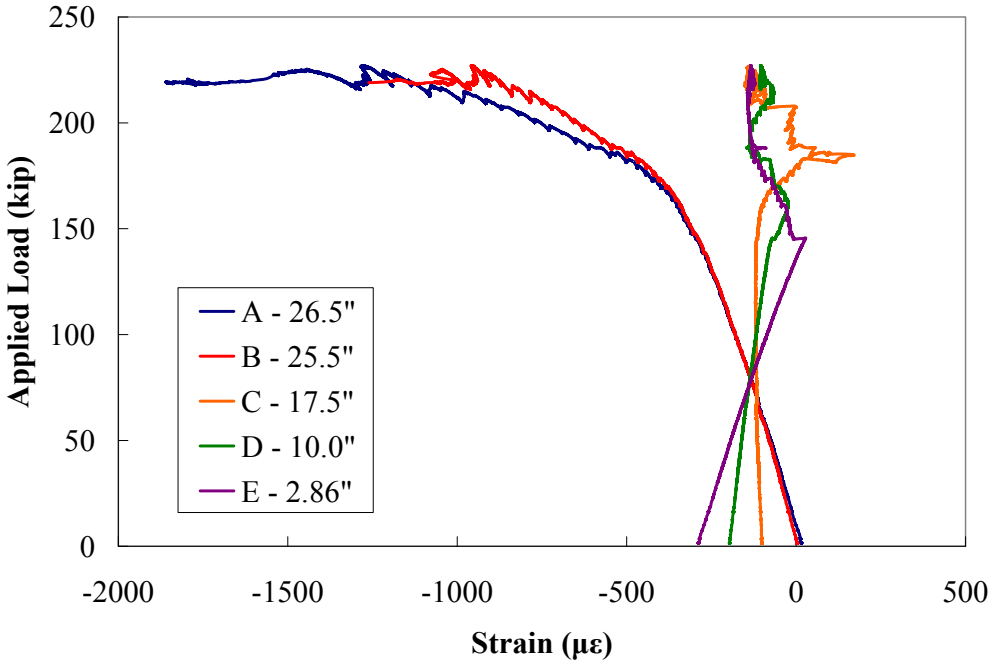

Figure 6.27: Longitudinal strains under loading for Box-1, North End

6.2.3 Flexural Test 3: Specimen Box-2, South End (A/D)

The third development length test was performed on the south end of specimen Box-2 (refer Figure 4.3). The date of testing was June 21, 2010; 299 days after casting. The total CL-to-CL distance between supports was 27 ft. The beam was placed under the loading frame such that the shear span was 5.42 ft. and the embedment was 68.5 in. As discussed in Section 4.7, an external CFRP wrap was placed around an 18-in. wide section of the beam to provide additional shear reinforcement. It was anticipated that the beam's shear capacity would then be sufficient to withstand the reaction required to reach the theoretical moment capacity; hence, the selected embedment was less than the predicted development length and the previous test's embedment.

Two unforeseen complications during the third test hindered the acquisition of digital data. The same loading protocol was followed as in the previous two tests; however, at an applied load of 184 kip, the manual pump advancing the hydraulic rams failed to develop any further pressure in the system. It was later determined that the pump's oil had unknowingly been depleted. The beam was unloaded, the data acquisition system was stopped, and the rams were disconnected from the manual pump. In order to proceed with the third test on the same day, the

rams were reconnected to an electric pump. The test was restarted (trial 2) using the same loading protocol as before. At the conclusion of the test, however, it was discovered that the data acquisition system had failed to record anything during this second trial. Later, it was determined that an internal limit within the data logger's code had been exceeded, preventing it from saving the data file despite successfully monitoring and displaying data throughout the test. As a result of these complications, no end-slip or strain readings from the second trial of test three are represented graphically, and all data reported for loads greater than 184 kip was obtained through visual observation and notes taken during the test.

The first visible flexural cracks occurred at an applied load of 149 kip. At an applied load of 188 kip, shear cracking initiated and was accompanied by "popping" noises generated by local de-bonding of the CFRP. Initial de-bonding occurred in the web of the beam. By the time the load had reached 208 kip, a portion of the CFRP had become fully delaminated from the side of the specimen, as seen in Figure 6.28. Also, from notes taken during the 208-kip load step, the strain gauge nearest the top of the beam had reached a value of 2040 microstrain. The specimen failed abruptly in shear at a maximum load of 217 kip; including the moment due to self-weight, this corresponds to a maximum experimental moment of 977.6 kip-ft. At failure, the CFRP on one side of the beam completely de-bonded after breaking at the corner of the beam; CFRP on the opposite side de-bonded only across the web. Both CFRP failures are shown in Figure 2.29. For reference, the load-deflection response for the test prior to 184 kip is shown in Figure 6.30.

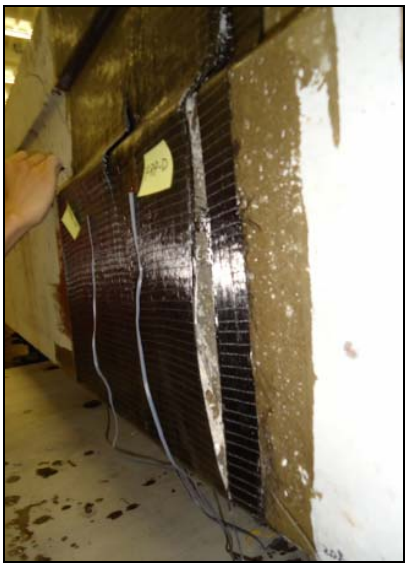

Figure 6.28: Portion of CFRP entirely de-bonded from Side D of Box-2

Figure 6.29: Final CFRP failure at Side D (left) and Side A (right) of Box-2

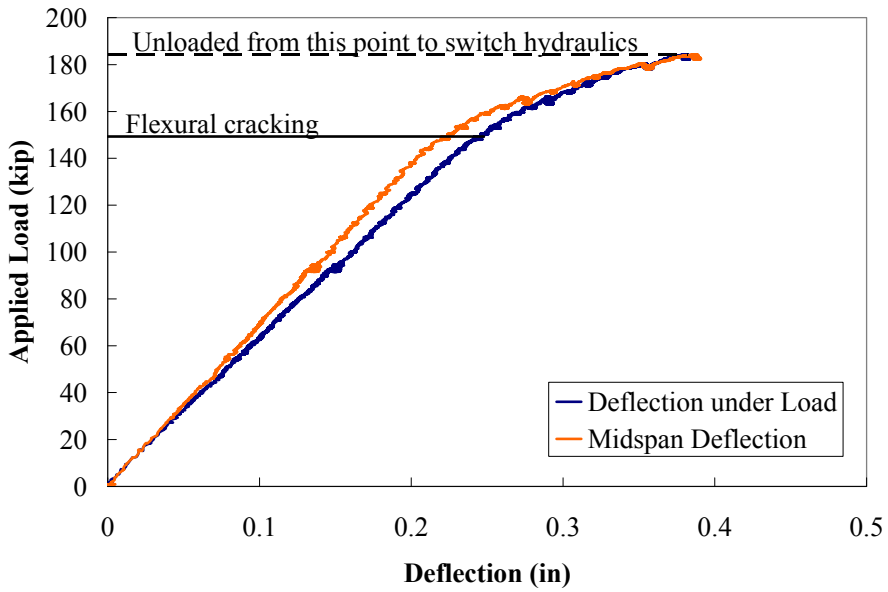

Figure 6.30: Partial load-deflection response for Box-2, South End

The final cracking pattern for the third test may be seen in Figures 6.31 and 6.32. While significant flexural cracks had developed, the ultimate failure mode paralleled what had been observed in the first two tests. In this case, however, the specimen was able to sustain considerable additional load past the point when shear cracking became prevalent. The external CFRP acted in tension to effectively confine the concrete when diagonal cracking would normally tend to split the specimen. Only when the CFRP failed did the specimen fail. As before, strand slip occurred only after shear cracks had propagated across the strands in the tension flange; however, exact end-slip data is unavailable for loads greater than 184 kip.

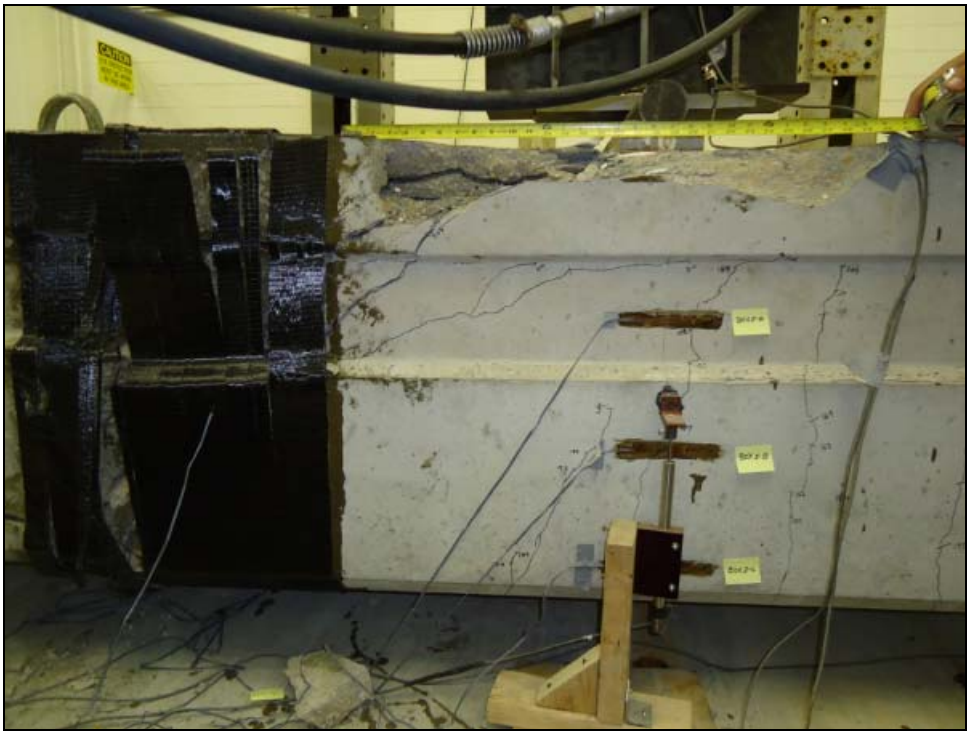

Figure 6.31: Crack pattern after failure for Box-2, South End, Side D

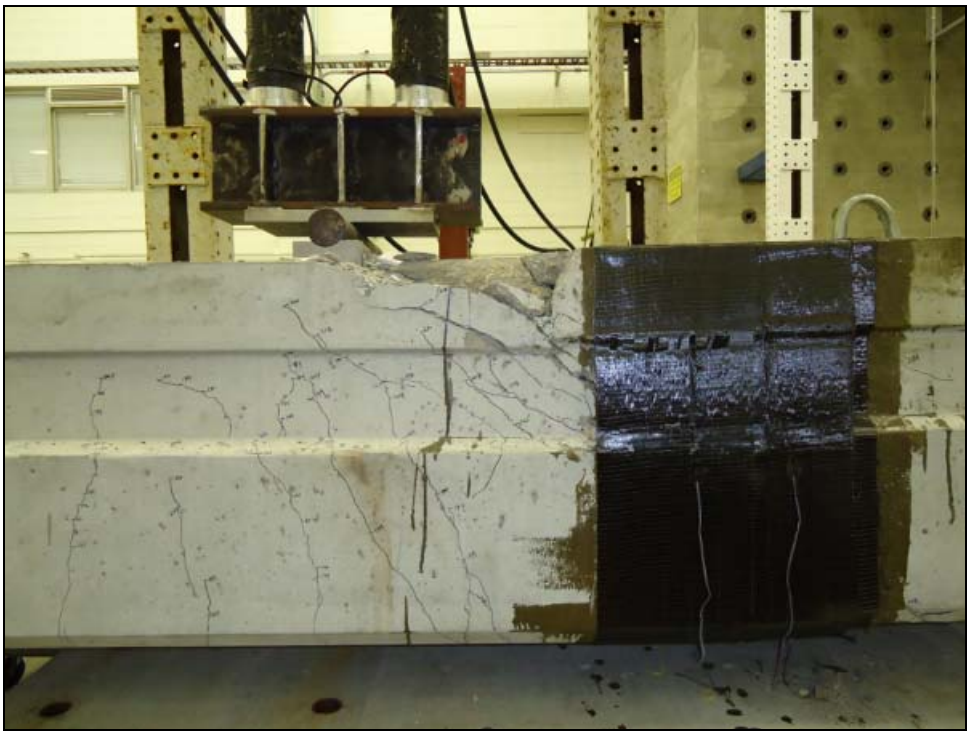

Figure 6.32: Crack pattern after failure for Box-2, South End, Side A

6.2.4 Flexural Test 4: Specimen Box-2, North End (B/C)

The fourth and final box girder development length test was performed on the north end of specimen Box-2 (refer to Figure 4.3). The date of testing was June 30, 2010; 308 days after casting. The total CL-to-CL distance between supports was 18.5 ft. The beam was placed under the loading frame such that the shear span was 6.67 ft. and embedment was 83.5 in. No external CFRP was utilized in this test since analysis predicted the beam's shear capacity could withstand the reaction produced with the given shear span.

The first visible flexural cracks occurred at an applied load of 161 kip, and shear cracking did not initiate until 235 kip. This specimen was not loaded until failure; rather, it was loaded until the induced moment exceeded the beam's theoretical moment capacity. The maximum applied load was 253 kip; including the moment due to self-weight, this corresponds to a maximum experimental moment of 1095 kip-ft. The load-deflection response for the specimen is shown in Figure 6.33. The maximum deflection under the point of loading was 0.94 in.

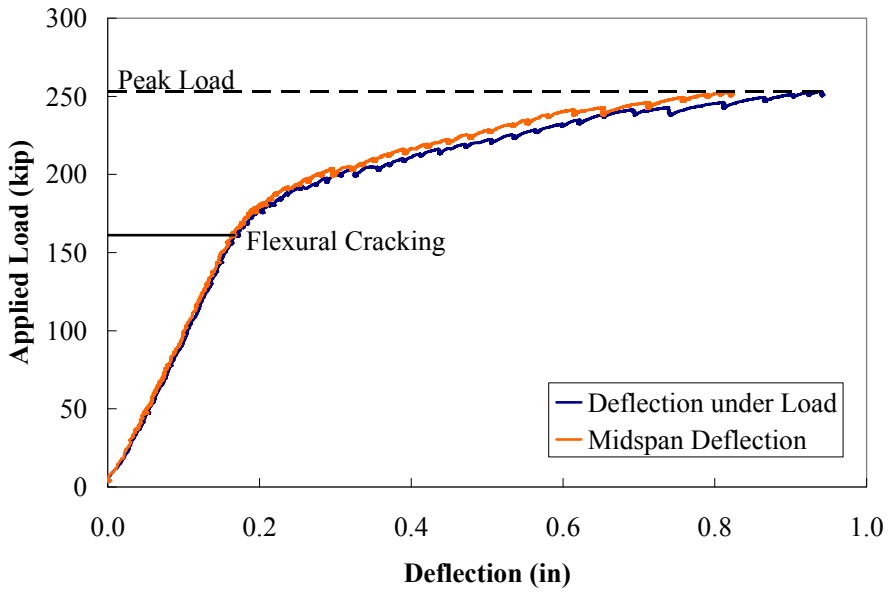

Figure 6.33: Load-deflection response for Box-2, North End

The final cracking pattern for the fourth box girder test may be seen in Figure 6.34 and Figure 6.35. As the figures show, cracking followed a flexural failure pattern and was symmetric about the point of loading. The one significant shear crack was observed only on one side of the beam (see Figure 6.35). The end-slip recorded for this test was minimal, even after the shear crack had propagated across through the tension flange. In Figure 6.36, end-slip is plotted with respect to the applied load for the strand which slipped furthest into the girder. End-slip responses of all eight strands in the girder are shown in Figure F.17 through Figure F.24 in Appendix F. The maximum end-slip values for individual strands are listed in Table 6.3.

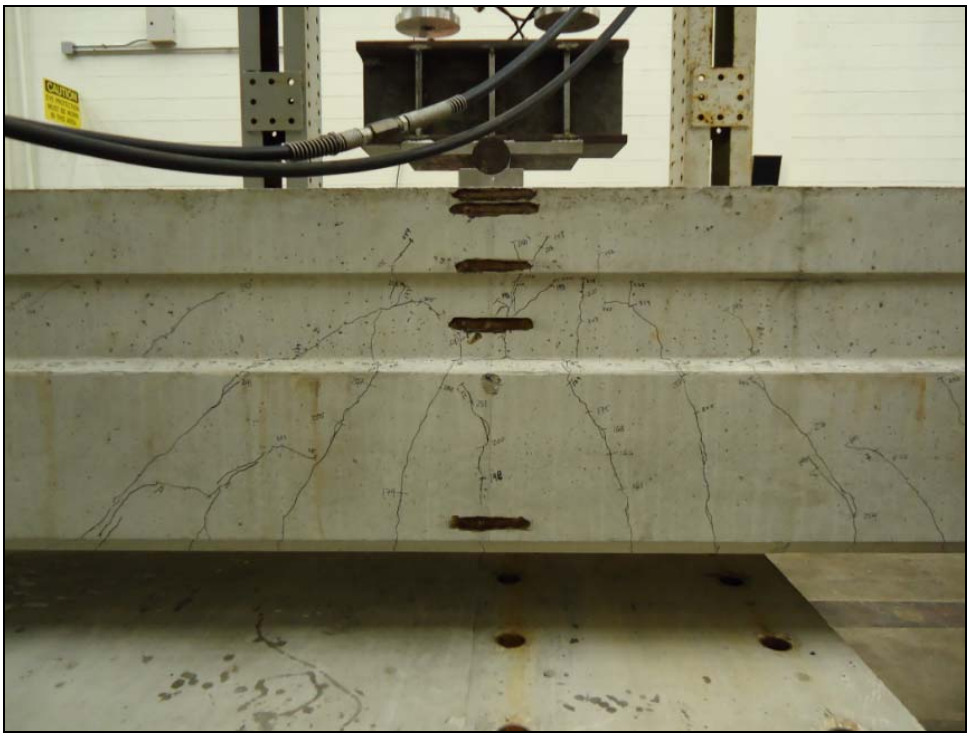

Figure 6.34: Crack pattern for Box-2, North End, Side B

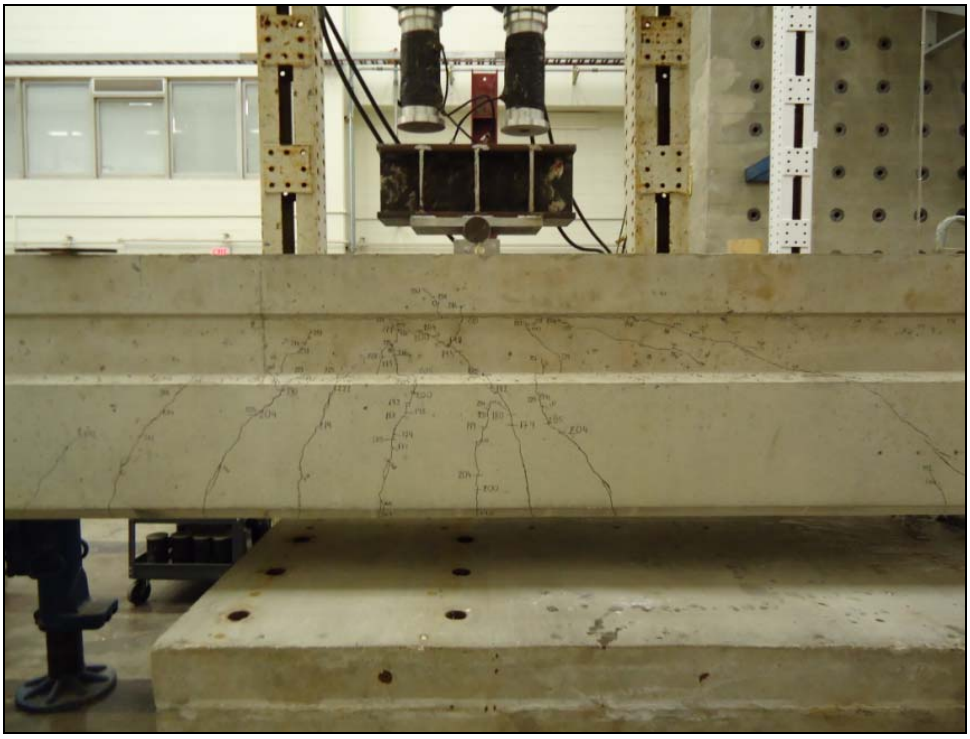

Figure 6.35: Crack pattern for Box-2, North End, Side C

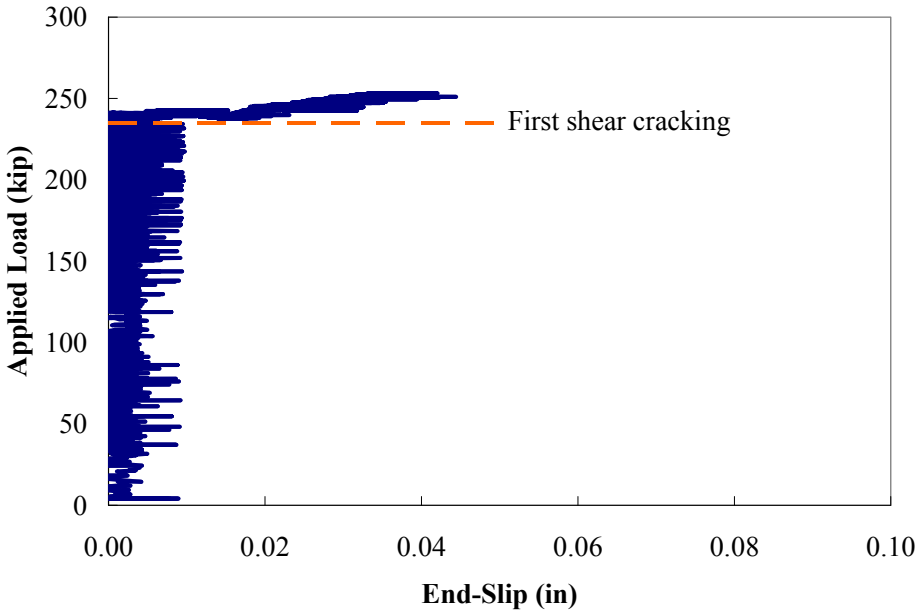

Figure 6.36: End-slip response of strand with greatest total slip (#7) for Box-2, North End

Table 6.3: Maximum End-Slip of Individual Strands for Box-2, North End

Strand	End-Slip (in)
1	0.000
2	0.005
3	0.001
4	0.035
5	0.012
6	0.038
7	0.044
8	0.001
Bottom Strands	**0.022**
Outer Strands (3 & 8)	**0.001**
Center Strands (4-7)	**0.032**

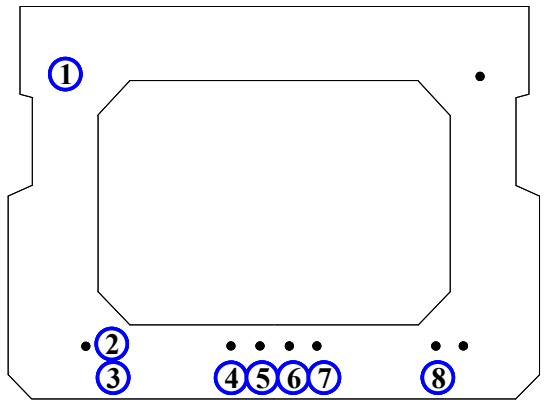

The longitudinal strain was monitored throughout the test at 5 locations under the point of loading. The strain output, adjusted for the initial strain in the concrete due to self-weight and the effective prestress, is shown in Figure 6.37. The distances listed in the legend indicate the location of each strain gauge with respect to the bottom fiber of the beam. Using a linear strain assumption, the maximum compressive strain at the top concrete fiber was 1941 microstrain. For scaling purposes, tensile strain readings exceeding 4000 microstrain are not plotted.

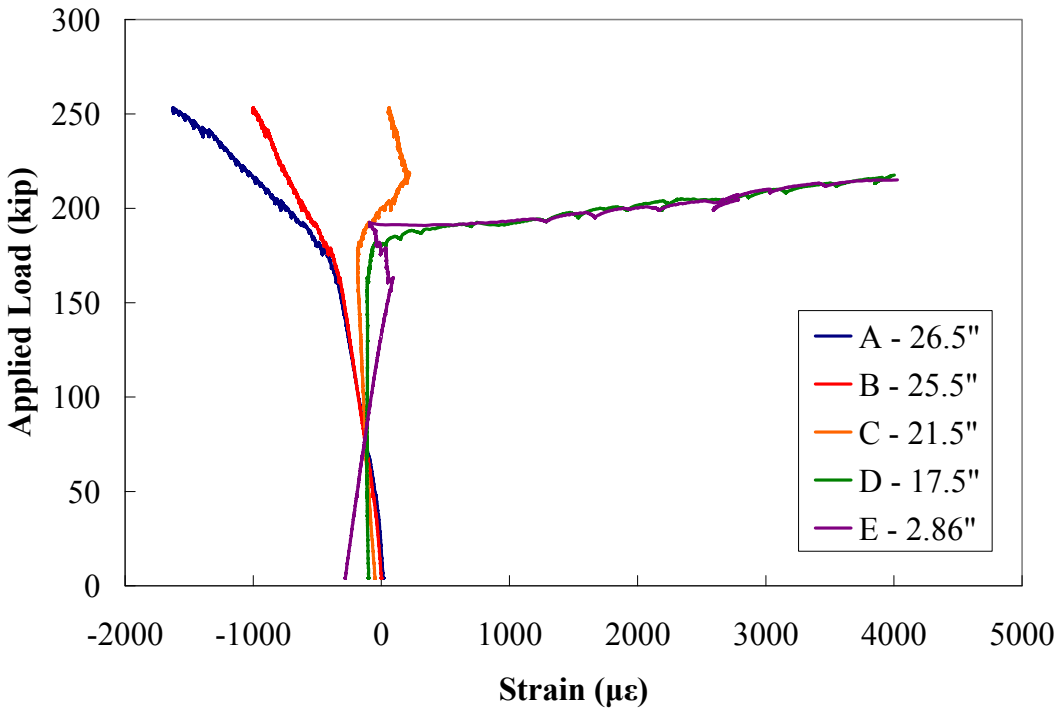

Figure 6.37: Longitudinal strains under loading for Box-2, North End

6.3 DISCUSSION OF DEVELOPMENT LENGTH RESULTS

This section summarizes the results of four flexural tests performed on full-scale SCC box girder specimens. First, the effective prestress in the specimens at the time of loading is calculated using the initial cracking observed in the tests and relationships of mechanics. This permits comparison to prestress losses calculated in Section 4.4. Then, experimental shear and moment capacities are compared to the sectional capacities calculated in Section 4.6. The effectiveness of external CFRP reinforcement in shear strengthening is also evaluated. Finally, although a single value for strand development length is indeterminate given the low number of test iterations, an upper bound and reasonable range for development length are established.

6.3.1 Prestress Losses from Initial Cracking

The effective prestress at the time of flexural testing may be back-calculated using the initial cracking load and relationships of mechanics, as presented in Equation 6.1. Two variables

in the calculation varied between tests: (1) the experimental cracking moment and (2) the concrete modulus of rupture. The average compressive strengths for SCC Batches 1, 2, and 3 (see Tables 3.3 and 3.5) at the time of testing were 7330 psi, 9480 psi, and 6820 psi, respectively. This includes data from all cylinders broken during the four flexural test iterations; it was assumed that any increase in concrete strength between iterations was negligible. Therefore, the average compressive strengths for Box-1 and Box-2 were taken as 8410 psi and 8150 psi, respectively. The modulus of rupture in all calculations was taken as $7.5\sqrt{f'_c}$.

$$f_{pe} = \frac{M_{cr} - f_r Z_b}{A_{ps}\left(e_o + \frac{Z_b}{A_c}\right)} \qquad \text{(Eq. 6-1)}$$

where: f_r = concrete modulus of rupture
Z_b = section modulus with respect to bottom fiber
M_{cr} = cracking moment

All variables not listed under Eq. 6-1 were previously defined in the text. The effective prestress values determined using initial cracking moments from each test are shown in Table 6.4. The back-calculated f_{pe} values for the second and third test are significantly lower than those predicted by any of the codes described in Section 4.4; otherwise, the value calculated for the first and last tests show excellent correlation to predicted values. Results in the table may have been more accurate if explicit modulus of rupture tests were performed instead of using estimates based on compressive strengths. Back-calculated effective stresses may have varied between tests conducted on the same girder because of SCC batch distribution within the girder.

Table 6.4: Effective Prestress from Initial Cracking

Test	f_c (psi)	M_{crack} (kip-ft)	f_{pe} (ksi)	*Average* f_{pe} by Beam (ksi)	*Average* f_{pe} (ksi)
1	8410	709	165.9	162.3	162.0
2	8410	687	158.6		
3	8150	683	158.5	161.7	
4	8150	703	165.0		

6.3.2 Experimental vs. Design Shear and Moment Capacities

The critical loads observed in each test are listed in Table 6.5, including loads at first flexural cracking, first shear cracking, and dominant shear cracking. Maximum sustained loads

and loads at failure are also listed. No dominant shear or failure loads are reported for the fourth test because shear cracking never governed and the specimen was not tested to failure. Experimental cracking moments are compared to theoretical values in Table 6.6; theoretical values were calculated using concrete strengths at testing and 167-ksi effective prestress.

Table 6.5: Critical Loads for All Box Girder Tests

Test 1	Applied P (kip)	Total V (kip)	Total M (kip-ft)
1st Flexural Cracking	165	141	709
1st Shear Cracking	165	141	709
Significant Shear Cracking	176	149	754
Maximum Load	197	167	841
Failure Load	192	162	817

Test 2	Applied P (kip)	Total V (kip)	Total M (kip-ft)
1st Flexural Cracking	155	109	687
1st Shear Cracking	218	152	957
Significant Shear Cracking	223	155	979
Maximum Load	227	158	996
Failure Load	219	153	961

Test 3	Applied P (kip)	Total V (kip)	Total M (kip-ft)
1st Flexural Cracking	149	125	683
1st Shear Cracking	188	156	852
Significant Shear Cracking	208	172	939
Maximum Load	217	179	978
Failure Load	217	179	978

Test 4	Applied P (kip)	Total V (kip)	Total M (kip-ft)
1st Flexural Cracking	161	104	703
1st Shear Cracking	235	151	1018
Significant Shear Cracking	-	-	-
Maximum Load	253	162	1095
Failure Load	-	-	-

Table 6.6: Experimental vs. Theoretical Cracking Moments

Test	$M_{cr\text{-}exp}$ (kip-ft)	$M_{cr\text{-}exp}/M_{cr\text{-}theory}$
1	709	1.00
2	687	0.96
3	683	0.96
4	703	0.99

The box girders consistently exceeded design and nominal shear values within the shear-vulnerable region for each test. Table 6.7 contains ratios between experimental and design shear values, and between experimental and nominal shear capacities. The nominal capacity was taken as the ACI 318-08 design capacity calculated at the interface of the hollow and filled cross-sections. The three trials without external reinforcement had an average ratio $V_u/\Phi V_n$ of 1.13. Meanwhile, the CFRP externally-wrapped specimen in test three had a $V_u/\Phi V_n$ ratio of 1.24, indicating the CFRP resulted in an 11% increase in shear capacity. The effectiveness of the CFRP was limited, however, by its early delamination from the irregularly-shaped girder, especially at the web indentation on either side of the beam (see Figure 6.29).

Table 6.7: Experimental vs. Theoretical Shear Capacity

Test	V_u (kip)	V_u/V_{design}	$V_u/\Phi V_n$
1	167	1.37	1.16
2	158	1.30	1.10
3	179	1.47	1.24
4	162	1.33	1.12

Ratios between experimental and design moments, and between experimental and nominal moment capacities, are presented in Table 6.8. In Test 1, shear cracking governed the response of the girder and only 81% of the nominal moment was achieved at maximum load. In Test 2, specimen damage was primarily due to flexural cracking, though the girder ultimately failed in shear with accompanying strand slip; the specimen developed 96% of the nominal moment. In Test 3, the specimen developed 94% of the nominal moment before failing abruptly due to shear cracking and CFRP delaminating from the sides of the beam. Finally, in Test 4, the girder experienced flexural damage with negligible strand slip and developed more than both the design moment and nominal moment capacity; as stated before, the specimen was not taken to ultimate failure. Strand slip in all tests occurred only after shear cracks had propagated across bottom strands. On average, center strands slipped 24% further into the girders than outer strands. This is likely the result of higher strand concentration and less concrete cover in the center of the girder than near the web sections. From the limited number of trials, no correlation was established between casting or strand release location and development length.

Table 6.8: Experimental vs. Theoretical Moment Capacity

Test	Embedment (in)	M_u (kip)	M_u/M_{design}	$M_u/\Phi M_n$	Failure Mode
1	62.8	841	0.83	0.81	Shear-Slip
2	77.5	996	0.98	0.96	Flexure-Shear
3	68.5	978	0.97	0.94	Shear-Slip
4	83.5	1095	1.08	1.06	Flexure

6.3.3 Experimental Development Length

A primary goal of this research was to compare an experimental development length with theoretical development lengths (see Section 4.5). Given the limited number of test trials, an experimental development length value was not explicitly determined. However, such a value may be interpolated from test data including nominal strand stress f_{ps} and embedment length. In any case where shear cracks propagated across bottom strands, the embedment length was effectively shortened as shown in Figure 6.38; this occurred in the first three flexural tests. As such, the nominal strand stress for the first three tests is determined at the end of the shortened embedment length, where cracking intersects bottom strands.

Nominal strand stress in each of the first three tests was calculated via the truss analogy method; in the method, the applied load is transferred to the reaction support via a series of compressive concrete struts in equilibrium with vertical stirrup forces and longitudinal strand tension forces. A depiction of such a truss is shown in Figure 6.39; the dashed lines represent struts originating at the support or the point of loading, while the dotted lines represent struts transferring load between stirrups. Each stirrup location comprised an upper U-shaped stirrup and a lower U-shaped stirrup with four legs overlapping in the girder's web. However, since they were being developed in opposite directions over a short overlapping distance, the four legs combined could only develop 75% of their total strength. Therefore, in the truss analogy, each set of U-shaped stirrups was assumed to carry a load of 36 kip rather than 48 kip. In maintaining equilibrium throughout the truss, the tension force in the prestressing strands was calculated along the embedment length. The nominal strand stress f_{ps} was taken as the tensile strand stress at the point where shear cracking crossed the center of gravity of bottom layer strands. For the third test, the reaction force was taken as 11% less than the maximum reaction to remove the effect of CFRP wrapping (see Section 6.3.2).

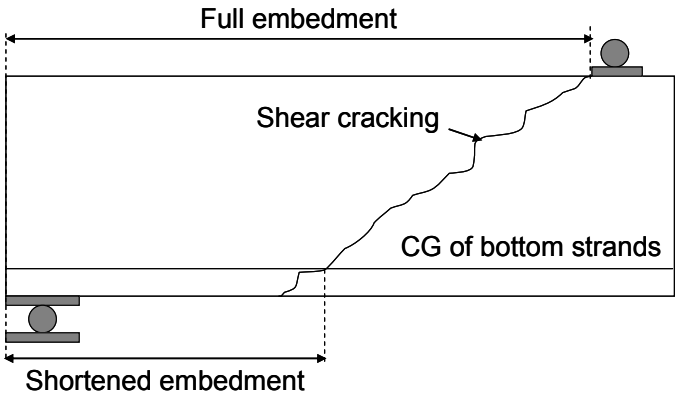

Figure 6.38: Embedment length before and after crack propagation across bottom strands.

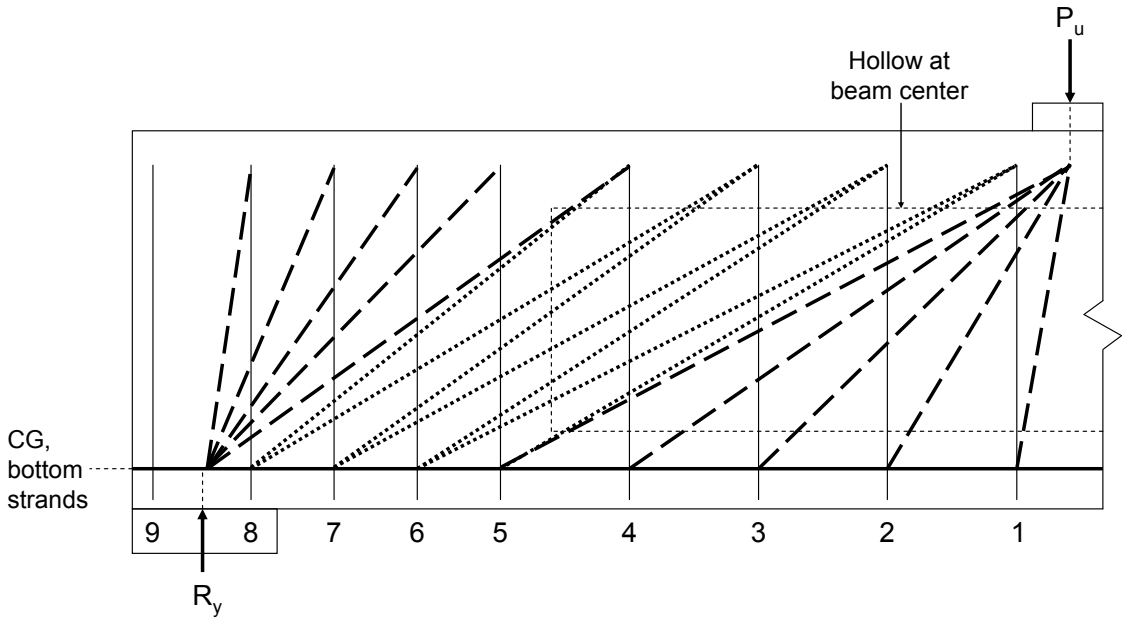

Figure 6.39: Truss analogy representation after shear cracking and stirrup yielding

For the fourth test, the truss analogy was not appropriate because stirrups could not be assumed to have yielded. Therefore, the nominal strand stress was calculated via basic flexural relationships using the experimental strain profile and experimental moment. Figure 6.40 shows the experimental nominal strand stress plotted against the shortened (post-cracking) embedment length for each trial; the full embedment length is utilized for the fourth test. The figure's data is approximated by a best-fit line. The embedment length corresponding to the intersection of the fitted line and a theoretical 253.8 ksi nominal strand stress (AASHTO estimate) may be taken as the interpolated development length L_d; in this case, L_d was approximately 75.6 in. This value is

approximately 4% greater than the 72.9 in. predicted development length. It should be restated, however, that the fourth test was terminated prior to reaching ultimate flexural failure of the girder. If the girder had reached ultimate failure, the strand stress utilized in Figure 6.40 for the fourth test would have increased; in turn, the interpolated development length value would have been lower.

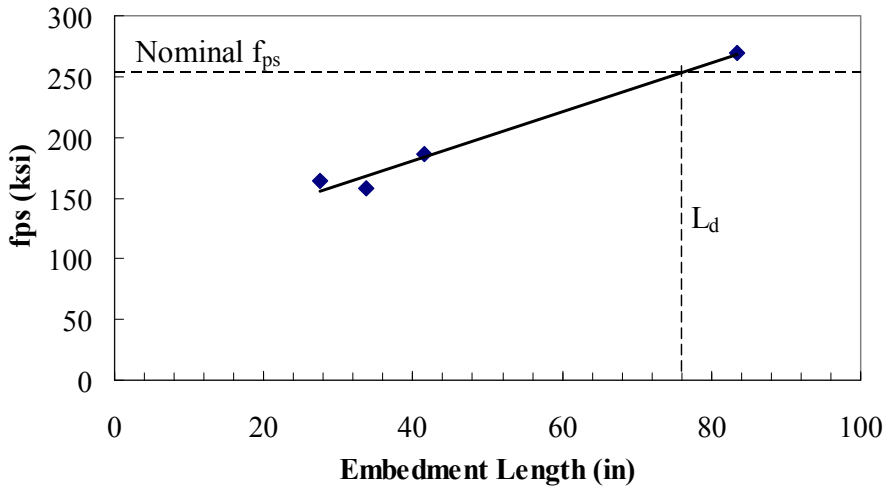

Figure 6.40: Maximum experimental moment vs. embedment length

The experimental development length obtained via Figure 6.40 may be utilized to assess whether the SCC mixture in this study is qualified for prestressed applications. This qualification may be demonstrated by comparing the experimental development length to development lengths predicted by analytical expressions in literature. Table 6.9 contains three such expressions, all postulated based on empirical data from conventional concrete specimens. The three expressions contain modifications to the ACI (2008) and AASHTO (2004) development length calculation (see Equation 2-2); the modifications are based on concrete strength, strand size, initial prestress, or member depth. First, Zia and Mostafa (1977) suggested development length is based on the initial prestress rather than the effective prestress, as well as concrete strength at the time of prestress transfer. Second, Deatherage et al. (1994) suggested applying a factor of 1.5 to only the flexural bond length component of development length. Finally, Shahawy (2001) proposed a third component in calculating development length to account for shear-flexure interaction in members with depth *h* greater than 24 in.

The analytical expressions in Table 6.9 encompass a broad range of development length predictions. As the table shows, analytical predictions ranged from 78.2 in. to 109.7 in. The upper bound value incorporated an additional length (1.47*h*) to account for flexure-shear interaction effects. The table provides ratios between the experimental development length obtained in this study and those obtained using the expressions. With an experimental-to-predicted development length ratio of 0.97, the experimental development length shows the best correlation to the analytical prediction by Zia and Mostafa (1977). The experimental value is also within 5% of the code-predicted value. Based on the conservatism of the analytical expressions, the ±5% variability between the experimental development length and those calculated using Zia and Mostafa (1977) and the ACI and AASHTO codes, and the overall structural performance of the SCC girders, it is reasonable to conclude that the SCC utilized in this study has comparable bond strength to conventional concrete and may be utilized in prestressed applications.

Reference	**L_d Expression**	**$L_{d\text{-}pred}$ (in)**	**$L_{d\text{-}exp} / L_{d\text{-}pred}$**
ACI (2008) AASHTO (2004)	$L_d = \frac{f_{pe} d_b}{3} + \left(f_{ps} - f_{pe}\right) d_b$	72.9	1.04
Zia and Mostafa (1977)	$L_d = 1.5 \frac{f_{pi}}{f_{ci}} d_b - 4.6 + 1.25(f_{ps} - f_{pe}) d_b$	78.2	0.97
Deatherage et al. (1994)	$L_d = \frac{f_{pi} d_b}{3} + 1.5(f_{ps} - f_{pe}) d_b$	100.6	0.75
Shahawy (2001)	$L_d = \frac{f_{pi} d_b}{3} + \frac{(f_{ps} - f_{pe}) d_b}{1.2} + 1.47h$	109.7	0.69

CHAPTER 7: FINITE ELEMENT ANALYSIS

Determining transfer and development lengths through experimental tests may be the most rigorous method for assessing bond between prestressing strands and SCC. However, such tests may be prohibitive in terms of time and cost when performed using large-scale specimens. A simple yet accurate analytical approach to predicting transfer or development length would be useful in situations where large-scale testing is not feasible. This chapter outlines a systematic method to predict transfer length in prestressed members using pullout test data and finite element analysis. The first step involves deriving bond stress-slip relationships from force-displacement responses obtained via pullout tests. With appropriate modification factors obtained from the literature, the relationships are then correlated to bond stress-slip behavior expected in transfer zones of prestressed members. The modified relationships define parameters in finite element models incorporating bond-slip via nonlinear spring elements. Analytical transfer lengths from the models are compared with the experimental results presented in Chapter 5. With proper refinement, the models may be extended to accurately predict development length.

7.1 MODELING PHILOSOPHY

All analyses for this study were conducted using three-dimensional models in the finite element program ANSYS (2007). This section describes the procedure followed to develop these models. Defined first was the solid model geometry including volumes for concrete sections, volumes for bearing plates, and lines for prestressing strands. Transverse steel reinforcement was not explicitly modeled; rather, it was incorporated as smeared reinforcement within concrete elements. The lines defining solid model entities were manually assigned size controls for meshing. Smaller mesh sizes were specified in areas of high stress concentration. Care was taken to ensure concrete nodes would coincide with steel nodes at locations of prestressing strands. Elements were created by sweeping volume entities and using the global mesh tool to mesh line elements (i.e. prestressing strands).

Each element was assigned a specific element type, set of real constants, and material model. In ANSYS (2007), an element's type defines its modeling capabilities and degrees of freedom; real constants define parameters which remain unchanged throughout analysis; and

material models define constitutive relationships which govern element behavior. After meshing all solid model entities, spring elements were defined at coincident nodes to incorporate the bond-slip mechanism between prestressing strands and concrete. Then, degree of freedom constraints were applied to represent appropriate boundary conditions. Finally, prior to executing the analysis, loads were applied directly to the solid model and solution parameters were selected; these included the desired element output, force or displacement convergence criteria, and maximum number of equilibrium equations.

7.2 ELEMENT TYPES AND MATERIAL MODELS

7.2.1 Concrete

Concrete was modeled using SOLID65 brick elements capable of cracking in three orthogonal directions, crushing, and plastic deformation. Each element was defined by eight nodes having three translational degrees of freedom, as shown in Figure 7.1. The real constant set for SOLID65 permits the user to input up to three volume ratios to incorporate smeared reinforcement. In the girder models, the smeared reinforcement capability was utilized to represent transverse reinforcement in any given flange or web section. As illustrated below in Figure 7.1, the orientation of smeared reinforcement was defined by specifying two angles relative to the element coordinate system. The reinforcement within the brick elements was capable of acting in tension and compression and could deform plastically.

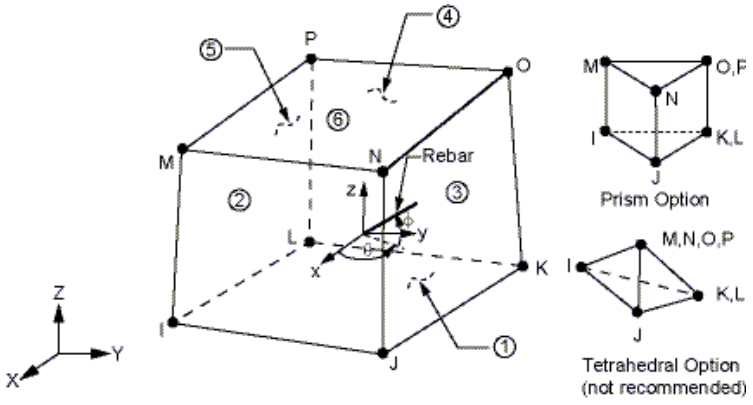

Figure 7.1: SOLID65 element geometry (ANSYS 2007)

The material model for concrete comprised four different components. A linear isotropic model was used to define the initial modulus; a multi-linear isotropic model was used to define a nonlinear stress-strain curve; non-metal plasticity was employed to define concrete behavior parameters; and density was specified to incorporate self-weight. The nonlinear stress-strain curve was based on the Todeschini (1964) stress-strain model shown in Equation 7-1. Here, f''_c is taken as $0.9f'_c$ to account for differences between cylinder and member strength, and the strain corresponding to maximum stress is taken per Equation 7-2 (MacGregor & Wight 2005). The concrete modulus of elasticity E_c was taken as $57000\sqrt{f'_c}$, and the 28-day concrete strength was taken as the average experimental compressive cylinder strength. As such, a unique concrete stress-strain relationship was used in each of the analyses of the four girders. The relationships incorporated strain softening after concrete reached its peak stress. To illustrate, the stress-strain curve utilized for the analysis of Box-1, with $f''_c = 0.9f'_c = 6750$ psi, is shown in Figure 7.2.

$$f_c = \frac{2f''_c\left(\frac{\varepsilon}{\varepsilon_o}\right)}{1+\left(\frac{\varepsilon}{\varepsilon_o}\right)^2} \qquad \text{(Eq. 7-1)}$$

$$\varepsilon_o = \frac{1.71f'_c}{E_c} \qquad \text{(Eq. 7-2)}$$

where: f_c = concrete stress at any strain ε

ε_o = strain at peak compressive strength f''_c

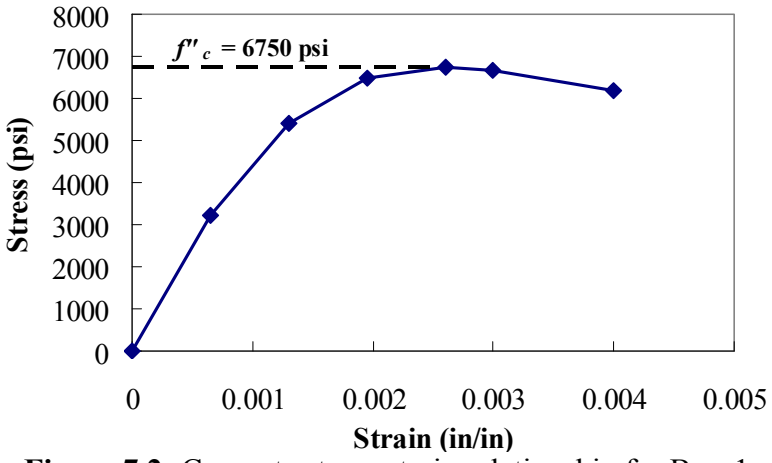

Figure 7.2: Concrete stress-strain relationship for Box-1

Concrete behavior parameters were defined according to the Willam and Warnke (1974) failure model. The nine parameters are listed in Table 7.1. The first two constants in the table relate to load transfer across open and closed cracks. For the analyses at hand, the coefficient for open cracks was taken as 0.3 and the coefficient for closed cracks was taken as 0.99. The third constant, the uniaxial cracking stress, was taken as the modulus of rupture determined using experimental concrete strengths. The fourth constant in the table was set to -1 to disable the SOLID65 element's crushing capability and avoid convergence problems. The five remaining parameters in Table 7.1 were set to ANSYS defaults.

Table 7.1: SOLID65 Concrete Material Model Parameters (ANSYS 2007)

Constant	Physical Representation
1	Shear transfer coefficient for an open crack
2	Shear transfer coefficient for a closed crack
3	Uniaxial tensile cracking stress
4	Uniaxial crushing stress
5	Biaxial crushing stress
6	Ambient hydrostatic stress state
7	Biaxial crushing stress under ambient hydrostatic stress
8	Uniaxial crushing stress under ambient hydrostatic stress
9	Stiffness multiplier for cracked tensile condition

7.2.2 Prestressing Strands

Prestressing strands were modeled using three-dimensional LINK8 spar elements capable of plastic deformation, stress stiffening, and large deflections. The elements resisted uniaxial tension and compression, but did not consider bending. Each element had two non-coincident nodes with three translational degrees of freedom each, as shown in Figure 7.3. The real constant set for LINK8 elements required two inputs. The first parameter defined the cross-sectional area of the spar, which in these analyses was 0.153 in^2. The second parameter defined the initial strain within the spar; it was through this initial strain that prestress within the girders was incorporated in the models. The material model for prestressing steel had two components, the first of which defined the elastic modulus of 28700 ksi. The second defined a nonlinear stress-strain curve typical of Grade 270, 0.5-in. diameter seven-wire strands.

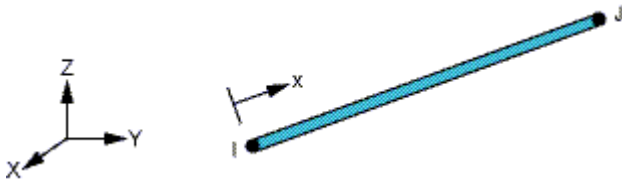

Figure 7.3: LINK8 spar element geometry (ANSYS 2007)

7.2.3 Transverse Reinforcement and Bearing Plates

As stated in Section 7.2.1, transverse steel within the girders was modeled via smeared reinforcement throughout SOLID65 elements. Steel loading and bearing plates were modeled using SOLID185 brick elements with plasticity, large deflection, and large strain capabilities. Brick elements had three translational degrees of freedom at each of their eight nodes and did not require real constant inputs. The material model for steel in the bearing plates and smeared reinforcement was taken as an elastic-perfectly-plastic curve with yielding occurring at 60 ksi.

7.2.4 Bond between Strands and Concrete

Perfect bond between prestressing strands and concrete was not assumed in this analysis. Instead, bond-slip relationships were incorporated via nonlinear COMBIN39 spring elements to permit the strand to displace relative to concrete. The springs were defined at coincident concrete and steel nodes with three translational degrees of freedom each. The springs resisted uniaxial tension and compression but considered neither bending nor torsion. The real constant set for COMBIN39 elements required general force-deflection inputs. The method in which these inputs were derived from experimental data is described in Section 7.3.

7.3 BOND-SLIP MECHANISM

7.3.1 Bond Stress-Slip Relationships

Idealized pullout responses were developed for each set of seven strands tested in SCC or NCC at various ages (see Chapter 3 for discussion of pullout tests). First, the average load was calculated at the points of first slip, peak load, ultimate failure, and midpoint between first slip and peak load. Average bond stress at each point was calculated by dividing the average load by the surface area of the 18-in. embedded portion of the strand. Normalized bond stress was obtained by dividing the average bond stress by $(f_c)^{1/2}$. An idealized pullout bond stress-slip

relationship is illustrated in Figure 7.4, where U is the average bond stress and U' is the normalized bond stress. Slip was calibrated using steel constitutive properties to eliminate the effect of the strand elongation that occurred between the concrete surface and the point at which the LVDT measured displacement (see Figure 3.5 for pullout test assembly). Figure 7.5 displays idealized bond stress-slip relationships for both concrete types at various curing ages. Until first slip occurred, SCC and NCC relationships were comparable. The peak normalized bond stress of SCC was 25% greater than that of NCC one day after concrete placement. After seven days the converse held true; peak normalized bond stress of NCC was approximately 25% greater than that of SCC. Differences between the concretes' peak bond stresses at 3 and 28 days were negligible.

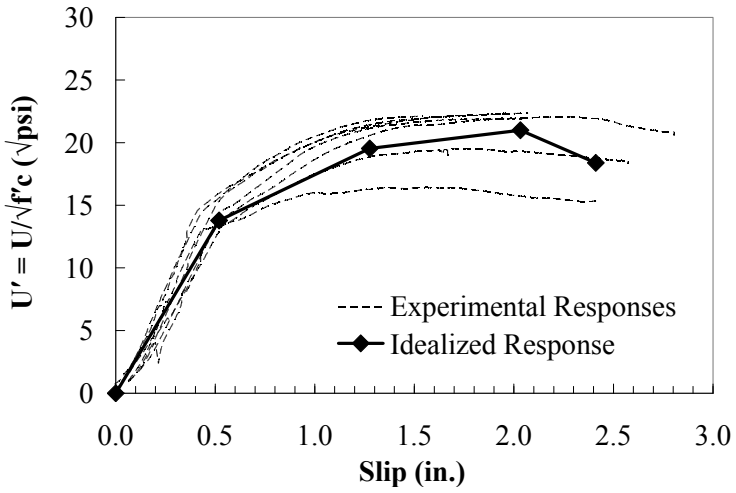

Figure 7.4: Idealized bond stress-slip curve derived from experimental curves for 3-day SCC

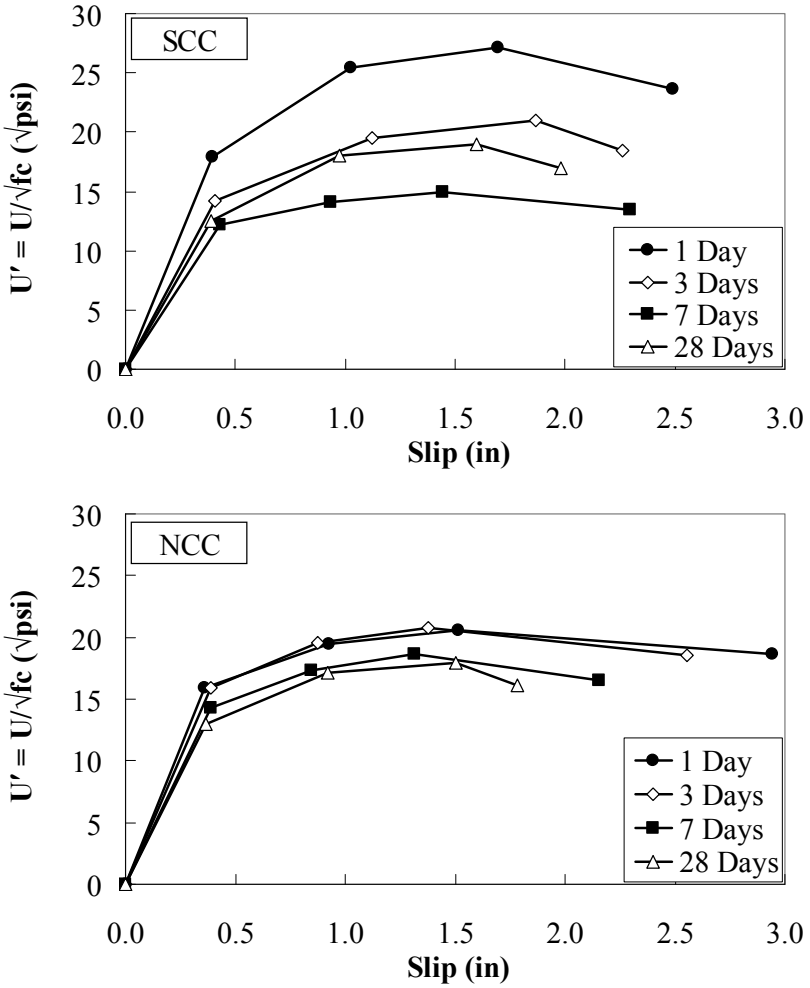

Figure 7.5: Idealized bond stress-slip relationships for SCC (top) and NCC (bottom)

7.3.2 Correlating Pullout Bond Stress to Transfer Bond Stress

Modification factors were derived to correlate pullout bond stress to transfer bond stress before experimental stress-slip relationships (Section 7.3.1) could be utilized in FE analyses to predict transfer lengths. Average bond stress-slip relationships derived from pullout data underestimate the stress-slip of strands in prestressed members for several reasons. First, for simplification, the average bond stresses are determined by assuming uniform bond stress distribution along the entire embedded strand; however, the actual bond stress varies with the depth of embedment as shown in Figure 7.6. The figure illustrates the location of peak stress shifting along the strand at increasing load increments. Similar progression patterns have been measured in steel reinforcing bars in concentric (Feldman & Bartlett 2007) and eccentric (Perry & Thompson 1966) pullout specimens. As such, the length of strand resisting pullout load is

much shorter than the full embedment length, especially at small loads. Second, the physical conditions in pullout blocks differ from those in transfer zones of prestressed members. As noted by Anderson, Rider and Sozen (1964), strands in pullout blocks undergo radial contraction while being pulled, yet strands in transfer zones expand when released from tension; this phenomenon, known as wedging action, exerts pressure on the surrounding concrete and increases the frictional component of bond. Finally, stirrup reinforcement in prestressed beams confines concrete in transfer zones, which has been shown to significantly improve the bond capacity of strands (Stocker and Sozen 1970); concrete in pullout tests is typically unconfined.

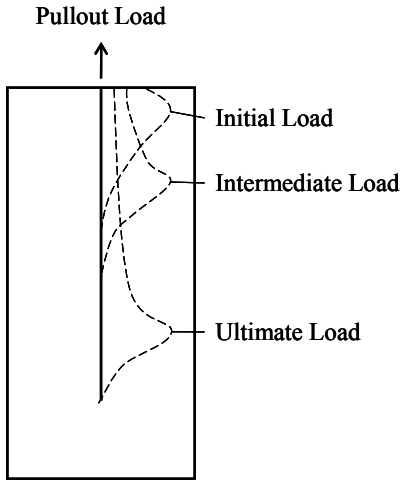

Figure 7.6: Variation of bond stress during pullout test

The impacts of non-uniform stress distribution, prestressing, and confinement on bond are excluded in deriving average pullout bond stress-slip relationships. For this study, to correlate pullout bond stress to transfer bond stress, modification factors were derived to account for non-uniform stress distribution and wedging action; no factor was utilized to account for confinement. Data from Anderson, Rider, and Sozen (1964) was utilized to calculate a ratio between maximum bond stress and average bond stress ($U_{max}/U_{avg} = 2.1$) in a pullout specimen with 18-in. embedment. Then, data from Cousins, Badeaux, and Moustafa (1992) was utilized to calculate a ratio between average bond stresses of prestressed and non-prestressed pullout specimens ($U_p/U_{np} = 1.91$) containing uncoated 0.5-in. diameter strands. A combined modification factor (MF) of 4.0 was obtained by multiplying the two aforementioned ratios, and was applied directly to the stress-slip relationships presented in Figure 7.5. The impact of this

modification is seen in Figure 7.7, which contrasts an unmodified and modified relationship. In the figure, the circled region shows where stress-slip behavior is most critical in determining transfer length; the range of slip in this region is reasonable for typical end-slip in prestressed members.

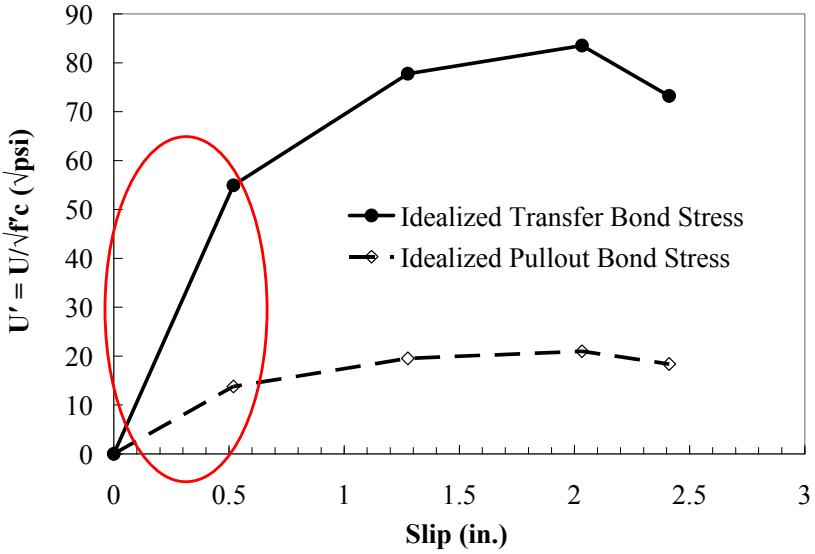

Figure 7.7: Transfer bond stress derived from pullout bond stress

7.4 PULLOUT MODEL

Before developing girder models to predict transfer lengths, a finite element pullout model was created to evaluate whether the COMBIN39 springs would effectively represent bond-slip. The model, as shown in Figure 7.8(a), comprised a 10 in. x 10 in. x 24 in. concrete prism surrounding one steel strand; preliminary analysis showed this size of prism could accurately capture the response observed experimentally. The prism was modeled with a single 0.5-in. diameter steel strand embedded 18 in. along its center axis. The strand extended to a point 24 in. above the concrete surface, where displacement was applied in 0.1-in. increments to simulate load transfer via a prestressing chuck. Nodal constraints allowed the steel strand to move only along the line of pullout action and restricted the concrete prism from movement at its upper surface.

To model bond-slip behavior at the concrete-strand interface, three COMBIN39 spring elements connected each pair of coincident concrete and steel nodes, as shown in Figure 7.8(b).

Two of the springs were rigid and acted only to prevent coincident nodes from slipping relative to each other in the horizontal plane. The third spring acted only in the direction of pullout and was characterized by nonlinear force-deflection inputs. The nonlinear parameters were derived from the idealized bond stress-slip relationships, with no modification factors applied. The global FE model output correlated well with experimental data and showed that nonlinear springs were capable of capturing bond-slip. For reference, Figure 7.9 shows a typical bond stress-slip relationship from the FE pullout model compared to the corresponding experimental bond stress-slip relationship.

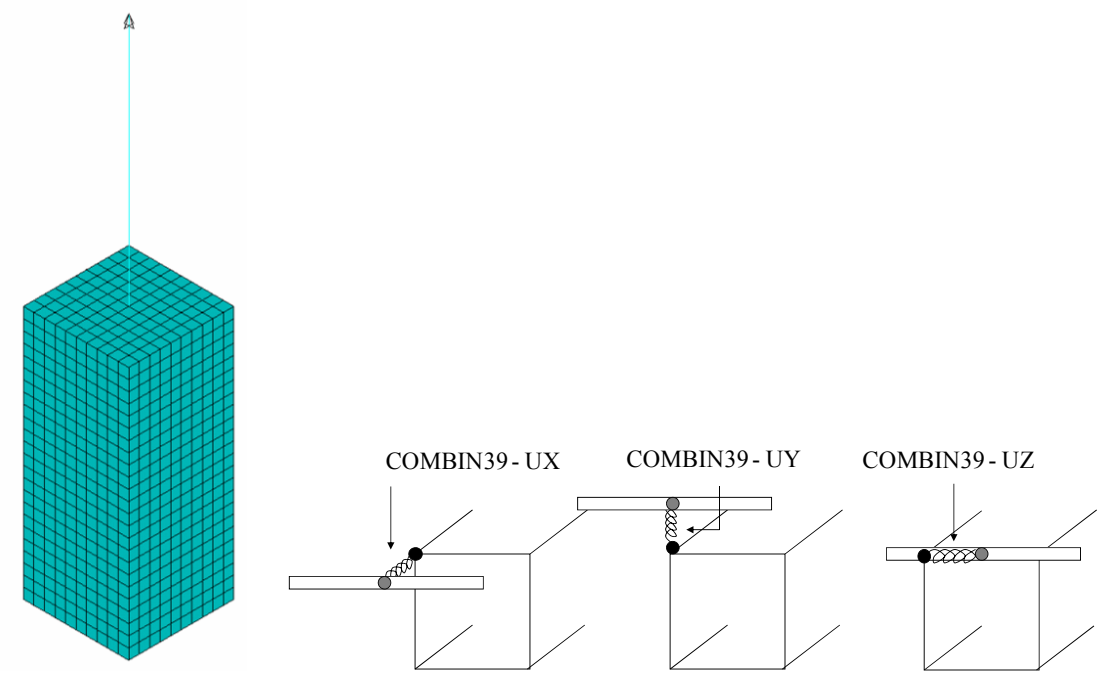

(a) Prism geometry (b) Concrete-strand interface

Figure 7.8: Pullout prism (a) and rheological representation of concrete-strand interface (b) with gray steel node and black concrete node

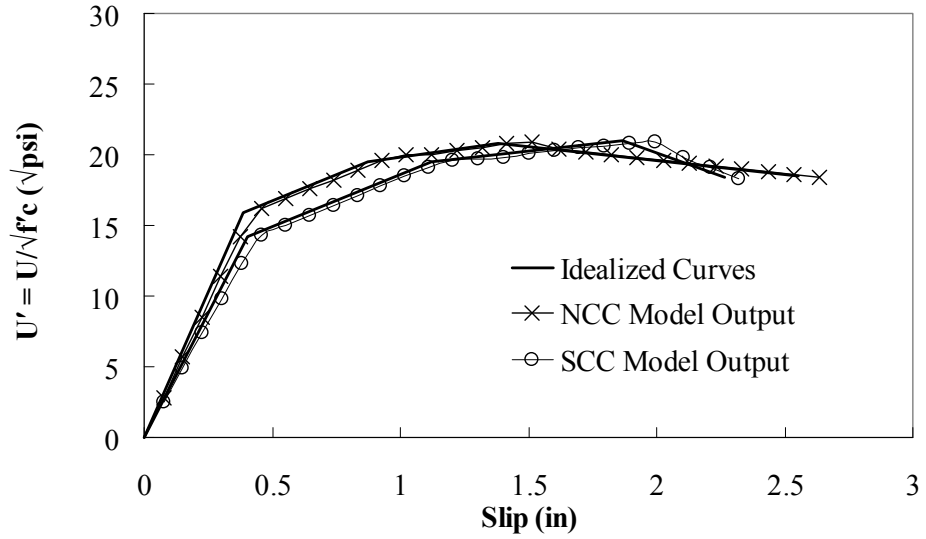

Figure 7.9: Ideal and analytical bond stress-slip relationships for SCC and NCC 3 days after concrete placement, normalized by $\sqrt{f'_c}$

7.5 GIRDER MODELS

7.5.1 Modeling Technique Validation

To validate the methodology and assumptions presented thus far, especially the assumed 4.0 modification factor (Section 7.3.2), analysis was conducted on a FE model of a beam tested experimentally by Haq (2005). The T-beam was 38 ft. long with the cross-sectional properties shown in Figure 7.10. The model's element types and material properties were defined per Section 7.2. Concrete material properties were derived using the 8035 psi 28-day strength reported for the study's SCC2B concrete mixture. An initial strain of 0.00579 in/in was assigned to LINK8 elements to impart an estimated prestress of 162 ksi. All concrete and steel elements in the model were 6 in. long. As in the pullout block model (Section 7.4), three COMBIN39 elements were affixed between each pair of coincident concrete and steel nodes to represent bond-slip along the beam's longitudinal axis. This method assumed camber was small enough to neglect the vertical component of prestressing force after beam deformation. The normalized average force-slip response from pullout tests using mixture SCC2B, multiplied by MF = 4.0, was utilized to derive parameters for the COMBIN39 springs. The average analytical end-slip, or the relative movement between the prestressing strand and the concrete surface at a beam's end, was found to be 0.1275 in. When compared to Haq's (2005) average experimental end-slip of

0.1301 in., the analysis yielded a relative error of 2%. Therefore, the assumptions regarding the modification factor MF = 4.0 and the overall FE modeling technique were deemed acceptable.

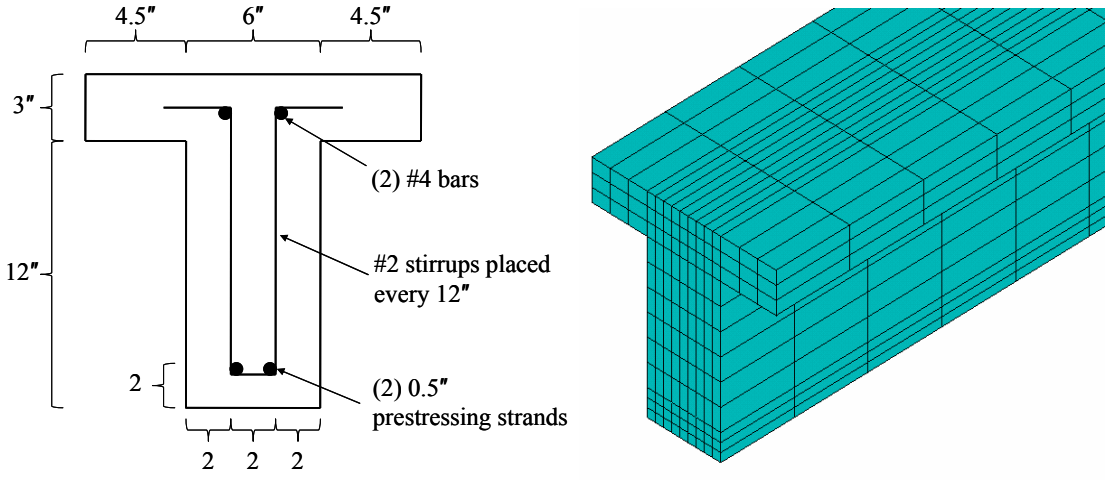

Figure 7.10: T-beam cross-section (left) and FE representation (right) from Haq (2005)

7.5.2 Box and I-Girder Models

After verifying spring elements could reasonably represent bond-slip and validating the modification factor of 4.0, two models were developed to analyze the full-scale specimens tested experimentally in this study. Both girders were modeled along axes of symmetry to reduce the required computational effort in analysis, as shown in Figures 7.11 through 7.13. All points along the cut cross-sections were restrained to prevent out-of-plane deformation. Elements defining concrete and prestressing strands were 6 in. long. To account for transverse reinforcement present in the experimental girders, appropriate steel volume ratios for smeared reinforcement were assigned to SOLID65 elements.

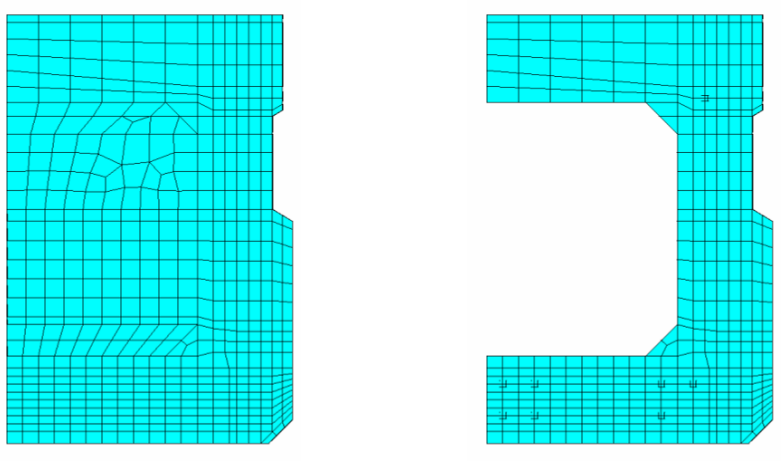

Figure 7.11: FE box girder cross-section at end of beam (left) and midspan (right)

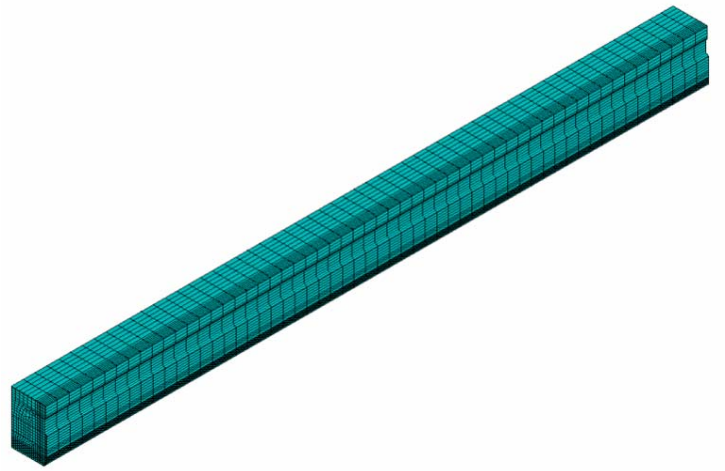

Figure 7.12: FE box girder modeled along one axis of symmetry

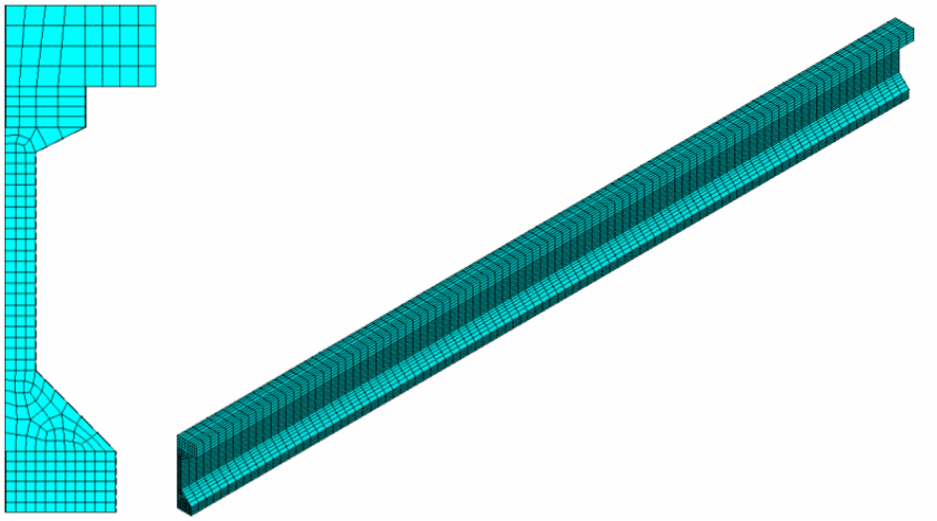

Figure 7.13: FE I-girder cross-section (left) and model (right) along one axis of symmetry

Two analyses were conducted for each girder model, differing primarily with respect to concrete strength. Per Section 7.2.1, concrete material properties were derived using the four experimental 28-day girder strengths (see Table 5.1). Concrete strength also affected the COMBIN39 force-deflection parameters, which were derived using the normalized bond stress-slip relationship for 28-day SCC. Higher strength resulted in higher spring stiffness and, accordingly, better bond.

Prestressing steel elements retained the same material properties as in the pullout model. However, initial strains were applied to impart prestressing force within the specimens. For the box girder model, LINK8 elements had initial strains of 0.006098 in/in, equivalent to a prestress of 175 ksi. Accounting for elastic shortening within the girder model, the effective prestress was 167 ksi. For the I-girder model, LINK8 elements had initial strains of 0.006063 in/in, equivalent to a prestress of 174 ksi. Accounting for elastic shortening within the model, the effective prestress was 166 ksi. The effect of prestressing on the girder models is shown in Figures 7.14 through 7.16.

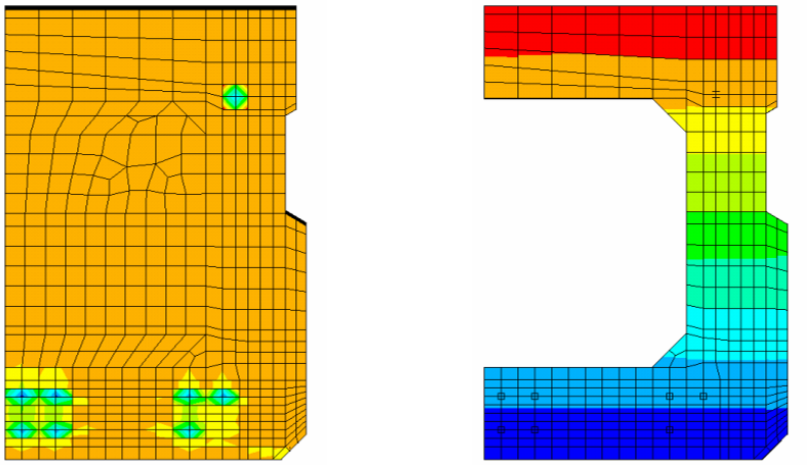

Figure 7.14: FE box girder cross-sections under prestressing load (stress gradient shown)

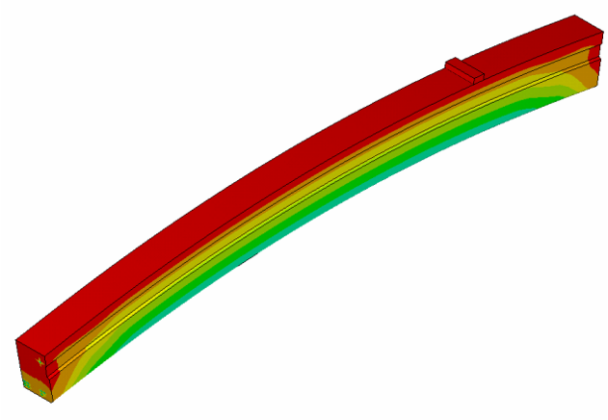

Figure 7.15: FE box girder deformation under prestressing load (stress gradient shown)

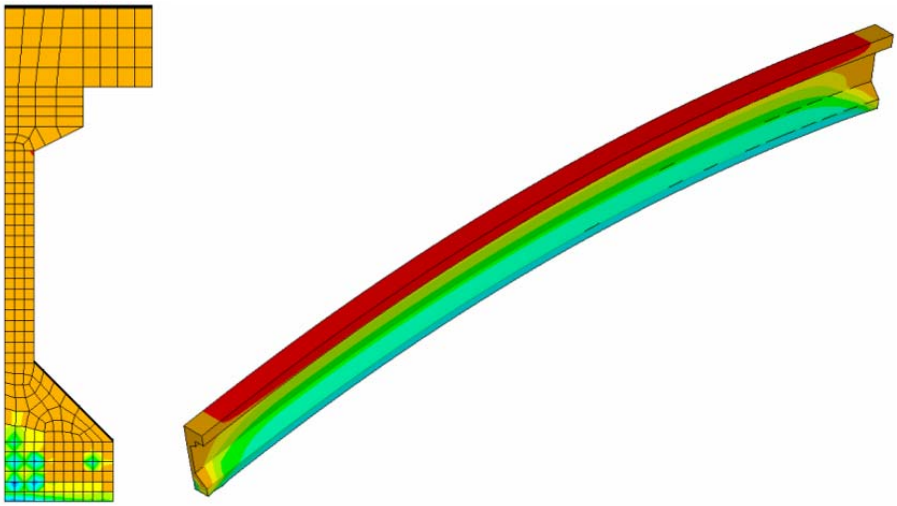

Figure 7.16: FE I-girder under prestressing load (stress gradient shown)

7.6 DISCUSSION OF FINITE ELEMENT RESULTS

Transfer lengths for the FE girders were obtained using the end-slip method. The relative slip Δ between the prestressing strand and the concrete surface at a beam's end is directly correlated to transfer length L_t as shown in Equation 7-4. A thorough review of this method may be found in Balazs (1993). The end-slip for each case was taken as the average of the end-slip values obtained for all strands within the girder, excluding the single top strand in the box girder model. The parameter α in Equation 7-4 is typically assigned a value between 2 and 3 depending on the assumed bond stress distribution within the transfer zone. A value of 2 corresponds to constant bond stress distribution, while a value of 3 corresponds to linear bond stress distribution. For 0.5-in. diameter strands, Balazs (1993) suggests taking α equal to 2.67.

$$L_t = \frac{\alpha E_{ps} \Delta}{f_{si}} \qquad \text{(Eq. 7-4)}$$

where: α = factor accounting for stress distribution along the strand
E_{ps} = strand's modulus of elasticity
f_{si} = strand's initial stress

Table 7.2 contains analytical end-slip values obtained from the four FE girder analyses, as well as corresponding transfer lengths calculated using α factors of 2 and 2.67. The last column in the table shows the average 28-day transfer lengths obtained experimentally in this study. The analytical transfer lengths calculated with α = 2 better correlated with experimental data than values calculated with α = 2.67. On average, analytical transfer lengths with α = 2 were 10.7% greater than experimental transfer lengths. In specimen Box-1, however, this percentage was only 3.3%. It may be concluded, therefore, that the finite element analysis described in this chapter could provide conservative estimates of transfer lengths in large-scale specimens.

Table 7.2: Analytical End-Slip and Transfer Length Values (in inches)

Specimen	Average End-Slip	L_t with α = 2	L_t with α = 2.67	Experimental L_t
Box-1	0.0764	22.93	30.61	22.20
Box-2	0.0763	22.90	30.57	19.70
I-1	0.0776	23.25	31.04	20.70
I-2	0.0775	23.24	31.03	20.95

CHAPTER 8: CONCLUSIONS

The primary goal of this research was to experimentally assess the bond behavior of prestressing strands in full-scale members cast with SCC adhering to IDOT specifications. First, pullout tests were conducted to compare the performance of seven-wire steel strands embedded in SCC to the performance of strands embedded in NCC. Then, transfer lengths of prestressing strands were determined experimentally in two prestressed SCC hollow box girders and two prestressed SCC I-girders. Finally, a series of flexural tests was used to determine the development length of strands in the two box girders. Results from these tests were compared to industry standards, code requirements, and theoretical predications to assess the acceptability of the IDOT-approved SCC mixture in current design and implementation techniques.

A secondary goal of this research was to assess the viability of various analytical transfer and development length prediction methods for specimens cast with SCC. Experimental data was compared to transfer and development length expressions proposed in the literature, and a method of finite element analysis was developed to predict transfer length in full-scale specimens using pullout test data. The research presented in this thesis affords the following observations:

1. Pullout test results at various ages showed strand performance in SCC to be comparable with strand performance in NCC. Normalized pullout loads differed between the two concrete types by as little as 1% after three days of curing.
2. Normalized first slip loads were lower in SCC than in NCC for all tests except those conducted one day after casting. At 28 days, the average normalized first slip load in SCC was 4% below that in NCC.
3. Normalized peak pullout loads were higher in SCC than in NCC for all tests except those conducted seven days after casting. At 28 days, the average normalized peak pullout load in SCC was 6% higher than that in NCC.
4. The strands and SCC mixture utilized in pullout tests were deemed acceptable for use in large-scale prestressed specimens for transfer and development length testing.
5. Average pullout bond stress-slip relationships obtained using experimental pullout data establish lower bounds for bond strength because they do not account for non-uniform stress

distribution along strands or radial expansion due to prestressing. A modification factor of 4.0 was derived in this study to correlate pullout bond stress-slip relationships to transfer zone bond stress-slip relationships.

6. A systematic method was developed to predict transfer lengths in large-scale specimens using pullout test data and finite element analysis. Analytical transfer lengths predicted using the method and assuming constant bond stress distribution were on average 10.7% larger than experimental values.
7. While the study utilized SCC adhering to IDOT standards, the analytical procedure relating pullout stress-slip relationships to transfer stress-slip relationships may be useful in analysis of any pretensioned specimen. In-depth research may be warranted to refine the stress-slip modification factor and validate the FE analysis.
8. Experimental transfer lengths at seven of the eight girder ends were below ACI and AASHTO code-required transfer lengths. Only at one end did experimental results consistently and significantly exceed code provisions. This end had the lowest concrete compressive strength of all locations and corresponded to the strand cutting location at prestress transfer.
9. Transfer lengths showed no correlation to casting location.
10. No correlation was observed between transfer length and girder type.
11. Overall, experimental transfer lengths were 86% of $50d_b$, 72% of $60d_b$, and 69% of $f_{pe}d_b/3$.
12. According to an analytical comparison study, experimental transfer lengths showed better correlation to predictions incorporating initial prestress and concrete compressive strength than to predictions incorporating effective prestress or no concrete strength. Expressions from Marti-Vargas et al. (2007-b) and Zia and Mostafa (1977) provided the most accurate transfer length predictions and may be utilized for SCC specimens.
13. On average, the as-built girders exceeded theoretical nominal shear capacities by 13%.
14. External CFRP shear reinforcement resulted in an approximate 11% increase in shear capacity of the box girder.
15. In three of the test iterations, strand slip occurred after shear cracks had propagated across the strands, effectively shortening the strand embedment length. On average, center strands slipped 24% further into the girders than outer strands, likely due to higher strand concentration and less concrete cover in the center of the box girder cross-section.

16. The box girder was able to develop at least 106% of the nominal moment capacity without experiencing significant strand slip when an embedment length of 83.5 in. was utilized. At iterations with shorter embedment lengths, failure was governed by shear which preceded strand slip; as such, the full flexural capacity of the girder was not realized.
17. Based on interpolated data, the experimental development length was estimated as 75.6 in. This experimental value is within 5% of the development lengths predicted using either the ACI (2008) and AASHTO (2004) design codes or the analytical expression proposed in literature by Zia and Mostafa (1977).
18. With satisfactory pullout behavior, adequate transfer and development lengths, and structural performance comparable to that of specimens cast with conventional concrete, it is reasonable to conclude that the SCC mixture in this study had sufficient bond to prestressing strands and would perform adequately in prestressed applications.

REFERENCES

AASHTO. (2004). *AASHTO LRFD Bridge Design Specifications*. Third Edition, American Association of State Highway and Transportation Officials, Washington, D.C.

ACI Committee 209. (2008). *Prediction of Creep, Shrinkage, and Temperature Effects in Concrete Structures (ACI 209R-92)*. American Concrete Institute, Farmington Hills, MI.

ACI Committee 318. (2008). *Building Code Requirements for Structural Concrete (ACI 318-08) and Commentary*. American Concrete Institute, Farmington Hills, MI.

ACI Committee 343. (2004). *Analysis and Design of Reinforced Concrete Bridge Structures (ACI 343R-95)*. American Concrete Institute, Farmington Hills, MI.

ACI Committee 440. (2008). *Guide for the Design and Construction of Externally Bonded FRP Systems for Strengthening Concrete Structures (ACI 440.2R-08)*. American Concrete Institute, Farmington Hills, MI.

Anderson, G., Rider, H., and Sozen, M. (1964). "Bond Characteristics of Prestressing Strands." Structural Research Series 283, University of Illinois at Urbana-Champaign, Urbana, IL.

Andrawes, B., Shin, M., and Pozolo, A. (2009). "Transfer and Development Length of Prestressing Tendons in Full-Scale AASHTO Prestressed Concrete Girders using Self-Consolidating Concrete." Report No. ICT-09-038, Illinois Center for Transportation, Urbana, IL.

ANSYS Structural Analysis Guide. (2007). Release 11.0, ANSYS, Inc., Canonsburg, PA.

ASTM C143 / C143M-10. (2010). "Standard Test Method for Slump of Hydraulic-Cement Concrete." ASTM International, West Conshohocken, PA.

ASTM C1611 / C1611M-09b. (2009). "Standard Test Method for Slump Flow of Self-Consolidating Concrete." ASTM International, West Conshohocken, PA.

ASTM C1621 / C1621M-09b. (2009). "Standard Test Method for Passing Ability of Self-Consolidating Concrete by J-Ring." ASTM International, West Conshohocken, PA.

Balazs, G. (1992). "Transfer Control of Prestressing Strands." *PCI Journal*, Vol. 37, No. 6, p. 60-71.

Balazs, G. (1993). "Transfer Length of Prestressing Strand as a Function of Draw-In and Initial Prestress." *PCI Journal*, Vol. 38, No. 2, p. 86-93.

Bonen, D. and Shah, S. (2004). "The Effects of Formulation on the Properties of Self-Consolidating Concrete." *Concrete Science and Engineering: A Tribute to Arnon Bentur*, Proceedings of the International RILEM Symposium, RILEM Publications, France, p. 43-56.

Bruggeling, A. and Huyghe, G. (1991). *Prefabrication with Concrete*. A.A. Balkema, Rotterdam, Netherlands.

Buckner, C. (1995). "A Review of Strand Development Length for Pretensioned Concrete Members." *PCI Journal*, Vol. 40, No. 2, p. 84-105.

Burgueno, R. and Haq, M. (2007). "Effect of SCC Mixture Proportioning on Transfer and Development Length of Prestressing Strand." ACI, SP-247-9, p. 105-116.

Chan, Y., Chen, Y., and Liu, Y. (2003). "Development of Bond Strength of Reinforcement Steel in Self-Consolidating Concrete." *ACI Structural Journal*, Vol. 100, No. 4.

Cousins, T., Johnston, D., and Zia, P. (1986). "Bond of Epoxy Coated Prestressing Strand." Report No. FHWA-NC-87-05, Center for Transportation Engineering Studies, North Carolina State University, Raleigh, NC.

Cousins, T., Johnston, D., and Zia, P. (1990). "Transfer and Development Length of Epoxy-Coated and Uncoated Prestressing Strand." *PCI Journal*, Vol. 35, No. 4, p. 92-103.

Cousins, T., Badeaux, M. and Moustafa, S. (1992). "Proposed Test for Determining Bond Characteristics of Prestressing Strands." *PCI Journal*, Vol. 33, No. 1, p. 66-73.

Darwin, D. et al. (1996). "Development Length Criteria for Conventional and High Relative Rib Area Reinforcing Bars." *ACI Structural Journal*, Vol. 98, No. 5.

Deatherage, J., Burdette, E., and Chew, C. (1994). "Development Length and Lateral Spacing Requirements of Prestressing Strand for Prestressed Concrete Bridge Girders." *PCI Journal*, Vol. 39, No. 1, p. 70-83.

Esfahani, M., Lachemi, M., and Kianoush, M. (2008). "Top-Bar Effect of Steel Bars in Self-Consolidating Concrete (SCC)." *Cement and Concrete Composites*, Vol. 30, Issue 1.

Feldman, L. and Bartlett, F. (2007). "Bond Stresses Along Plain Steel Reinforcing Bars in Pullout Specimens." *ACI Structural Journal*, Vol. 104, No. 6.

Girgis, A. and Tuan, C. (2005). "Bond Strength and Transfer Length of Pretensioned Bridge Girders Cast with Self-Consolidating Concrete." *PCI Journal*, Vol. 50, No. 6, p. 72-87.

Hanson, N. and Kaar, P. (1959). "Flexural Bond Tests of Pretensioned Prestressed Beams." *ACI Journal*, Proceedings, Vol. 55, No. 7, p. 783-803.

Haq, M. (2005). "Effect of Self Consolidating Concrete (SCC) Mix Proportioning on Transfer and Development Length of Prestressing Strands." MS Thesis, Michigan State University, East Lansing, MI.

IDOT. (2007). "Self-Consolidating Concrete for Precast Products (BDE)." Bureau of Materials and Physical Research, Illinois Department of Transportation, Springfield, IL.

Kachlakev, D. and McCurry, D. (2000). "Testing of Full-Size Reinforced Concrete Beams Strengthened with FRP Composites: Experimental Results and Design Methods Verification." Report No. FHWA-OR-00-19, U.S. Department of Transportation Federal Highway Administration.

Labonte, T. and Hamilton, H. (2005). "Self-Consolidating Concrete (SCC) Structural Investigation." Report No. BD545 RPWO #21, Florida Department of Transportation, Gainesville, FL.

Lange, D. et al. (2008). "Performance and Acceptance of Self-Consolidating Concrete: Final Report." Report No. FHWA-ICT-08-020, Illinois Center for Transportation, Urbana, IL.

Larson, K., Peterman, R., and Esmaeily, A. (2007). "Evaluating the Time-Dependent Deformations and Bond Characteristics of a Self-Consolidating Concrete Mix and the Implication for Pretensioned Bridge Applications." Final Report No. FHWA-KS-07-1, Kansas Department of Transportation, Topeka, KS.

Logan, D. (1997). "Acceptance Criteria for Bond Quality of Strand for Pretensioned Prestressed Concrete Applications." *PCI Journal*, Vol. 42, No. 2, p. 52-90.

MacGregor, J. and Wight, J. (2005). *Reinforced Concrete: Mechanics and Design*. 4th Edition, Prentice Hall, Upper Saddle River, NJ.

Mahmoud, Z., Rizkalla, S. and Zaghloul, E. (1999). "Transfer and Development Lengths of Carbon Fiber Reinforcement Polymers Prestressed Reinforcement." *ACI Structural Journal*, Vol. 96, No. 4, p. 594-602.

Marti-Vargas, J., Arbelaez, C., Serna-Ros, P., and Castro-Bugallo, C. (2007-a). "Reliability of Transfer Length Estimation from Strand End Slip." *ACI Structural Journal*, Vol. 104, No. 4, p. 487-494.

Marti-Vargas, J. et al. (2007-b). "Analytical Model for Transfer Length Prediction of 13 mm Prestressing Strand." *Structural Engineering and Mechanics*, Vol. 26, No. 2, p. 211-229.

Mitchell, D. and Marzouk, H. (2007). "Bond Characteristics of High-Strength Lightweight Concrete." *ACI Structural Journal*, Vol. 104, No. 1.

Mitchell, D. et al. (1993). "Influence of High Strength Concrete on Transfer and Development Length of Pretensioning Strand." *PCI Journal*, Vol. 38, No. 3, p. 52-66.

Moustafa, S. (1974). "Pullout Strength of Strand and Lifting Loops." Technical Bulletin 74-B5, Concrete Technology Associates, Tacoma, WA.

Naito, C. et al. (2006). "Performance of Bulb-Tee Girders Made with Self-Consolidating Concrete." *PCI Journal*, Vol. 51, No. 6, p. 72-85.

Neville, A. (1996). *Properties of Concrete*. Fourth Edition, John Wiley and Sons, Inc., New York.

Nijhawam, C. (1978). Discussion of "Development Length of Prestressing Strand." *PCI Journal*, Vol. 23, No. 4, p. 97-07.

Norris, T., Saadatmanesh, H., and Ehsani, M. (1997). "Shear and Flexural Strengthening of R/C Beams with Carbon Fiber Sheets." *Journal of Structural Engineering*, Vol. 123, No. 7, p. 903-911.

Okamura, H. and Ouchi, M. (2003). "Self-Compacting Concrete." *Journal of Advanced Concrete Technology*, Vol. 1, No. 1, p. 5-15.

Olesniewicz, A. (1975). *Statistical Evaluation of Transmission Length of Strand*. Research and Design Centre for Industrial Building, Warsaw, Poland.

Ouchi, M. Nakamura, S. Osterberg, T. and Lwin, M. (2003). "Applications of Self-Compacting Concrete in Japan, Europe, and the United States." Proceedings of the International Symposium on High-Performance Concrete, Orlando, FL.

PCI. (2003-a). *Interim Guidelines for the Use of Self-Consolidating Concrete in Precast/Prestressed Concrete Member Plants*. Precast/Prestressed Concrete Institute, Chicago, IL.

PCI. (2003-b). *PCI Bridge Design Manual*. Precast/Prestressed Concrete Institute, Chicago, IL.

PCI. (2004). *PCI Design Handbook: Precast and Prestressed Concrete*. Sixth Edition, Precast/Prestressed Concrete Institute, Chicago, IL.

Perry, E. and Thompson, J. (1966). "Bond Stress Distribution on Reinforcing Steel in Beams and Pullout Specimens." *Proceedings of the Journal of the American Concrete Institute*, Vol. 63, No. 8.

Russell, B. and Burns, N. (1993). "Design Guidelines for Transfer, Development and Debonding of Large Diameter Seven Wire Strands in Pretensioned Concrete Girders." Research Report 1210-5F, Center for Transportation Research, University of Texas at Austin, Austin, TX.

Russell, B. and Burns, N. (1996). "Measured Transfer Lengths of 0.5 and 0.6 in. Strands in Pretensioned Concrete." *PCI Journal*, Vol. 41, No. 5, p. 44-65.

Russell, B. and Rose, D. (1996). "Investigation of Standardized Tests to Measure the Bond Performance of Prestressing Strand." Research Report, Fears Structural Engineering Laboratory, University of Oklahoma, Norman, OK.

Schindler, A., Barnes, R., Roberts, J. and Rodriguez, S. (2007). "Properties of Self-Consolidating Concrete for Prestressed Members." *ACI Materials Journal*, p. 53-61.

Shahawy, M. (2001). "A Critical Evaluation of the AASHTO Provisions for Strand Development Length of Prestressed Concrete Members." *PCI Journal*, Vol. 46, No. 4, p. 94-117.

Shahawy, M., Moussa, I., and Batchelor, B. (1992). "Strand Transfer Lengths in Full Scale AASHTO Prestressed Concrete Girders." *PCI Journal*, Vol. 37, No. 3, p. 84-96.

Staton, B., Do, N., Ruiz, E., and Hale, W. (2009). "Transfer Lengths of Prestressed Beams Cast with Self-Consolidating Concrete." *PCI Journal*, Vol. 54, No. 2, p. 64-83.

Stocker, M. and Sozen, M. (1970). "Investigation of Prestressed Reinforced Concrete for Highway Bridges, Part V: Bond Characteristics of Prestressing Strand." Engineering Experiment Station Bulletin 503, University of Illinois at Urbana-Champaign, Urbana, IL.

Tadros, M. and Baishya, M. (1996). Discussion of "A Review of Strand Development Length for Pretensioned Concrete Members." *PCI Journal*, Vol. 41, No. 2, p. 112-127.

Todeschini, C., Albert, B., and Kesler, C. (1964). "Behavior of Concrete Columns Reinforced with High Strength Steels." *Proceedings of the Journal of the American Concrete Institute*, Vol. 61, Issue 6, p. 701-716.

Trent, J. (2007). "Transfer Length, Development Length, Flexural Strength, and Prestress Losses Evaluation in Pretensioned Self-Consolidating Concrete Members." M.S. Thesis, Virginia Polytechnic Institute and State University, Blacksburg, VA.

Wehbe, N., Sigl, A., Gutzmer, Z., and Stripling, C. (2009). "Structural Performance of Prestressed Self-Consolidating Concrete Bridge Girders Made with Limestone Aggregates." The Mountain Plains Consortium, Upper Great Plains Transportation Institute at North Dakota State University.

Willam, K. and Warnke, E. (1974). "Constitutive Model for the Triaxial Behaviour of Concrete. Seminar on Concrete Structures Subjected to Triaxial Stresses." International Association of Bridge and Structural Engineering Conference, Bergamo, Italy.

W.R. Grace & Co. (2005). "Test Methods for Self-Consolidating Concrete." Technical Bulletin TB-1506, Cambridge, MA.

Zia, P. and Mostafa, T. (1977). "Development Length of Prestressing Strands." *PCI Journal*, Vol. 22, No. 5, p. 54-65.

Zia, P., Nunez, R., and Mata, L. (2005). “Implementation of Self-Consolidating Concrete for Prestressed Concrete Girders.” FHWA-NC-2006-30 Final Report, North Carolina Department of Transportation, Raleigh, NC.

APPENDIX A: PULLOUT TEST FORCE-DISPLACEMENT RESPONSES

This appendix contains figures of the force-displacement responses generated during the pullout tests described in Chapter 3, as well as the first slip and peak pullout loads obtained for all pullout specimens. Figures A.1-A.4 show responses for strands embedded in normally-consolidated blocks at various curing ages, while Figures A.5-A.8 show responses for stands embedded in SCC blocks at various curing ages. No data is presented for strand N3-E in Figure A.2 because the LVDT became dislodged during testing, requiring an abrupt stop to the servo-controlled loading mechanism; the LVDT and load cell were recalibrated prior to testing the next strand. Displacement values in the figures are those measured by the pullout apparatus LVDT (see Figure 3.5) at a position 20 in. above the upper surface of the pullout blocks; the figures do not account for strand elongation and, thus, are not force-slip responses. Table A.1 summarizes the first slip and peak pullout loads for all pullout test specimens.

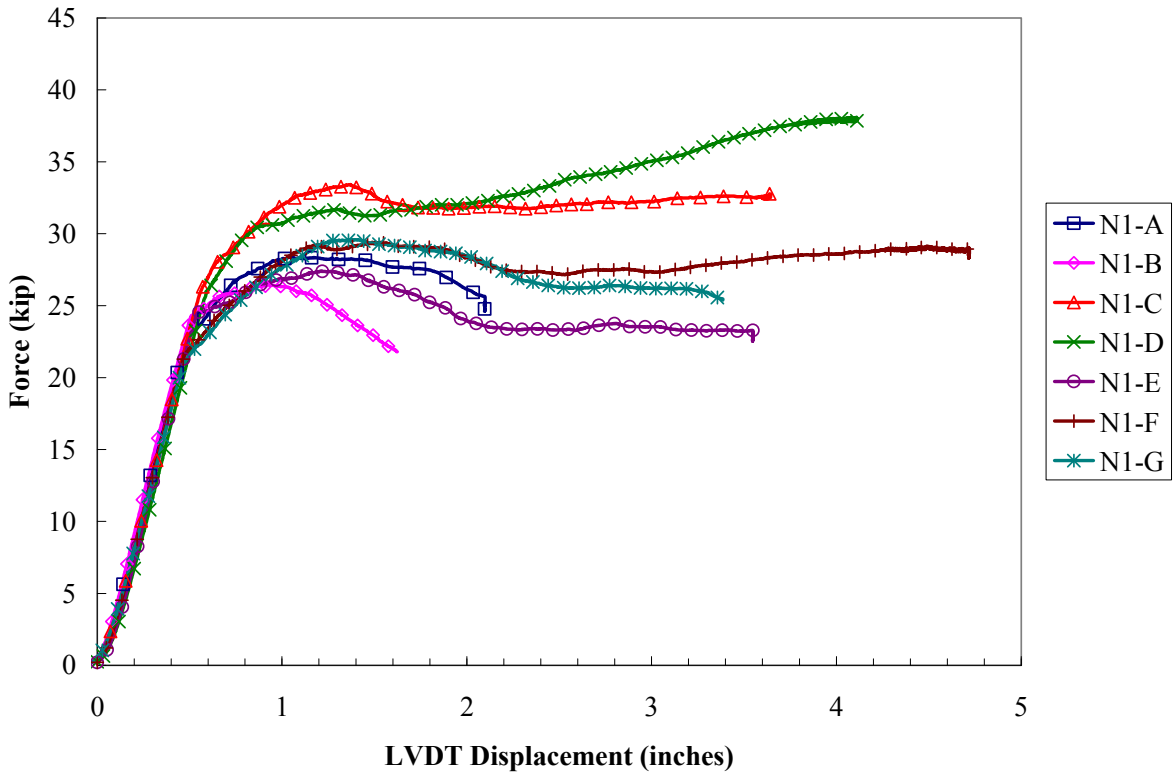

Figure A.1: Force-displacement responses for strands in NCC 1 day after casting

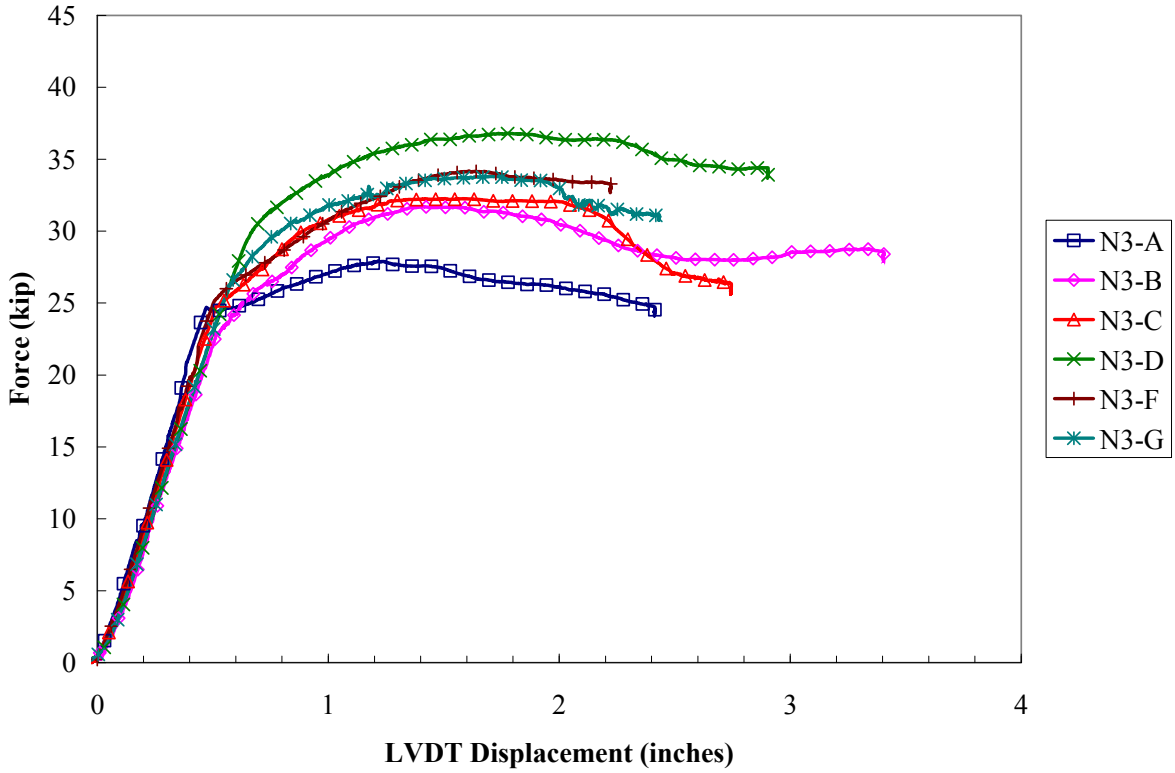

Figure A.2: Force-displacement responses for strands in NCC 3 days after casting

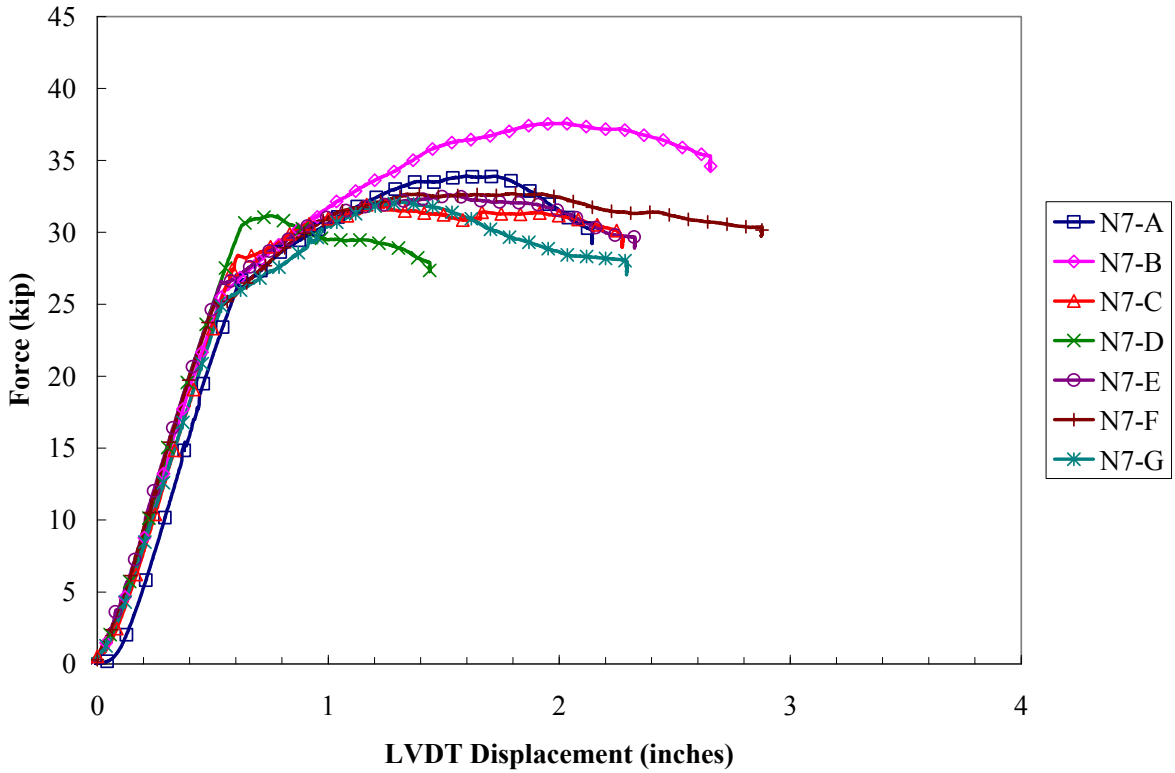

Figure A.3: Force-displacement responses for strands in NCC 7 days after casting

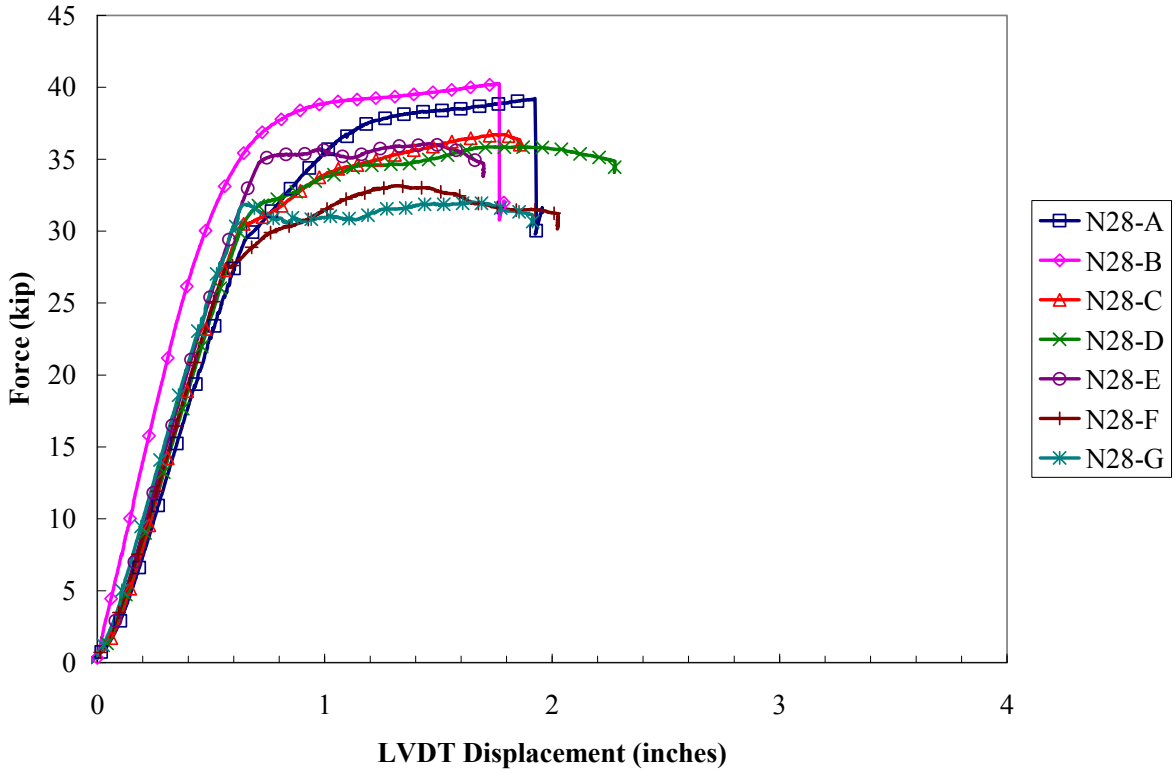

Figure A.4: Force-displacement responses for strands in NCC 28 days after casting

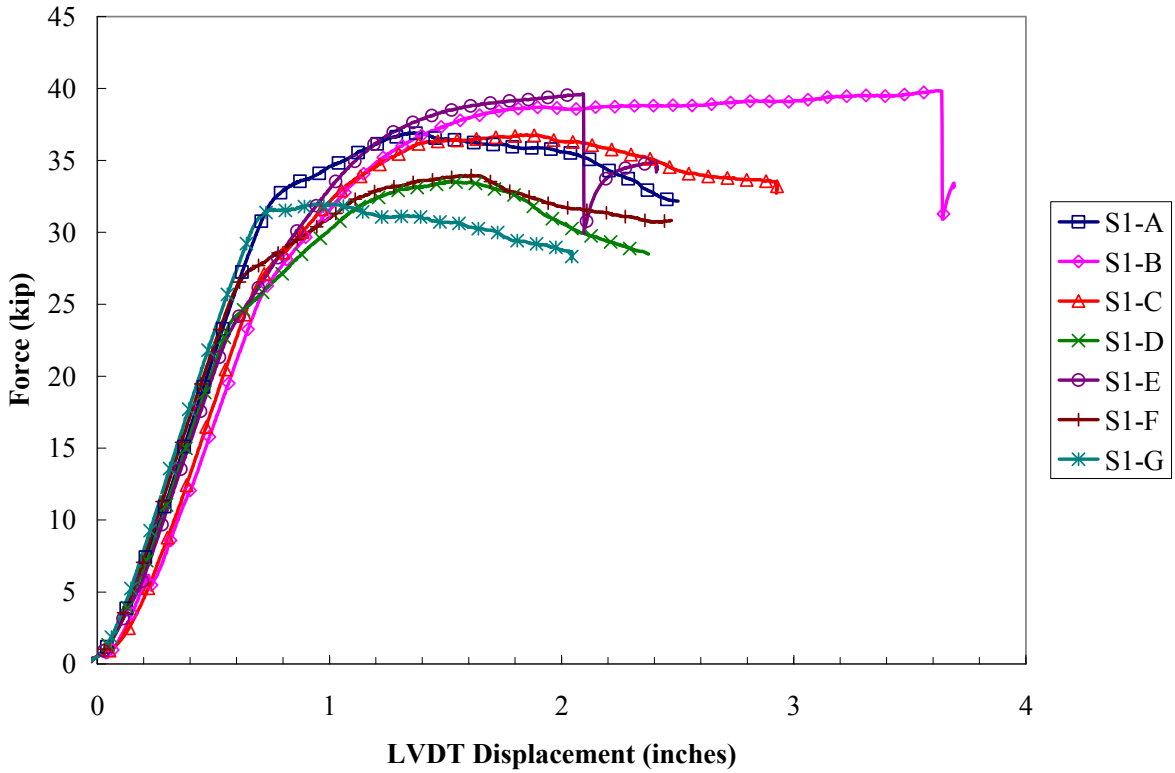

Figure A.5: Force-displacement responses for strands in SCC 1 day after casting

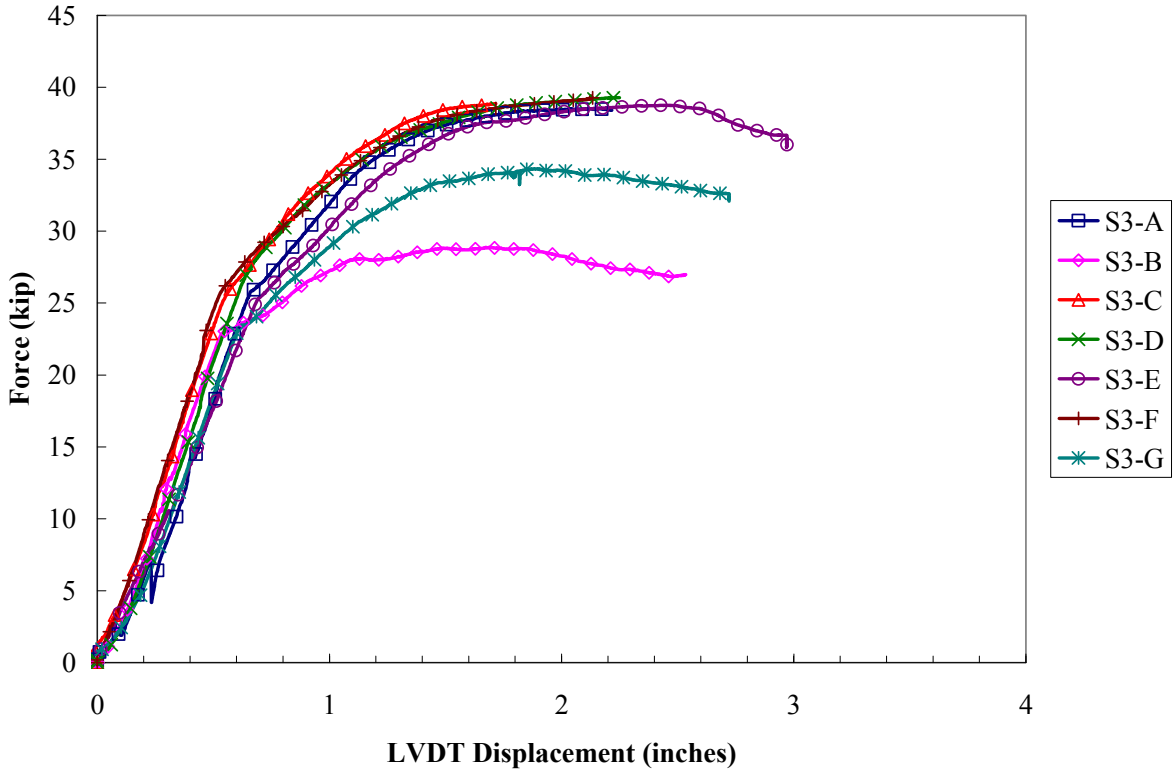

Figure A.6: Force-displacement responses for strands in SCC 3 days after casting

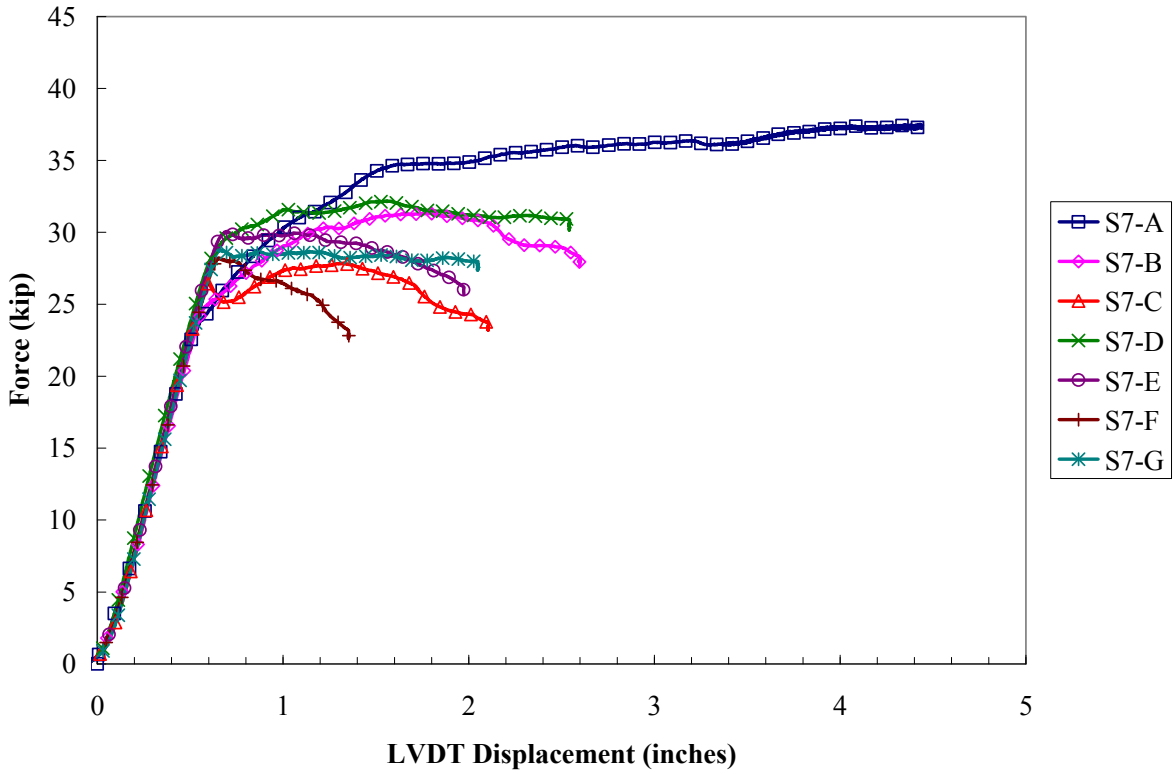

Figure A.7: Force-displacement responses for strands in SCC 7 days after casting

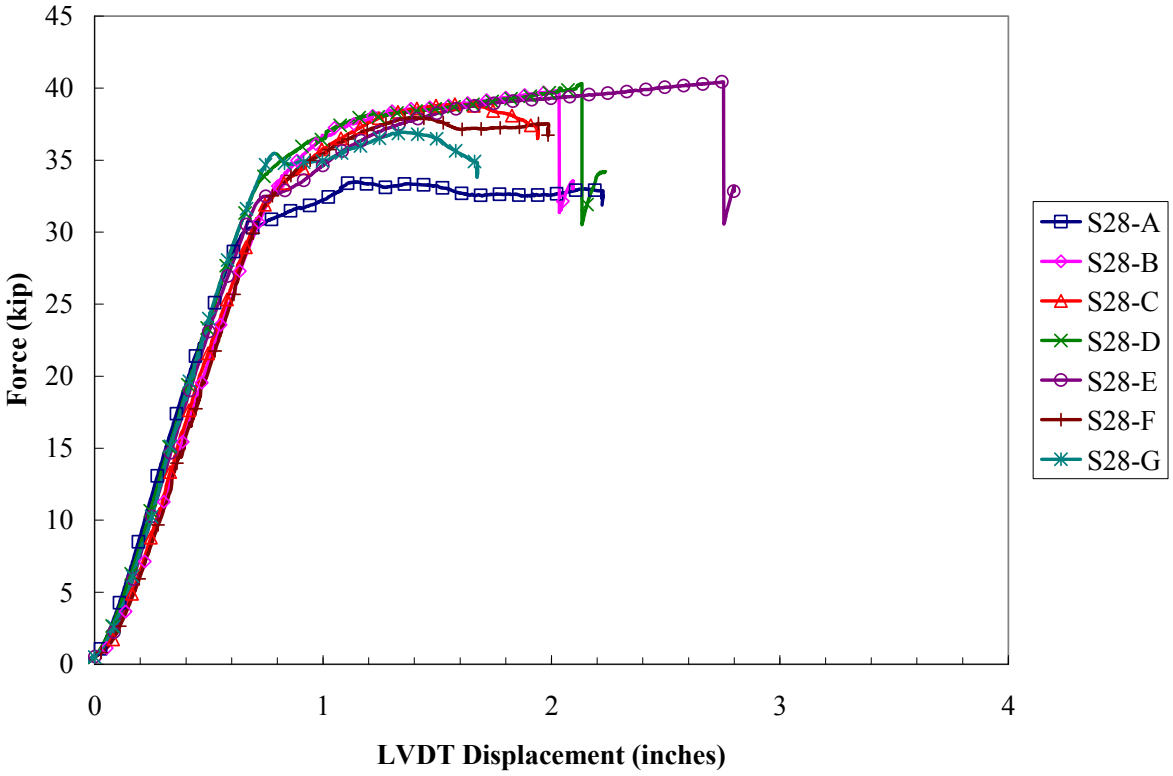

Figure A.8: Force-displacement responses for strands in SCC 28 days after casting

Table A.1: First Slip and Peak Pullout Loads for all Pullout Tests

	First Slip Loads (kip)				Peak Pullout Loads (kip)			
NCC	**1 Day**	**3 Day**	**7 Day**	**28 Day**	**1 Day**	**3 Day**	**7 Day**	**28 Day**
A	22.8	24.5	26.6	24.0	28.4	27.9	33.9	39.2
B	24.3	23.1	26.1	27.0	26.5	31.7	37.6	40.3
C	25.8	24.5	26.5	23.0	33.4	32.3	32.0	36.7
D	25.4	28.5	21.7	27.5	38.1	36.8	31.2	35.9
E	23.2	-	26.4	27.0	27.4	-	32.6	36.1
F	21.8	25.0	24.9	28.0	29.4	34.2	32.7	33.2
G	21.1	25.1	25.5	27.5	29.6	33.8	32.1	32.0
Average	**23.5**	**25.1**	**25.4**	**26.3**	**30.4**	**32.8**	**33.2**	**36.2**
Std. Dev.	**1.8**	**1.8**	**1.7**	**2.0**	**4.1**	**3.0**	**2.1**	**3.0**

	First Slip Loads (kip)				Peak Pullout Loads (kip)			
SCC	**1 Day**	**3 Day**	**7 Day**	**28 Day**	**1 Day**	**3 Day**	**7 Day**	**28 Day**
A	28.5	25.7	23.4	23.5	36.9	38.5	37.5	33.5
B	23.5	23.1	24.9	25.5	39.8	29.5	31.3	39.8
C	24.1	25.5	25.9	26.0	36.8	38.9	27.8	38.9
D	23.1	25.6	26.1	23.0	33.6	39.3	32.2	40.3
E	21.9	25.6	26.9	24.0	39.6	38.8	30.1	40.4
F	22.3	25.4	23.2	28.0	34.0	39.4	28.2	38.0
G	23.3	23.5	26.4	27.0	32.0	34.3	28.8	36.9
Average	**23.8**	**24.9**	**25.3**	**25.3**	**36.1**	**36.9**	**30.8**	**38.3**
Std. Dev.	**2.2**	**1.1**	**1.5**	**1.9**	**3.0**	**3.7**	**3.4**	**2.5**

APPENDIX B: FABRICATION DRAWINGS FOR FULL-SCALE GIRDERS

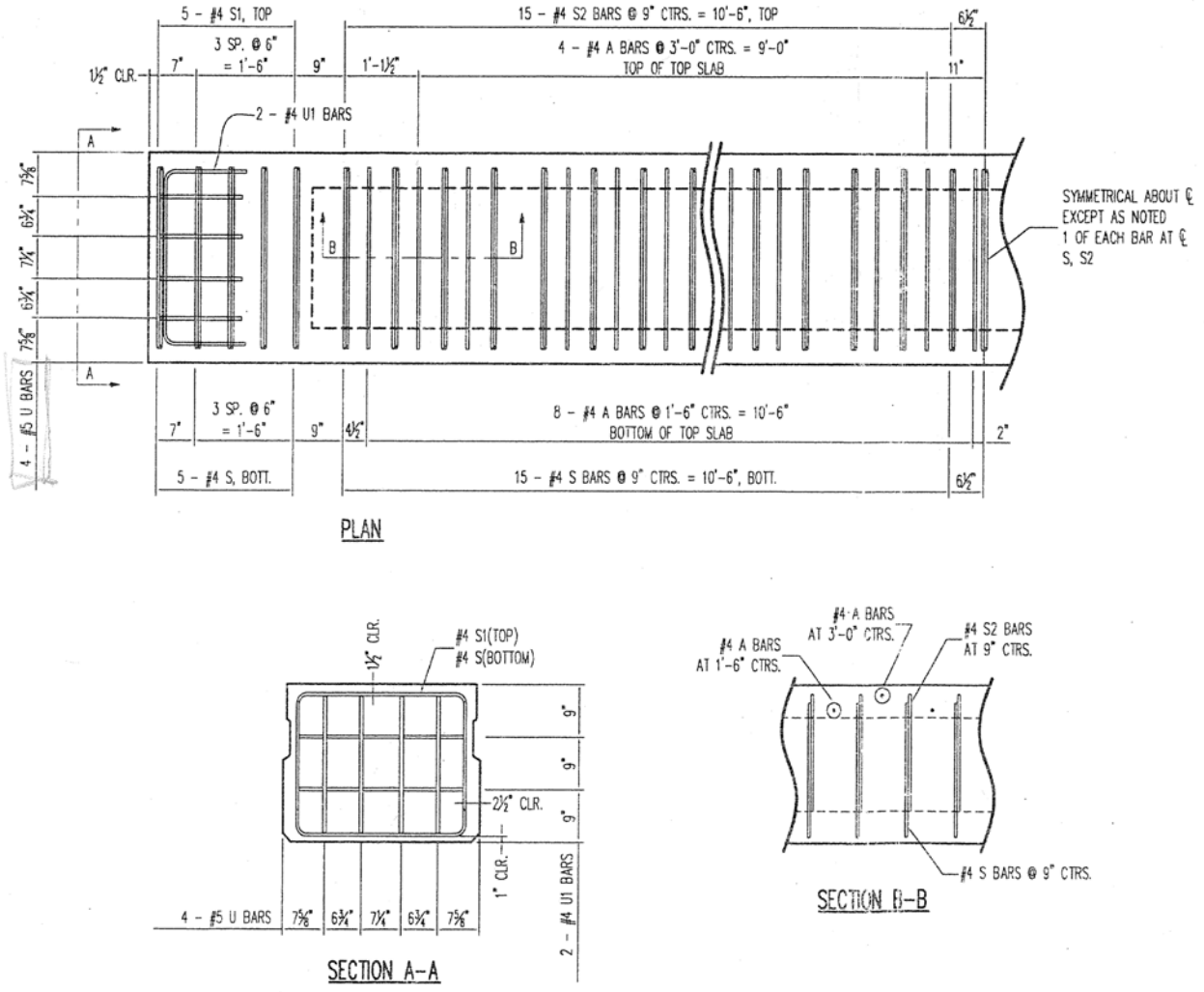

Figure B.1: Reinforcement layout for hollow box girders

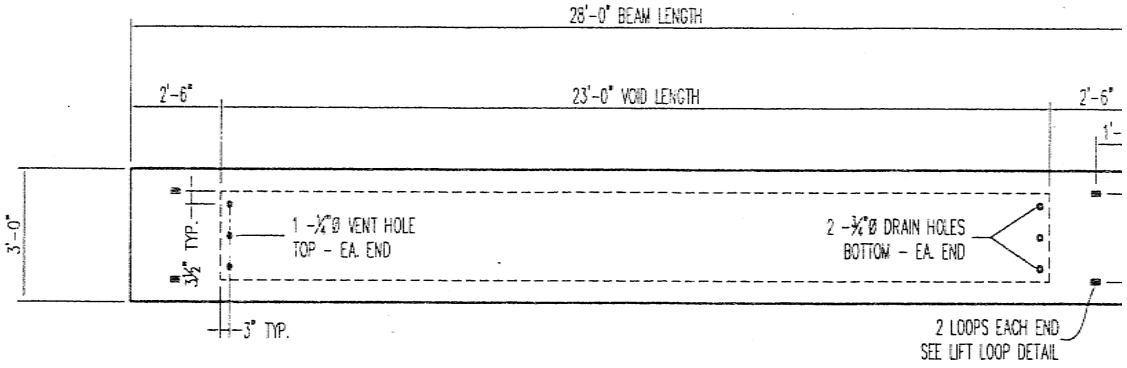

Figure B.2: Plan for hollow box girders showing center void

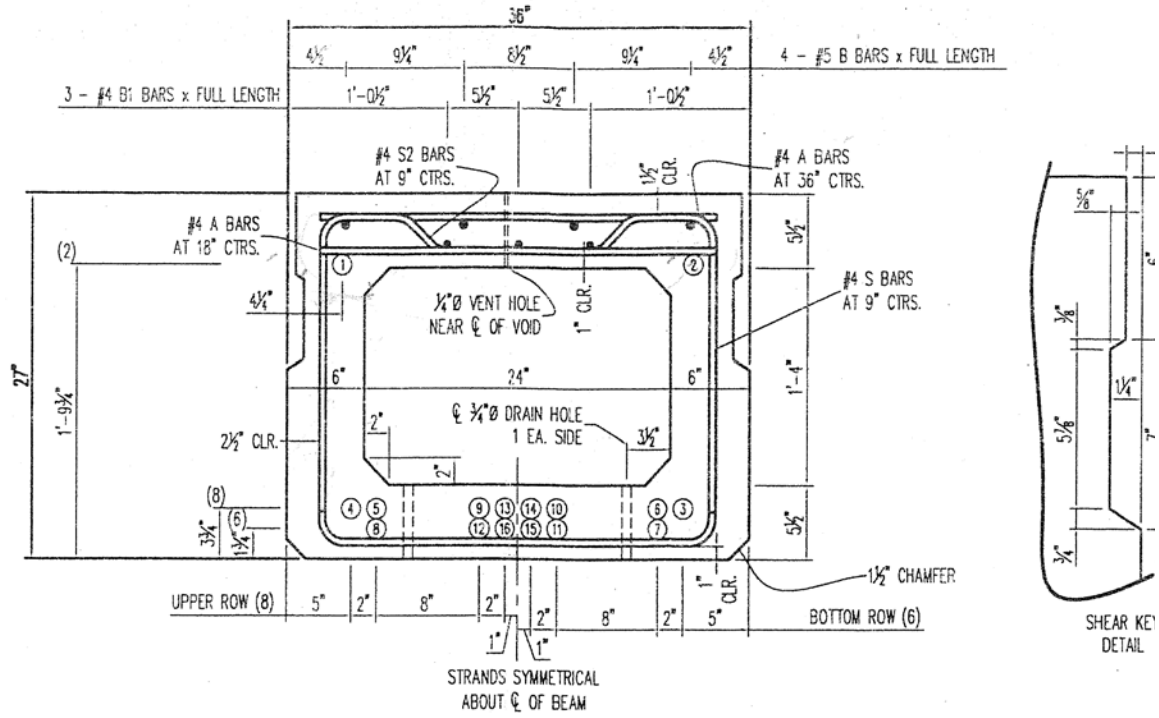

Figure B.3: Strand pattern and cross-section geometry for hollow box girders

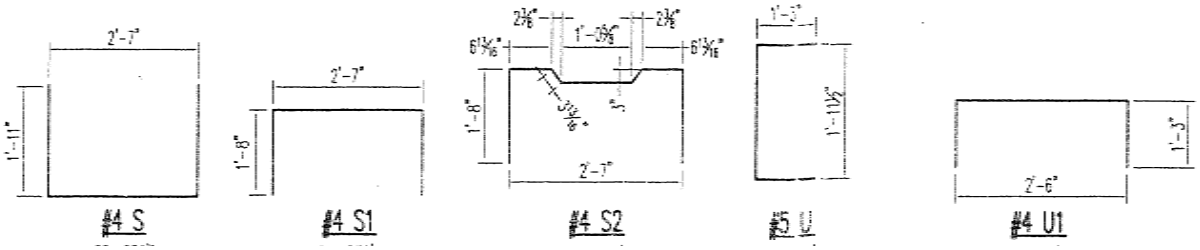

REINFORCEMENT BARS						
BAR	SIZE	NO. / BM.	LENGTH	SHAPE	T. REQ'D	LBS.
A	#4	8	2'-7"	——	16	28
B	#5	4	27'-9"	——	8	232
B1	#4	3	27'-9"	——	6	111
S	#4	41	6'-5"	⌊⌋	82	351
S1	#4	10	5'-11"	⌐¬	20	79
S2	#4	31	6'-2"	⌐¬	62	255
U	#5	8	4'-6"	⊏	16	75
U1	#4	4	5'-0"	⌐¬	8	27

Figure B.4: Reinforcement specifications for hollow box girders

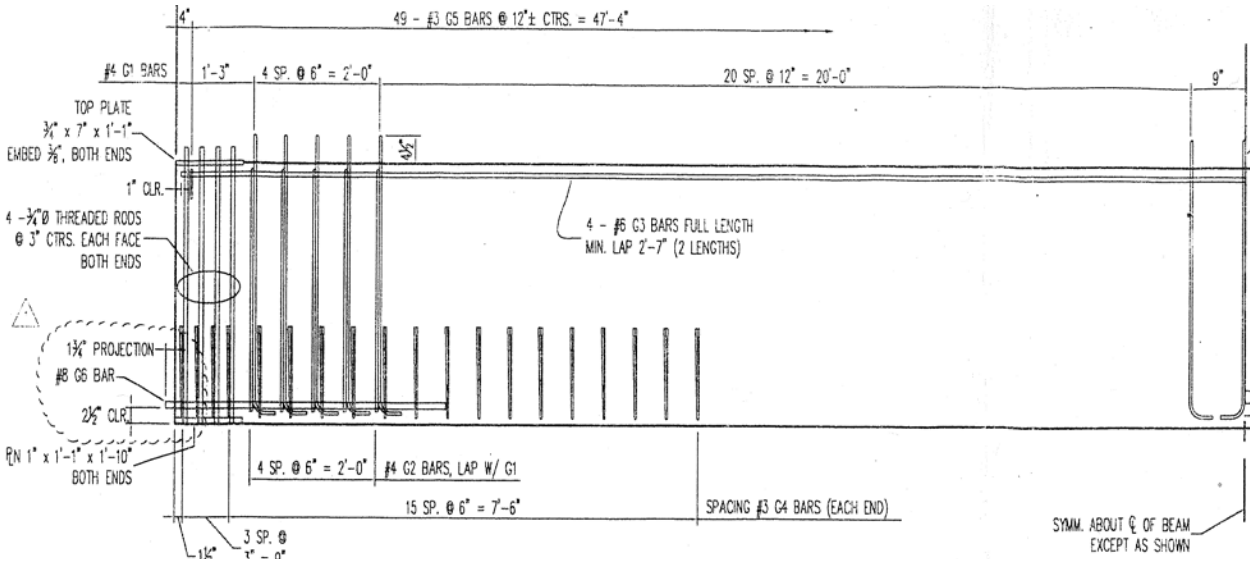

Figure B.5: Reinforcement layout for I-girders

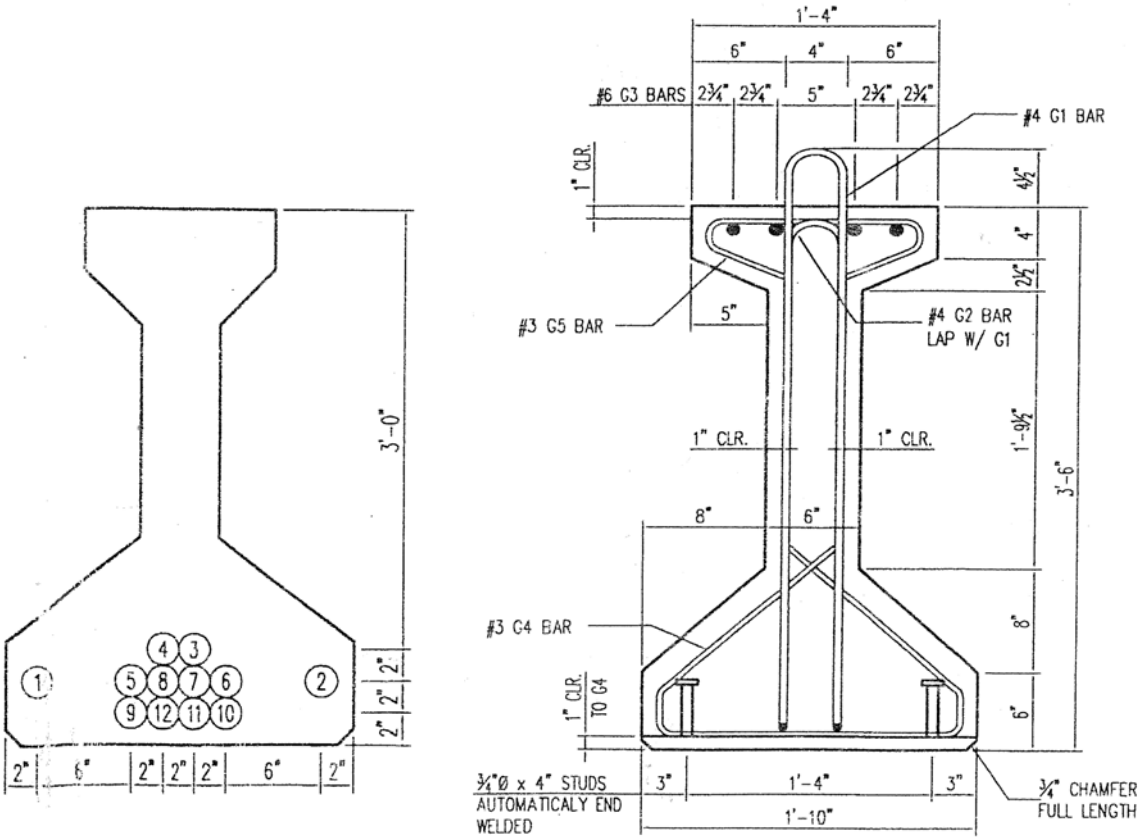

Figure B.6: Strand pattern and cross-section geometry for I-girders

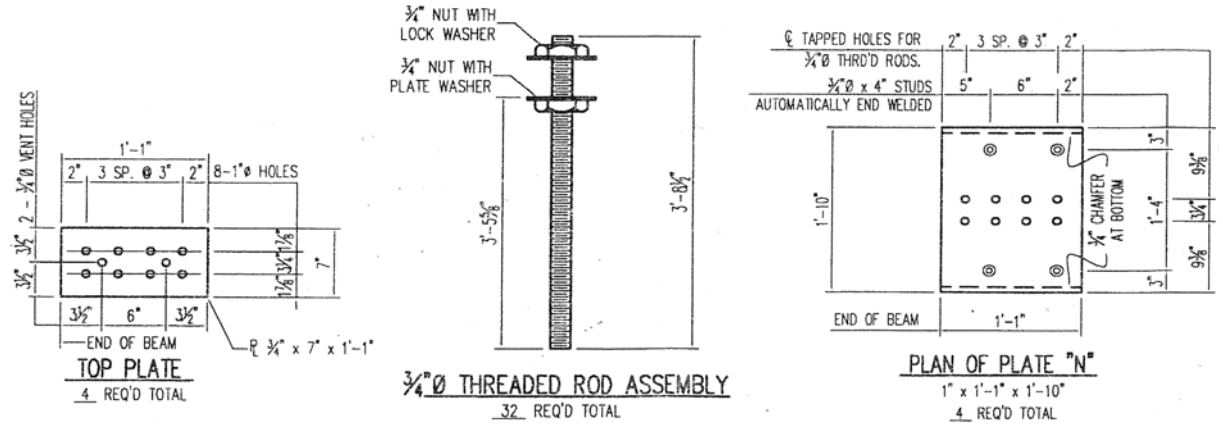

Figure B.7: Hardware details for I-girders

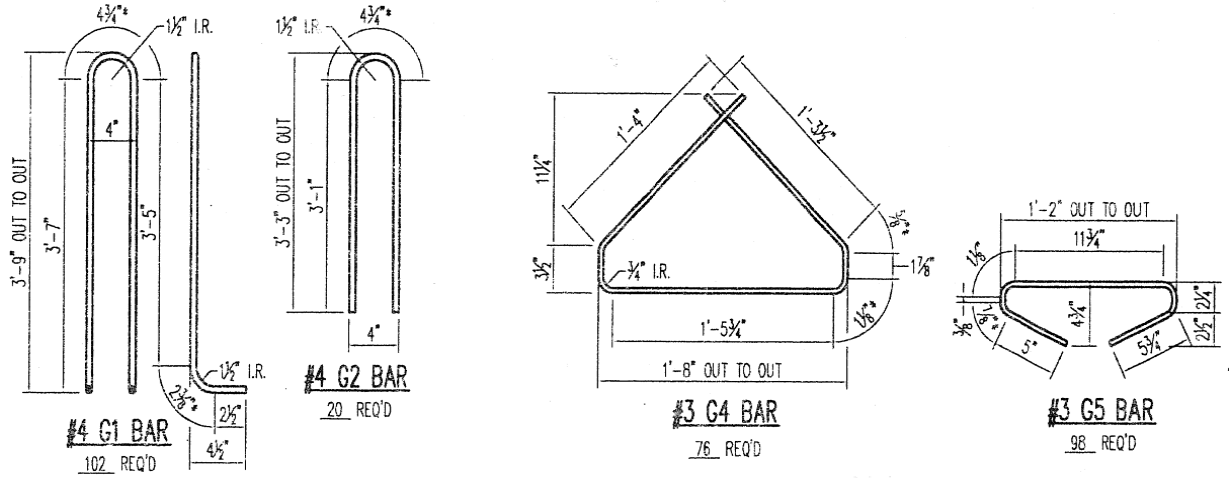

REINFORCEMENT BARS – ALL BEAMS						
BAR	SIZE	REQ'D	*LENGTH	SHAPE	REQ'D	LBS.
G1	#4	51	8'-1"	⊓L	102	551
G2	#4	10	6'-7"	⊓	20	88
G3	#6	8	25'-3"	—	16	607
G4	#3	38	4'-8"	⌓	76	133
G5	#3	49	2'-3"	⊐	98	83
G6	#8	4	4'-6"	—	8	96

Figure B.8: Reinforcement specifications for I-girders

APPENDIX C: EXAMPLE CALCULATIONS OF PRESTRESS LOSSES

Example C.1 – Box Girder 1 – Prestress Losses – AASHTO Separate Lump Sum Method

Steel Relaxation before Transfer:

$$\Delta f_{pR1=1} = \frac{\log(24.0t)}{40.0}\left(\frac{f_{pJ}}{f_{py}} - 0.55\right) f_{pJ} = \frac{\log(24.0)}{40.0}\left(\frac{202}{243} - 0.55\right)202 = 2ksi$$

Elastic Shortening:

$$w = 18300/28000 = 0.65klf$$

$$M_{sw} = \frac{wL^2}{8} = \frac{0.65(12)(28^2)}{8} = 769kip \cdot ft$$

$$f_{cgp} = \left(\frac{f_{pi}A_{ps}}{A_c} + \frac{f_{pi}A_{ps}e^2}{I}\right) - \frac{M_{sw}e}{I}$$

$$= \left(\frac{191.2(2.448)}{568.8} + \frac{191.2(2.448)(8.04)^2}{49684}\right) - \frac{769(8.04)}{49684} = 1.31ksi$$

$$\Delta f_{pES} = \frac{E_{ps}}{E_{ci}} f_{cgp} = \frac{28700}{57\sqrt{5660}}(1.31) = 8.8ksi$$

Check $f_{pi} = f_{pJ} - f_{pR1} - f_{pES} = 202 - 2 - 8.8 = 191.2ksi$

Shrinkage:

$$\Delta f_{pS} = 17.0 - 0.15H = 17.0 - 0.15(75) = 5.8ksi$$

Creep:

$$\Delta f_{pC} = 12.0 f_{cgp} - 7.0\Delta f_{cdp} = 12.0(1.31) - 0 = 15.7ksi$$

Steel Relaxation after Transfer:

$$\Delta f_{pR2} = 0.30\left[20.0 - 0.4(8.8) - 0.2(5.8 + 15.7)\right] = 3.66ksi$$

Total Losses:

$$\Delta f_{pT} = \Delta f_{pES} + \Delta f_{pSR} + \Delta f_{pCR} + \Delta f_{pR} = 8.8 + 5.8 + 15.7 + 3.66 + 2 = 35.8ksi$$

Effective Prestress:

$$f_{pe} = f_{pJ} - \Delta f_{pT} = 202 - 35.8 = 166.1ksi$$

Example C.2 – Box Girder 1 – Prestress Losses – PCI Method

Elastic Shortening (ES):

$$f_{pi} = 194.1 ksi$$

$$P_i = A_{ps} f_{pi} = 2.448(194.1) = 475.1 kip$$

$$f_{cir} = K_{cir}\left(\frac{P_i}{A_g} + \frac{P_i e^2}{I_g}\right) - \frac{M_g e}{I_g} = 0.9\left(\frac{475}{568.8} + \frac{475(8.04)^2}{49684}\right) - \frac{769(8.04)}{49684} = 1.18 ksi$$

$$ES = \frac{K_{es} E_{ps} f_{cir}}{E_{ci}} = \frac{1(28700)(1.18)}{57\sqrt{5660}} = 7.92 ksi$$

Check $f_{pi} = f_{pJ} - ES = 202 - 7.92 = 194.1 ksi$

Creep (CR):

$$f_{cds} = \frac{M_{sd} e}{I_g} = 0$$

$$CR = \frac{K_{cr} E_{ps}}{E_c}\left(f_{cir} - f_{cds}\right) = \frac{2(28700)}{\left(57\sqrt{7500}\right)}(1.18 - 0) = 14 ksi$$

Shrinkage (SH):

$$SH = \left(8.06 \times 10^{-6}\right) K_{sh} E_{ps}\left(1 - 0.06\frac{V}{S}\right)(100 - RH)$$

$$= \left(8.06 \times 10^{-6}\right)(1)(28700)(1 - 0.06(3.24))(100 - 75) = 4.7 ksi$$

Steel Relaxation (RE):

$$\frac{f_{pi}}{f_{pu}} = \frac{202 - ES}{270} = \frac{202 - 7.92}{270} = 0.72 \rightarrow \qquad C = \frac{0.72}{0.21}\left[\frac{0.72}{0.9} - 0.55\right] = 0.85$$

$$RE = \left[5000 - 0.04\left(4.7 + 14 + 7.92\right)\right](0.85) = 3.35 ksi$$

Total Losses:

$$TL = 7.9 + 14.0 + 4.7 + 3.4 = 30 ksi$$

Effective Prestress:

$$f_{pe} = 202 - 30 = 172 ksi$$

Example C.3 – Box Girder 1 – Prestress Losses – ACI Committee 209 Method

Steel Relaxation before Transfer:

$$f_{pi} = 191.9 ksi$$

$$P_i = A_{ps} f_{pi} = 2.448(191.9) = 469.7 kip$$

$$\left(f_{sr}\right)_t = 0.005\left(f_{pi}\right)\log(t) = 0.005\left(191.9\right)\log(1) = 1.32 ksi$$

Elastic Shortening:

$$n = \frac{E_{ps}}{E_{ci}} = \frac{28700}{57\sqrt{5660}} = 6.693$$

$$f_c = \left(\frac{P_i}{A_g} + \frac{P_i e^2}{I_g}\right) - \frac{M_g e}{I_g} = \left(\frac{470}{568.8} + \frac{470\left(8.04\right)^2}{49684}\right) - \frac{769\left(8.04\right)}{49684} = 1.31 ksi$$

$$\left(nf_c\right) = 6.693(1.31) = 8.79 ksi$$

Check: $f_{pi} = f_{pJ} - ES - R_1 = 202 - 8.79 - 1.32 = 191.9 ksi$

Creep:

$$\gamma_{vs} = \frac{2}{3}\left(1 + 1.13e^{\left(-0.54\frac{V}{S}\right)}\right) = \frac{2}{3}\left(1 + 1.13e^{(-0.54(3.24))}\right) = 0.798$$

$$\gamma_{la} = 1.25\left(t_{la}\right)^{-0.118} = 1.25\left(7\right)^{-0.118} = 0.994$$

$$\gamma_{\lambda} = 1.27 - 0.0067\lambda = 1.27 - 0.0067(75) = 0.768$$

$$\gamma_c = \gamma_{la}\gamma_{\lambda}\gamma_{vs} = 0.994(0.768)(0.978) = 0.608$$

$$v_u = 2.35\gamma_c = 2.35(0.608) = 1.43$$

$$v_{t=28} = \frac{t^{0.60}}{10 + t^{0.60}} v_u = \frac{28^{0.60}}{10 + 28^{0.60}}(1.43) = 0.607$$

$$\left(nf_c\right)v_t\left(1 - \frac{F_t}{2F_o}\right) = \left(8.79\right)\left(0.607\right)\left(1 - \frac{0.10}{2}\right) = 5.07 ksi$$

Shrinkage:

$$\gamma_{vs} = 1.2e^{\left(-0.12\frac{V}{S}\right)} = 1.2e^{(-0.12(3.24))} = 0.81$$

$$\gamma_{\lambda} = 1.40 - 0.010\lambda = 1.40 - 0.010\left(75\right) = 0.65$$

$$\gamma_{cp} = 1.2$$

$$\gamma_{sh} = \gamma_{\lambda}\gamma_{vs}\gamma_{cp} = 0.65(0.81)(1.2) = 0.63$$

$$\left(\varepsilon_{sh}\right)_u = 780\gamma_{sh} \times 10^{-6} = 780(0.63) \times 10^{-6} = 0.000495$$

$$\left(\varepsilon_{sh}\right)_{t=28} = \frac{t}{35 + t}\left(\varepsilon_{sh}\right)_u = \frac{28}{35 + 28}\left(0.000495\right) = 0.00022$$

$$\xi_s = 1 + \frac{e^2}{\left(I/A\right)} = 1 + \frac{8.04^2}{\left(49684/568.8\right)} = 1.74$$

$$\frac{\left(\varepsilon_{sh}\right)_t E_s}{1 + n\rho\xi_s} = \frac{\left(0.00022\right)\left(28700\right)}{1 + 6.69(0.0043)(1.74)} = 6.6ksi$$

Steel Relaxation after Transfer:

$$\left(f_{sr}\right)_{t=28} = 0.005\left(f_{si}\right)\log(t) - 0.005\left(f_{si}\right)\log(1) = 0.005\left(191.9\right)\log(28) - 1.32 = 1.39ksi$$

Total Losses:

$$\lambda_t = \left(nf_c\right) + \left(nf_c\right)v_t\left(1 - \frac{F_t}{2F_o}\right) + \frac{\left(\varepsilon_{sh}\right)_t E_s}{1 + n\rho\xi_s} + \left(f_{sr}\right)_t = 8.8 + 5.1 + 6.6 + 1.32 + 1.39 = 23.21ksi$$

Effective Prestress:

$$f_{pe} = 202 - 23.2 = 178.8ksi$$

APPENDIX D: EXAMPLE SHEAR AND MOMENT CAPACITY CALCULATIONS

Example D.1 – Box Girder 1 – Flexural Capacity via AASHTO Refined Method

A_{ps}	= 2.448	in^2	A_c	= 568.8	in^2	e_o	= 8.04	in
E_{ps}	= 28700	ksi	E_c	= 4415	ksi	I_{xx}	= 49684	in^4
d_p	= 21.75	in	f'_c	= 6.0	ksi	b_f	= 34.75	in

$$\beta_1 = 0.85 - 0.05(f'_c - 4) = 0.85 - 0.05(6-4) = 0.75 \geq 0.65$$

$$k = 2\left(1.04 - \frac{f_{py}}{f_{pu}}\right) = 2\left(1.04 - \frac{243}{270}\right) = 0.28$$

$$c = \frac{A_{ps}f_{pu} + A_s f_y - A'_s f_y}{0.85\beta_1 f'_c b + kA_{ps}f_{pu}/d_p} = \frac{2.448(270) - 1.84(60)}{0.85(0.75)(6)(34.75) + 0.28(2.448)(270)/(21.75)} = 3.89"$$

Since $c < 3d_s'$, the contribution from compression reinforcement may be neglected:

$$c = \frac{A_{ps}f_{pu} + A_s f_y}{0.85\beta_1 f'_c b + kA_{ps}f_{pu}/d_p} = \frac{2.448(270)}{0.85(0.75)(6)(34.75) + 0.28(2.448)(270)/(21.75)} = 4.67"$$

$$\frac{c}{d} = \frac{4.67}{21.75} = 0.21 \leq 0.42 \quad \text{and} \quad a = \beta_1 c = 0.75(4.67) = 3.51"$$

$$f_{ps} = f_{pu}\left(1 - \frac{kc}{d_{ps}}\right) = 270\left(1 - \frac{0.28(4.67)}{21.75}\right) = 253.8 \text{ k*ft}$$

Taking Φ = 1.0 for prestressed member: $\Phi M_n = 1.0\left[2.448(253.8)\left(21.75 - \frac{3.51}{2}\right)\right] = 1035$ k*ft

$$Z_b = \frac{I}{y_b} = \frac{49684}{13.29} = 3738.5 \text{ in}^3$$

$$f_r = 7.5\sqrt{f'_c} = 7.5\sqrt{6000} = 0.581 \text{ ksi}$$

$$M_{crack} = A_{ps}f_{pe}\left(e_o + \frac{Z_b}{A_c}\right) + f_r Z_b = \frac{2.448(167)}{12}\left(8.04 + \frac{3739}{568.8}\right) + \frac{0.581(3739)}{12} = 679 \text{ k*ft}$$

Check $\frac{\Phi M_n}{M_{crack}} = \frac{1035}{679} = 1.53 > 1.2$ OK

Example D.2 – Box Girder 1 – Shear Capacity via AASHTO Method

$$d_v = \max\begin{cases} 0.9d_e = 0.9(21.75) = 19.58 \\ 0.72h = 0.72(27.0) = 19.44 \end{cases} = 19.58"$$

$$b_v = 2(4.75) = 9.5"$$

$V_p = f_{pe} A_{ps} \sin\alpha = 0$ (tendons straight)

Consider section 36 in. from end of specimen, where cross-section is hollow and stirrups are spaced 9 in. apart. Take applied shear and moment from respective envelopes.

$V_u = 129.6$ kip

$M_u = 4904$ k*in

$M_u \geq V_u d_v = 129.6(19.58) = 2537$ k*in

Assume θ = 30 degrees:

$$\varepsilon_x = \frac{\frac{M_u}{d_v} + 0.5N_u + 0.5(V_u - V_p)\cot\theta - A_{ps}f_{po}}{2(E_s A_s + E_p A_{ps})}$$

$$\varepsilon_x = \frac{\frac{4904}{19.58} + 0.5(129.6)\cot 30 - 2.448(167)}{2(28700)(2.448)} = -0.3278$$

Since strain negative, use:

$$\varepsilon_x = \frac{\frac{M_u}{d_v} + 0.5N_u + 0.5(V_u - V_p)\cot\theta - A_{ps}f_{po}}{2(E_c A_{cf} + E_s A_s + E_p A_{ps})}$$

$$\varepsilon_x = \frac{\frac{4904}{19.58} + 0.5(129.6)\cot 30 - 2.448(167)}{2\left[4415(312) + 28700(2.448)\right]} = -0.016$$

$$v = \frac{V_u - \phi V_p}{\phi b_v d_v} = \frac{129.6}{0.9(9.5)(19.58)} = 0.7743 \text{ ksi}$$

$$\frac{v}{f_c'} = \frac{0.7743}{6} = 0.129$$

From AASHTO (2004) interpolation tables: θ = 23.63 degrees ≠ 30 degrees.

Iterate to find: θ = 23.84 degrees, β = 2.85

$$V_c = 0.0316\beta b_v d_v \sqrt{f_c'} = 0.0316(2.85)(9.5)(19.58)\sqrt{6} = 41 \text{ kip}$$

Steel contribution considering only one leg on each side of hollow:

$$V_s = \frac{A_v f_y d_v \cot\theta}{s} = \frac{0.4(60)(19.58)\cot 23.84}{9} = 118.1 \text{ kip}$$

Total Shear:

$$\Phi V_n = \Phi(V_c + V_s + V_p) = 0.9(41+118.1) = 143.3 \text{ kip}$$

$$\Phi V_{n,limit} = \Phi(0.25 f'_{c,28-day} b_v d_v + V_p) = 0.9(0.25)(6)(9.5)(19.58) = 251 \text{ kip OK}$$

Example D.3 – Box Girder 1 – Shear Capacity via ACI Method

$$d_v = \max\begin{cases} d_p = 21.75 \\ 0.8h = 0.8(27) = 21.6 \end{cases} = 21.6"$$

$$b_w = 9.5"$$

Check both V_{ci} and V_{cw} to find V_c:

$$M_{cr} = Z_b\left[6\sqrt{f_c'} + \frac{F}{A_c}\left(1 + \frac{e_o A_c}{Z_b}\right)\right] = \frac{3738}{12000}\left[6\sqrt{6} + \frac{409}{568.8}\left(1 + \frac{8.04(568.8)}{3738}\right)\right] = 643 \text{ kip*ft}$$

$$\Delta M_{cr} = M_{cr} - M_G = 632 - 24.5 = 618 \text{ kip*ft}$$

$$V_{ci} = 0.6\lambda b_w d_p \sqrt{f_c'} + V_G + \frac{\Delta V_u \Delta M_{cr}}{\Delta M_u} \geq 1.7\lambda b_w d_p \sqrt{f_c'}$$

$$V_{ci} = \frac{0.6(9.5)(21.75)\sqrt{6000}}{1000} + 7.2 + \frac{618}{(36/12)} = 222.8 \text{ kip} \geq \frac{1.7(9.5)(21.75)\sqrt{6000}}{1000} = 27.2 \text{ kip}$$

$$V_{cw} = (3.5\lambda\sqrt{f_c'} + 0.3\sigma_g)b_w d_p + V_p = \left[3.5\sqrt{6000} + 0.3\left(\frac{409}{568.8}\right)\right]\frac{(9.5)(21.75)}{1000} = 100.6 \text{ kip}$$

$$V_c = \min\left(V_{cf}, V_{ci}\right) = 100.6 \text{ kip}$$

Steel contribution considering only one leg on each side of hollow:

$$V_s = \frac{A_v f_y d}{s} = \frac{0.4(60)(21.75)}{9} = 58 \text{ kip}$$

$$V_{s,\text{limit}} = 8b_w d_p \sqrt{f_c'} = \frac{8(9.5)(21.75)\sqrt{6000}}{1000} = 128 \text{ kip}$$

Shear Capacity:

$$\Phi V_n = \Phi(V_c + V_s) = 0.75(100.6 + 58) = 119 \text{ kip}$$

Example D.4 – I-Girder 1 – Flexural Capacity via AASHTO Refined Method

A_{ps}	= 1.836	in^2	A_c	= 704.5	in^2	e_o	= 23.6	in
E_{ps}	= 28700	ksi	E_c	= 4415	ksi	I_{xx}	= 219262	in^4
d_p	= 46.3	in	f'_c	= 6.0	ksi	b_f	= 30	in

$$\beta_1 = 0.85 - 0.05(f'_c - 4) = 0.85 - 0.05(6-4) = 0.77 \geq 0.65$$

$$k = 2\left(1.04 - \frac{f_{py}}{f_{pu}}\right) = 2\left(1.04 - \frac{243}{270}\right) = 0.28$$

$$c = \frac{A_{ps}f_{pu} + A_s f_y - A'_s f_y}{0.85\beta_1 f'_c b + kA_{ps}f_{pu}/d_p} = \frac{1.836(270) - 2.31(60)}{0.85(0.75)(6)(30) + 0.28(1.836)(270)/(46.3)} = 5.38"$$

Since $c < 3d_s'$, the contribution from compression reinforcement may be neglected:

$$c = \frac{A_{ps}f_{pu} + A_s f_y}{0.85\beta_1 f'_c b + kA_{ps}f_{pu}/d_p} = \frac{1.836(270)}{0.85(0.75)(6)(30) + 0.28(1.836)(270)/(46.3)} = 4.21"$$

$$\frac{c}{d} = \frac{4.21}{46.3} = 0.09 \leq 0.42 \quad \text{and} \quad a = \beta_1 c = 0.75(4.21) = 3.16"$$

$$f_{ps} = f_{pu}\left(1 - \frac{ck}{d_{ps}}\right) = 270\left(1 - \frac{4.21(0.28)}{46.3}\right) = 263.1 \text{ ksi}$$

Taking Φ = 1.0 for prestressed member: $\Phi M_n = 1.0\left[1.836(263.1)\left(46.3 - \frac{3.16}{2}\right)\right] = 1800$ k*ft

Cracking Moment:

$$Z_b = \frac{I}{y_b} = \frac{219262}{27.3} = 8032 \text{ in}^3$$

$$f_r = 7.5\sqrt{f'_c} = 7.5\sqrt{6000} = 0.58 \text{ ksi}$$

$$M_{crack} = A_{ps}f_{pe}\left(e_o + \frac{Z_b}{A_c}\right) + f_r Z_b = \frac{1.836(163)}{12}\left(23.6 + \frac{8032}{704.5}\right) + \frac{0.58(8032)}{12} = 1263 \text{ k*ft}$$

Check $\frac{\Phi M_n}{M_{crack}} = \frac{1800}{1263} = 1.43 > 1.2$ OK

Example D.5 – I-Girder 1 – Shear Capacity via AASHTO Method

$$d_v = \max\begin{cases} 0.9d_e = 0.9(46.3) = 41.7 \\ 0.72h = 0.72(50) = 36.0 \end{cases} = 41.7"$$

$$b_v = 6"$$

$V_p = f_{pe} A_{ps} \sin\alpha = 0$ (tendons straight)

Consider section 60 in. from end of specimen, where stirrups are spaced 12 in. apart. Take applied shear and moment from respective shear and moment envelopes.

$V_u = 174.1$ kip
$M_u = 10890$ k*in
$M_u \geq V_u d_v = 174.1(41.67) = 7253$ k*in

Assume θ = 35.1 degrees: $$\varepsilon_x = \frac{\frac{M_u}{d_v} + 0.5N_u + 0.5(V_u - V_p)\cot\theta - A_{ps} f_{po}}{2(E_s A_s + E_p A_{ps})}$$

$$\varepsilon_x = \frac{\frac{10890}{41.7} + 0.5(174.1)\cot 35.1 - 1.836(163)}{2(28700)(1.836)} = .814$$

$$v = \frac{V_u - \phi V_p}{\phi b_v d_v} = \frac{174.1}{0.9(6)(41.7)} = 0.774 \text{ ksi}$$

$$\frac{v}{f_c'} = \frac{0.774}{6.0} = 0.129$$

From AASHTO (2004) interpolation tables: θ = 35.1, β = 2.22

$$V_c = 0.0316\beta b_v d_v \sqrt{f_c'} = 0.0316(2.22)(6)(41.7)\sqrt{6.0} = 42.9 \text{ kip}$$

$$V_s = \frac{A_v f_y d_v \cot\theta}{s} = \frac{0.4(60)(41.7)\cot 35.1}{12} = 118.4 \text{ kip}$$

$$\Phi V_n = \Phi(V_c + V_s + V_p) = 0.9(42.9 + 118.4) = 145.2 \text{ kip}$$

$$\Phi V_{n,limit} = \Phi(0.25 f_c' b_v d_v + V_p) = 0.9(0.25)(6)(6)(41.7) = 337.5 \text{ kip}$$

Example D.6 – I-Girder 1 – Shear Capacity via ACI Method

$$d_v = \max\begin{cases} d_p = 46.3 = 46.3 \\ 0.8h = 0.8(50) = 40 \end{cases} = 46.3"$$

$$b_w = 6"$$

Check both V_{ci} and V_{cw} to find V_c:

$$M_{cr} = Z_b\left[6\sqrt{f_c'} + \frac{F}{A_c}\left(1 + \frac{e_o A_c}{Z_b}\right)\right] = \frac{8032}{12000}\left[6\sqrt{6000} + \frac{299}{704.5}\left(1 + \frac{23.6(704.5)}{8032}\right)\right] = 1185 \text{ kip*ft}$$

$$\Delta M_{cr} = M_{cr} - M_G = 1185 - 79 = 1106 \text{ kip*ft}$$

$$V_{ci} = 0.6\lambda b_w d_p \sqrt{f_c'} + V_G + \frac{\Delta V_u \Delta M_{cr}}{\Delta M_u} \geq 1.7\lambda b_w d_p \sqrt{f_c'}$$

$$V_{ci} = \frac{0.6(6)(46.3)\sqrt{6000}}{1000} + 13.9 + \frac{1185}{(60/12)} = 248 \text{ kip} \geq \frac{1.7(6)(46.3)\sqrt{6000}}{1000} = 37 \text{ kip}$$

$$V_{cw} = (3.5\lambda\sqrt{f_c'} + 0.3\sigma_g)b_w d_p + V_p = \left[3.5\sqrt{6000} + 0.3\left(\frac{299}{704.5}\right)\right]\frac{(6)(46.3)}{1000} = 110.7 \text{ kip}$$

Steel Contribution:

$$V_s = \frac{A_v f_y d}{s} = \frac{0.4(60)(46.3)}{12} = 92.6 \text{ kip}$$

$$V_{s,\text{limit}} = 8b_w d_p \sqrt{f_c'} = \frac{8(6)(46.3)\sqrt{6000}}{1000} = 172 \text{ kip}$$

Shear Capacity:

$$\Phi V_n = \Phi(V_c + V_s) = 0.75(110.7 + 92.6) = 152.5 \text{ kip}$$

APPENDIX E: STRAIN PROFILES FOR 95% AMS TRANSFER LENGTH

This appendix contains all strain readings recorded for the transfer length measurements described in Chapter 5. Each of the following figures contains the smoothed strain profiles generated for one location of one specimen at all testing ages. Figures E.1-E.4 show profiles for specimen Box-1; Figures E.5-E.8 show profiles for specimen Box-2; Figures E.9-E.12 show profiles for specimen I-1; Figures E.13-E.16 show profiles for specimen I-2.

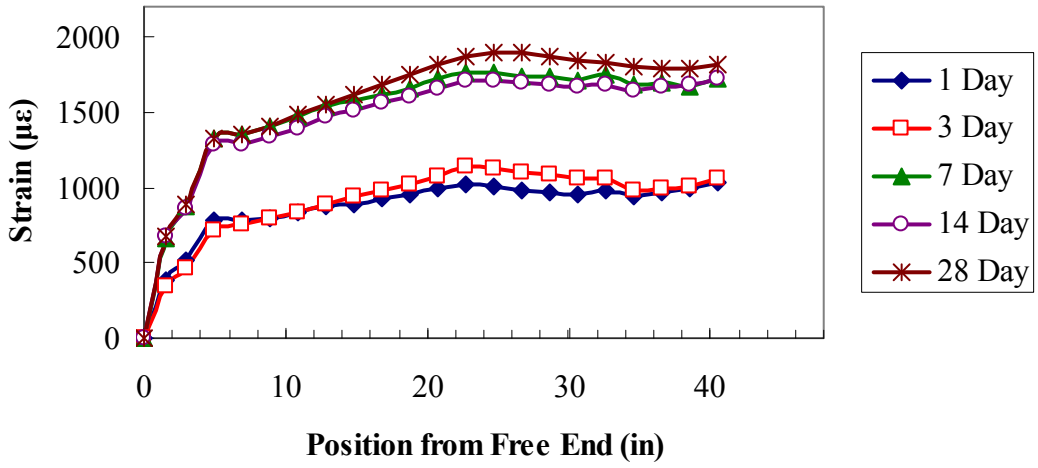

Figure E.1: Strain readings at Box-1, Starting End, Side A

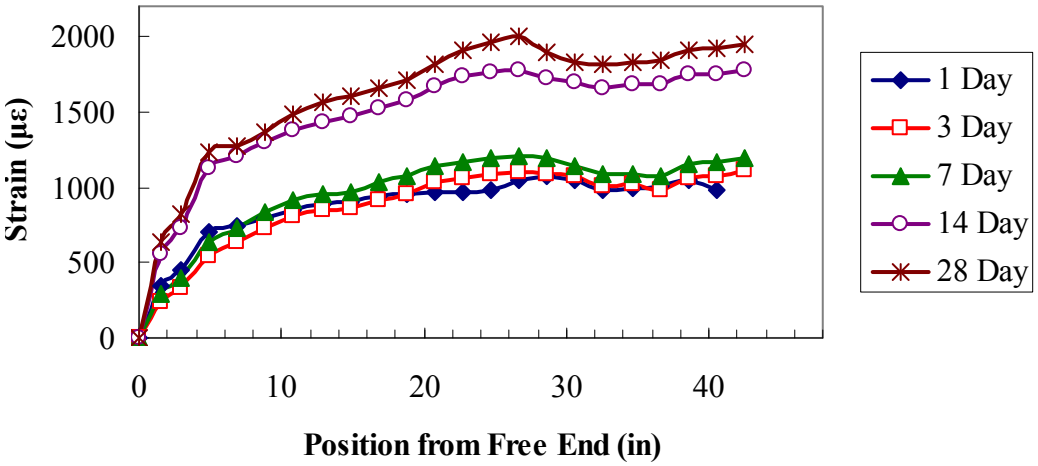

Figure E.2: Strain readings at Box-1, Starting End, Side D

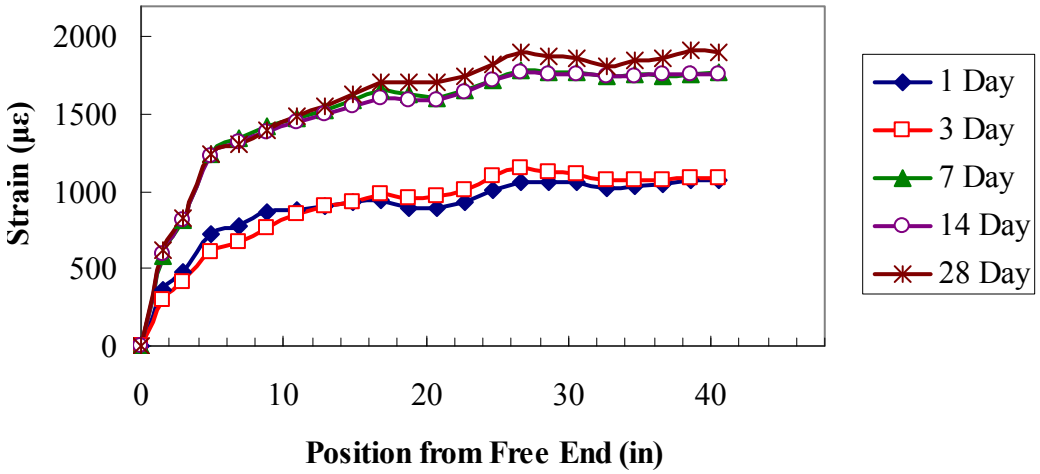

Figure E.3: Strain readings at Box-1, Far End, Side B

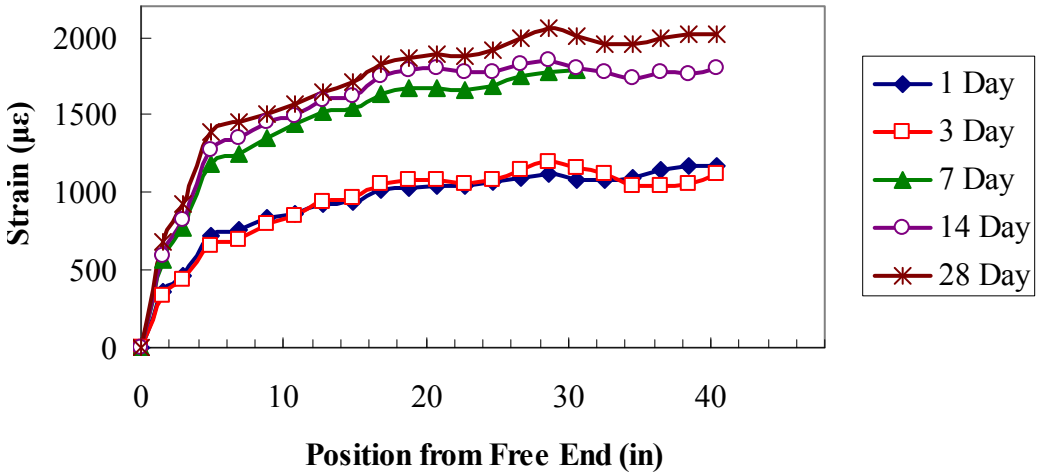

Figure E.4: Strain readings at Box-1, Far End, Side C

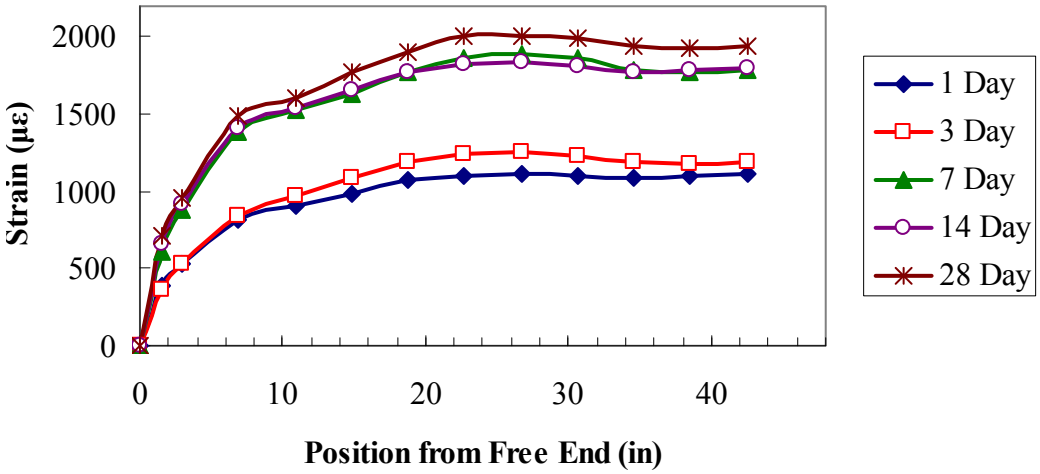

Figure E.5: Strain readings at Box-2, Starting End, Side A

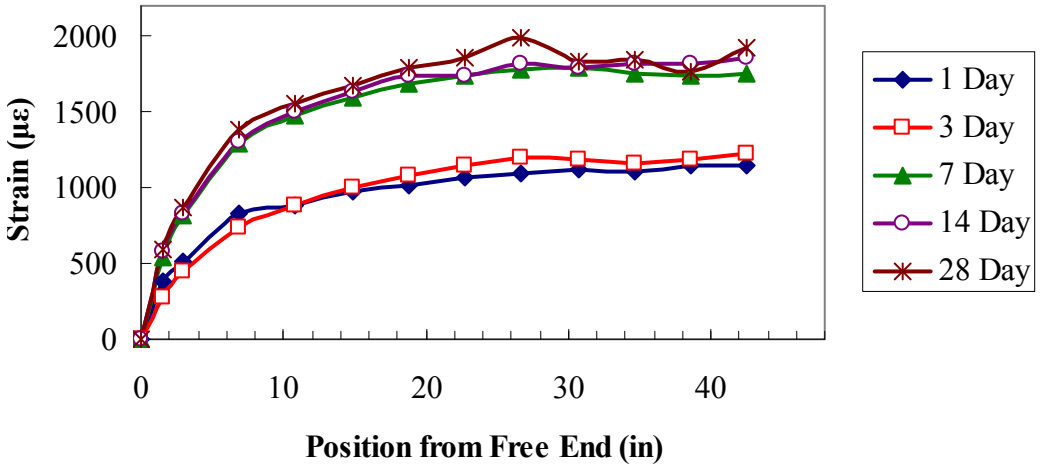

Figure E.6: Strain readings at Box-2, Starting End, Side D

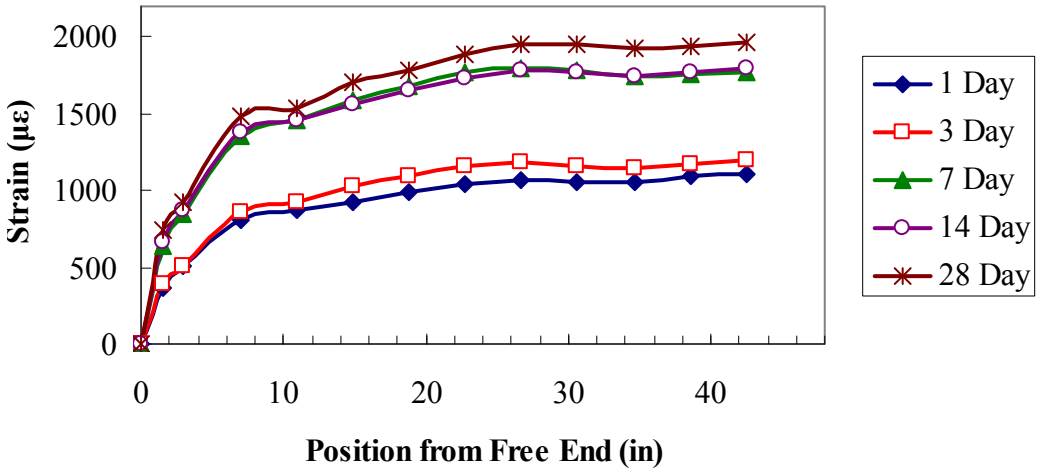

Figure E.7: Strain readings at Box-2, Far End, Side B

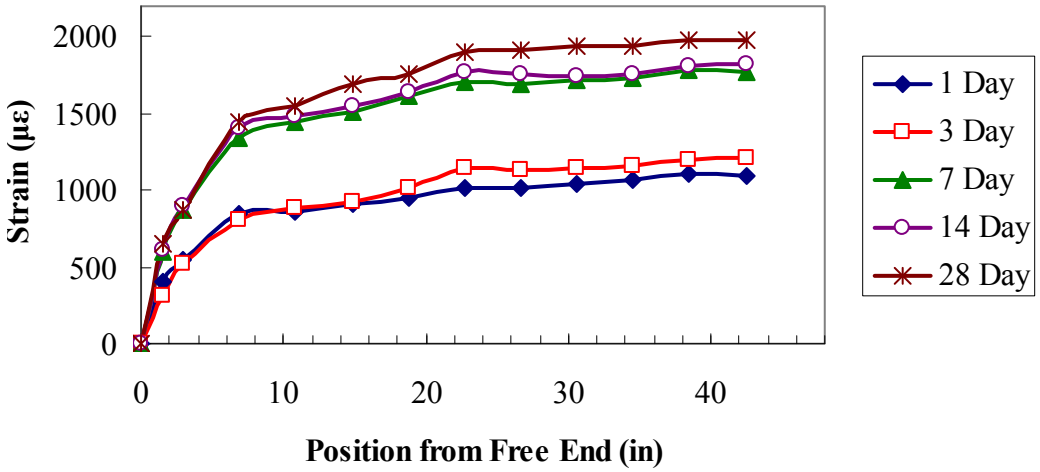

Figure E.8: Strain readings at Box-2, Far End, Side C

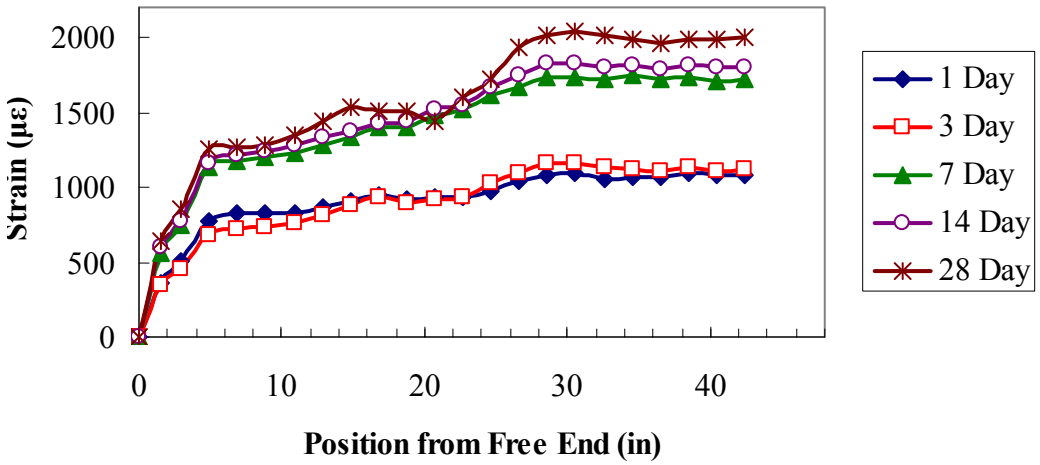

Figure E.9: Strain readings at I-1, Starting End, Side B

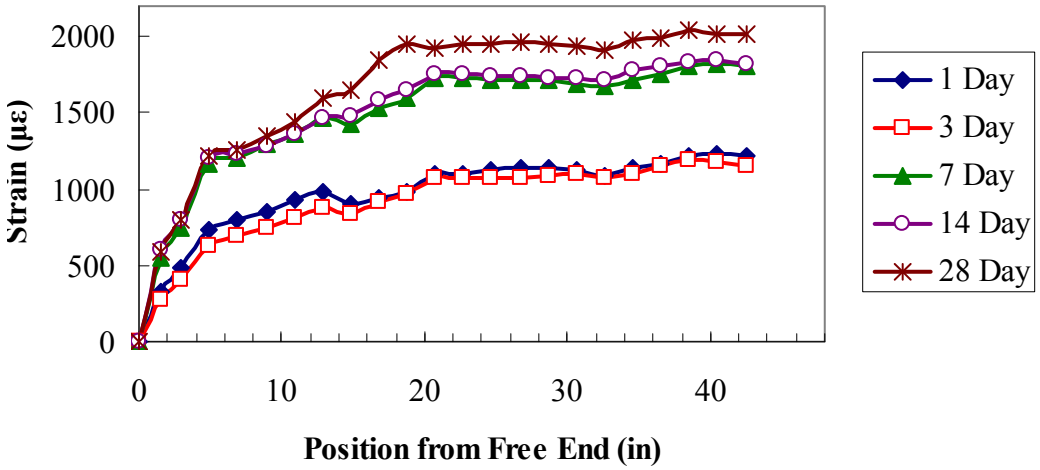

Figure E.10: Strain readings at I-1, Starting End, Side C

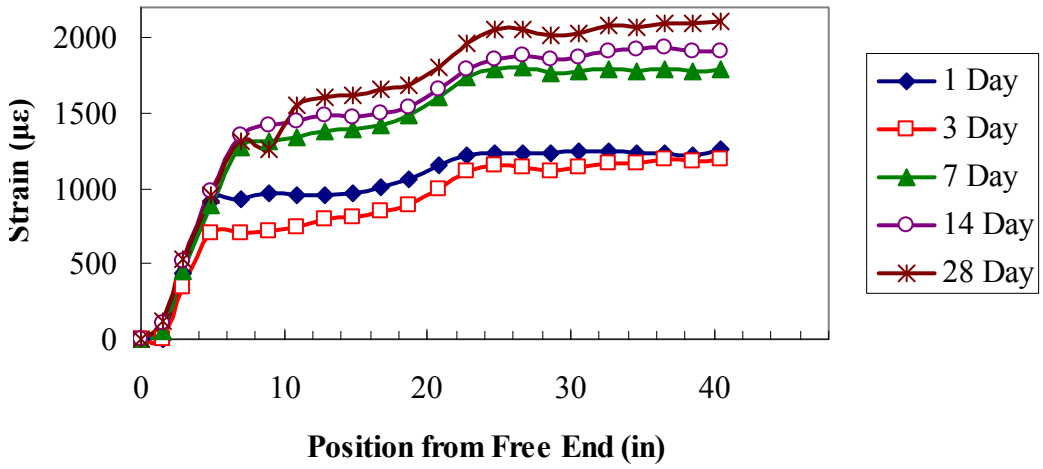

Figure E.11: Strain readings at I-1, Far End, Side A

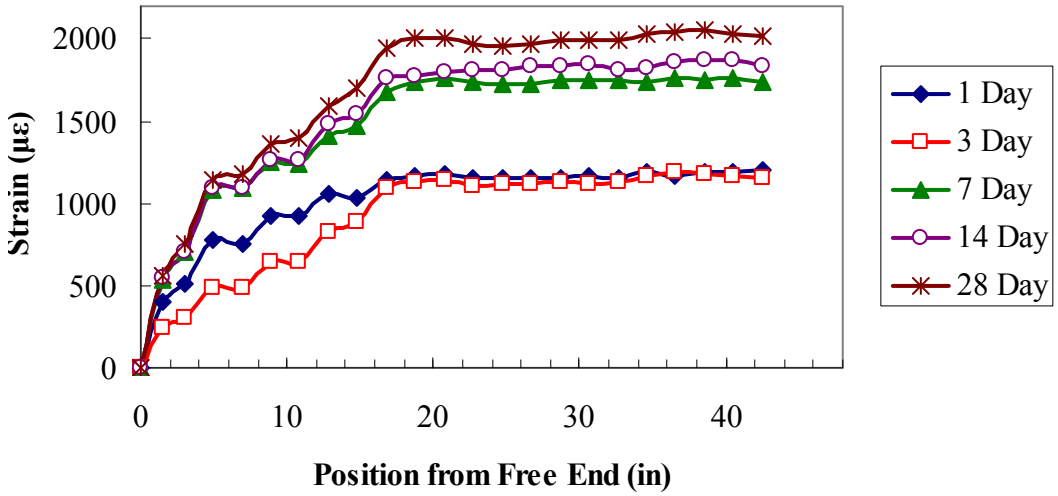

Figure E.12: Strain readings at I-1, Far End, Side D

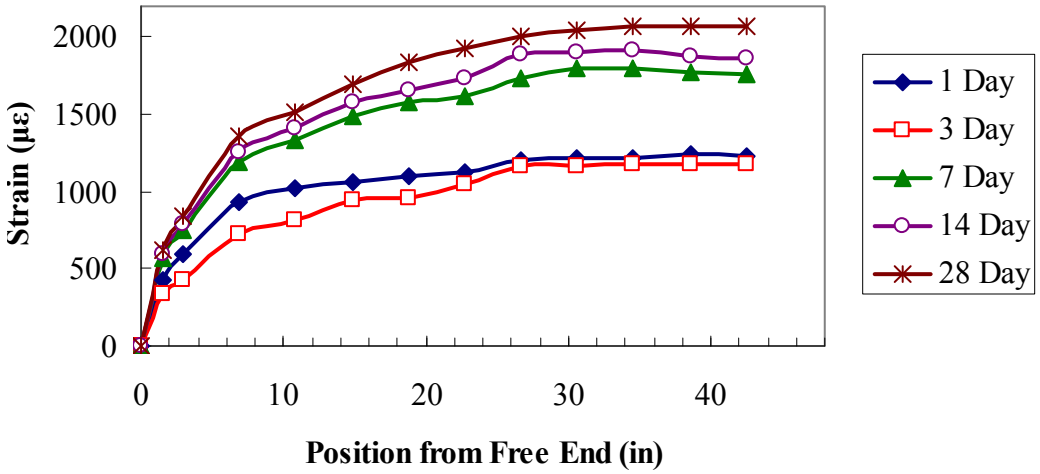

Figure E.13: Strain readings at I-2, Starting End, Side B

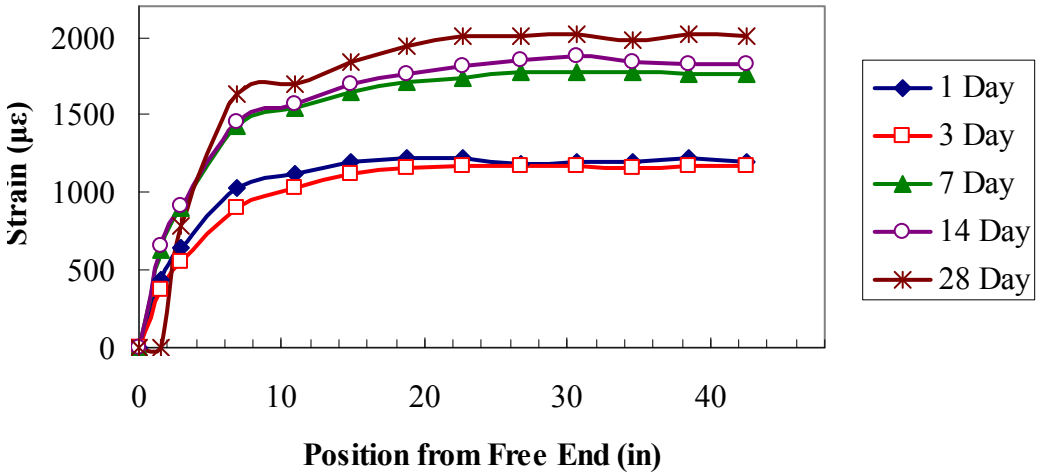

Figure E.14: Strain readings at I-2, Starting End, Side C

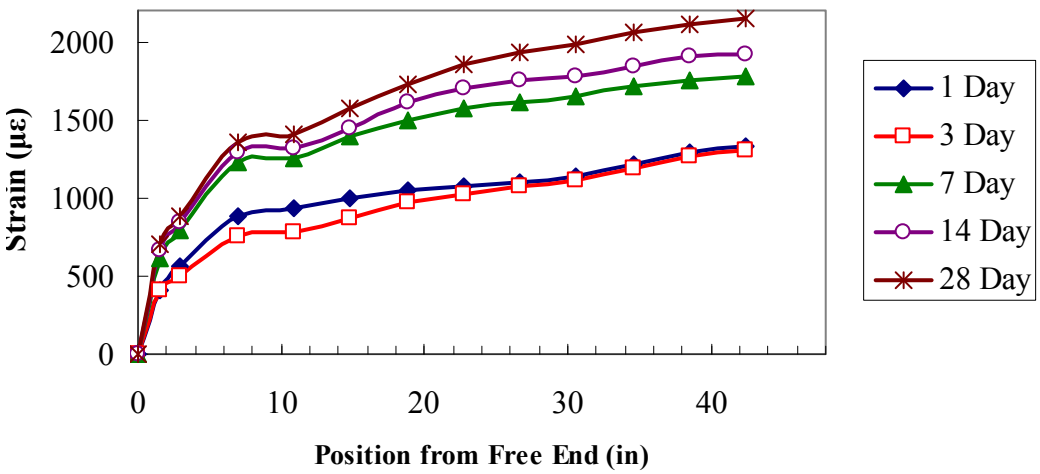

Figure E.15: Strain readings at I-2, Far End, Side A

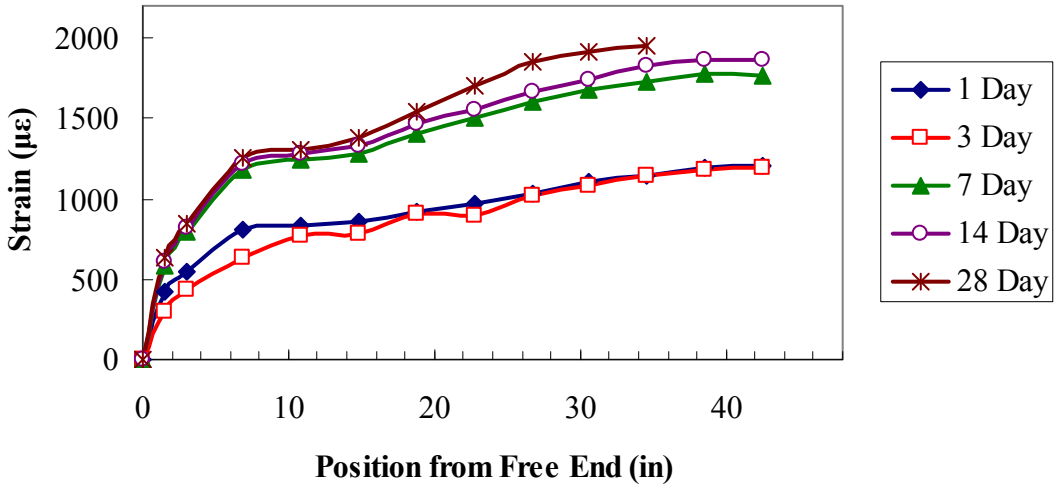

Figure E.16: Strain readings at I-2, Far End, Side D

APPENDIX F: END-SLIP RESPONSES FOR FLEXURAL TESTS

This appendix contains all end-slip responses plotted against applied loads in the first, second, and fourth development length tests. End-slip data is not available for the third flexural test (see Section 6.2.3). For strand numbering, see Figure 6.9.

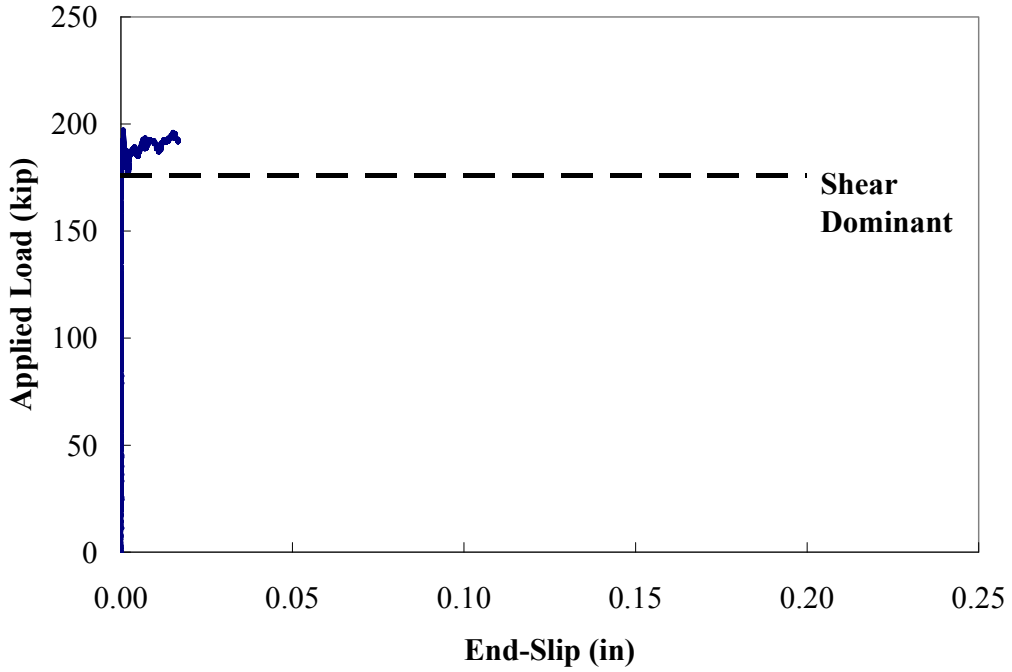

Figure F.1: End-slip response of strand #1 for Box-1, South End (A/D)

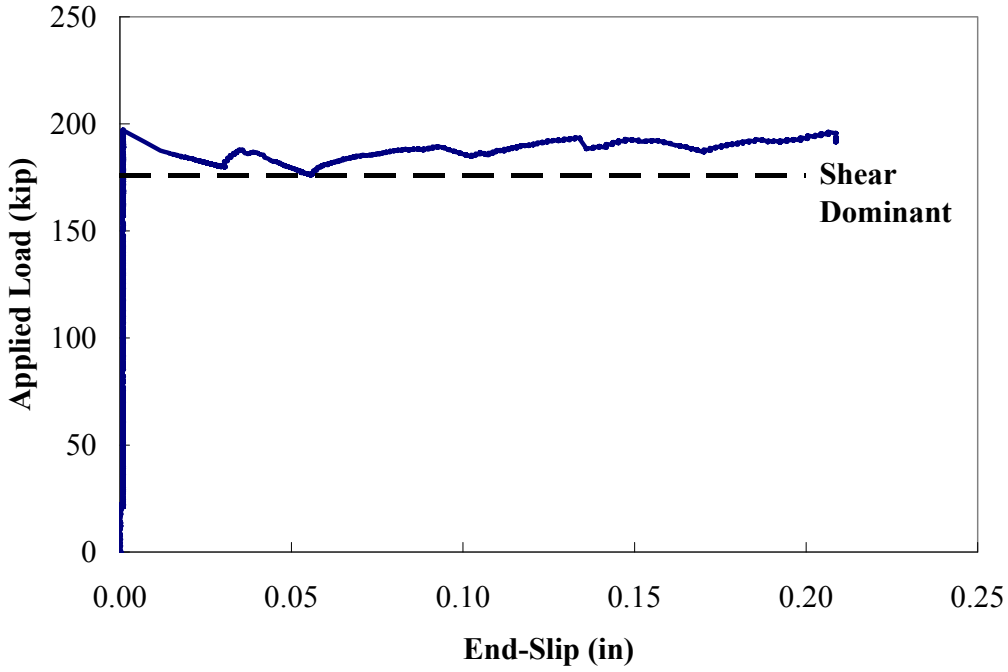

Figure F.2: End-slip response of strand #2 for Box-1, South End (A/D)

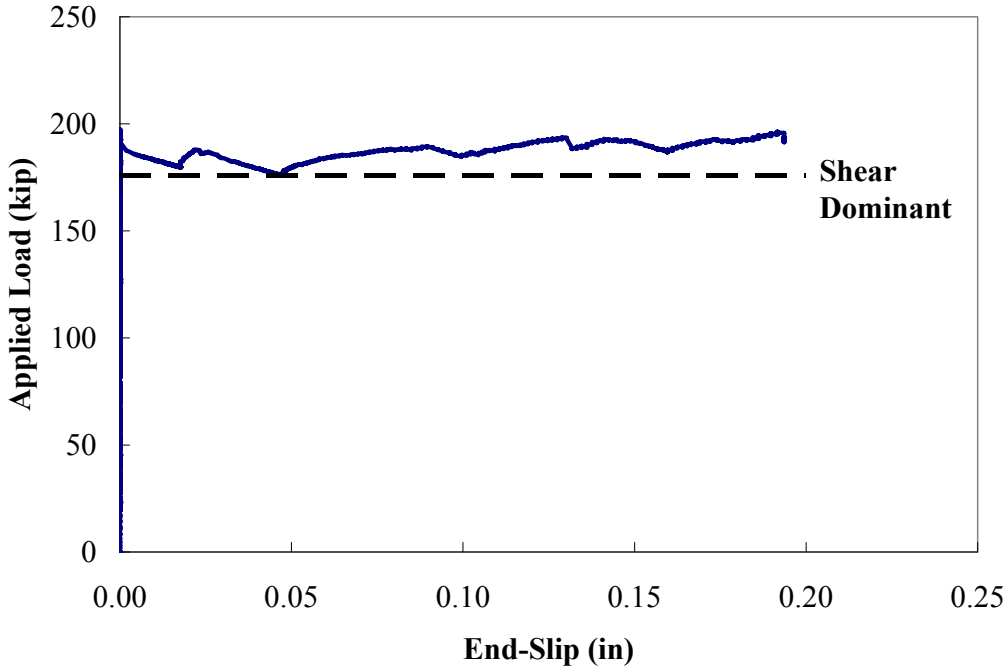

Figure F.3: End-slip response of strand #3 for Box-1, South End (A/D)

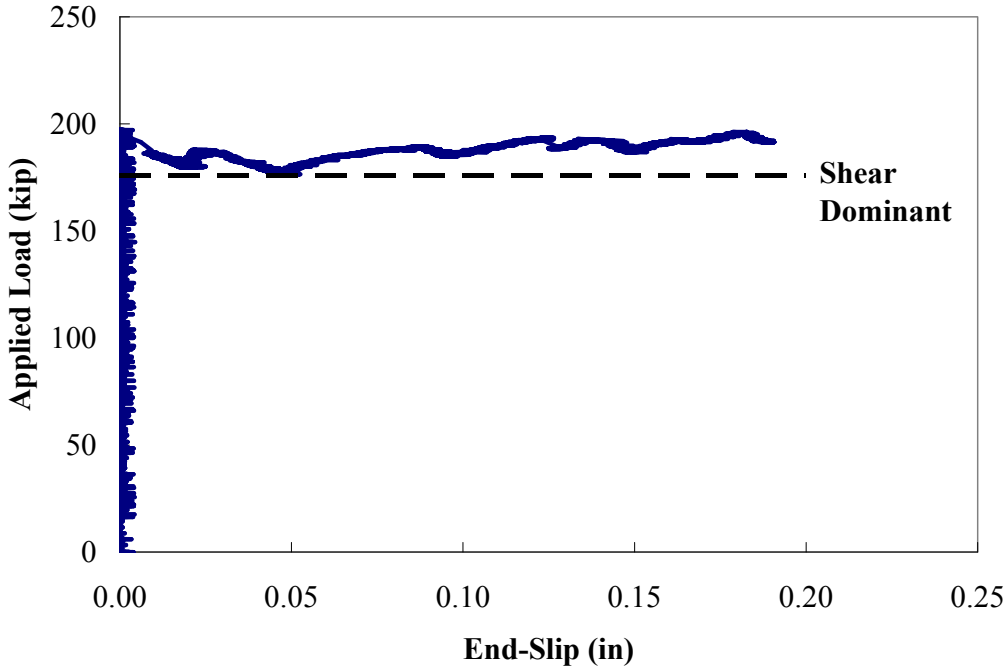

Figure F.4: End-slip response of strand #4 for Box-1, South End (A/D)

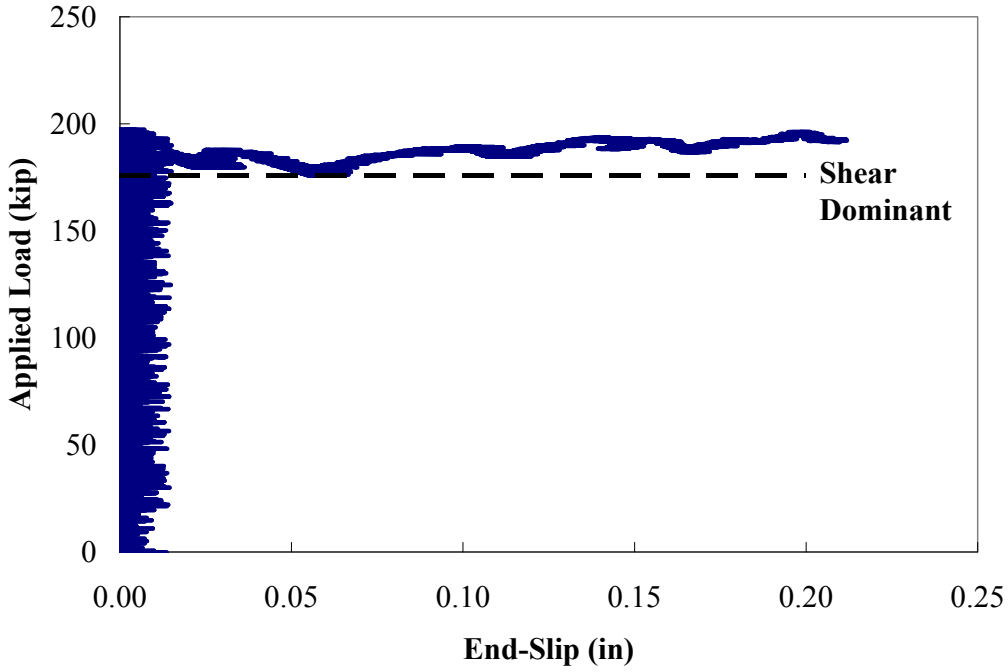

Figure F.5: End-slip response of strand #5 for Box-1, South End (A/D)

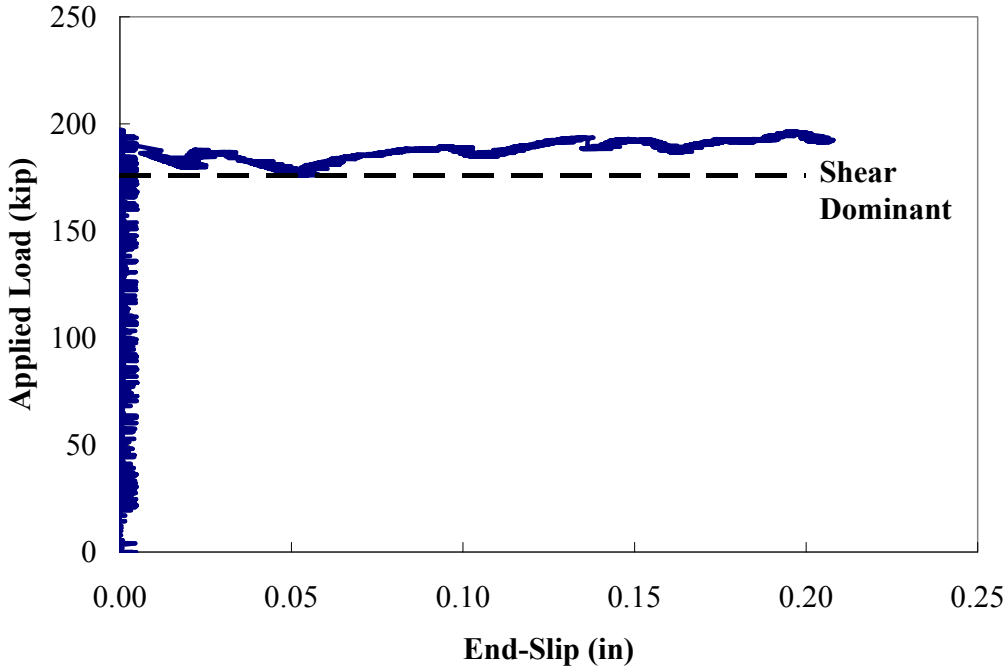

Figure F.6: End-slip response of strand #6 for Box-1, South End (A/D)

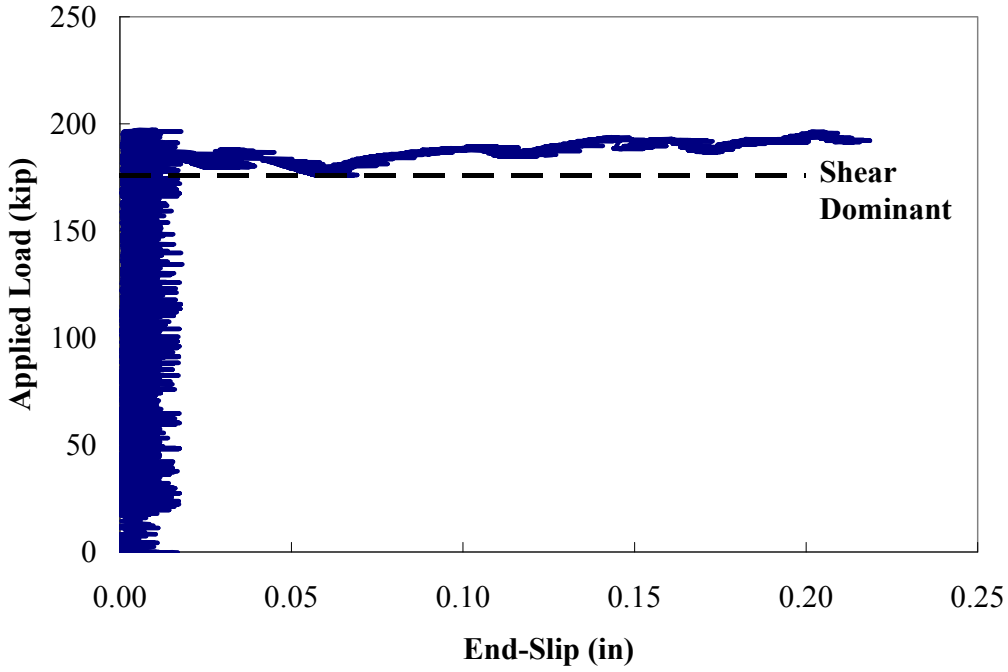

Figure F.7: End-slip response of strand #7 for Box-1, South End (A/D)

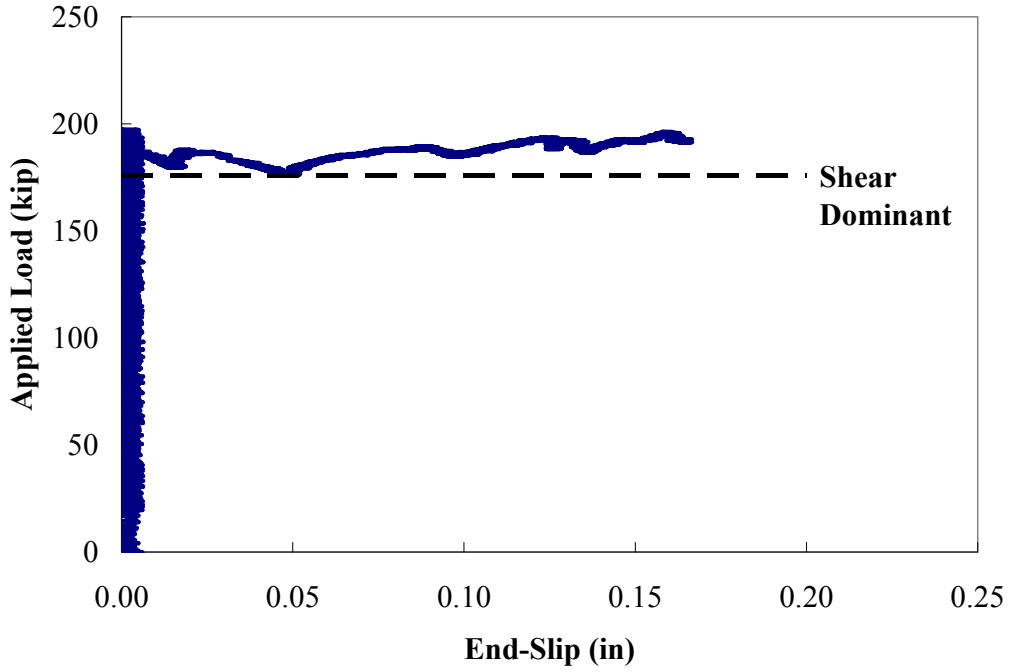

Figure F.8: End-slip response of strand #8 for Box-1, South End (A/D)

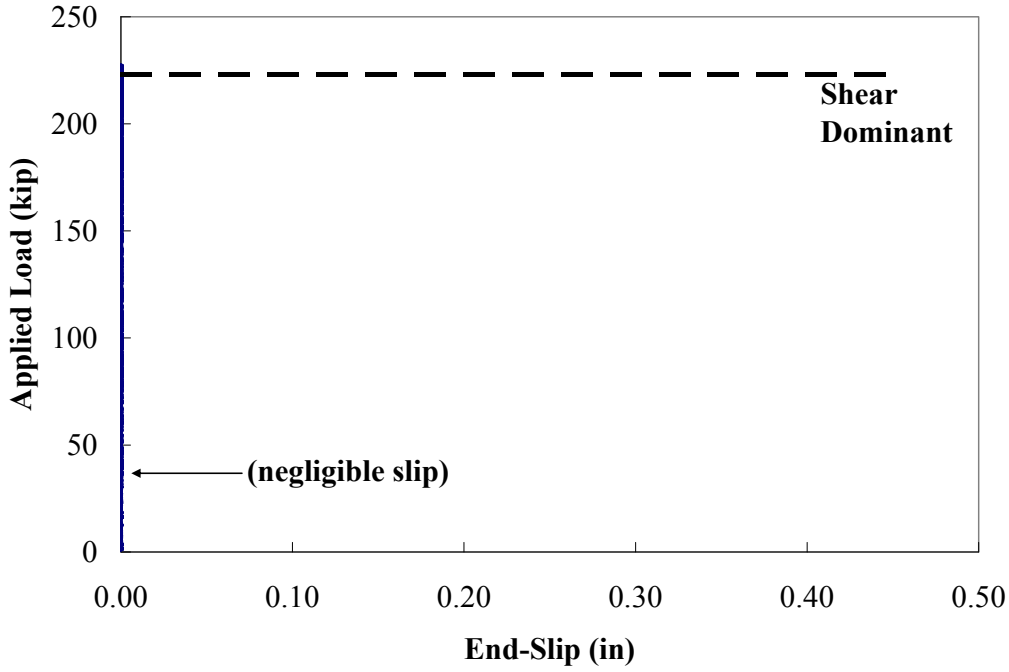

Figure F.9: End-slip response of strand #1 for Box-1, North End (B/C)

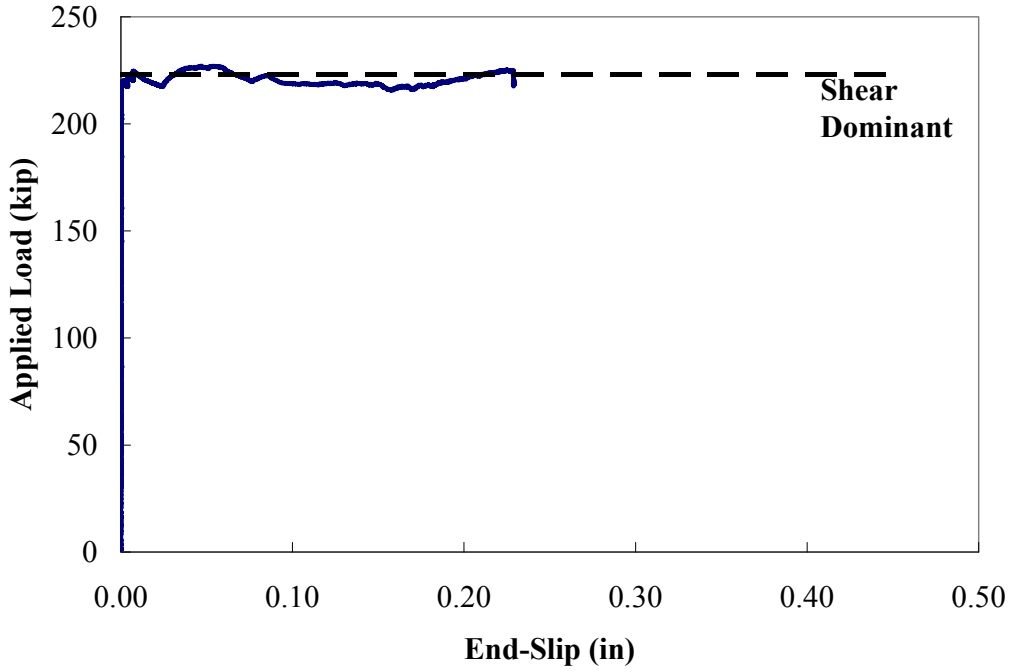

Figure F.10: End-slip response of strand #2 for Box-1, North End (B/C)

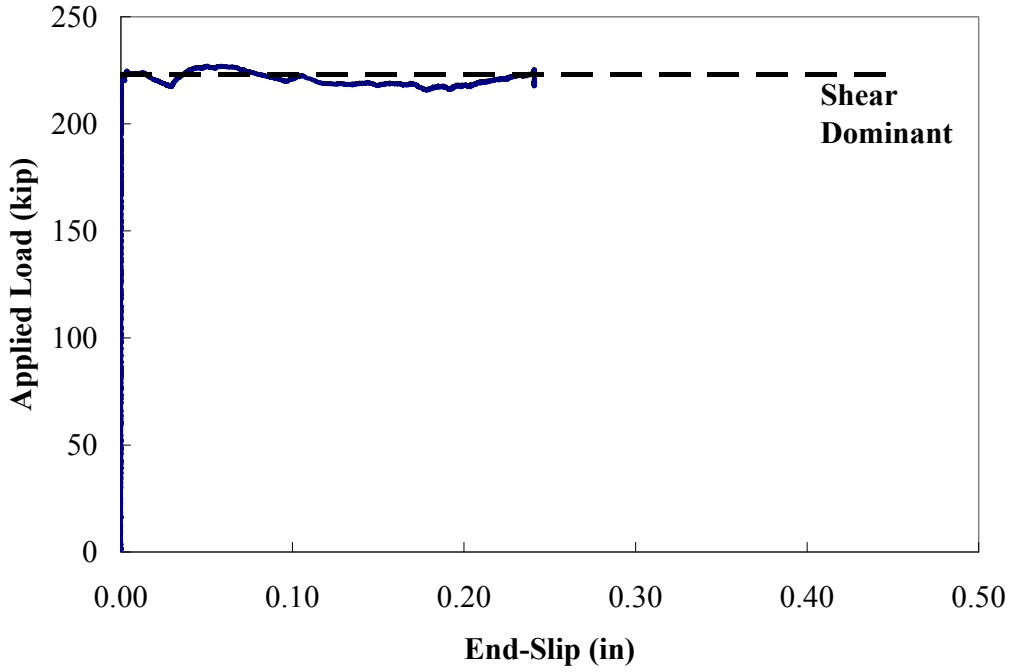

Figure F.11: End-slip response of strand #3 for Box-1, North End (B/C)

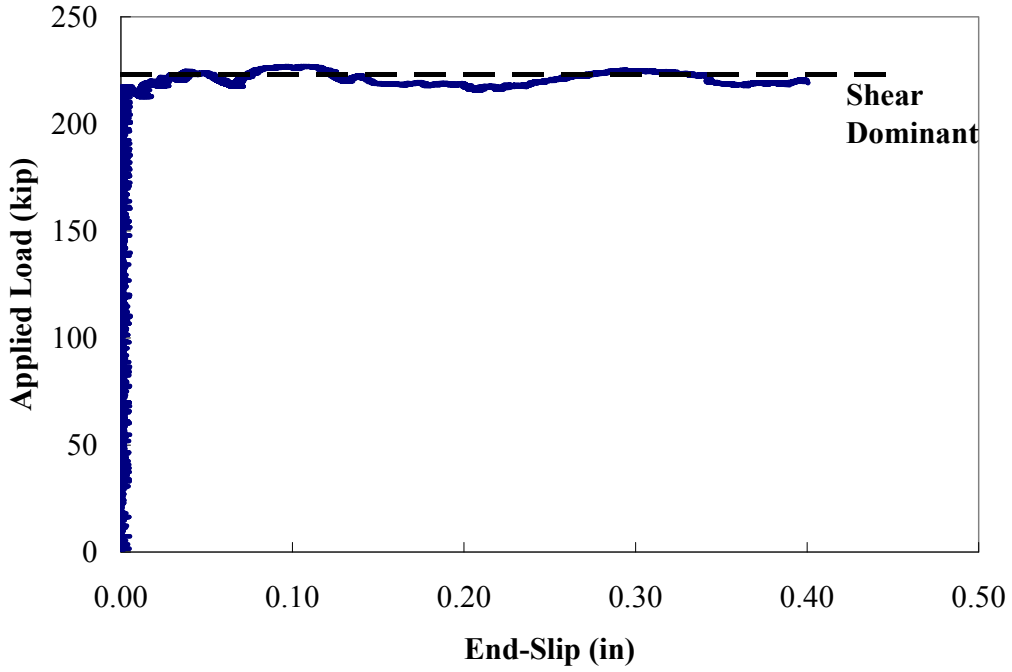

Figure F.12: End-slip response of strand #4 for Box-1, North End (B/C)

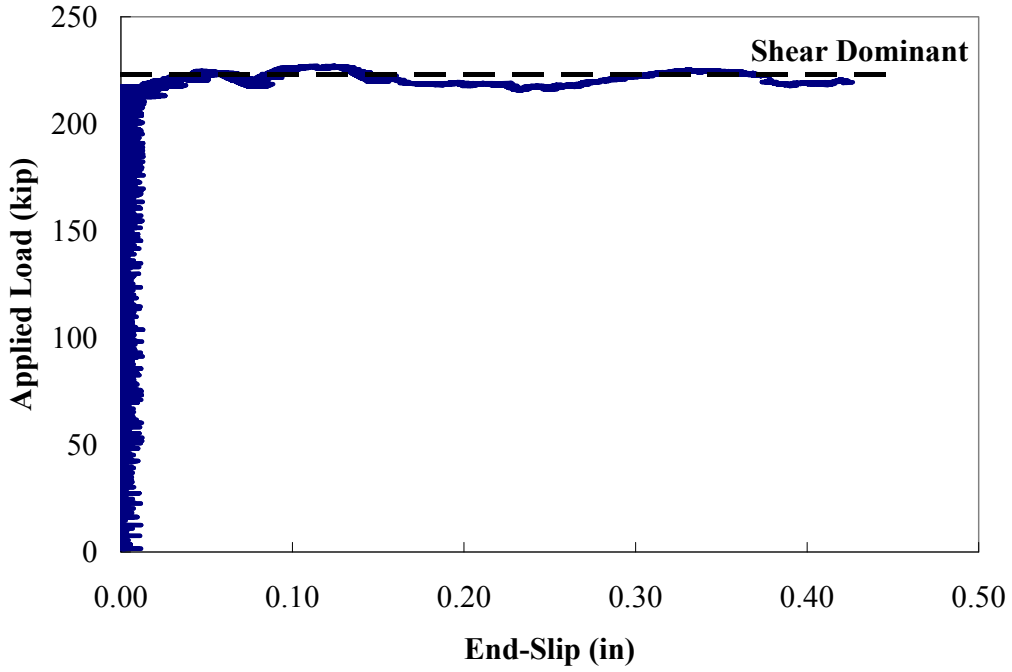

Figure F.13: End-slip response of strand #5 for Box-1, North End (B/C)

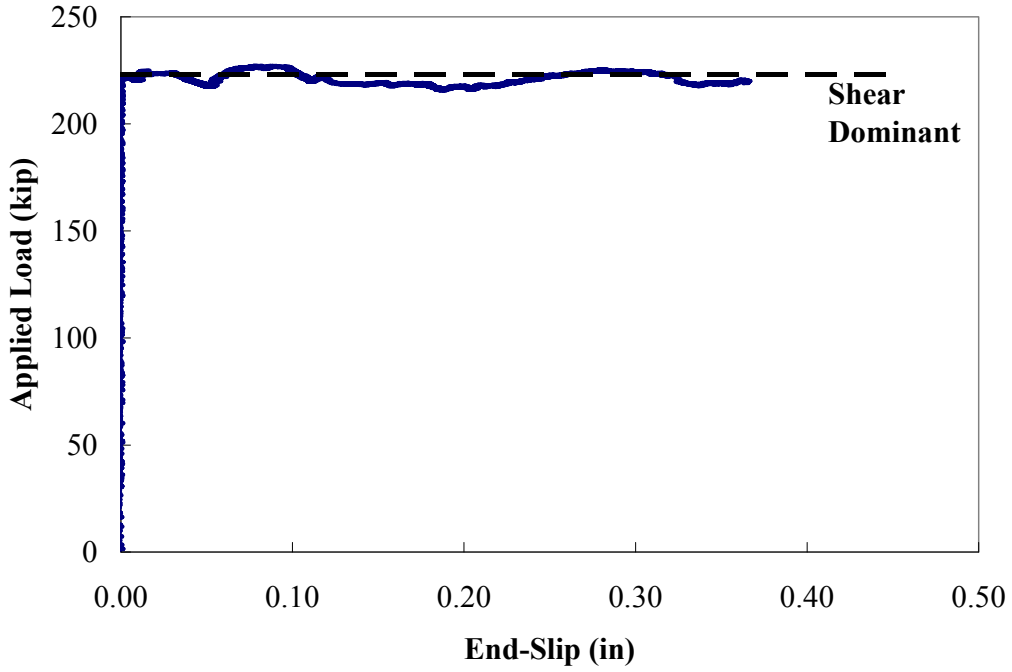

Figure F.14: End-slip response of strand #6 for Box-1, North End (B/C)

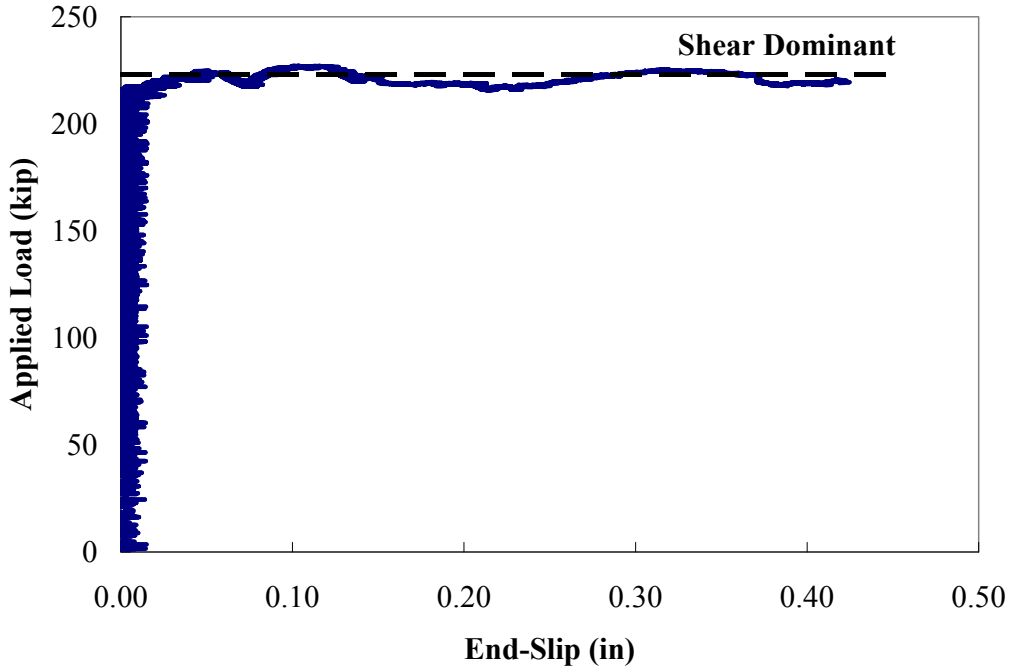

Figure F.15: End-slip response of strand #7 for Box-1, North End (B/C)

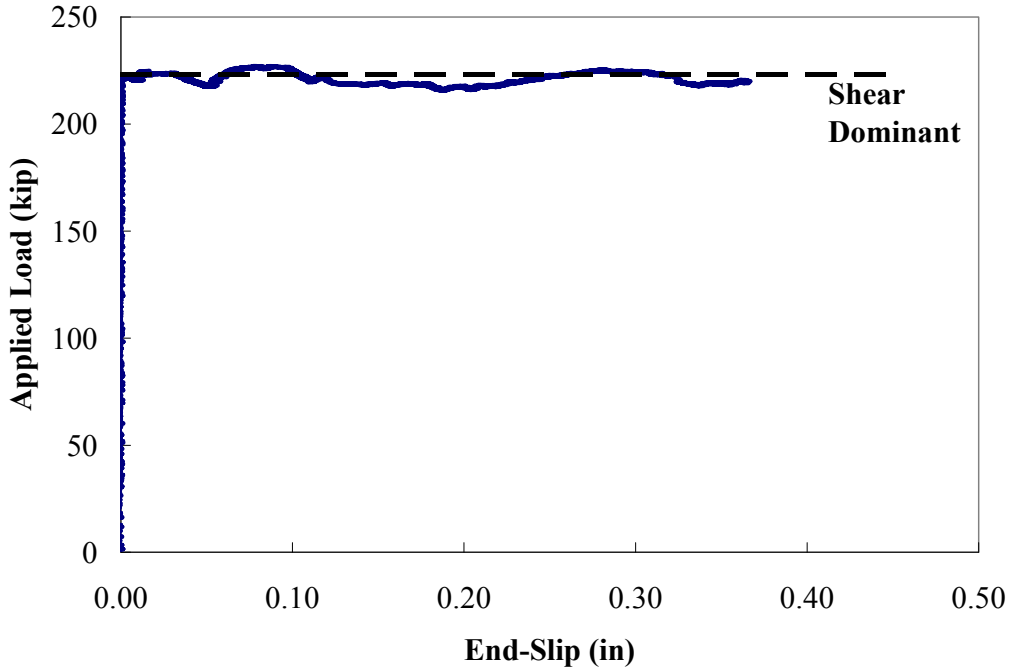

Figure F.16: End-slip response of strand #8 for Box-1, North End (B/C)

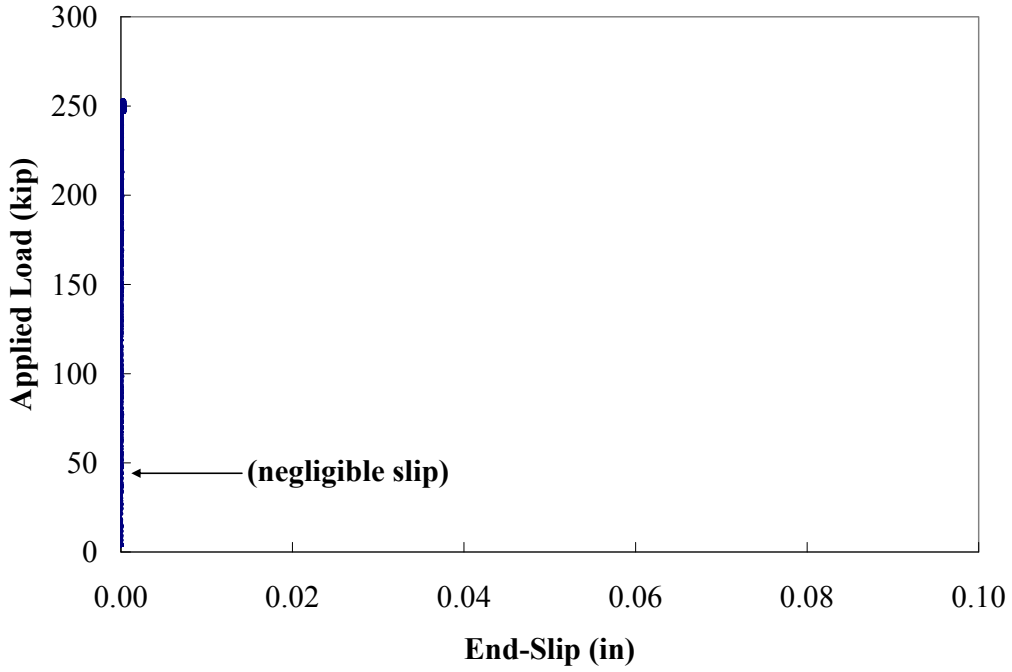

Figure F.17: End-slip response of strand #1 for Box-2, North End (B/C)

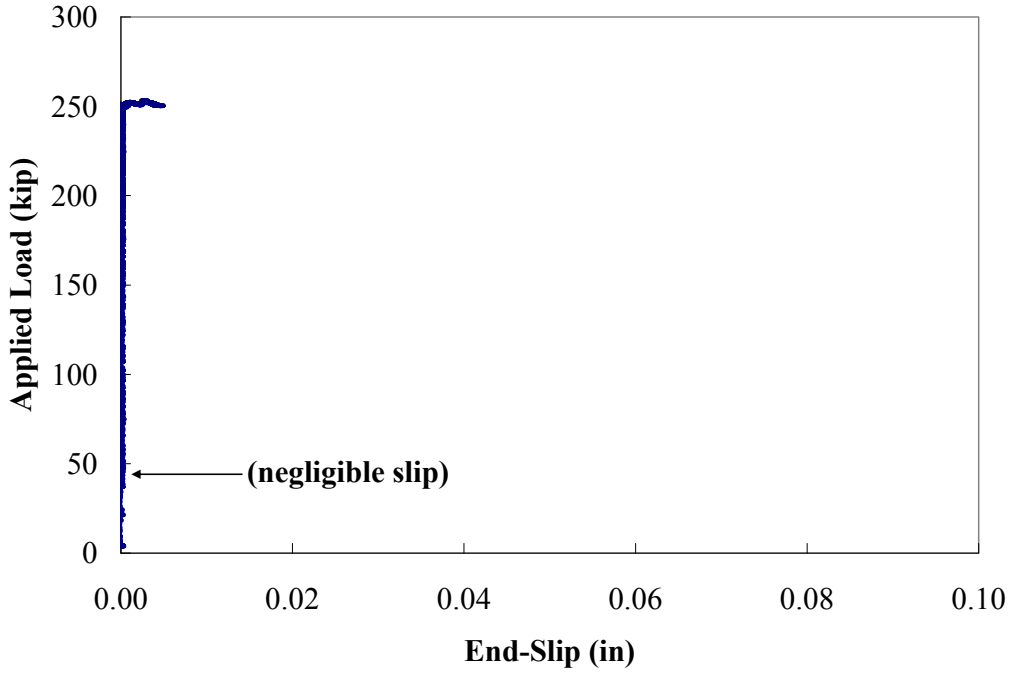

Figure F.18: End-slip response of strand #2 for Box-2, North End (B/C)

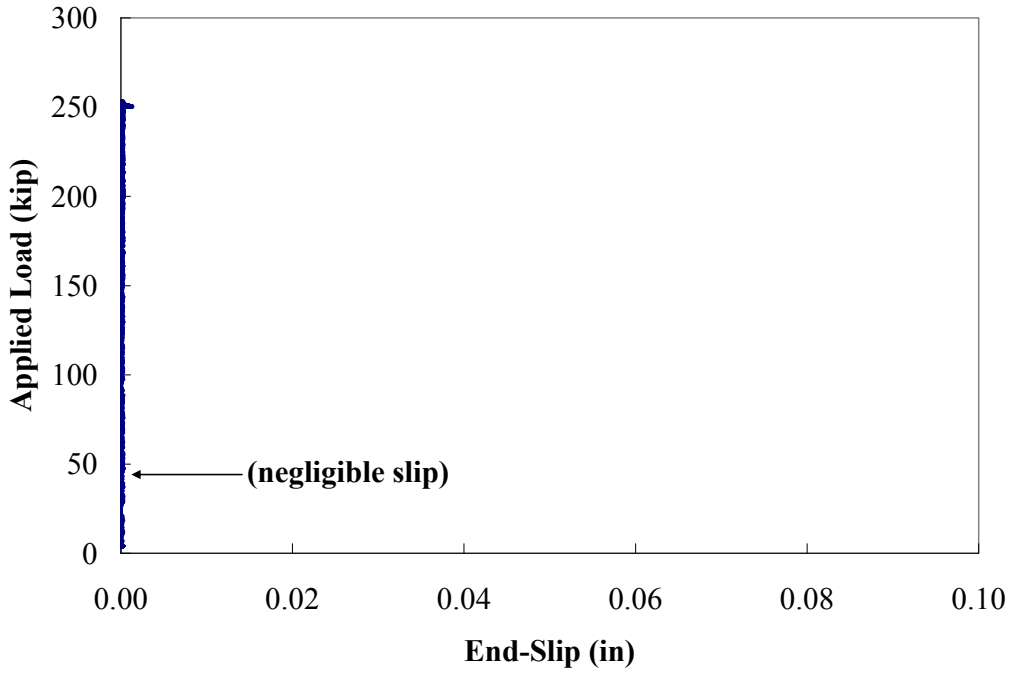

Figure F.19: End-slip response of strand #3 for Box-2, North End (B/C)

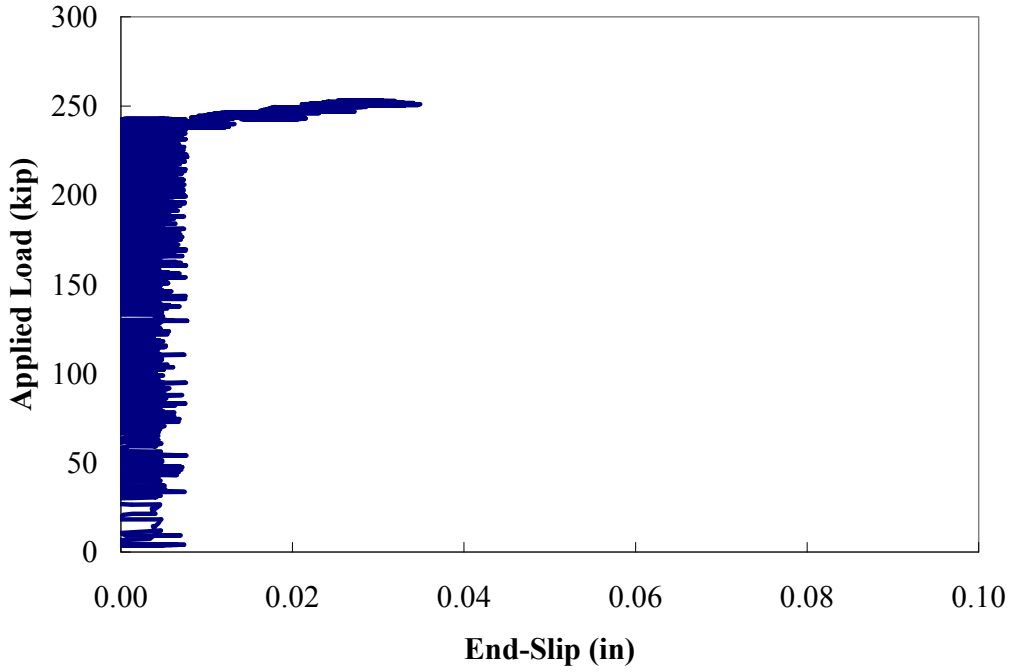

Figure F.20: End-slip response of strand #4 for Box-2, North End (B/C)

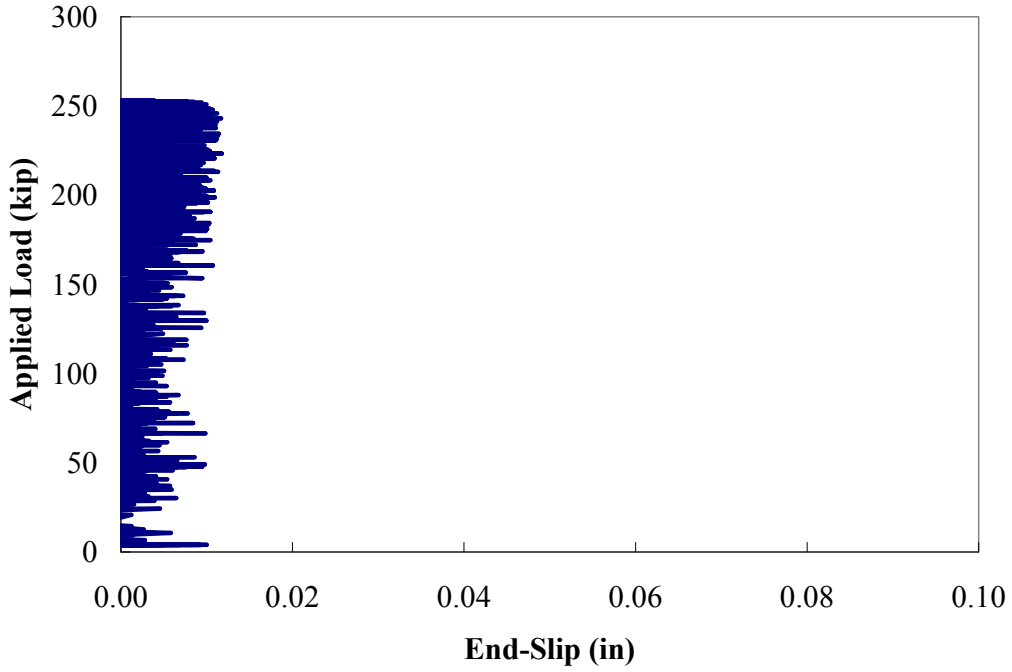

Figure F.21: End-slip response of strand #5 for Box-2, North End (B/C)

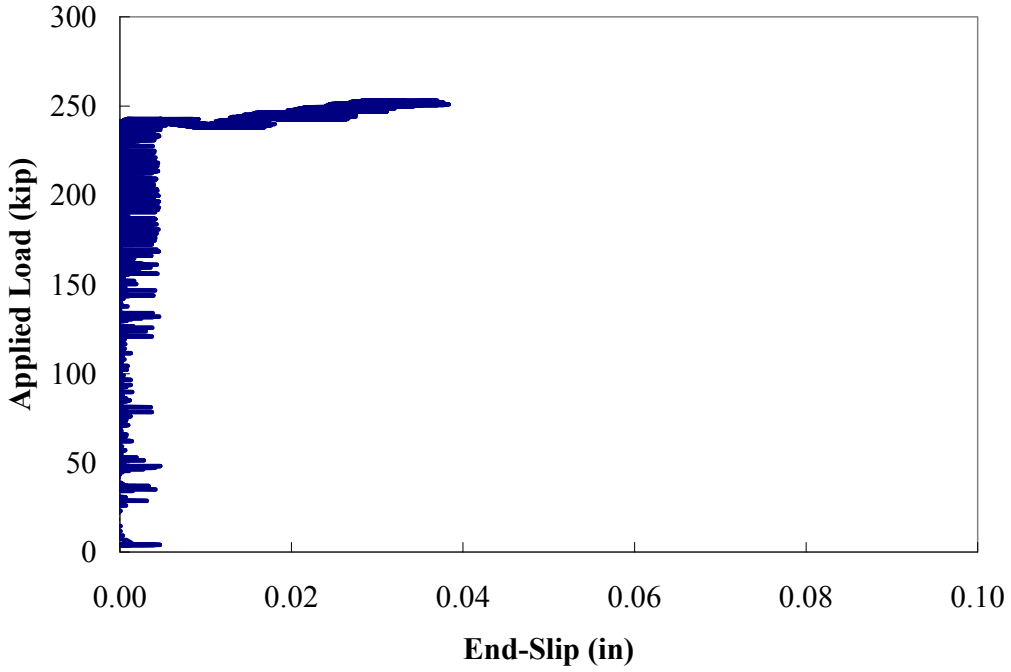

Figure F.22: End-slip response of strand #6 for Box-2, North End (B/C)

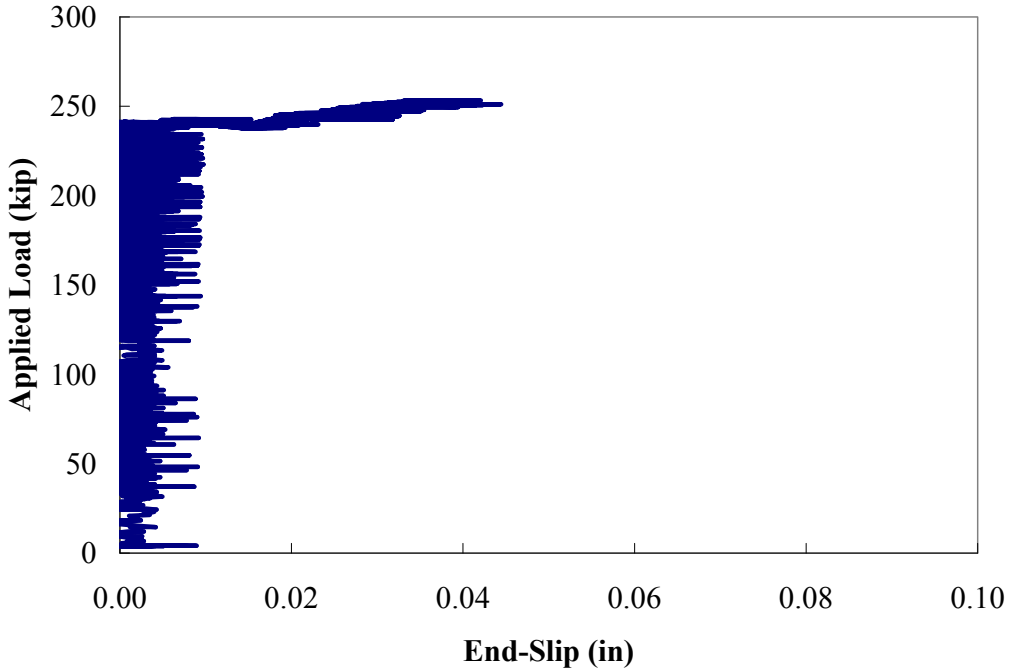

Figure F.23: End-slip response of strand #7 for Box-2, North End (B/C)

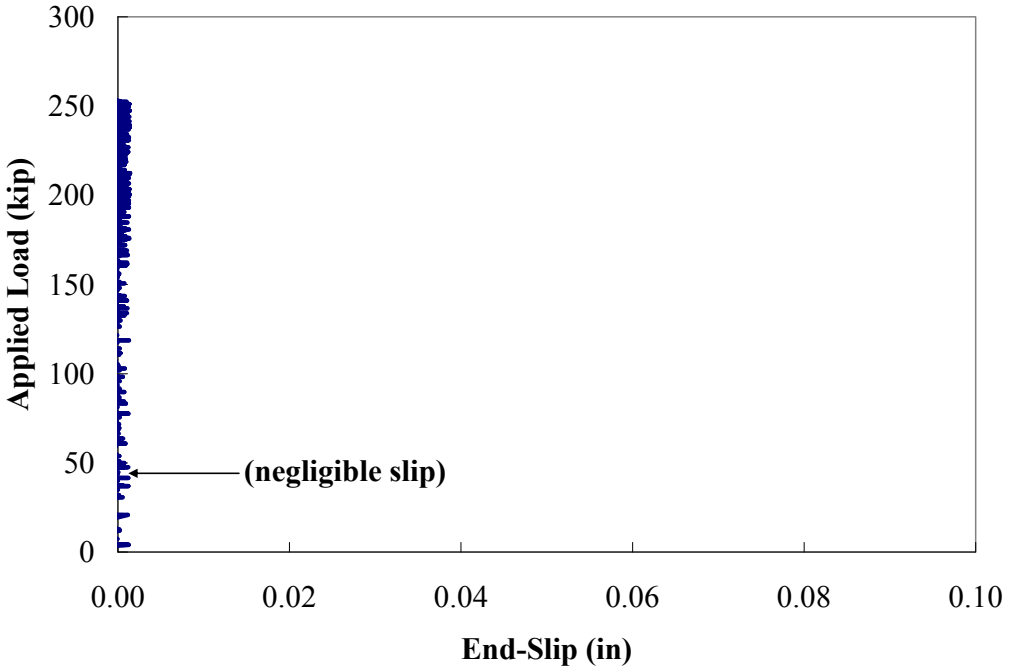

Figure F.24: End-slip response of strand #8 for Box-2, North End (B/C)